UNIVERSITY OF SASKATCHEWAN

CONTRACT SERIAL NUMBER 69121-01-SQ
DSS REQUISITION NUMBER 23440-6-9121
CONTRACTOR: POTASH CORPORATION OF SASK.

A REPORT TO DEPARTMENT OF SUPPLY AND SERVICES

CONTRACT # 04SQ-23440-5-9121
6-9121

ON

RESEARCH IN MICROSEISMIC TECHNOLOGY

VOLUME I

FEBRUARY 1988

83pp

MICROMEDIA

TABLE OF CONTENTS

SECTION 1: REPORT OF THE RESULTS OF SEISMIC MONITORING AT PCS MINING, LANIGAN DIVISION, NOVEMBER AND DECEMBER 1987

SECTION 2: REPORT OF THE RESULT OF THE SEISMIC MONITORING AT THE IMC-K2 POTASH MINE, DECEMBER 1987

SECTION 3: REPORT OF THE RESULTS OF SEISMIC MONITORING AT PCS MINING, ROCANVILLE DIVISION, JULY AND OCTOBER 1988

SECTION 4: REPORT OF THE RESULTS OF SEISMIC MONITORING AT THE COMINCO POTASH MINE, OCTOBER 1985

PRELIMINARY RESULTS OF SEISMIC MONITORING AT THE PCS LANIGAN POTASH MINE, (LANIGAN SASKATCHEWAN), NOVEMBER AND DECEMBER 1987.

Arnfinn Prugger
Don Gendzwill
Department of Geological Sciences
University of Saskatchewan
Saskatoon, Saskatchewan
(S7N-0W0)

January 31, 1988.

Summary :

A seismic monitoring array was continuously operated underground at the Lanigan potash mine in the period November 5 through December 7, 1987. A total of 37 seismic events were observed in 33 full days of recording. Events occurred regularly throughout the recording period; there were never more than 3 events in a single day. Arrival times were used to calculate event locations, which are plotted on a mine map. Most events occurred in a very localized region of Panel 321, in an old, abandoned region of the mine. No active mining was carried out near the geophone array during the recording period.

1.1 Background :

Seismic traces are records of ground vibration observed through time at that point in (or on) the Earth where a vibration sensor, or geophone, has been set up. "Vibration" in this context means particle displacement of the region of rock that the geophone is attached to. The geophone sensors used at Lanigan measure the velocity of particle displacement (in micro-meters per second). The vibration record that is observed results from rock fracture occurring some distance away from the sensor. Since seismic energy travels at finite velocities through rock, vibrations emanating from a rock fracture will in general arrive at different times at different geophones. The arrival times are used to calculate the location of the rock fracture using the "Simplex Method" of source location described in Prugger and Gendzwill, 1988.

Micro-seismic activity has been observed at every potash mine in Saskatchewan where monitoring instruments have been set up. As well, seismic events strong enough to be noticed by persons living in the vicinity of mines have occurred at five of the provinces ten mines to date : IMC-K1 and IMC-K2 at Esterhazy, PCS at Cory, CCP at Colonsay, and PCA at Patience Lake. These events have been in the Richter magnitude range 2.0 - 3.5 (Gendzwill et al., 1982). This corresponds to noticed effects ranging from "I thought a truck ran into the house", or "It felt like the furnace blew up", to (in a few cases) cracked wall plaster.

Noticeable macro-seismic activity has NOT been observed in the Lanigan area to date. Although high frequency acoustic emissions have been monitored at Lanigan using a "roof-fall warning" system, seismicity was not monitored prior to the experiment described here.

1.2 Instrument Setup :

6 vertical component geophones (channels 1 - 6) were set up to form a "plus-sign" array configuration in a central region of the Lanigan mine,

as shown in Figure 1. The coordinate system used was chosen for convenience and DOES NOT correspond to mine coordinates. All distances are in feet. In Figure 1 true north is 45 degrees west of the map north. All sensors were at roughly the same elevation in the mine, at 950 m depth. The recording instruments were located near the center of the array, just south of geophone 1 at coordinates (0N,0E). The array configuration was chosen to monitor an old abandoned region of the mine, Panels 311 and 321. Geophone coordinates in feet are :

2085 590.

Channel 1 :	(10E,	820N)	
Channel 2 :	(920E,	-20N)	
Channel 3 :	(2870E,	0N)	
Channel 4 :	(-3140E,	-30N)	-1485, -1340
Channel 5 :	(-1650E,	-70N)	
Channel 6 :	(650E,	-1630N)	

Each station consisted of two high impedance Mark Products Model L-1 (4.5 Hz) geophones connected in series, and connected by up to 3000 feet of two-conductor telephone wire to amplifiers at the instrument site. The seismic recorders used were two Terra Technology model DCS-302 three-channel digital recorders (connected to a common clock). This system monitors seismic activity continuously, but only records the incoming vibration signal when an event is "recognized" as a seismic event by the program that controls the unit. Details of the operation of the Terra-Technology system are given in Prugger and Gendzwill, 1983.

2.1 Frequency of Occurrence of Seismic Events :

Seismicity was monitored continuously, with virtually no downtime, during the recording period. During the period November 27 - 30 channels 4 and

5 were disconnected due to a cable break. Nine events were therefore recorded on only 4 rather than 6 channels. Although the accuracy of event locations was decreased during this period, the loss of the two channels did not diminish the ability of the system to recognize and record events when they occurred. A histogram showing number of events per day over the recording period is given in Figure 2. 36 microseismic events were recorded in 33 consecutive full days of monitoring. The level of seismicity of 0 to 3 events per day remained steady over the 33 day monitoring period. Most events were recorded on all six channels. In addition, 8 dynamite blasts from south-east of the geophone array and a magnitude 6.9 Alaska earthquake that occurred on November 17 were recorded.

2.2 Event Locations :

The arrival time of seismic energy at each sensor was picked from plotted seismograms of each recorded event. These differences in arrival times were used to calculate the location of the rock fracture that gave rise to the observed seismograms. Source location was calculated using a variety of programs written by Prugger (U of S) that use the "Simplex Method" of direct iteration for earthquake location (described in Prugger and Gendzwill, 1988). Seismogram records for a typical event on day 339 (December 5) at 23:18:17, located at coordinates (E 2085, N 590), are shown in Figure 3. Event locations for all recorded events are plotted on a mine map in Figure 4. The location accuracy is poor for those events that occurred north and east of Panel 321, well outside the array of geophones. Notice the total abscence of seismicity in Panel 311, and the concentration of events near the south/central region of the adjacent (and similar) Panel 321. The blasts that were recorded occurred off the map in Panel 051 and have not been plotted.

2.3 Spectral Analysis :

Analysis of the frequency content of the recorded seismic signals is often used to estimate parameters relating to the rock fracture mechanism for recorded seismic events (Aki, 1967; Brune, 1971; Wyss and Hanks, 1972; Spottiswoode and McGarr, 1975). Spectral analysis involves transforming seismogram records into the frequency domain, and looking at the spectrum of vibrations generated by the rock fracture. The general idea is that small fractures produce short wavelength (high frequency) vibrations while large fractures produce long wavelengths (lower frequencies). After converting the recorded velocity data to particle displacements these data are plotted on a log-log graph. Velocity and displacement spectra for the event plotted in Figure 3 are given in Figures 5 and 6. A Butterworth function is fitted to the displacement spectra to give estimates of the zero-frequency intercept (AZRO), the corner frequency (FCNR), and the high frequency attenuation (SLOP). The fitting was done using the simplex method to optimize the three parameters for a best-fit to the data.

Using the determined values of AZRO and FCNR the following estimates for seismic moment (Mo), local Richter magnitude (ML), radiated vibration energy (E), (NOT released energy), an fault surface radius (Rf) were calculated for event 339 at 23:18:17 (December 5, 1987) :

Mo = 2.0 * 10**8 Newton - meters

ML = -1.9

E = 750 Joules (Watt-sec)

Rf = 25 meters / 85 feet

Recall that the Richter magnitude scale is logarithmic : this event was about 100,000 times smaller than a magnitude 3.0 event that would certainly be noticed on surface. The radiated energy value is small, but keep in mind that it is released over a very short time (0.5 to 1.5 seconds). The calculated value for fault surface area is much larger than seems reasonable for an event as small the one shown in Figure 3. Significant attenuation of high frequency energy along the source to receiver travel path (which in our experience is common in potash) may account for incorrect high fault radius values. Results of the spectral analysis of all events recorded at Lanigan during the fall, 1987 monitoring experiment will be the topic of a future report.

3.1 Concluding Remarks :

There is nothing extraordinary about the level of seismicity - about one event per day, on average - observed at Lanigan. This level of seismicity is lower than the 10 to 20 events per day observed at the Cominco mine at Vanscoy, but higher than the 1 event every week or two seen at PCS Rocanville. However, the locations of the events in a very localized region of Panel 321 is surprising. The mining pattern is similar throughout Panel 321, as well as in Panel 311, and neither region was mined recently, so it is difficult to imagine that the pattern of seismicity seen in Figure 4 is the result of mining alone. Why are there no events in Panel

311 ? Why are there no events in the north, west, and east regions of Panel 321 ? The obvious conclusion is that there is something unusual about the geology in the area of Panel 321 where the seismicity is occurring. Seismicity is more likely to occur in regions where the Dawson Bay limestone, which overlies the salts of the Prairie Evaporite, is weak (ie.- porous or fractured). In our experience, these weak zones are characterized by low seismic propagation velocities in the limestone (seen in well logs and/or refraction data) and often occur in areas where the mine-to-limestone salt cover is thinner than usual. An interesting follow-up to this seismic monitoring project would be to carry out a refraction line running east-west, crossing close to the unusual region in Panel 321, to see if any variation in either salt-back thickness or limestone velocity can be seen. It may also be worth returning to the area to carry out a more detailed followup survey (using more geophones, and if possible, a better recording system) to see if the pattern observed in November, 1987 has changed in time.

4.1 Acknowledgement :

We wish to acknowledge the Saskatchewan Potash Producers Association, under the direction of Parviz Mottahed, and the Department of Energy Mines and Resources of Canada for providing funding for this project. We also thank the Potash Corporation of Saskatchewan (PCS) Mining Ltd., Lanigan Division and mine manager Dale Jackson for allowing us access to the Lanigan mine. Thanks are extended to Jack Arnold of the University of Saskatchewan for assistance in keeping the instruments running. And finally sincere thanks are extended to PCS employee Dave Greenberg

for his conscientious help in installing, operating, and repairing the monitoring system throughout the recording experiment.

5.1 References

Aki, K., 1967; Scaling law of seismic spectrum; Journal of Geophysical Research, V. 72, pp. 1217 - 1231.

Brune, J. N., 1970; Tectonic stress and spectra of seismic shear waves from earthquakes; Journal of Geophysical Research, V. 75, pp. 4997 - 5009.

Gendzwill, D. J., R. B. Horner, and H. S. Hasegawa, 1982; Induced earthquakes at a potash mine near Saskatoon, Canada; Canadian Journal of Earth Sciences, V. 19, pp. 466 - 475.

Prugger, A. F. and D. J. Gendzwill, 1983; Earthquake monitoring system used at the PCS Mining, Cory Division potash mine near Saskatoon, Canada; Potash '83, Pergamon Press, pp. 191 - 196.

Prugger, A. F. and D. J. Gendzwill, 1988; Micro-earthquake location : a non-linear approach that makes use of a simplex stepping procedure; Bulletin of the Seismological Society of America, in press (April, 1988 issue).

Spottiswoode, S. M. and A. McGarr, 1975; Source parameters of tremors in a deep level gold mine; Bulletin of the Seismological Society of America, V. 65, pp. 93 - 112.

Wyss, M. and T. C. Hanks, 1972; The source parameters of the San Fernando earthquake inferred from teleseismic body waves; Bulletin of the Seismological Society of America, V. 62, pp. 591 - 602.

6.1 Figure Headings

Figure 1 : Mine plan and geophone locations (dots) for seismic monitoring experiment in November and December, 1987.

Figure 2 : Histogram of seismic events per day over the November 5 through December 7 (1987) recording period.

Figure 3 : Seismogram records for Lanigan event 339 (Dec. 5, 1987) at local time 23:18:17.

Figure 4 : Mine plan showing seismic events locations (stars).

Figure 5 : Velocity spectra of seismograms shown in Figure 3.

Figure 6 : Displacement spectra of seismograms shown in Figure 3.

FIGURE 1.

PCS LANIGAN

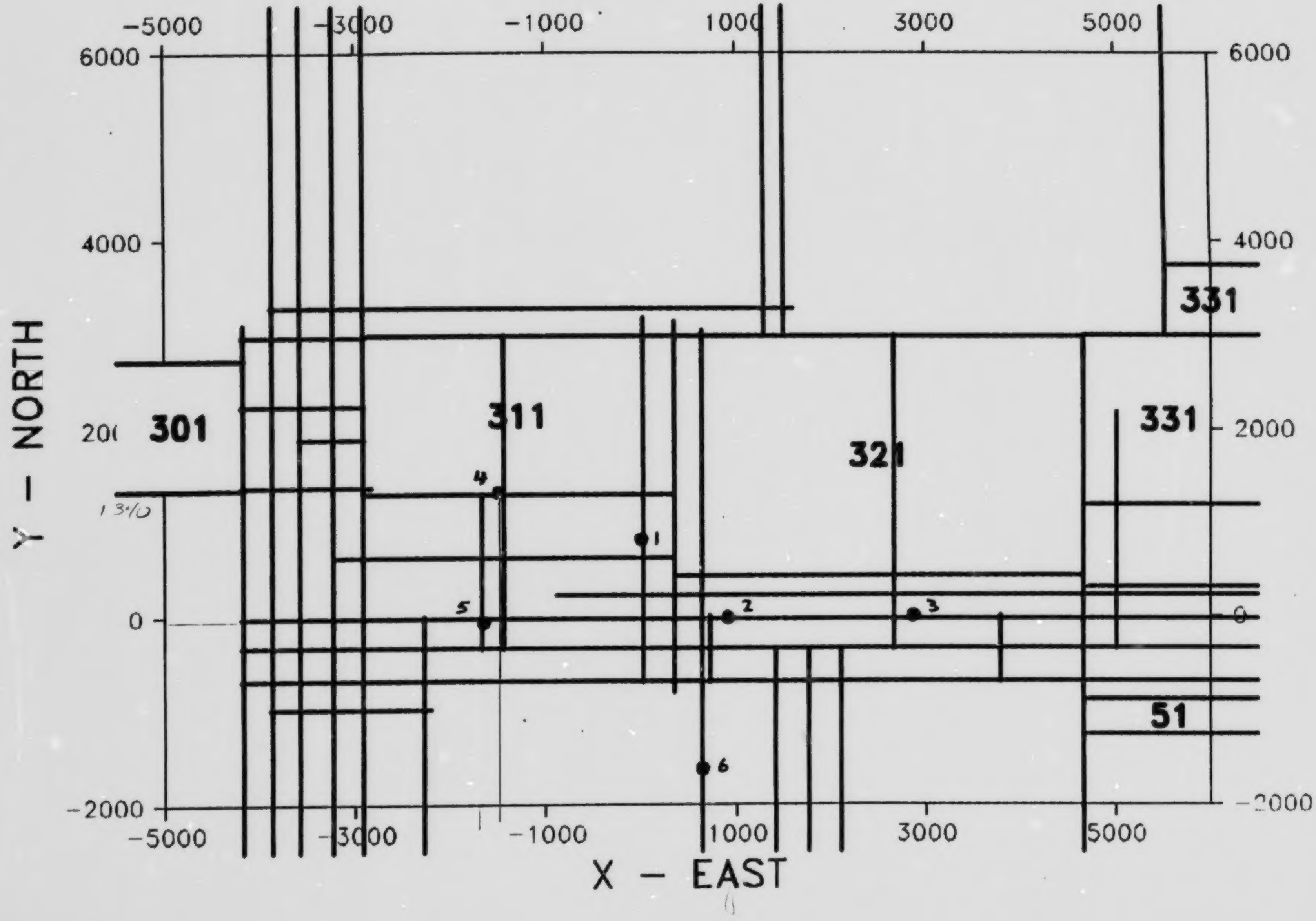
-5000
-3000
-1000
1000
3000
5000
6000
4000
200
2000
0
-2000
Y - NORTH
X - EAST
301
311
321
331
331
51
1
2
3
4
5
6
1340

Figure 2.

PCS LANIGAN

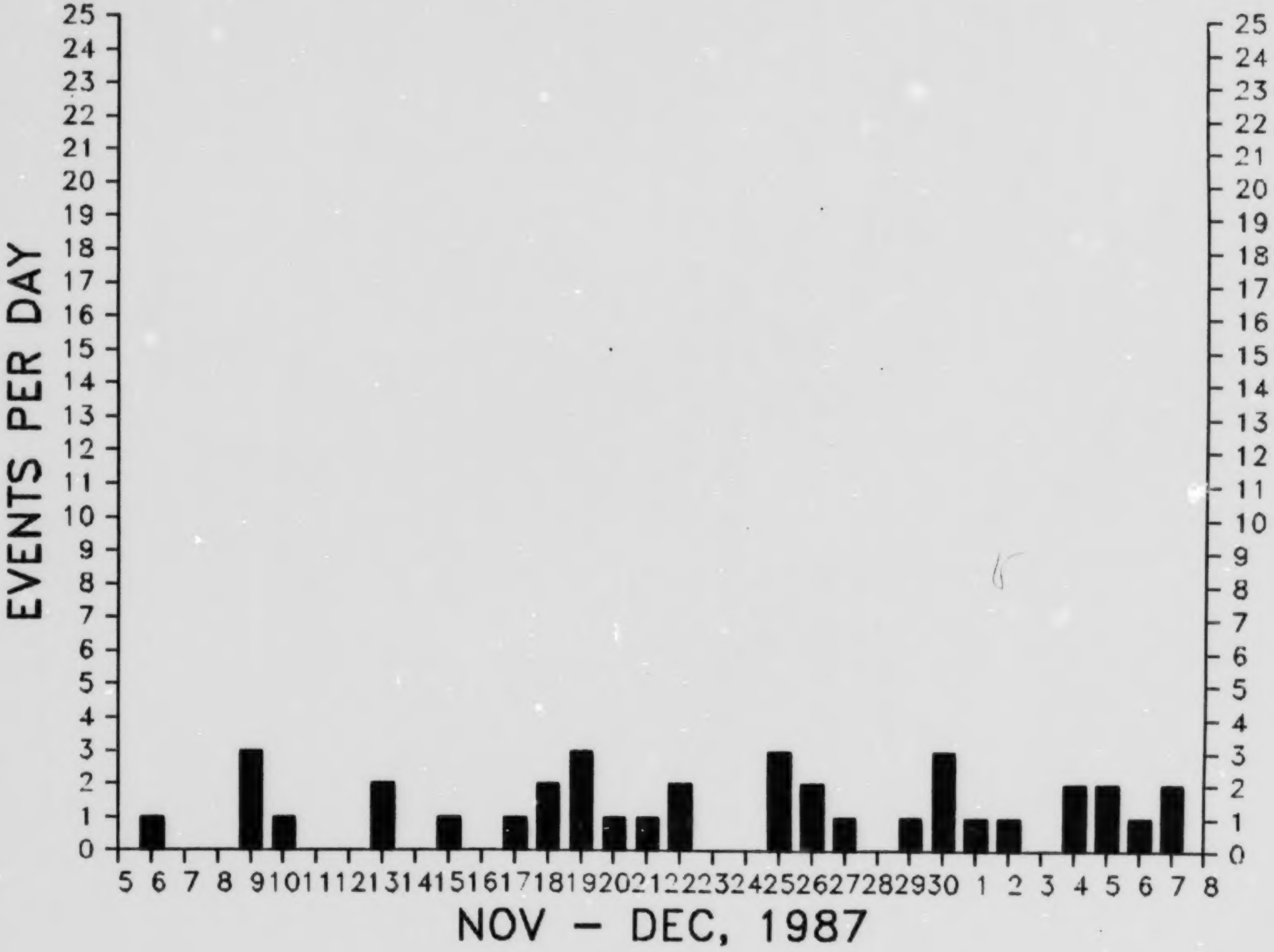

FIGURE 3.

MICRO–EARTHQUAKE SEISMOGRAMS (1987/339/23/18/17)

(VELOCITY DATA IN μmeters / second)

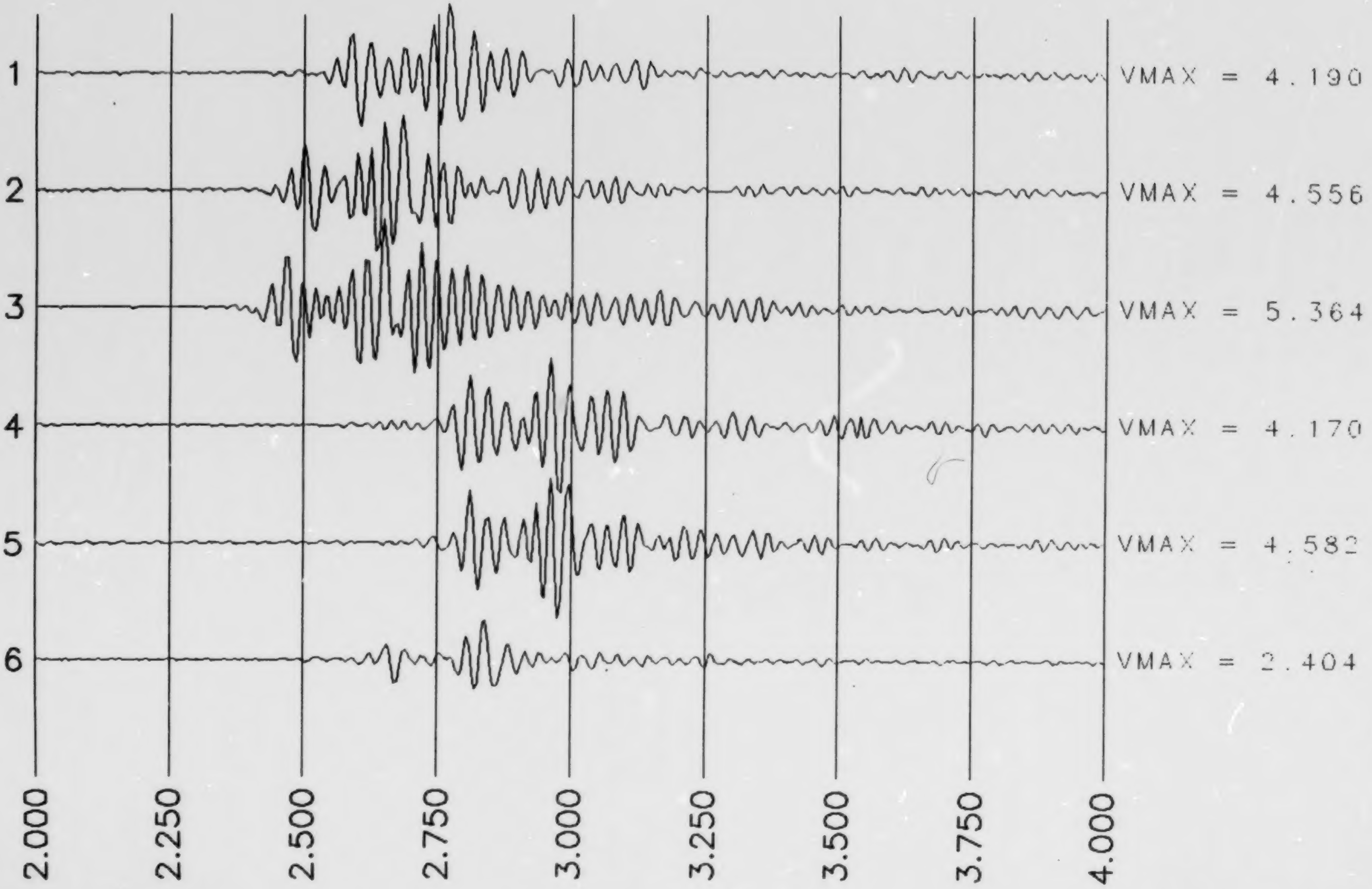

PCS LANIGAN

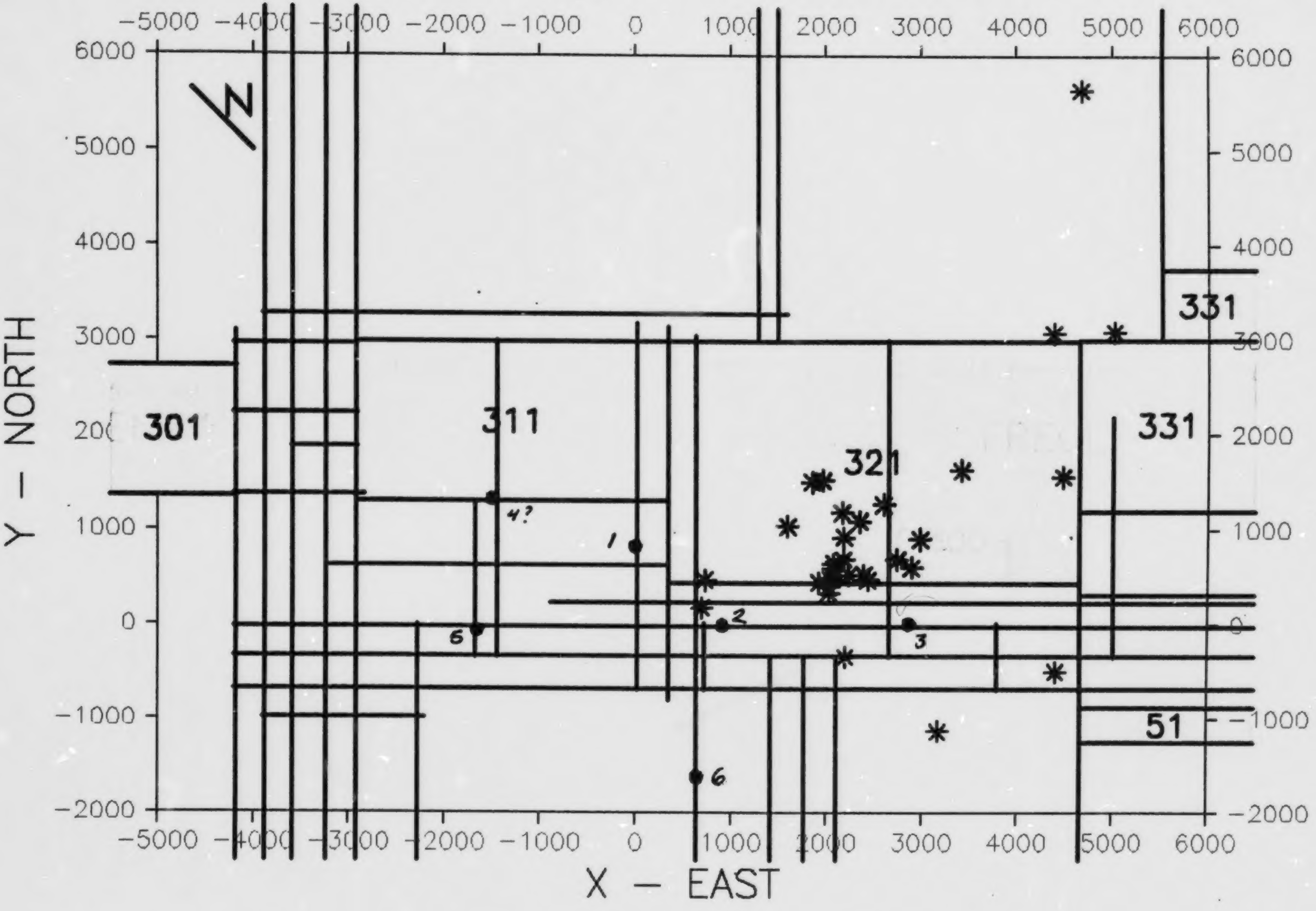

-5000
-4000
-3000
-2000
-1000
0
1000
2000
3000
4000
5000
6000
X — EAST
Y — NORTH
-2000
-1000
0
1000
2000
3000
4000
5000
6000
N
301
311
321
331
331
51
1
2
3
4?
5
6

FIGURE 5.

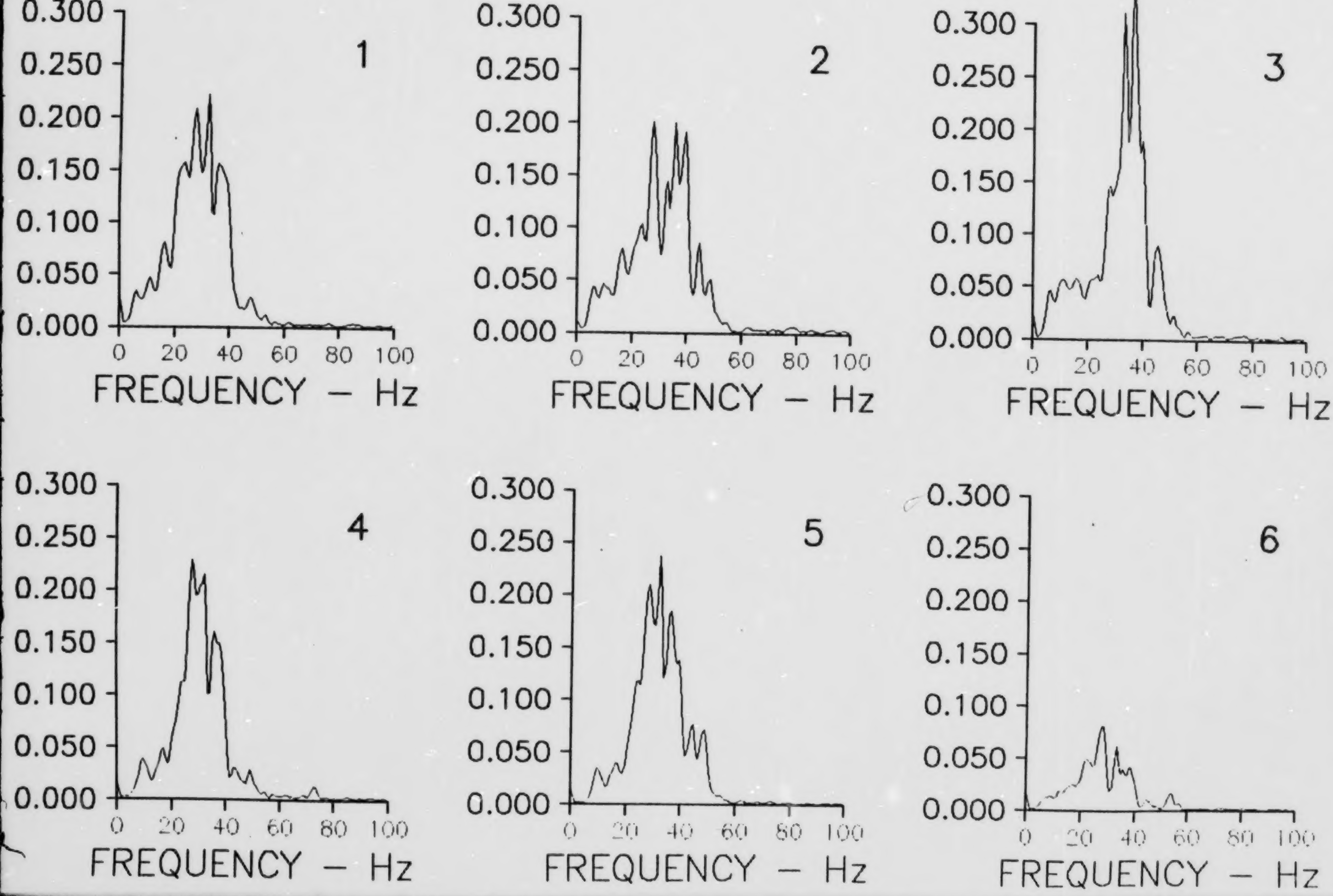

EVENT : 1987/339/23/18/17
256 POINT FFT OF VELOCITY (μmeter/sec) DATA

FIGURE 6.

EVENT : 1987/339/23/18/17
256 POINT FFT OF DISPLACEMENT (μmeter) DATA

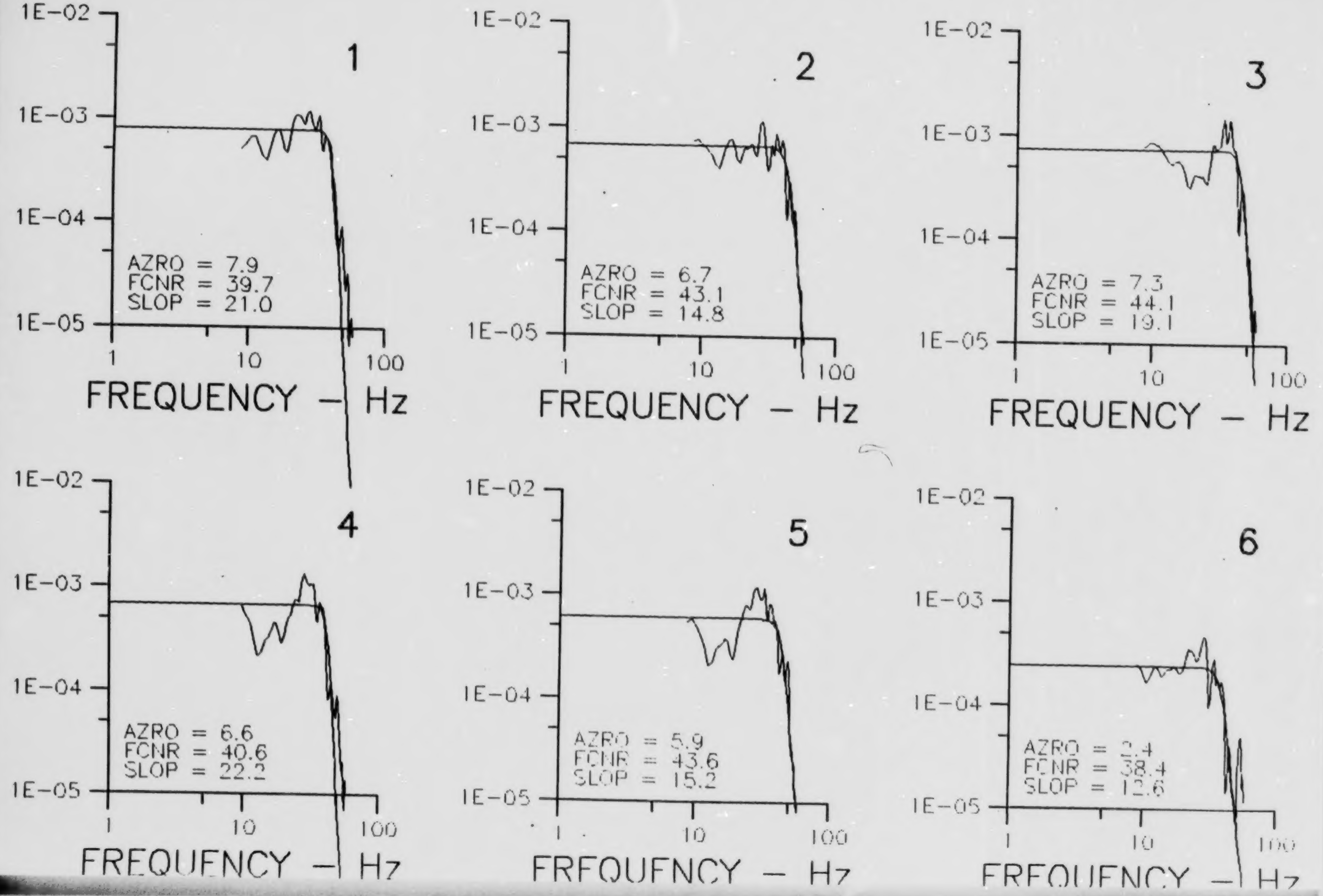

7.1 Appendix : List of Microseismic Events, Lanigan 1987.

EVENT #	DATE & LOCAL TIME	LOCATION (feet)	
1.	310 (NOV 06) 02:30:37	E 2205. N -345.	
2.	313 (NOV 09) 06:33:00	E 735. N 465.	
3.	313 (NOV 09) 12:53:14	E 2085. N 645.	
4.	313 (NOV 09) 21:58:22	E 700. N 175.	
5.	314 (NOV 10) 01:56:16	E 2360. N 1090.	
6.	317 (NOV 13) 06:49:58	E 2035. N 395.	
7.	317 (NOV 13) 21:30:47	E 2400. N 525.	
8.	319 (NOV 15) 01:55:11	E 1940. N 1235.	
***	(NOV 17) ALASKA MAGNITUDE 6.9 EARTHQUAKE / recorded		
	(NOV 17) BLASTING at 04:45 / not recorded		
9.	321 (NOV 17) 11:34:28	E 4390. N 3070.	
10.	322 (NOV 18) 15:25:24	E 1860. N 1500.	
11.	322 (NOV 18) 18:07:01	E 14160.? N 7215.?	(poor solution)
12.	323 (NOV 19) 06:06:31	E 1600. N 1035.	
13.	323 (NOV 19) 13:25:42	E 1975. N 1515.	
***	(NOV 19) BLASTING at 17:30 / recorded :		
	323 (NOV 19) 17:28:41	E 64300.? N-19900.?	(poor solution)
***	(NOV 19) BLASTING at 18:15 / recorded :		
	323 (NOV 19) 18:07:31	E 5805. N -2165.	
***	(NOV 20) BLASTING at 05:00 / recorded :		
	324 (NOV 20) 04:49:13	E 8270. N -1175.	
14.	325 (NOV 21) 09:00:59	E 31950. N 13587.	(poor solution)
15.	326 (NOV 22) 04:50:54	E 2175. N 1180.	
16.	326 (NOV 22) 07:49:51	E 2610. N 1265.	
***	(NOV 24) BLASTING at 18:30 / recorded :		
	328 (NOV 24) 18:30:19	E 4120. N -1815.	

```
17.     329 (NOV 25) 15:00:39      E  2195.  N    920.
18.     329 (NOV 25) 16:26:28      E  2185.  N    690.
19.     329 (NOV 25) 21:37:54      E  2900.  N    600.
20.     330 (NOV 26) 02:12:52      E  4680.? N   5640.?  (poor solution)
21.     330 (NOV 26) 15:42:16      E  2245.  N    525.
22.     331 (NOV 27) 16:16:02      E  7580.? N   2615.?  (poor solution)
***     (NOV 28) BLASTING at 06:1  / recorded :
        332 (NOV 28) 06:08:24      E  3915.  N -1730.

***     (NOV 28) BLASTING at 16:15 / recorded :
        332 (NOV 28) 16:13:22      E 58600.? N-20300.? (poor solution)

***     (NOV 28) BLASTING at 18:45 / recorded :
        333 (NOV 28) 18:43:59      E  2885.  N  -835.
23.     332 (NOV 28) 23:33:16      E  2440.  N    470.
24.     333 (NOV 29) 01:14:11      E  8820.  N   1815.   (poor solution)
***     (NOV 29) BLASTING at 21:45 / recorded :
        333 (NOV 29) 21:38:52      E 51909.? N-11110.? (poor solution)
25.     334 (NOV 30) 00:55:05      E  3425.  N   1625.
        (NOV 30) BLASTING AT 01:40 / not recorded
26.     334 (NOV 30) 06:17:40      E  2995.  N    900.
27.     334 (NOV 30) 14:37:46      E  4490.  N   1555.
28.     335 (DEC 01) 06:12:18      E  4405.  N   -500.
29.     336 (DEC 02) 08:59:21      E  2750.  N    685.
30.     338 (DEC 04) 05:38:22      E  2030.  N    330.
31.     338 (DEC 04) 21:22:29      E  2050.  N    485.
32.     339 (DEC 05) 09:10:19      E  3170.  N  -1135.
33.     339 (DEC 05) 23:18:17      E  2085.  N    590.
34.     340 (DEC 06) 12:57:54      E 60790.? N 16430.?  (poor solution)
```

PRELIMINARY RESULTS OF SEISMIC MONITORING AT THE IMC - K2 POTASH MINE, (ESTERHAZY SASKATCHEWAN), IN DECEMBER 1987.

Arnfinn Prugger
Don Gendzwill
Department of Geological Sciences
University of Saskatchewan
Saskatoon, Saskatchewan
(S7N-0W0)

January 31, 1988.

Summary :

A seismic monitoring array was continuously operated underground in the south eastern region ("H Block") of the IMC - K2 potash mine near Esterhazy in the period December 15, 1987 through January 2, 1988. Only one seismic event was observed in 18 full days of recording. Arrival times were used to calculate a location for the event, which is plotted on a mine map. No active mining was carried out near the geophone array during the recording period.

1.1 Background :

Seismic traces are records of ground vibration observed through time at that point in (or on) the Earth where a vibration sensor, or geophone, has been set up. "Vibration" in this context means particle displacement of the region of rock that the geophone is attached to. The geophone sensors used at Lanigan measure the velocity of particle displacement (in micro-meters per second). The vibration record that is observed results from rock fracture occurring some distance away from the sensor. Since seismic energy travels at finite velocities through rock, vibrations emanating from a rock fracture will in general arrive at different times at different geophones. The arrival times are used to calculate the location of the rock fracture using the "Simplex Method" of source location described in Prugger and Gendzwill, 1988.

Micro-seismic activity has been observed at every potash mine in Saskatchewan where monitoring instruments have been set up. As well, seismic events strong enough to be noticed by persons living in the vicinity of mines have occurred at five of the provinces ten mines to date : IMC-K1 and IMC-K2 at Esterhazy, PCS at Cory, CCP at Colonsay, and PCA at Patience Lake. These events have been in the Richter magnitude range 2.0 - 3.5 (Gendzwill et al., 1982). This corresponds to noticed effects ranging from "I thought a truck ran into the house", or "It felt like the furnace blew up", to (in a few cases) cracked wall plaster.

Noticeable macro-seismic events have occurred at the IMC-K2 mine since 1981, but to date no large events are known to have occurred in the H-Block area of the mine. And although seismicity has been monitored in various regions of the mine, the monitoring experiment described here is the first period of monitoring in H-Block.

1.2 Instrument Setup and Event Location :

8 vertical component geophones were set up to form a "plus-sign" array configuration covering the entire H-Block region of the IMC - K2 mine as shown in Figure 1. The coordinate system used was chosen for convenience

and DOES NOT correspond to mine coordinates. All distances are in feet. True north corresponds to map north. All sensors were at roughly the same elevation in the mine, at 3050 feet depth. The recording instruments were located near the center of the array, just north of geophone 8. The array configuration was chosen to monitor a region of the K2 mine that is, in a sense, a small mine (complete with old mined-out regions as well as areas of ongoing active mining) isolated from older mine workings that are 15000 feet to the north-west. Geophone coordinates in feet are :

	12,000	-2560
Channel 1 :	(10325E,	0N)
Channel 2 :	(11840E,	0N)
Channel 3 :	(14480E,	0N)
Channel 4 :	(16300E,	0N)
Channel 5 :	(13045E,	3400N)
Channel 6 :	(13250E,	-3100N)
Channel 7 :	(13045E,	2145N)
Channel 8 :	(13045E,	-800N)

Each station consisted of two high impedance Mark Products Model L-1 (4.5 Hz) geophones connected in series, and connected by up to 3500 feet of two-conductor telephone wire to amplifiers at the instrument site. The seismic recorders used were three Terra Technology model DCS-302 three-channel digital recorders (connected to a common clock). This system monitors seismic activity continuously, but only records the incoming vibration signal when an event is "recognized" as a seismic event by the program that controls the unit. Details of the operation of the Terra-Technology system are given in Prugger and Gendzwill, 1983.

During the 18 day recording period only one event was recorded on five channels on day 350 (December 16) at local time 00:40:25. The arrival time of seismic energy at each sensor was picked from plotted seismograms of the recorded event. These differences in arrival times were used to calculate the location of the rock fracture that gave rise to the observed seismograms. Source location was calculated using a variety of programs written by Prugger (U of S) that use the "Simplex Method" of direct iteration for earthquake location (described in Prugger and Gendzwill, 1988). The calculated event location, (12000E, -2560N), is plotted as a star in Figure 1. Seismogram records for the event are plotted in Figure 2.

1.3 Spectral Analysis :

Analysis of the frequency content of the recorded seismic signals is often used to estimate parameters relating to the rock fracture mechanism for recorded seismic events (Aki, 1967; Brune, 1971; Wyss and Hanks, 1972; Spottiswoode and McGarr, 1975). Spectral analysis involves transforming seismogram records into the frequency domain, and looking at the spectrum of vibrations generated by the rock fracture. The general idea is that small fractures produce short wavelength (high frequency) vibrations while large fractures produce long wavelengths (lower frequencies). After converting the recorded velocity data to particle displacements these data are plotted on a log-log graph. Velocity and displacement spectra for the event plotted in Figure 2 are given in Figures 3 and 4. A Butterworth function is fitted to the displacement spectra to give estimates of the zero-frequency intercept (AZRO), the corner frequency (FCNR), and the high frequency attenuation (SLOP). The fitting was done using the simplex method to optimize the three parameters for a best-fit to the data.

Using the determined values of AZRO and FCNR the following estimates for seismic moment (Mo), local Richter magnitude (ML), radiated vibration energy (E), (NOT released energy), an fault surface radius (Rf) were calculated for event 350 at local time 00:40:25 (December 16, 1987) :

Mo = 3.0 * 10**9 Newton - meters

ML = -1.0

E = 10500 Joules (Watt-sec)

Rf = 35 meters / 115 feet

Recall that the Richter magnitude scale is logarithmic : this event was about 10,000 times smaller than a magnitude 3.0 event that would certainly be noticed on surface. The radiated energy value is small, but keep in mind that it is released over a very short time (0.5 to 1.5 seconds). The calculated value for fault surface area is much larger than seems reasonable for an event as small the one shown in Figure 2. Significant attenuation of high frequency energy along the source to receiver travel path (which in our experience is common in potash) may account for incorrect high fault radius values.

2.1 Concluding Remarks :

The level of seismic activity seen in the H-Block region of the IMC - K2 mine during December, 1987 is lower (ie.- fewer events per week) than has been observed in older regions of the mine. However, this low rate of seismicity is similar to the rate of 1 event every week or two seen at PCS Rocanville. Seismicity is more likely to occur in regions where the Dawson Bay limestone, which overlies the salts of the Prairie Evaporite, is weak (ie.- porous or fractured). In our experience, these weak zones are characterized by low seismic propagation velocities in the limestone (seen in well logs and/or refraction data) and often occur in areas where the mine-to-limestone salt cover is thinner than usual. It follows that both salt cover and limestone velocity should be higher in the H-Block region of IMC - K2 than in the regions of the mine that are more seismically active. It also follows that salt cover and limestone velocity are similar at Rocanville and the H-Block region of IMC - K2.

In a region where seismic activity occurs infrequently two weeks of monitoring is not enough. It is important to return to the H-Block area to carry out a similar survey over a much longer time period to really nail down the seismic pattern in the region.

3.1 Acknowledgement :

We wish to acknowledge the Saskatchewan Potash Producers Association, under the direction of Parviz Mottahed, and the Department of Energy Mines and Resources of Canada for providing funding for this project. We also thank the International Minerals and Chemical Corp. (Canada) Ltd. (IMC) and K2 mine manager Julian Kopchynski for allowing us access to the IMC - K2 mine. Thanks are extended to Jack Arnold of the University of Saskatchewan for assistance in keeping the instruments running, and to IMC employees Tom Olson, Derek Gugulyn, and Blaine Kunkel for assistance in setting up and maintaining the monitoring system.

4.1 References

Aki, K., 1967; Scaling law of seismic spectrum; Journal of Geophysical Research, V. 72, pp. 1217 - 1231.

Brune, J. N., 1970; Tectonic stress and spectra of seismic shear waves from earthquakes; Journal of Geophysical Research, V. 75, pp. 4997 - 5009.

Gendzwill, D. J., R. B. Horner, and H. S. Hasegawa, 1982; Induced earthquakes at a potash mine near Saskatoon, Canada; Canadian Journal of Earth Sciences, V. 19, pp. 466 - 475.

Prugger, A. F. and D. J. Gendzwill, 1983; Earthquake monitoring system used at the PCS Mining, Cory Division potash mine near Saskatoon, Canada; Potash '83, Pergamon Press, pp. 191 - 196.

Prugger, A. F. and D. J. Gendzwill, 1988; Micro-earthquake location : a non-linear approach that makes use of a simplex stepping procedure; Bulletin of the Seismological Society of America, in press (April, 1988 issue).

Spottiswoode, S. M. and A. McGarr, 1975; Source parameters of tremors in a deep level gold mine; Bulletin of the Seismological Society of America, V. 65, pp. 93 - 112.

Wyss, M. and T. C. Hanks, 1972; The source parameters of the San Fernando earthquake inferred from teleseismic body waves; Bulletin of the Seismological Society of America, V. 62, pp. 591 - 602.

5.1 Figure Headings

Figure 1 : Mine plan showing geophone locations (dots) and microseismic event location (star) for seismic monitoring experiment at IMC - K2 in December, 1987.

Figure 2 : Seismogram records for event 350 (Dec. 16, 1987) at local time 00:40:25.

Figure 3 : Velocity spectra of seismograms shown in Figure 2.

Figure 4 : Displacement spectra of seismograms shown in Figure 2.

IMCK2 ESTERHAZY

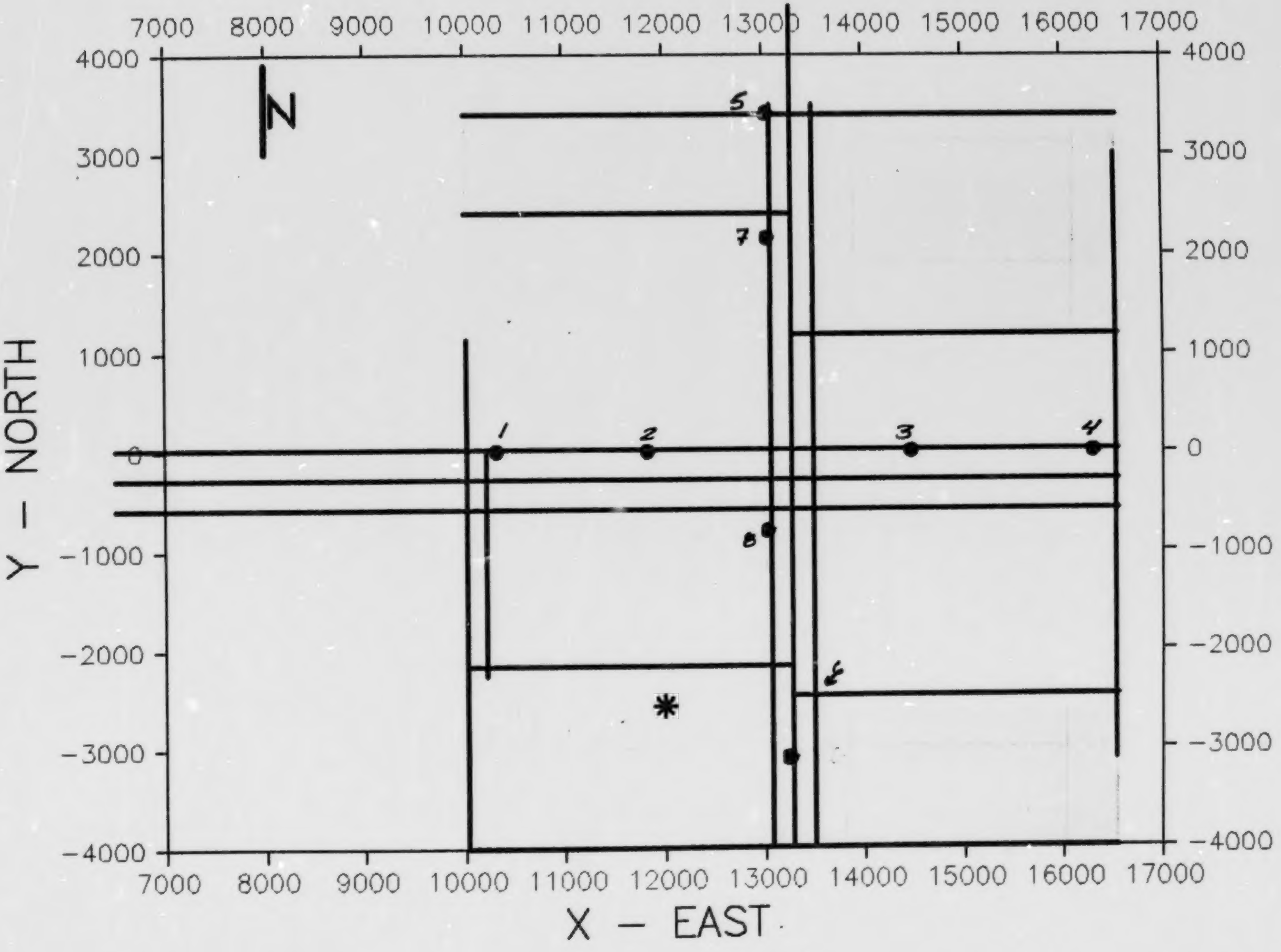

7000
8000
9000
10000
11000
12000
13000
14000
15000
16000
17000
4000
3000
2000
1000
0
-1000
-2000
-3000
-4000
N
1
2
3
4
5
6
7
8
Y - NORTH
X - EAST

MICRO-EARTHQUAKE SEISMOGRAMS (1987/350/0/40/25)
(VELOCITY DATA IN μmeters / second)

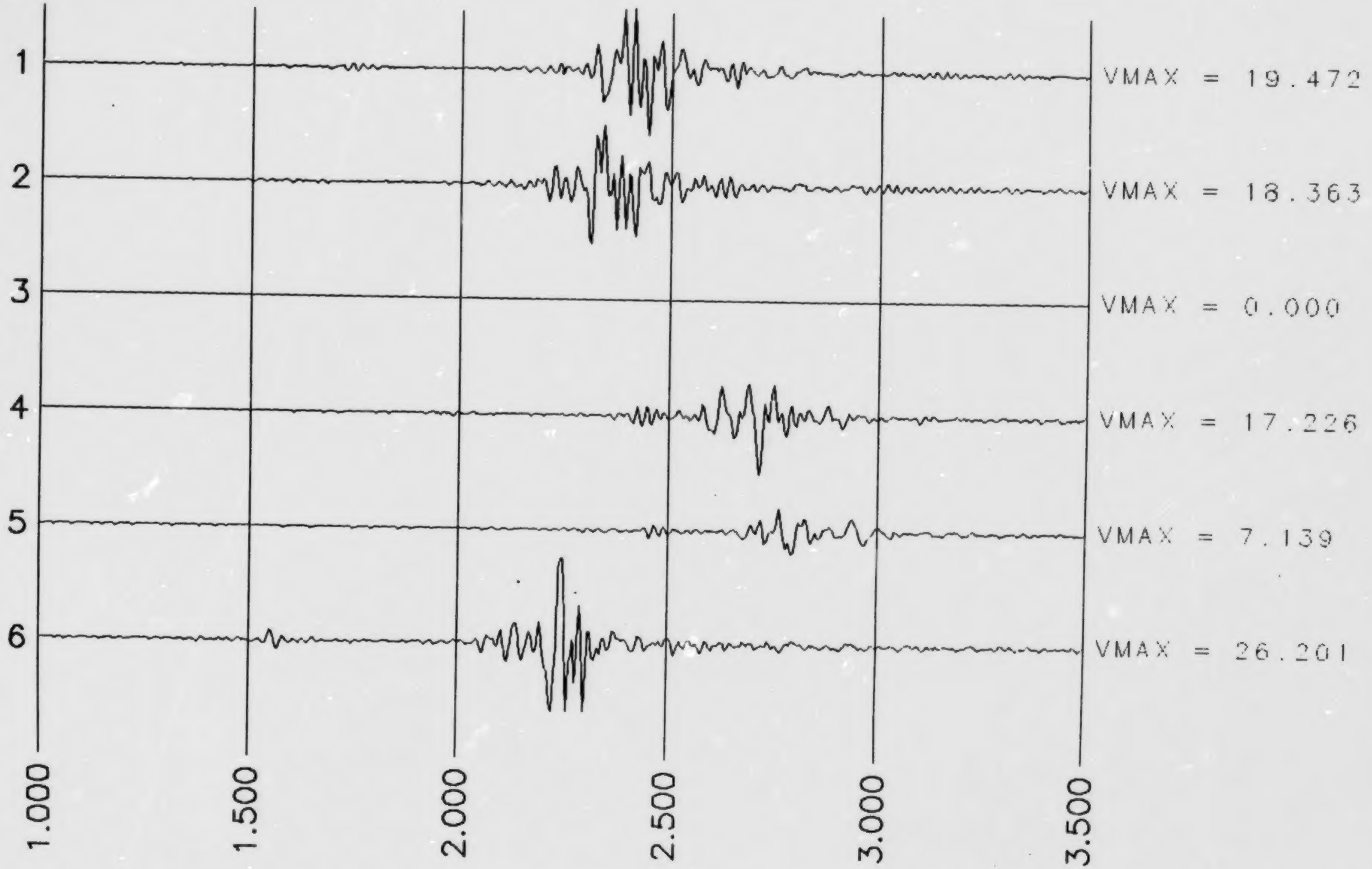

EVENT : 1987/350/0/40/25
256 POINT FFT OF VELOCITY (μmeter/sec) DATA

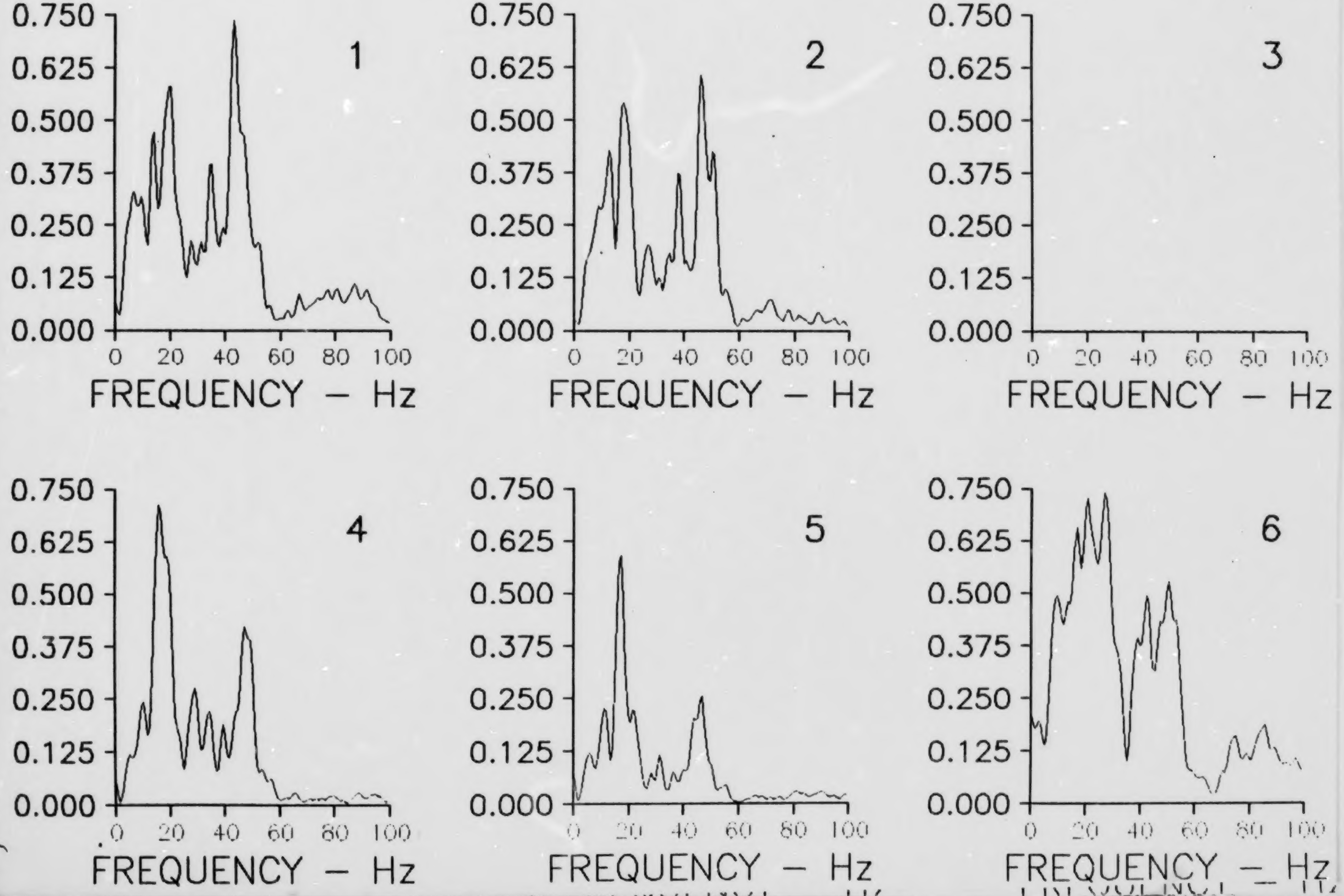

EVENT : 1987/350/0/40/25

256 POINT FFT OF DISPLACEMENT (μmeter) DATA

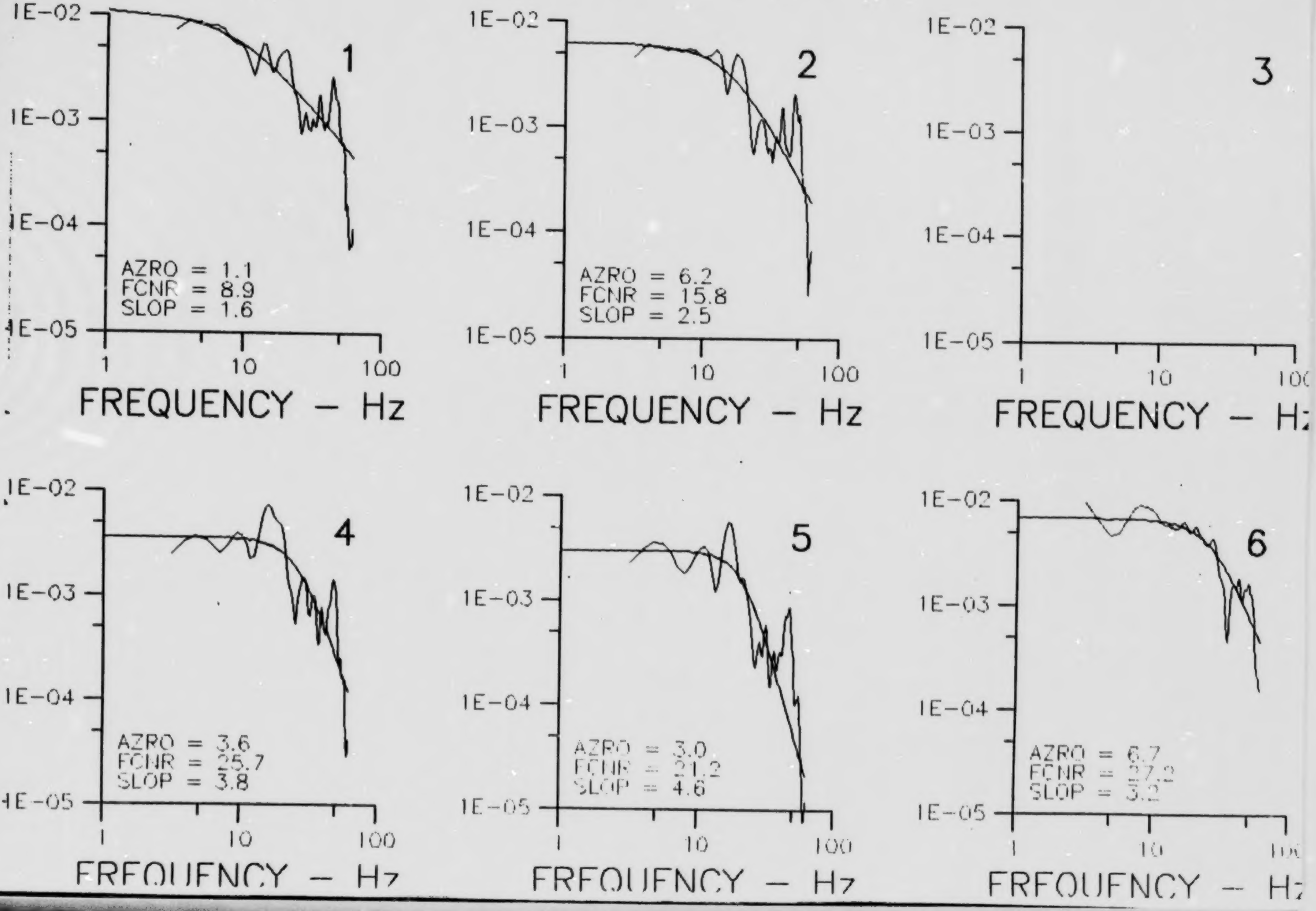

PRELIMINARY REPORT OF THE RESULTS OF SEISMIC MONITORING AT THE COMINCO POTASH MINE, (VANSCOY SASKATCHEWAN), OCTOBER THROUGH DECEMBER, 1985.

Arnfinn Prugger
Don Gendzwill
Department of Geological Sciences
University of Saskatchewan
Saskatoon, Saskatchewan
(S7N-0W0)

January 31, 1988.

CONTENTS :

Summary p. 1
1.1 Background p. 1
1.2 Instrument Setup p. 3
2.1 Frequency of Occurrence of Seismic Events p. 4
2.2 Event Locations p. 5
2.3 Propagation Velocities p. 6
2.4 Spectral Analysis p. 6
3.1 Concluding Remarks p. 7
4.1 Acknowledgement p. 9
5.1 References p. 10
6.1 Figure Headings p. 11
Figures pp. 12 - 19
7.1 Appendix : List of Event Locations p. 20

PRELIMINARY REPORT OF THE RESULTS OF SEISMIC MONITORING AT THE PCS ROCANVILLE POTASH MINE, (ROCANVILLE SASKATCHEWAN), JULY AND OCTOBER, 1987.

Arnfinn Prugger
Don Gendzwill
Department of Geological Sciences
University of Saskatchewan
Saskatoon, Saskatchewan
(S7N-0W0)

January 31, 1988.

CONTENTS :

Summary p. 1
1.1 Background p. 2
1.2 Instrument Setup p. 3
2.1 Frequency of Occurrence of Seismic Events p. 4
2.2 Event Locations p. 6
2.3 Spectral Analysis p. 7
3.1 Concluding Remarks p. 8
4.1 Acknowledgement p. 9
5.1 References p. 10
6.1 Figure Headings p. 11
Figures pp. 12 - 22
7.1 Appendix : List of Event Locations p. 23

PRELIMINARY RESULTS OF SEISMIC MONITORING AT THE PCS ROCANVILLE POTASH MINE, (ROCANVILLE SASKATCHEWAN), JULY AND OCTOBER 1987.

Arnfinn Prugger
Don Gendzwill
Department of Geological Sciences
University of Saskatchewan
Saskatoon, Saskatchewan
(S7N-0W0)

January 31, 1988.

Summary :

A seismic monitoring array was operated underground at the Rocanville potash mine in the periods July 15 - 28 and October 13 - 27, 1987. A total of 4 seismic events were observed in 28 full days of recording ; 4 events in 4 weeks of monitoring is a very low level of seismicity. Two microseismic events occurred during the first recording period and a "double" roof-fall event (two events 12 seconds apart) occurred on October 26, near the end of the second recording period. The roof-fall was large enough to be noticed by virtually everyone working in the southern region of the mine when it occurred. Since the event was localized in an abandoned region of the mine damage was limited to "blowing out" a few ventilation brattices. Arrival times were used to calculate event locations, which are plotted on a mine map. All four events occurred in the same region of the mine, in Panel 301 just north of the geophone array. It follows that the July microseisms may have been precursors to the much larger roof-fall event that occurred in October.

In addition to the 4 local seismic events, a Richter magnitude 3.2 earth-

quake which occurred at the IMC mine near Esterhazy (50 km. north-west of Rocanville) was recorded on October 21.

1.1 Background :

Seismic traces are records of ground vibration observed through time at that point in (or on) the Earth where a vibration sensor, or geophone, has been set up. "Vibration" in this context means particle displacement of the region of rock that the geophone is attached to. The geophone sensors used at Rocanville measure the velocity of particle displacement (in micro-meters per second). The vibration record that is observed results from rock fracture occurring some distance away from the sensor. Since seismic energy travels at finite velocities through rock, vibrations emanating from a rock fracture will in general arrive at different times at different geophones. The arrival times are used to calculate the location of the rock fracture using the "Simplex Method" of source location described in Prugger and Gendzwill, 1988.

Micro-seismic activity has been observed at every potash mine in Saskatchewan where monitoring instruments have been set up. As well, seismic events strong enough to be noticed by persons living in the vicinity of mines have occurred at five of the provinces ten mines to date : IMC-K1 and IMC-K2 at Esterhazy, PCS at Cory, CCP at Colonsay, and PCA at Patience Lake. These events have been in the Richter magnitude range 2.0 - 3.5 (Gendzwill et al., 1982). This corresponds to noticed effects ranging from "I thought a truck ran into the house", or "It felt like the furnace blew up", to (in a few cases) cracked wall plaster.

Noticeable macro-seismic activity has not been observed in the Rocanville area to date. However, microseismic events were observed in the winter of 1984-85 during a serious brine inflow into the mine (Vance and Mottahed, 1985). During 3 months of monitoring 51 events were recorded, virtually all located near the inflow point in Panel 306 in the southern region of the mine (see Figure 1). After the inflow was shut off, the event rate dropped from several per week to virtually none (Vance and Mottahed, 1985).

1.2 Instrument Setup :

9 vertical component geophones (channels 1 - 9) and one triaxial geophone (channels 10 - 12) were set up to form a "plus-sign" array configuration in the south region of the Rocanville mine, as shown in Figure 2. The coordinate system used was chosen for convenience and DOES NOT correspond to mine coordinates. All distances are in feet. In Figure 2 true north is 57 degrees east of the map north. All sensors were at roughly the same elevation in the mine, at 950 m depth. The recording instruments were located near the triaxial sensor at the center of the array. The array configuration was chosen to monitor two regions of active mining in Panels 303 and 304, and to investigate Panel 306, where a water inflow into the mine had occurred in the winter of 1984-85 (Vance and Mottahed, 1985). Geophone coordinates in feet are :

Channel 1 :	(7500E,	-4400N)
Channel 2 :	(7550E,	-2445N)
Channel 3 :	(7595E,	670N)
Channel 4 :	(11880E,	0N)
Channel 5 :	(8890E,	0N)
Channel 6 :	(10400E,	0N)
Channel 7 :	(6925E,	0N)
Channel 8 :	(5925E,	0N)
Channel 9 :	(7595E,	1670N)

Channel 10 : (8000E, 50N) / vertical
Channel 11 : (8000E, 50N) / north
Channel 12 : (8000E, 50N) / east

Stations 1 - 9 consisted of two high impedance Mark Products Model L-1 (4.5 Hz) geophones connected in series, and connected by up to 4000 feet of two-conductor telephone wire to an amplifier system located at the central instrument site. The triaxial sensor was a single Mark Products Model L-28 (4.5 Hz) geophone located 50 feet from the recorders.

Two recording systems were used at different times during the recording periods : a MicroSeis System (with a separate 12-channel amplifier set) and three Terra Technology model DCS-302 three-channel digital recorders (connected to a common clock). The triaxial sensor was not connected when the Terra-Technology system was used. Each of these systems monitors seismic activity continuously, but only records the incoming vibration signal when an event is "recognized" as a seismic event by the programs that control the units. Details of the operation of the Terra-Technology system are given in Prugger and Gendzwill, 1983.

2.1 Frequency of Occurrence of Seismic Events :

After installation of the seismic monitoring system in early July, 1987 problems with the recording unit developed. These problems plagued the monitoring experiment during the first half of July and throughout August. As a result, seismicity was monitored continuously for only a two week period during the summer : July 15 - 28. Both recording systems were utilized at different times (and sometimes in tandem) in this period. A recording system based on the Terra-Technolgy instruments was subsequently re-installed on October 13. During this second recording phase, seismicity was continuously monitored for a second two-week period, October 13 - 27. A geotomography experiment was carried out around the perimeter of Panel 306 during the October recording period. In the period July 15 - 28 two microseismic events were observed :

1. July 16 (day 197) at 11:01:48
2. July 26 (day 207) at 17:45:57

In the period October 13 - 27 thirty-one dynamite blasts (from the tomography experiment), the signal from a Richter magnitude 3.2 earthquake that occurred at Esterhazy on October 21, and two roof-fall events were recorded :

Oct. 21 : 3 dynamite blasts
Oct. 21 (day 294) at 22:34:45 : Esterhazy earthquake
Oct. 22 : 20 dynamite blasts
Oct. 24 : 8 dynamite blasts

3. Oct. 26 (day 299) at 11:44:39 (roof-fall, noticed underground)
4. Oct. 26 (day 299) at 11:44:51 (roof-fall, noticed underground)

A histogram of the number of seismic events per day is shown in Figure 3 ; note that there is a two month time gap in the middle of the plot.

Event 1 was recorded on only three channels (1, 2, & 3) using the Terra-Technology system. Event 2 was recorded on all 12 channels using the MicroSeis recording system. The dynamite blasts and the Esterhazy earthquake were recorded on channels 1 - 5 and 7 - 9, and events 3 and 4 were recorded on channels 1 - 5 using the Terra-Technology recording system.

Seismogram records for events 2, 3, and 4 are given in Figures 4 - 6. Note that vibration signals from events 3 and 4 were so strong that the amplifiers were saturated, and the signals clipped.

2.2 Event Locations :

The arrival time of seismic energy at each sensor was picked from plotted seismograms of each of the four recorded events. These differences in arrival times were used to calculate the location of the rock fracture that gave rise to the observed seismograms. Source location was calculated using a variety of programs written by Prugger (U of S) that use the "Simplex Method" of direct iteration for earthquake location (described in Prugger and Gendzwill, 1988). Event locations are plotted on a mine map in Figure 7. The location accuracy is poor for event 1 since it was recorded on only three channels. Events 2, 3, and 4 are estimated to be accurate to +/- 1000 feet. Notwithstanding these large uncertainties, it is very probable that all events occurred in the southern region of Panel 301, close to where they have been plotted. Since all events occurred well north of the set of geophones, event locations were checked by drawing the "errorspace" for each event ; (see Prugger and Gendzwill, 1988 for a full explanation of errorspaces). Errormaps for the two roof-fall events are shown in Figures 8 and 9. In both figures, the earthquake location lies within the region of the closed contours. Note that the first event was located substantially further from the geophones in Panel 301 than the second event, (which occurred only 11 seconds after the first event).

2.3 Spectral Analysis :

Analysis of the frequency content of the recorded seismic signals is often used to estimate parameters relating to the rock fracture mechanism for recorded seismic events (Aki, 1967; Brune, 1971; Wyss and Hanks, 1972; Spottiswoode and McGarr, 1975). Spectral analysis involves transforming seismogram records into the frequency domain, and looking at the spectrum of vibrations generated by the rock fracture. The general idea is that small fractures produce short wavelength (high frequency) vibrations while large fractures produce long wavelengths (lower frequencies). After converting the recorded velocity data to particle displacements these data are plotted on a log-log graph. Velocity and displacement spectra for event 2, channels 1 - 6, are given in Figures 10 and 11. A Butterworth function is fitted to the displacement spectra to give estimates of the zero-frequency intercept (AZRO), the corner frequency (FCNR), and the high frequency attenuation (SLOP). The fitting was done using the simplex method to optimize the three parameters for a best-fit to the data.

Using the determined values of AZRO and FCNR the following estimates for seismic moment (Mo), local Richter magnitude (ML), radiated vibration energy (E), (NOT released energy), an fault surface radius (Rf) were calculated for event 2. at Day 207/11:45:57 (July 26, 1987) :

Mo = 9.3 * 10**7 Newton - meters

ML = -2.3

E = 250 Joules (Watt-sec)

Rf = 16 meters / 50 feet

This analysis was not done for events 3 and 4 since the recorded signal was clipped for these two events. Recall that the Richter magnitude scale is logarithmic : event 2 was about 100,000 times smaller than a magnitude 3.0 event that would certainly be noticed on surface. The radiated energy value is small, but keep in mind that it is released over a very short time (0.5 to 1.5 seconds). The calculated value for fault surface area is much larger than seems reasonable for an event as small as event 2. Significant attenuation of high frequency energy along the source to receiver travel path (which in our experience is common in potash) may account for incorrect high fault radius values.

3.1 Concluding Remarks :

The most striking aspect of the Rocanville seismic monitoring project is the very low level of seismicity observed in the south region of the mine. No seismicity was observed in Panels 303 or 304, the regions of active mining. No seismicity was observed in Panel 306, the region in which 51 microseismic events were observed during a three month period of water inflow. Seismicity was only observed in a region of the mine where ground conditions are known to be poor from observation of room closure and roof falls : Panel 301. It is likely that ground subsidence measured on surface will be greater over Panel 301 than over other regions in the south part of the mine (at least, during the fall of 1987). There is either something unusual about the geology near Panel 301, or, if room age is the determining factor, it may be that a similar pattern of seismicity will develop in other panels when they have stood open as long as Panel 301 has.

Seismicity is more likely to occur in regions where the Dawson Bay limestone, which overlies the salts of the Prairie Evaporite, is weak (ie.- porous or fractured). In our experience, these weak zones are characterized by low seismic propagation velocities in the limestone (seen in well-logs and/or refraction data) and often occur in areas where the mine-to-limestone salt cover is thinner than usual. An interesting follow-up to this seismic monitoring project would be to carry out a refraction survey in a variety of regions of the Rocanville mine to see if Panel 301 is indeed anomalous.

4.1 Acknowledgement

We wish to acknowledge the Saskatchewan Potash Producers Association, under the direction of Parviz Mottahed, and the Department of Energy Mines and Resources of Canada for providing funding for this project. We also thank the Potash Corporation of Saskatchewan (PCS) Mining Ltd., Rocanville Division and mine manager Garth Moore for allowing us access to the Rocanville mine. Sincere thanks are extended to Jack Arnold of the University of Saskatchewan for assistance in keeping the instruments running. And finally we gratefully acknowledge the help and assistance in installing and operating the system of PCS employees Jim Vance, Mike Wooley, Mo Molavi, Bob Franklin, and George Williams.

5.1 References

Aki, K., 1967; Scaling law of seismic spectrum; Journal of Geophysical Research, V. 72, pp. 1217 - 1231.

Brune, J. N., 1970; Tectonic stress and spectra of seismic shear waves from earthquakes; Journal of Geophysical Research, V. 75, pp. 4997 - 5009.

Gendzwill, D. J., R. B. Horner, and H. S. Hasegawa, 1982; Induced earthquakes at a potash mine near Saskatoon, Canada; Canadian Journal of Earth Sciences, V. 19, pp. 466 - 475.

Prugger, A. F. and D. J. Gendzwill, 1983; Earthquake monitoring system used at the PCS Mining, Cory Division potash mine near Saskatoon, Canada; Potash '83, Pergamon Press, pp. 191-196.

Prugger, A. F. and D. J. Gendzwill, 1988; Micro-earthquake location : a non-linear approach that makes use of a simplex stepping procedure; Bulletin of the Seismological Society of America, in press (April, 1988 issue).

Spottiswoode, S. M. and A. McGarr, 1975; Source parameters of tremors in a deep level gold mine; Bulletin of the Seismological Society of America, V. 65, pp. 93 - 112.

Vance, J. B. and P. Mottahed, 1985; AE/MS applications to potash mining problems; Proceedings of the Fourth Symposium on Acoustic Emissions and Microseismicity, Pennsylvania State University, State College, Pennsylvania, U.S.A.

Wyss, M. and T. C. Hanks, 1972; The source parameters of the San Fernando earthquake inferred from teleseismic body waves; Bulletin of the Seismological Society of America, V. 62, pp. 591 - 602.

6.1 Figure Headings

Figure 1 : Microseismic events in Panel 306 during a water inflow, winter 1984/1985, Rocanville. Seismic events are drawn as stars, geophone locations as dots ; (from Vance and Mottahed, 1985).

Figure 2 : Mine plan and geophone locations (dots) for seismic monitoring experiment in July and October, 1987.

Figure 3 : Histogram of seismic events per day over the July 15 - 28 and October 13 - 27 (1987) recording periods.

Figure 4 : Seismogram records for Rocanville event 2, 1987 day 207 (July 26) at local time 17:45:57 .

Figure 5 : Seismogram records for Rocanville event 3, 1987 day 299 (Oct. 26) at local time 11:44:39 .

Figure 6 : Seismogram records for Rocanville event 4, 1987 day 299 (Oct. 26) at local time 11:44:51 .

Figure 7 : Mine plan showing seismic event locations (stars).

Figure 8 : Errormap for event 299/11/44/39 ; this event is located within the closed error contours (dark region).

Figure 9 : Errormap for event 299/11/44/51 ; this event is located within the closed error contours (dark region).

Figure 10 : Velocity spectra of channel 1 - 6 seismograms for event 2 (207/17/45/57) .

Figure 11 : Displacement spectra of channel 1 - 6 seismograms for event 2 (207/17/45/57) .

PCS ROCANVILLE

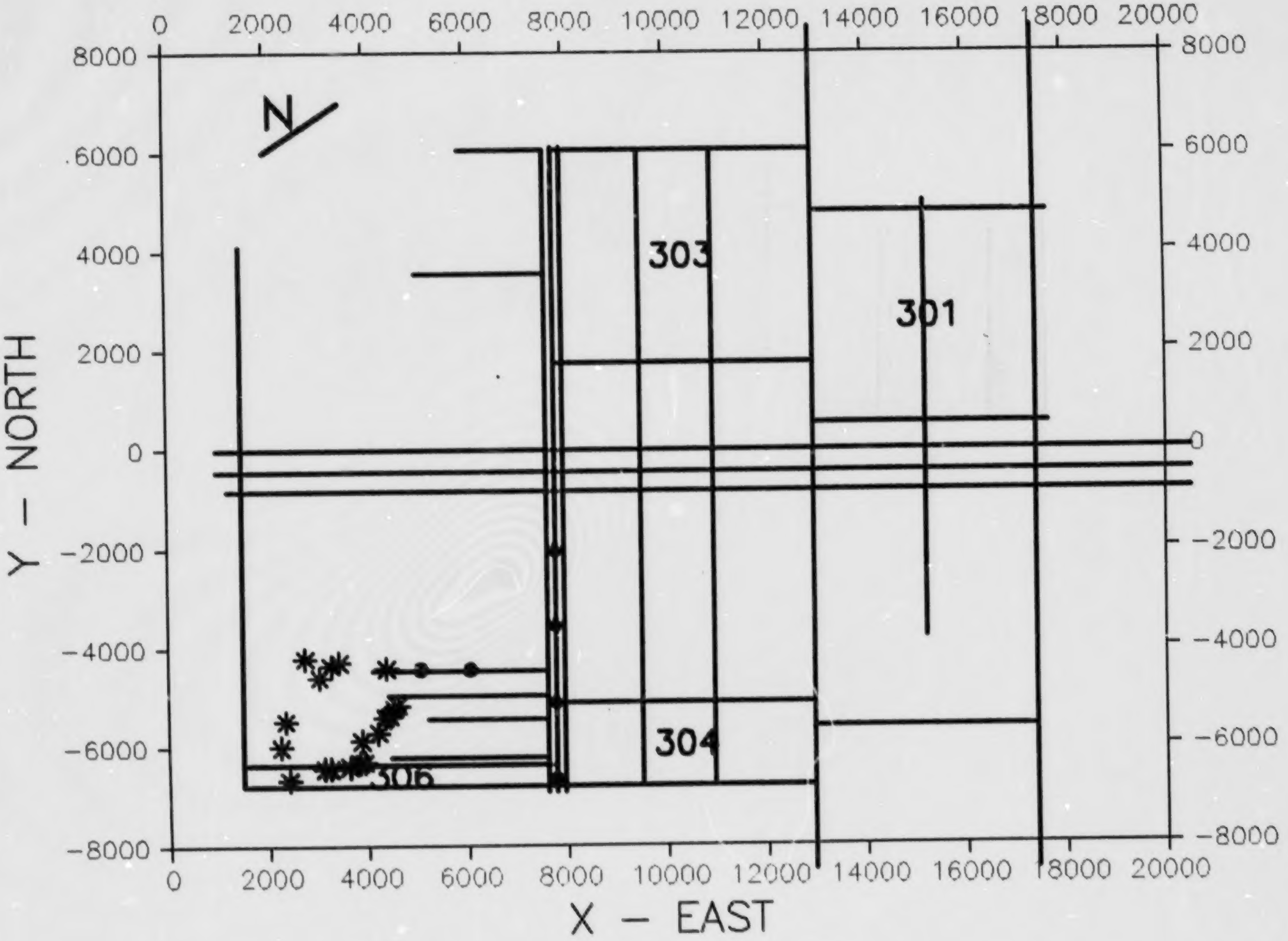
N
303
301
304
306
Y – NORTH
X – EAST
0
2000
4000
6000
8000
10000
12000
14000
16000
18000
20000
8000
6000
4000
2000
0
-2000
-4000
-6000
-8000

PCS ROCANVILLE

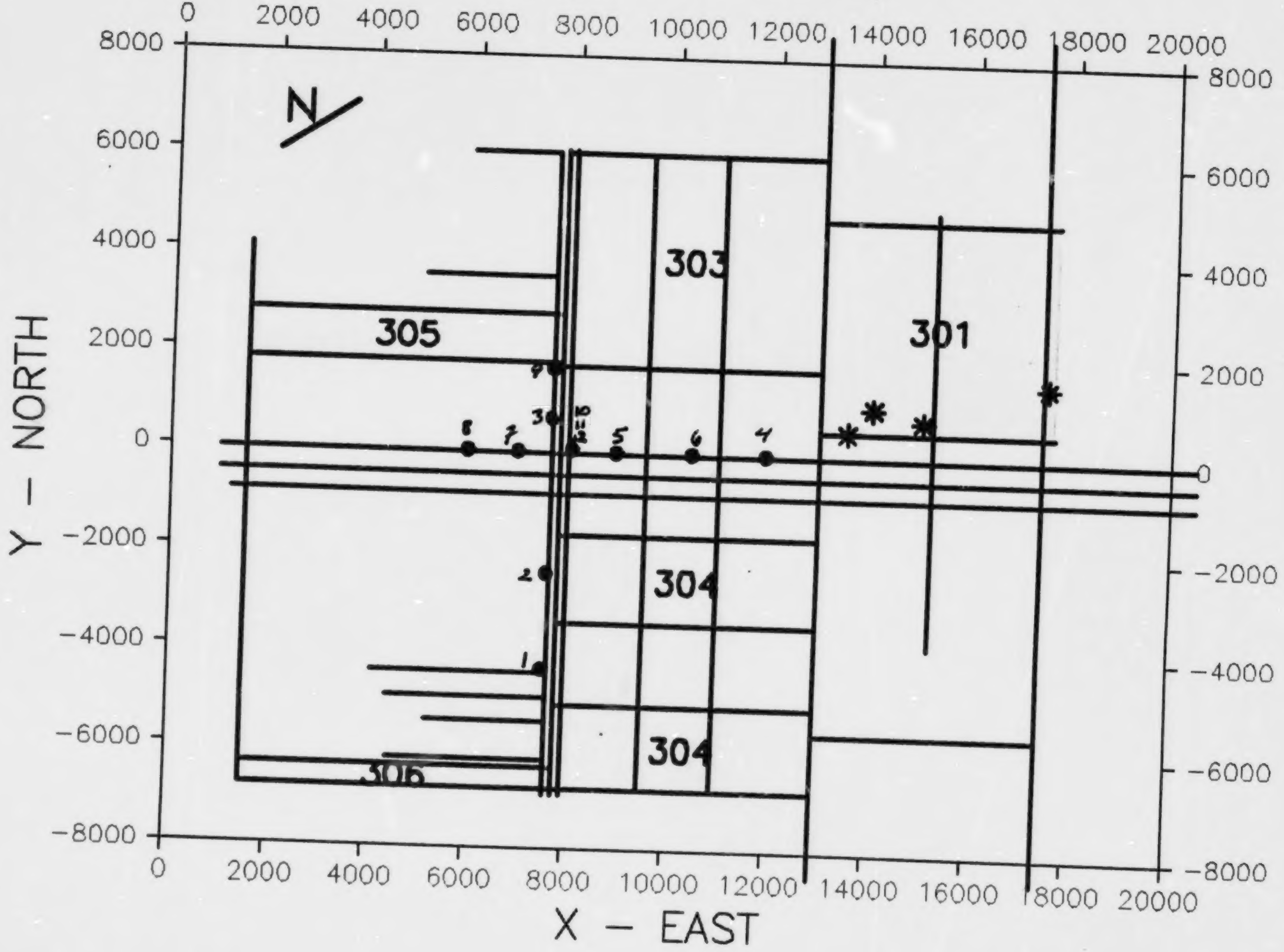

N
301
303
304
304
305
306
1
2
30
4
5
6
7
8
9
10
11
12
Y - NORTH
X - EAST
8000
6000
4000
2000
0
-2000
-4000
-6000
-8000
0
2000
4000
6000
8000
10000
12000
14000
16000
18000
20000

Figure 3.

PCS ROCANVILLE

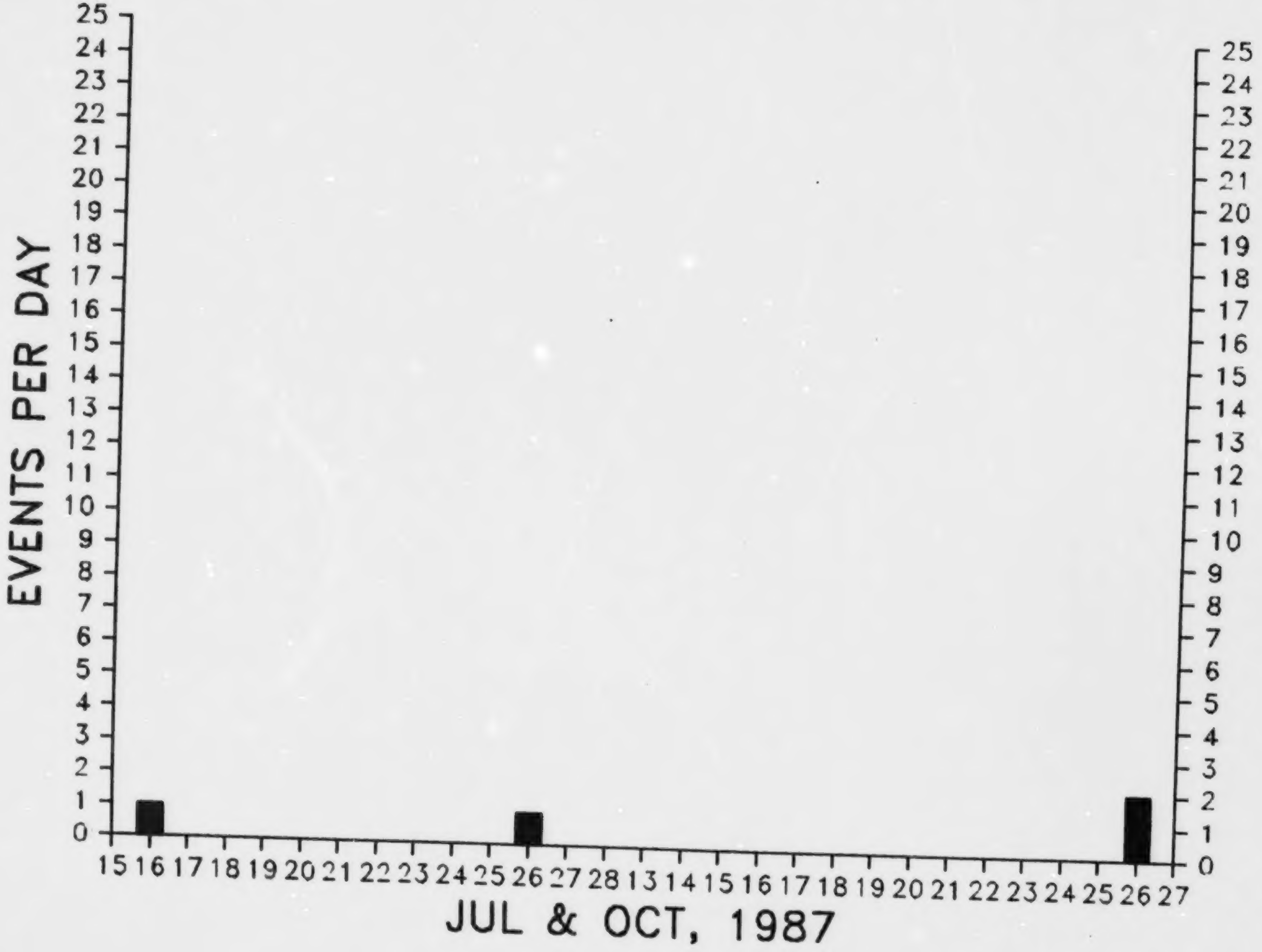

Figure 4.

MICRO–EARTHQUAKE SEISMOGRAMS (1987/207/17/45/57)
(VELOCITY DATA IN μmeters / second)

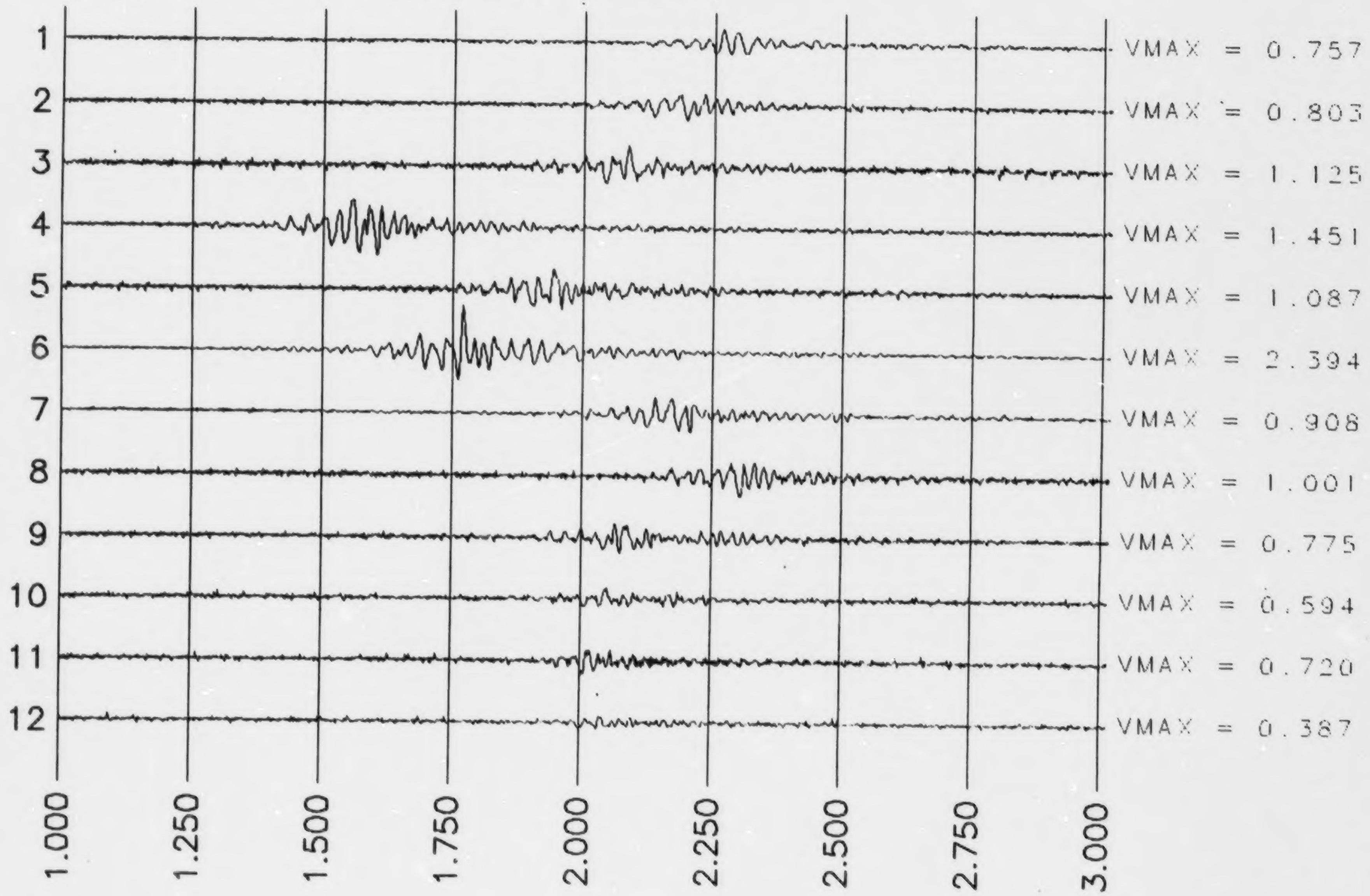

Figure 5.

MICRO-EARTHQUAKE SEISMOGRAMS (1987/299/11/44/39)
(VELOCITY DATA IN μmeters / second)

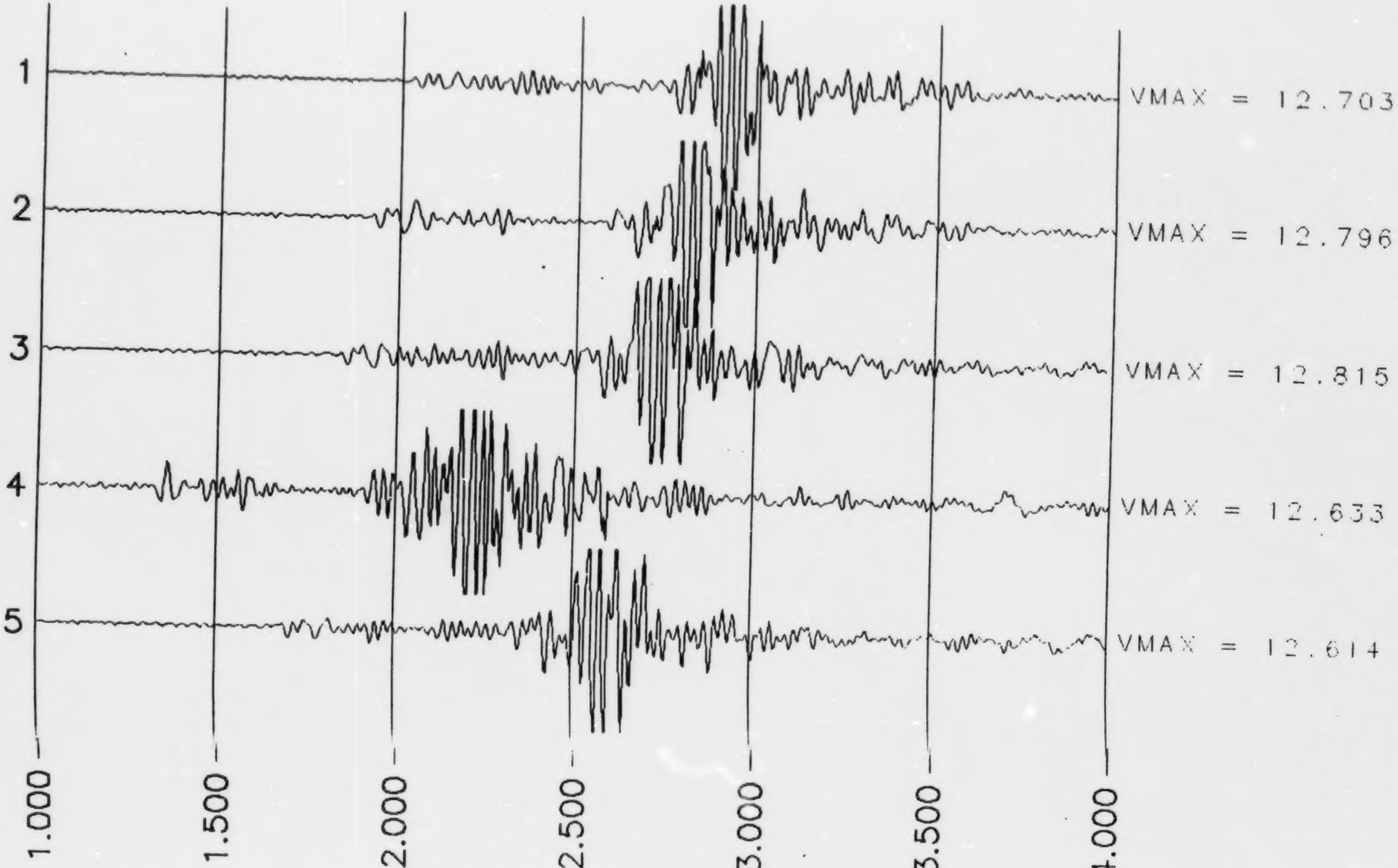

FIGURE 6.

MICRO–EARTHQUAKE SEISMOGRAMS (1987/299/11/44/51)

(VELOCITY DATA IN μmeters / second)

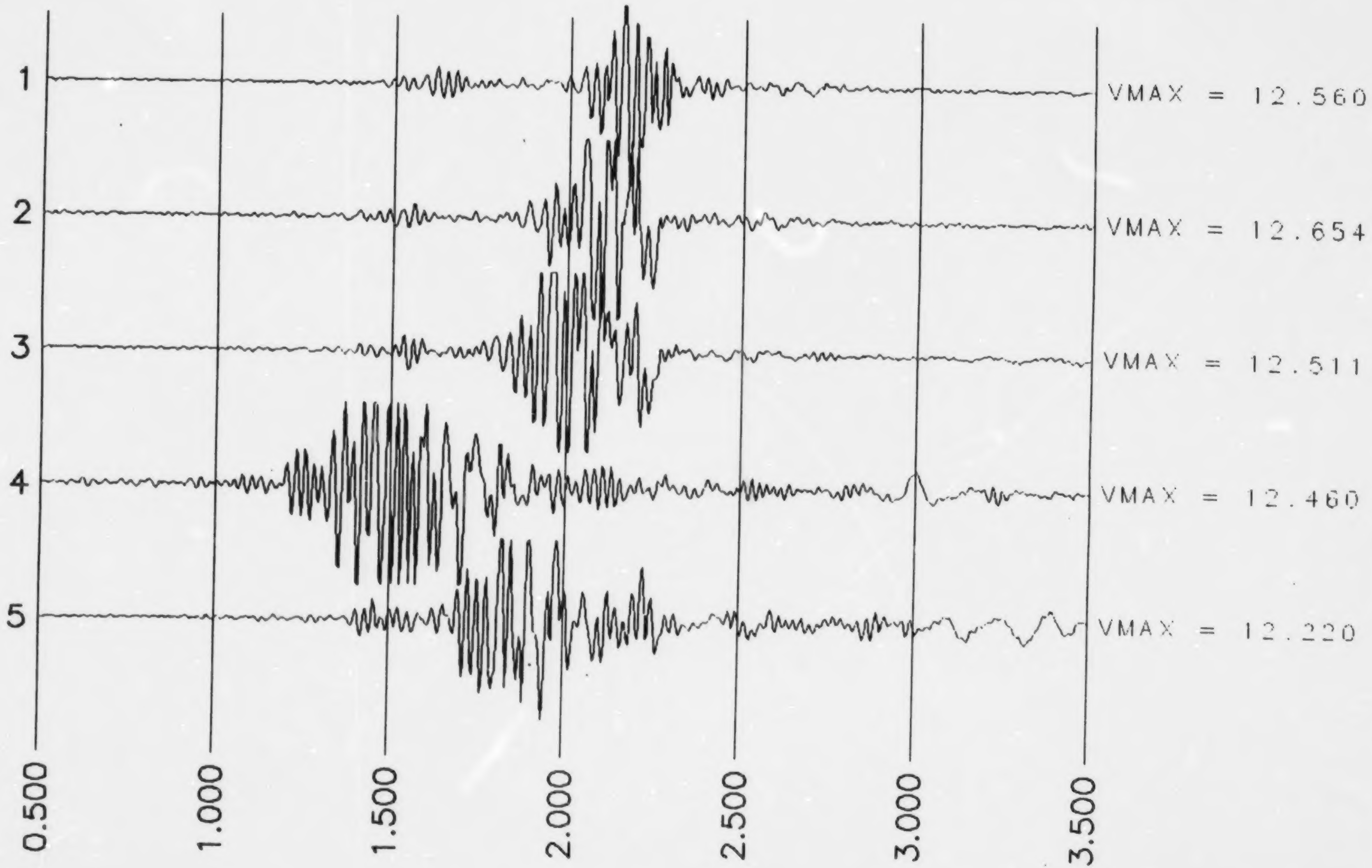

FIGURE 7.
PCS ROCANVILLE

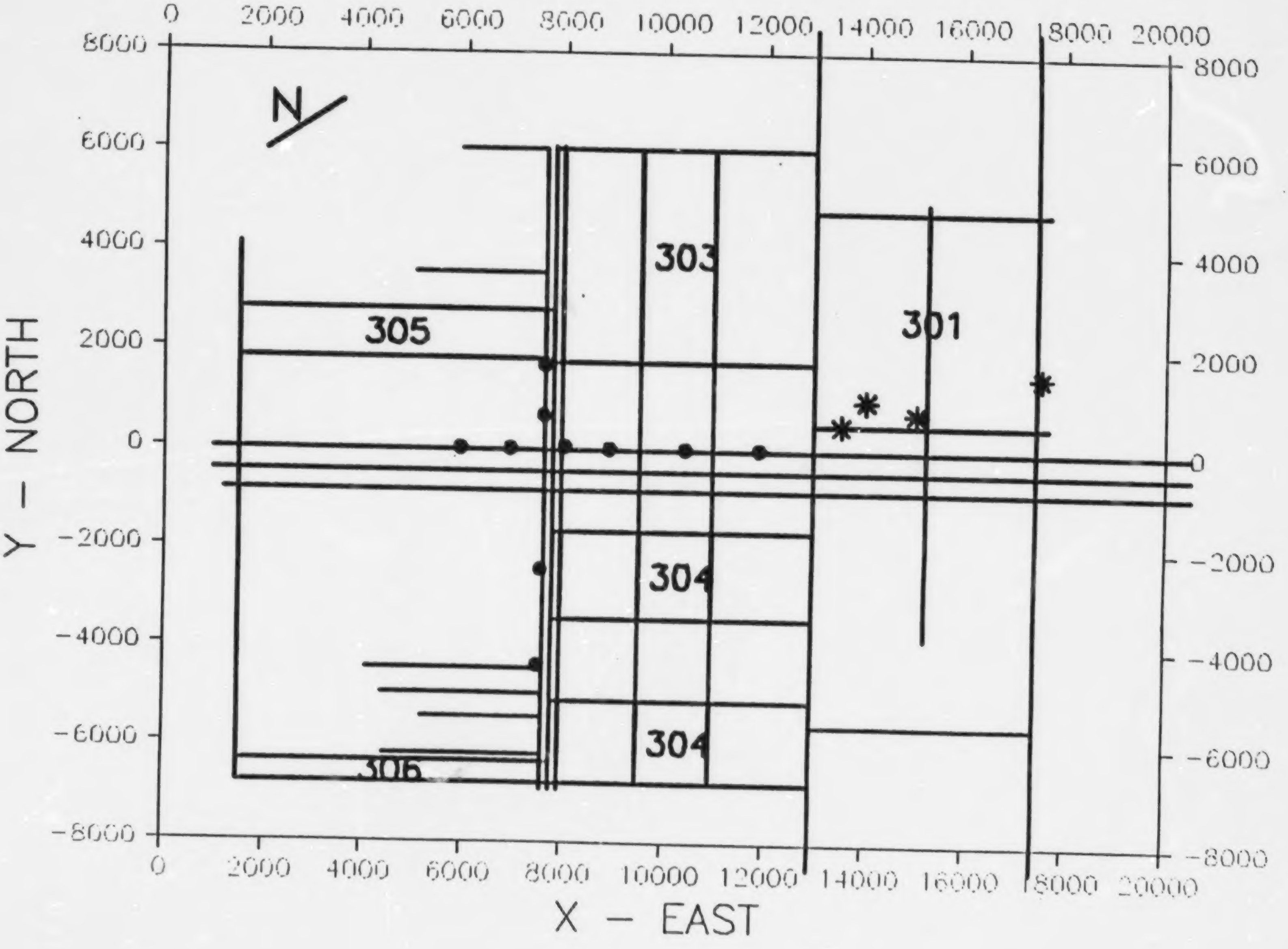

N
301
303
304
304
305
306
Y - NORTH
X - EAST
8000
6000
4000
2000
0
-2000
-4000
-6000
-8000
0
2000
4000
6000
8000
10000
12000
14000
16000
18000
20000

FIGURE 8

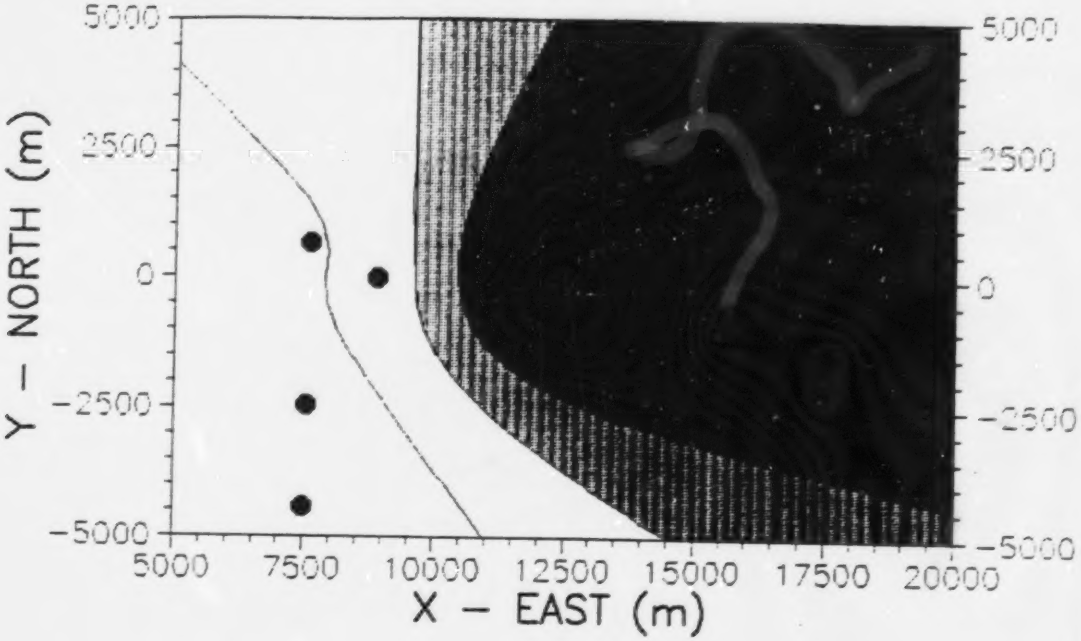

ERRORMAP FOR EVENT: 1987/299/11/44/39

Y - NORTH (m)
X - EAST (m)
5000
2500
0
-2500
-5000
5000
7500
10000
12500
15000
17500
20000

FIGURE 9

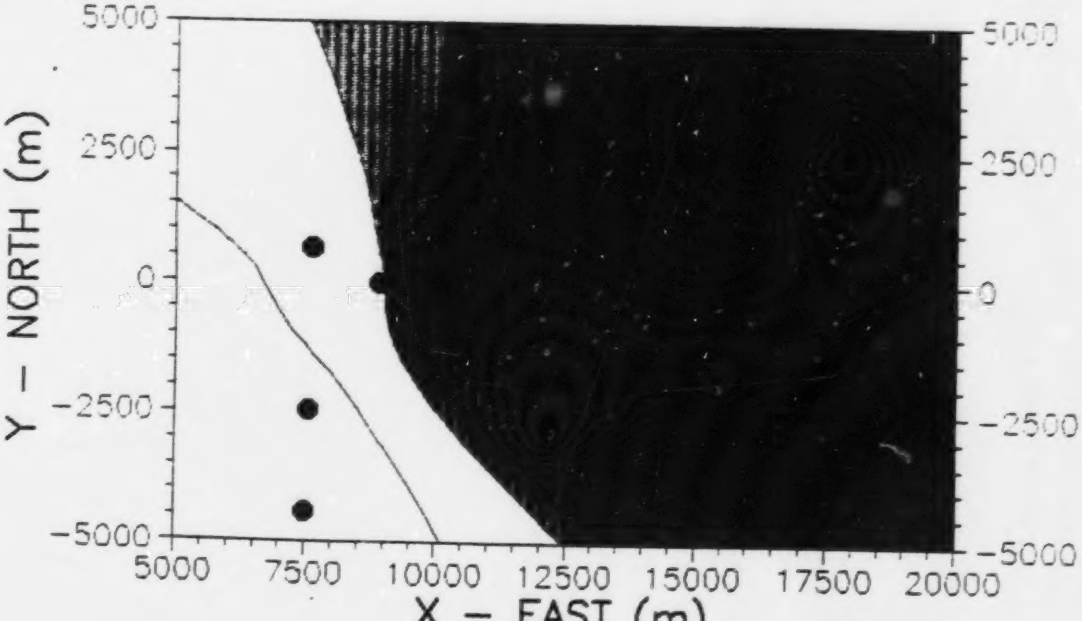

ERRORMAP FOR EVENT: 1987/299/11/44/51

Y - NORTH (m)
X - EAST (m)
5000
2500
0
-2500
-5000
5000
7500
10000
12500
15000
17500
20000

Figure 8

ERRORMAP FOR EVENT: 1987/299/11/44/39

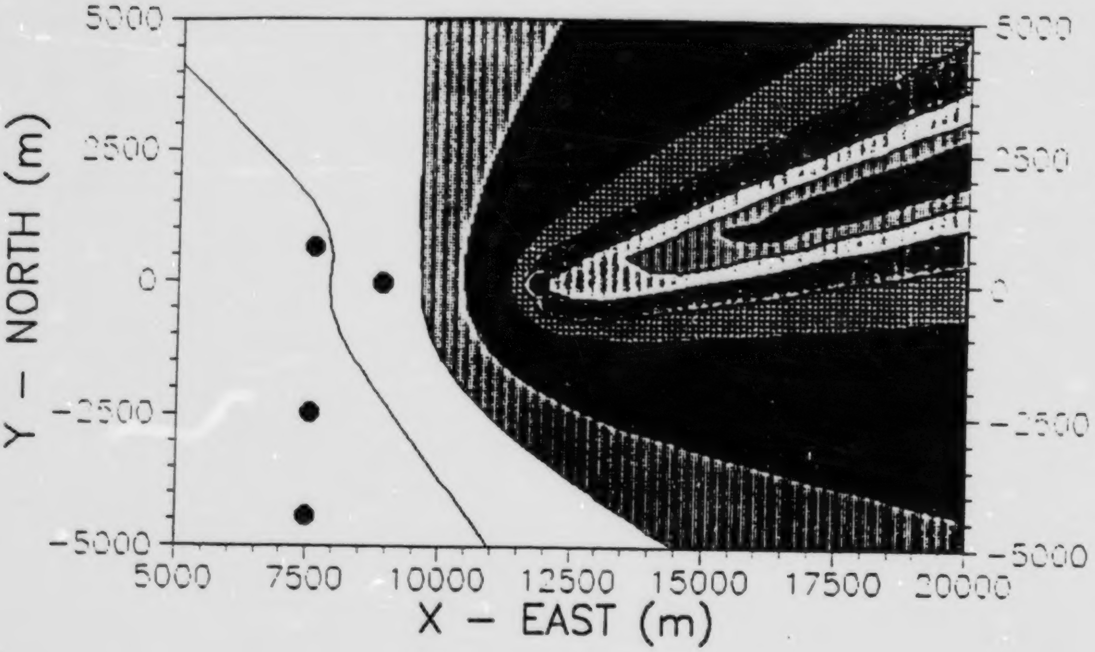

Figure 9

ERRORMAP FOR EVENT: 1987/299/11/44/51

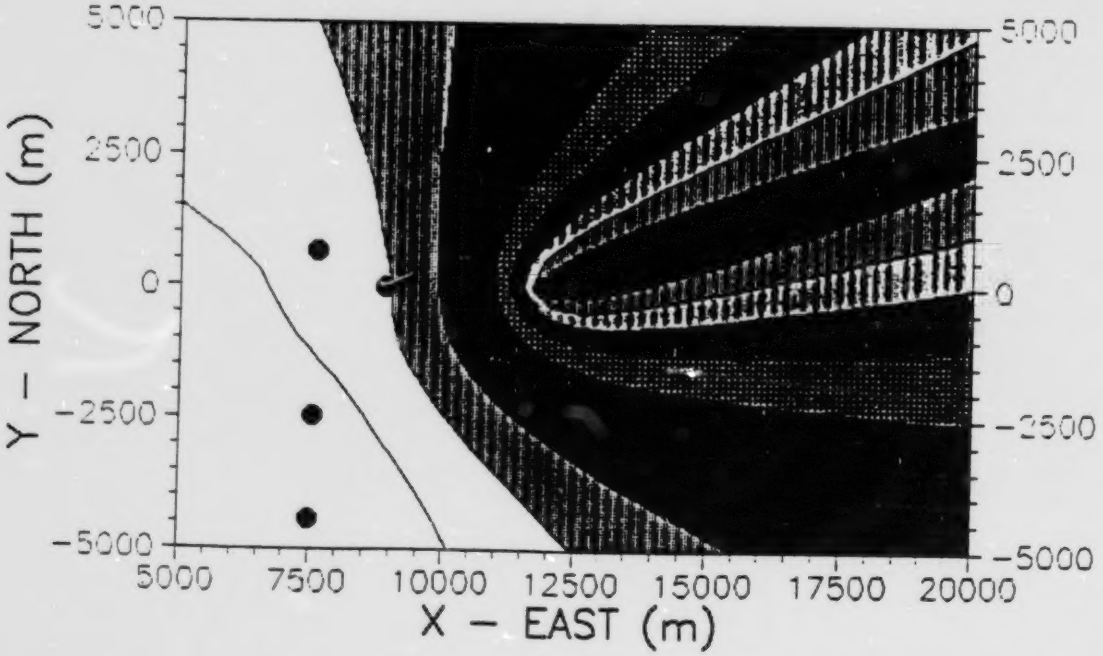

Figure 10.

EVENT : 1987/207/17/45/57
512 POINT FFT OF VELOCITY (μmeter/sec) DATA

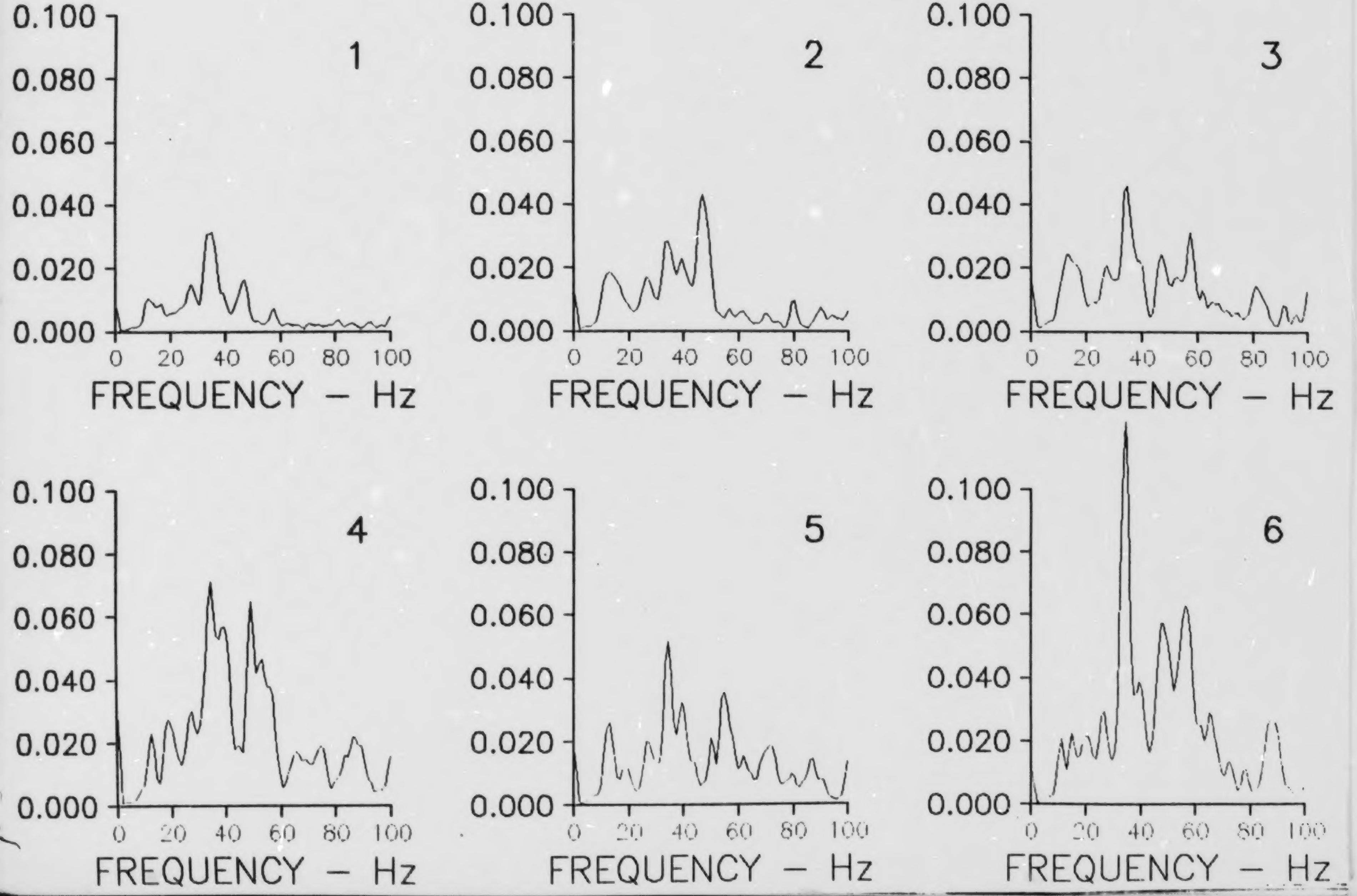

.FIGURE II.

EVENT : 1987/207/17/45/57
512 POINT FFT OF DISPLACEMENT (μmeter) DATA

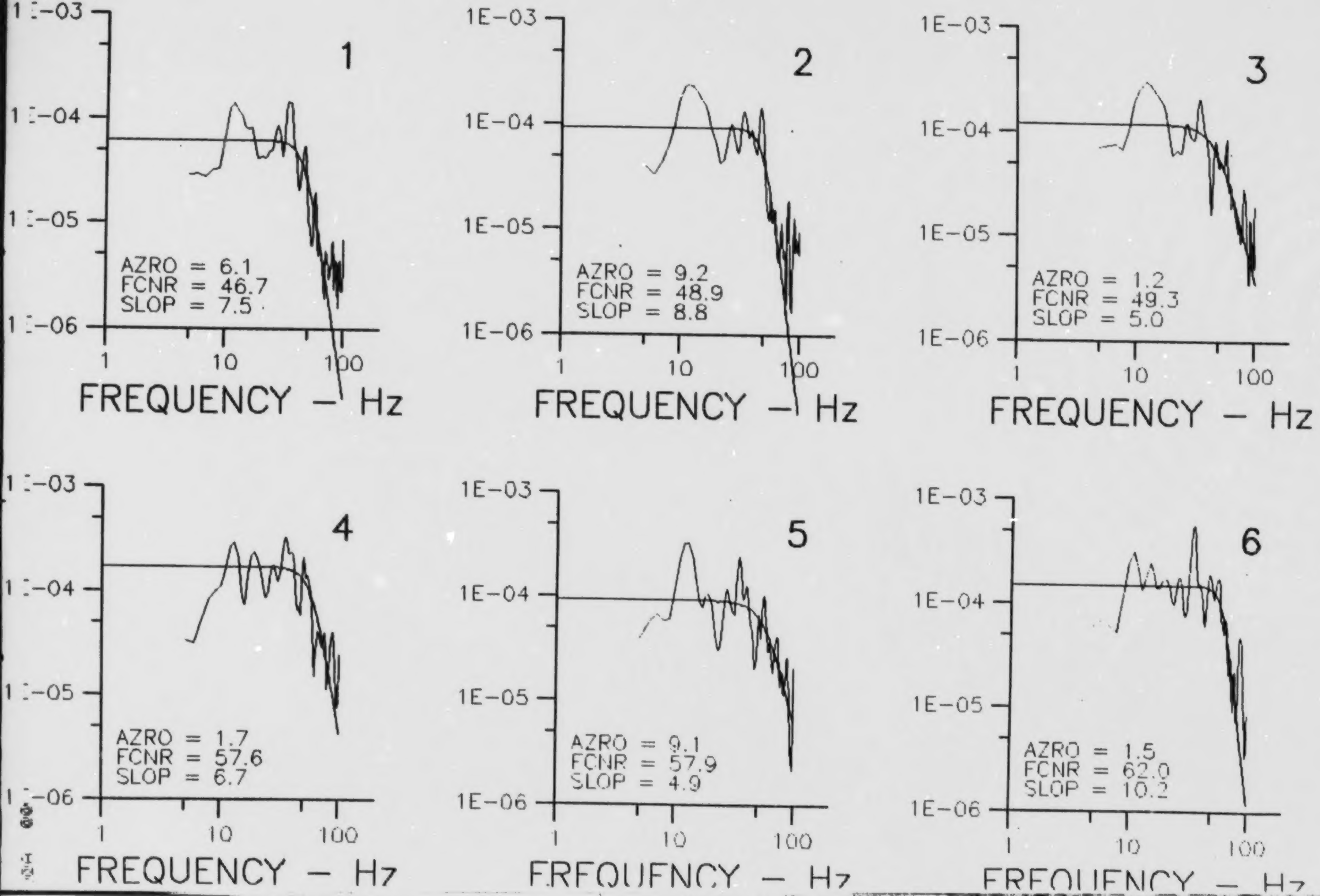

7.1 Appendix : List of Microseismic Events, Rocanville, 1987.

1. Day 197 (July 16) at local time 11:01:45,
   poor record (weak signal), recorded only on 3 backup channels;
   Location estimate : E 14000 ft. / N 1000 ft.
2. Day 207 (July 26) at local time 17:45:57,
   weak signal, recorded on 12 channels;
   Location : E 15000 ft. / N 750 ft.
3. Day 299 (October 26) at local time 11:44:39,
   good record (strong signal), recorded on 5 channels;
   Location : E 17500 ft. / N 1500 ft.
4. Day 299 (October 26) at local time 11:44:51,
   good record (strong signal), recorded on 5 channels;
   Location : E 13500 ft. / N 500 ft.

PRELIMINARY REPORT OF THE RESULTS OF SEISMIC MONITORING AT THE COMINCO POTASH MINE, (VANSCOY, SASKATCHEWAN), OCTOBER THROUGH DECEMBER, 1985.

Arnfinn Prugger
Don Gendzwill
Department of Geological Sciences
University of Saskatchewan
Saskatoon, Saskatchewan
(S7N-OWO)

January 31, 1988

Summary :

A seismic monitoring array was operated underground at the Cominco potash mine in the period October 9 through December 5, 1985. A total of 336 seismic events were observed in 34 full days of recording, amounting to an average of 10 events per day. As many as 23 events, or one every hour, were observed on November 23. Arrival times were used to calculate event locations, which have been plotted on a mine map. Events were scattered over a large region of the mine, but tended to occur more often where total surface subsidence is greatest, near the center of old mined out areas. A magnitude calculation was carried out on one of the larger events, which shows that most events recorded were smaller than $M = -1.5$.

1.1 Background :

Seismic traces are records of ground vibration observed through time at that point in (or on) the Earth where a vibration sensor, or geophone, has been set up. "Vibration" in this context means particle displacement of the region of rock that the geophone is attached to. The geophone sensors used at Rocanville measure the velocity of particle displacement (in micro-meters per second). The vibration record that is observed results from rock fracture occurring some distance away from the sensor. Since seismic energy travels at finite velocities through rock, vibrations emanating from a rock fracture will in general arrive at different times at different geophones. The arrival times are used to calculate the location of the rock fracture using the "Simplex Method" of source location described in Prugger and Gendzwill, 1988.

Micro-seismic activity has been observed at every potash mine in Saskatchewan where monitoring instruments have been set up. As well, seismic events strong enough to be noticed by persons living in the vicinity of mines have occurred at five of the provinces ten mines to date : IMC-K1 and IMC-K2 at Esterhazy, PCS at Cory, CCP at Colonsay, and PCA at Patience Lake. These events have been in the Richter magnitude range 2.0 - 3.5 (Gendzwill et al., 1982). This corresponds to noticed effects ranging from "a truck ran into the house", or "the furnace blew up", to (in a few cases) cracked wall plaster.

Noticeable macro-seismicity has not been observed in the Cominco area to date. Microseismicity was monitored from surface over various mining areas during the fall and summer of 1980 using a single drum recorder. Events could not be located with only one channel records, (and many apparent seismic events may in fact have been spurious noise events), but on days of good recording there were as many as 20 microseisms per 24 hour period over the mine.

1.2 Instrument Setup :

Three vertical component geophones were set up in the north-west region of the Cominco mine on October 9, 1985. On October 29 one of these channels was moved further east, and a triaxial geophone was set up in its place. The final four channel geophone array is shown in Figure 1; (in the first month of recording the array consisted of channels 1, 2, and 4). Recording continued until December 5, 1985. The coordinate system used corresponds to the mine coordinate system. All distances are in meters. Map north coincides with true north. All sensors were at roughly the elevation in the mine, at 1000 m depth. The recording instruments were located near the triaxial sensor, geophone 4. The array configuration was chosen to monitor seismicity in the old regions of the mine north of the array, to investigate whether any seismicity was associated with a minor water inflow into the mine (located near 105,000N / 99,000E), and to see if any seismicity was associated with a mining machine cutting the rooms just south of geophones 1 and 4 (near 103,000N / 99,000E). Geophone coordinates in meters are :

Channel 1 :	N 104205.0 m ,	E 98951.5 m	
Channel 2 :	N 104242.0 m ,	E 100774.0 m	
Channel 3 :	N 105160.5 m ,	E 99819.0 m	
Channel 4 :	N 104205.0 m ,	E 99748.5 m	
Channel 5 :	N 104205.0 m ,	E 99748.5 m	(east)
Channel 6 :	N 104205.0 m ,	E 99748.5 m	(north)

Stations 1 - 3 consisted of two vertical component Mark Products model L-1 (4.5 Hz) geophones connected in series, strapped to the mine roof, connected by up to 1000 meters of two-conductor telephone wire to an amplifier system at the central instrument site. The tri-axial sensor was a pair of Mark Products model L-28 (4.5 Hz) geophones connected in series.

The recording system was a pair of Terra-Technology model DCS-302 three-channel digital recorders (connected to a common clock). These units monitor seismicity contiuously, but only record the incoming vibration signal when an event is "recognized" as a seismic event by the program that controls the units. Details of the operation of the Terra-Technology system are given in Prugger and Gendzwill, 1983.

2.1 Frequency of Occurrence of Seismic Events :

A histogram plot of the number of seismic events recorded per day is given in Figure 2. Note that there are many gaps in the record, indicating times of no recording, (usually for reasons of instrument malfunction). In the period October 9, 1985 through December 5, 1985 a total of 336 seismic events were observed in about 34 full days of recording. This amounts to an average of 10 events per day, (with as many as 23 events, or one every hour, recorded on November 23). This is roughly the same level of seismicity as was observed during the spring 1980 monitoring period. However, seismic events occur at a far higher rate at the Cominco mine than at either PCS Lanigan, where the average is one event per day, or PCS Rocanville, where the average rate is one event every one or two weeks.

2.2 Event Locations :

The arrival time of seismic energy at each sensor was picked from plotted seismograms of each recorded event. These differences in arrival times were used to calculate the location of the rock fracture that gave rise to the observed seismograms. A typical six-channel seismogram is shown in Figure 3 ; (channels 1 - 4 are vertical component geophones, channel 5 is the east-west component at channel 4, and channel 6 is the north-south component at channel 4). Source location was calculated using a variety of programs written by Prugger (U of S) that use the "Simplex Method" of direct iteration for earthquake location (described in Prugger and Gendzwill, 1988). Event locations are plotted on a mine map in Figure 4. Events recorded in October (roughly half of the events plotted) were located using arrival times at only three geophones, and are therefore less accurately located than events recorded in November and December. But since there are so many events, and since the general pattern seen in October was much the same as the general pattern seen in November, no distiction has been made between the two sets of data here.

An attempt was made to smooth the scattered pattern of event locations seen in Figure 4 by drawing the seismic event density map shown in Figure 5. This is a map of contours of number of seismic events within a 500 meter radius of positions on a systematic grid covering the north region of the mine. Although any individual location point may be in error (for a variety of reasons) the event contour map is an accurate representation of the pattern of seismicity during the recording period.

2.3 Propagation Velocities :

In one version of the location programs that were run, arrival times were used to solve for propagation velocity as well as X-east and Y-north location. The velocity data are plotted in Figure 6 as a histogram of the number of seismic events per velocity interval. Calculated velocities range from 1500 m/s to 5250 m/s, with two clear peaks in the distribution at 2750 m/s and 4300 m/s. These values are close to the S and P wave velocities for seismic wave propagation in salt. The result that energy from most events arrives across the geophone array at S wave velocities came as a surprise. A similar pattern of predominantly "apparent" S-wave arrivals has been observed at every other potash mine where seismicity has been monitored underground. This observation may indicate that most microseismic events in potash mines are generated in the salts near the mining level, and have nothing to do with the large macro-earthquakes observed at some mines.

2.4 Spectral Analysis :

Analysis of the frequency content of the recorded seismic signals is often used to estimate parameters relating to the rock fracture mechanism for recorded seismic events (Aki, 1967; Brune, 1971: Wyss and Hanks, 1972; Spottiswoode and McGarr, 1975). Spectral analysis involves transforming seismogram records into the frequency domain, and looking at the spectrum of vibrations generated by the rock fracture. The general idea is that small fractures produce short wavelength (high frequency) vibrations while large fractures produce long wavelengths (lower frequencies). After converting the recorded velocity data to particle displacements these data are plotted on a log-log graph. Velocity and displacement spectra of vertical component sensors for the event shown in Figure 3 are given in Figures 7 and 8. A Butterworth function is fitted to the displacement spectra to give estimates of the zero-frequency intercept (AZRO), the corner frequency (FCNR), and the high frequency attenuation (SLOP). The fitting was done using the simplex method to optimize the three parameters for a best-fit to the data.

Using the determined values of AZRO and FCNR the following estimates for seismic moment (Mo), local Richter magnitude (ML), radiated vibration energy (E), (NOT released energy), an fault surface radius (Rf) were calculated :

Mo = 5.0 * 10**8 Newton - meters
ML = -1.5
E = 1500 Joules (Watt-sec)
Rf = 25 meters

Recall that the Richter magnitude scale is logarithmic : this event was about 30,000 times smaller than a magnitude 3.0 event that would certainly be noticed on surface. The radiated energy value is small, but keep in mind that it is released over a very short time (0.5 10 1.5 seconds). The calculated fault surface area is much larger than seems reasonable for an event as small as the one shown here. Significant attenuation of high frequency energy along the source to receiver travel path (which in our experience is common in potash) may account for incorrectly high fault radius values.

3.1 Concluding Remarks :

The most striking aspects of the seismic monitoring experiment at the Cominco mine are the large number of events per day shown in Figure 2 and the scattered "shotgun blast" pattern of seismicity seen in Figure 4. 10 to 20 events per day is far more than the 0 to 3 per day at Lanigan, or the 1 event per week at Rocanville, but this rate is consistent with results from an earlier monitoring experiment carried out in 1980. And there does not appear to be any of the clear localization of seismicity seen at Lanigan and Rocanville. Although seismicity tends to occur towards the center of old mining regions, (rather than near abutment pillars at the edge of mine workings), it seems possible for events to occur anywhere in the mine. The linear pattern of events north-south along coordinate E 99500 (between N 103000 and N 104000), was likely caused by the mining machine that was cutting in the area throughout the recording period.

The contour pattern in Figure 5 is similar in shape to the map of total subsidence measured on surface ; at Cominco rock fracture tends to occur where total subsidence is greatest (at least, this was the case in the Fall of 1985). Having the greatest number of events in the middle of the subsidence zone may be another indication that most events are generated in the salt (the greatest crushing of pillars is where room closure in the mine and subsidence on surface are greatest). But in our experience seismicity is more likely to occur in regions where the Dawson Bay limestone, which overlies the salts of the Prairie Evaporite, is weak (ie.- porous or fractured). In the middle of a large subsidence zone the limestone is being let down more or less uniformly, with the greatest flexural deformation occurring at abutment pillars (where little, or no, seismicity is observed). It may be that most small events occur in the middle of mined out areas in the salt, and that larger events occur near abutment pillars in the limestone. Since large seismic events have not been noticed at Cominco in 20 years of mining, one is tempted to conclude that elastic strain energy built up during subsidence of strata above the mine is released as many small fractures at Cominco rather than as a few large failures at mines where macro-seismicity has been observed. But this might be true if ALL of the observed events occurred in the limestones overlying the mine level ; (the idea is that strain energy is released as a small fracture before the rock can build up enough strain to generate a large event). In any case, given that many small events DO NOT make a large one in other seismic areas, as well as the indications that most of the events at Cominco are in salts near the mine level, it would be fallacious to assume that a large event could never occur at Cominco.

Weak zones in the limestone that overlie Saskatchewan potash mines are characterized by low seismic propagation velocities (seen in well-logs and/or refraction data) and often occur in areas where the mine-to-limestone salt cover is thinner than usual. An interesting follow-up to this seismic monitoring project would be to carry out a refraction survey to compare the limestone velocity in the seismic area to the velocity in non-seismic areas of the mine.

4.1 Acknowledgement

We wish to acknowledge the Department of Energy Mines and Resources of Canada for providing funding for this project. We also thank the Cominco Fertilizers, Potash Division Ltd. and mine manager Don Boyle for allowing us access to the Cominco mine. Sincere thanks are extended to Jack Arnold of the University of Saskatchewan for assistance in getting and keeping the instruments running. We gratefully acknowledge the assistance in installing and operating the system of Cominco employees Dave MacKintosh and Don Gugliellmin. And finally sincere thanks are extended to George McVittie and Dave MacKintosh for ideas and suggestions, and for their constructive criticism of the first version of this report.

5.1 References

Aki, K., 1967; Scaling law of seismic spectrum; Journal of Geophysical Research, V. 72, pp. 1217 - 1231.

Brune, J. N., 1970; Tectonic stress and spectra of seismic shear waves from earthquakes; Journal of Geophysical Research, V. 75, pp. 4997 - 5009.

Gendzwill, D. J., R. B. Horner, and H. S. Hasegawa, 1982; Induced earthquakes at a potash mine near Saskatoon, Canada; Canadian Journal of Earth Sciences, V. 19, pp. 466 - 475.

Prugger, A. F. and D. J. Gendzwill, 1983; Earthquake monitoring system used at the PCS Mining, Cory Division potash mine near Saskatoon, Canada; Potash '83, Pergamon Press, pp. 191-196.

Prugger, A. F. and D. J. Gendzwill, 1988; Micro-earthquake location : a non-linear approach that makes use of a simplex stepping procedure; Bulletin of the Seismological Society of America, in press (April, 1988 issue).

Spottiswoode, S. M. and A. McGarr, 1975; Source parameters of tremors in a deep level gold mine; Bulletin of the Seismological Society of America, V. 65, pp. 93 - 112.

Wyss, M. and T. C. Hanks, 1972; Bulletin of the Seismological Society of America, V. 62, pp. 591 - 602.

6.1 Figure Headings

Figure 1 : Mine plan and geophone locations (dots) for seismic monitoring experiment in October through December, 1985.

Figure 2 : Histogram of seismic events per day over the October 9 through December 5 (1985) recording period; note that there are numegaps in the record, days of no recording.

Figure 3 : Seismogram records for Cominco event 1985 day 338 (December 4) at local time 9:59:54 .

Figure 4 : Mine plan showing seismic events locations (stars).

Figure 5 : Mine plan showing seismic event density contours (ie.- number of seismic events within a 500 meter radius) ; contour interval is 10 events.

Figure 6 : Histogram of the number of seismic events per velocity interval.

Figure 7 : Velocity spectra of channel 1 - 4 seismograms for event (338/ 9:59:54) .

Figure 8 : Displacement spectra of channel 1 - 4 seismograms for event (338/9:59:54) .

Figure 1.

COMINCO VANSCOY

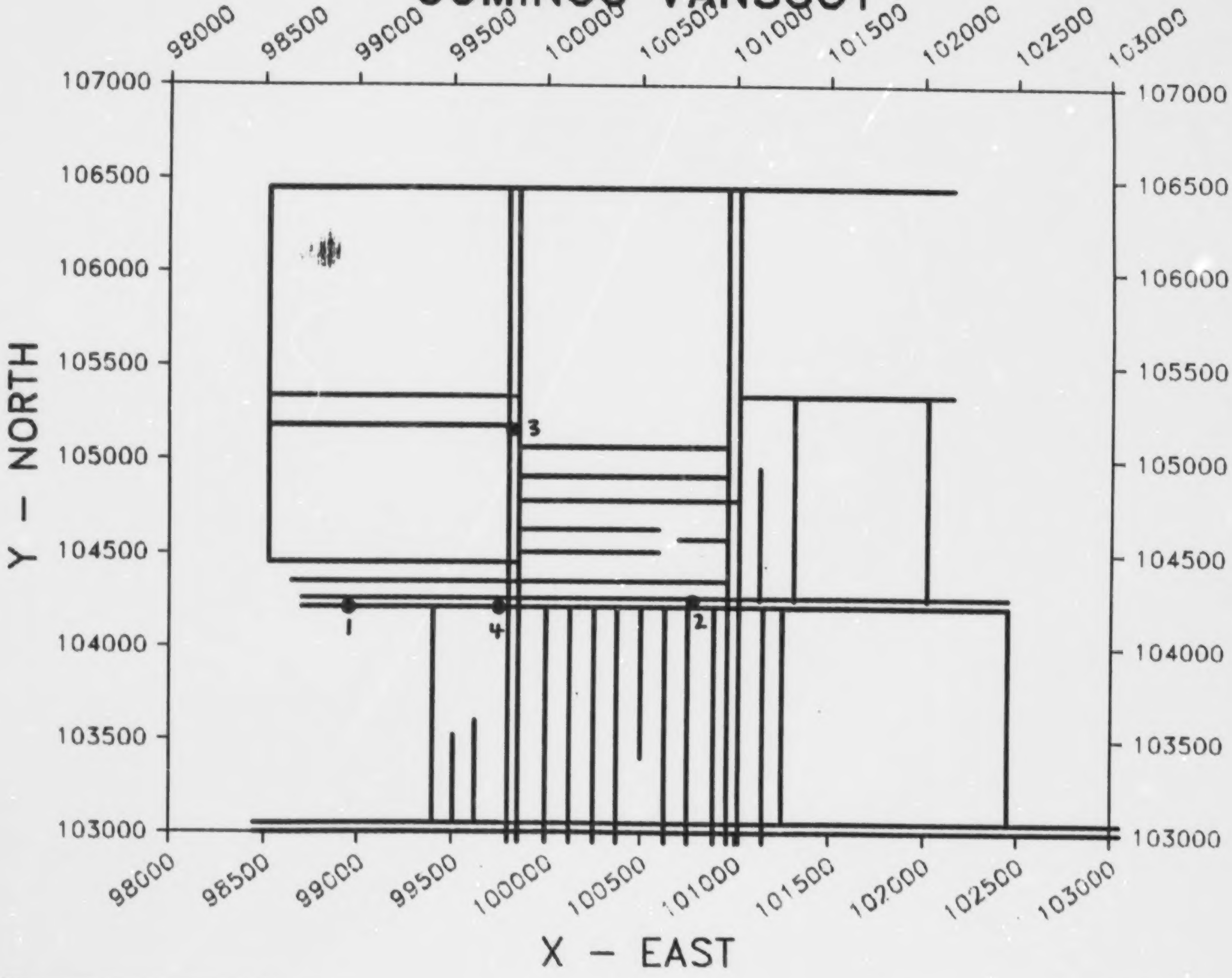
98000
98500
99000
99500
100000
100500
101000
101500
102000
102500
103000
107000
106500
106000
105500
105000
104500
104000
103500
103000
Y - NORTH
X - EAST
1
2
3
4

FIGURE 2.

COMINCO VANSCOY

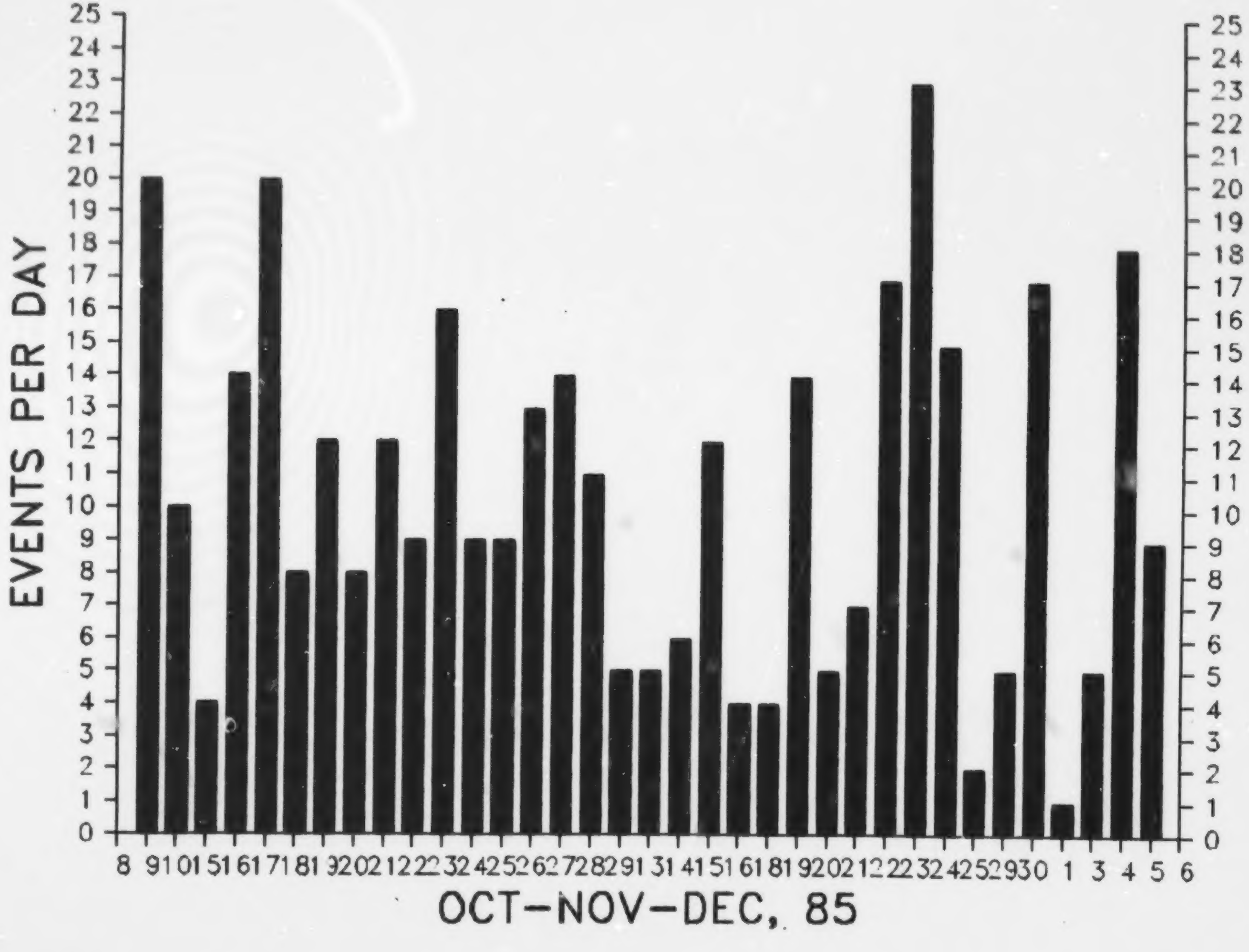

FIGURE 3.

MICRO–EARTHQUAKE SEISMOGRAMS (1985/338/9/59/54)
(VELOCITY DATA IN μmeters / second)

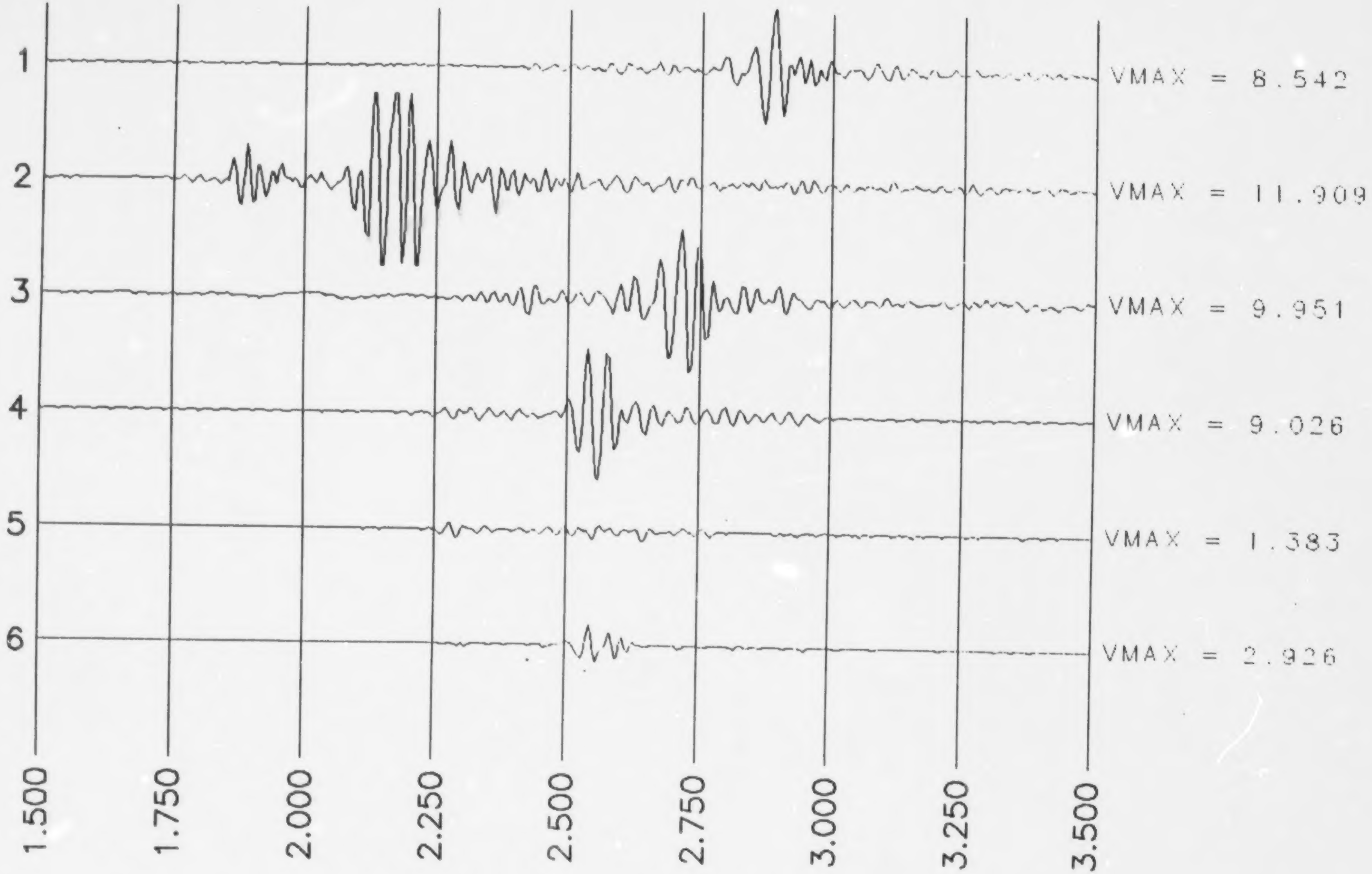

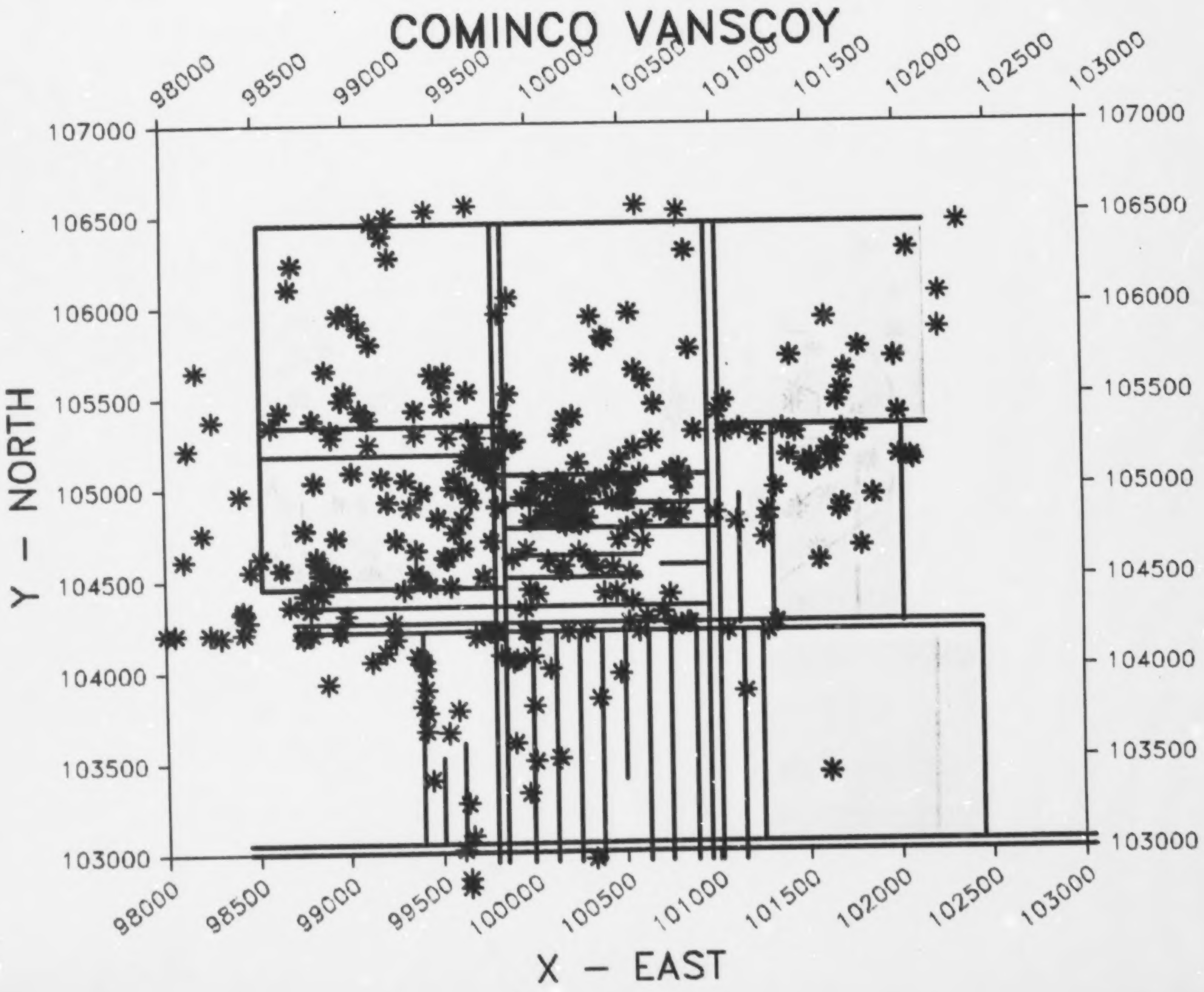

COMINCO VANSCOY

Y - NORTH
X - EAST
98000
98500
99000
99500
100000
100500
101000
101500
102000
102500
103000
103000
103500
104000
104500
105000
105500
106000
106500
107000

COMINCO VANSCOY

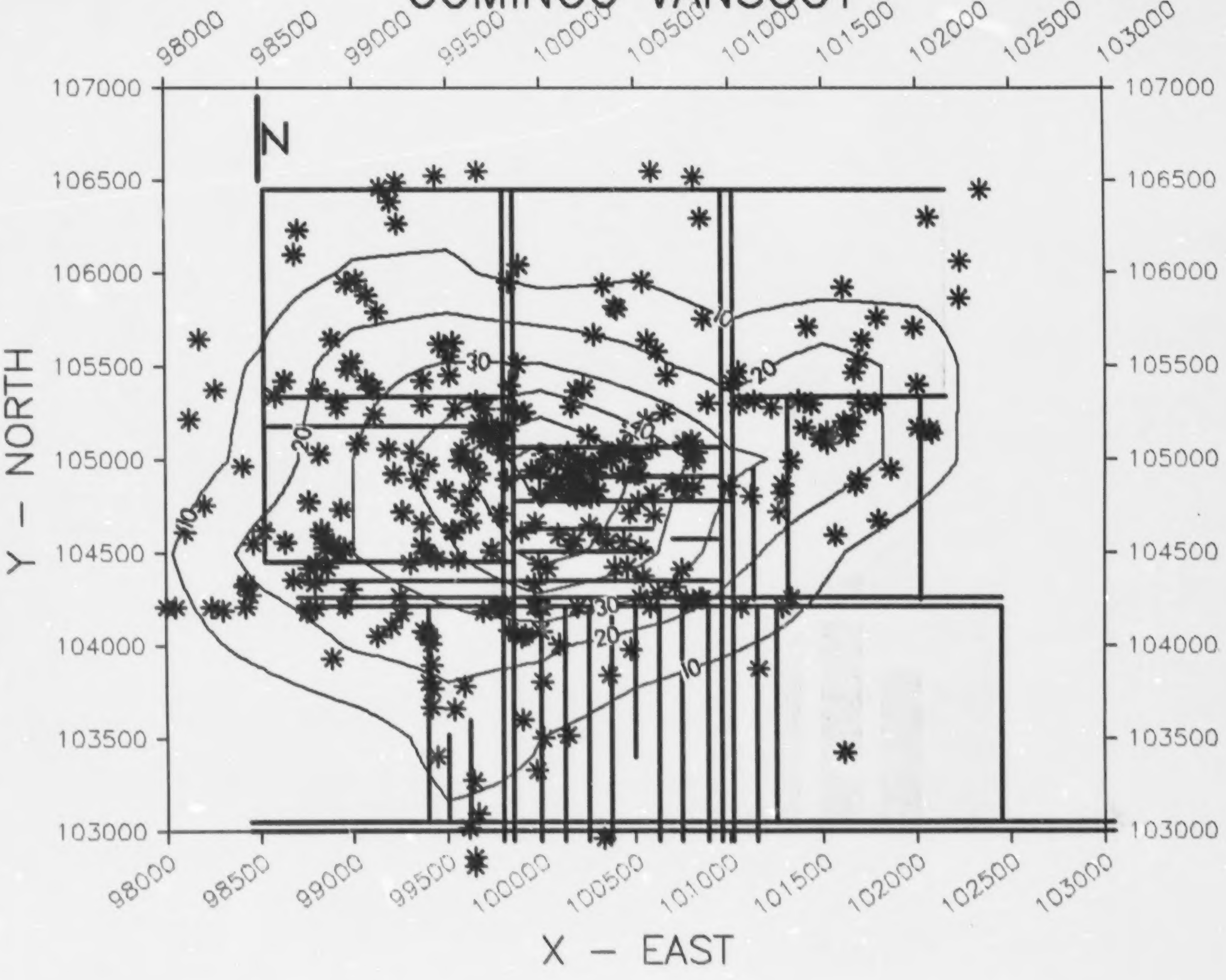
N
98000
98500
99000
99500
100000
100500
101000
101500
102000
102500
103000
107000
106500
106000
105500
105000
104500
104000
103500
103000
10
20
30
40
Y - NORTH
X - EAST

Figure 6.

COMINCO VANSCOY

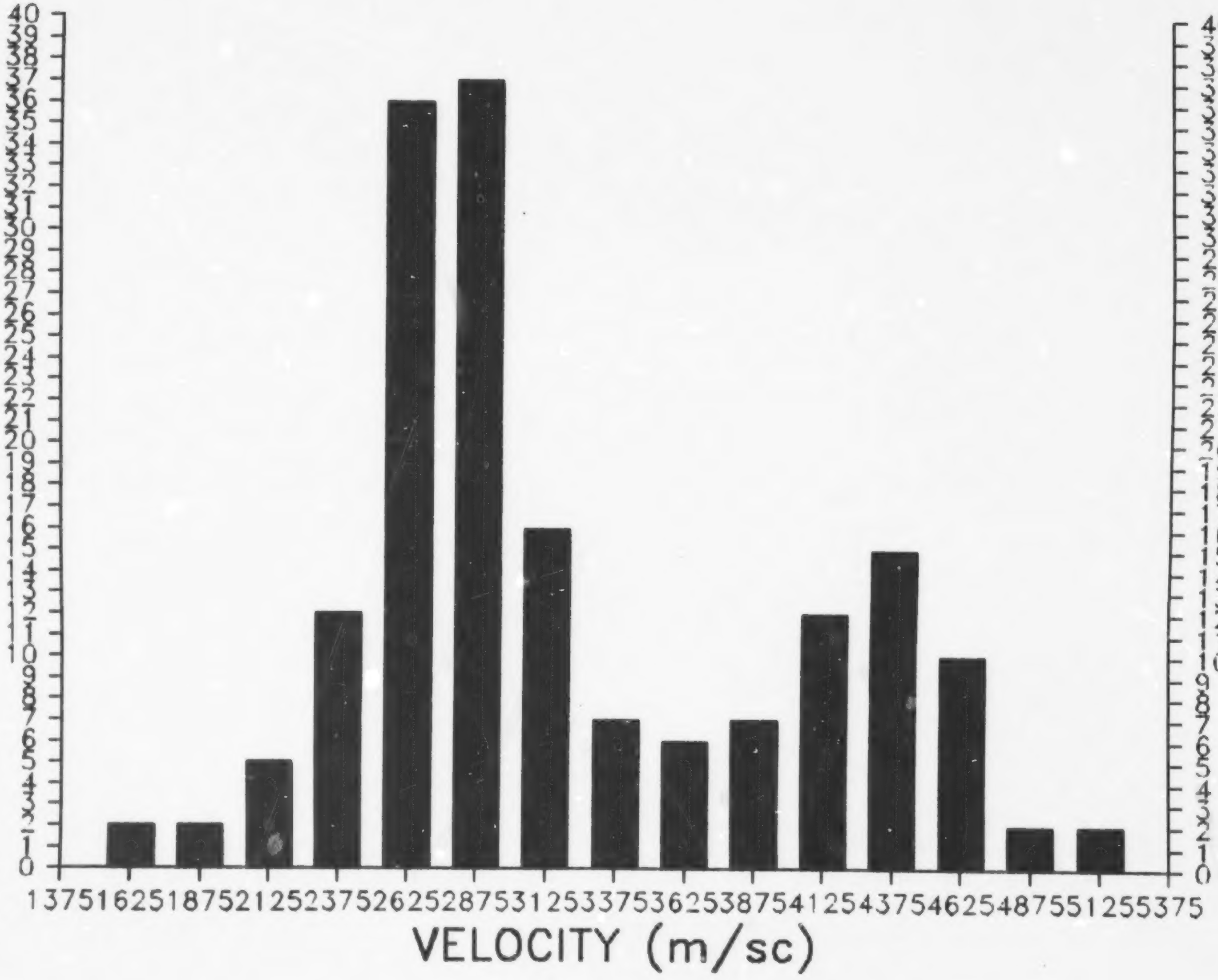

FIGURE 7.

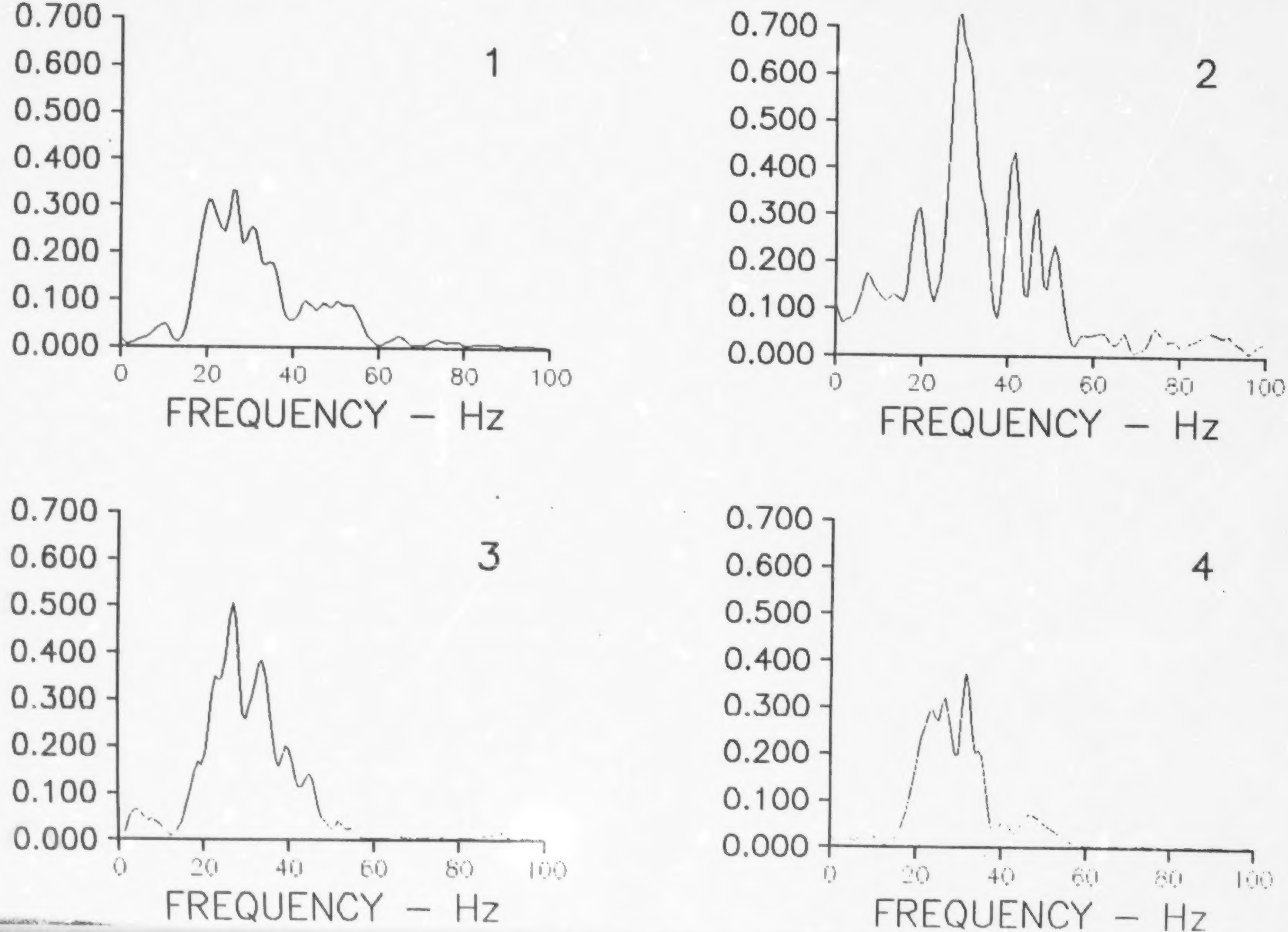

EVENT : 1985/338/9/59/54

256 POINT FFT OF VELOCITY (μmeter/sec) DATA

FIGURE 8.

EVENT : 1985/338/9/59/54
256 POINT FFT OF DISPLACEMENT (μmeter) DATA

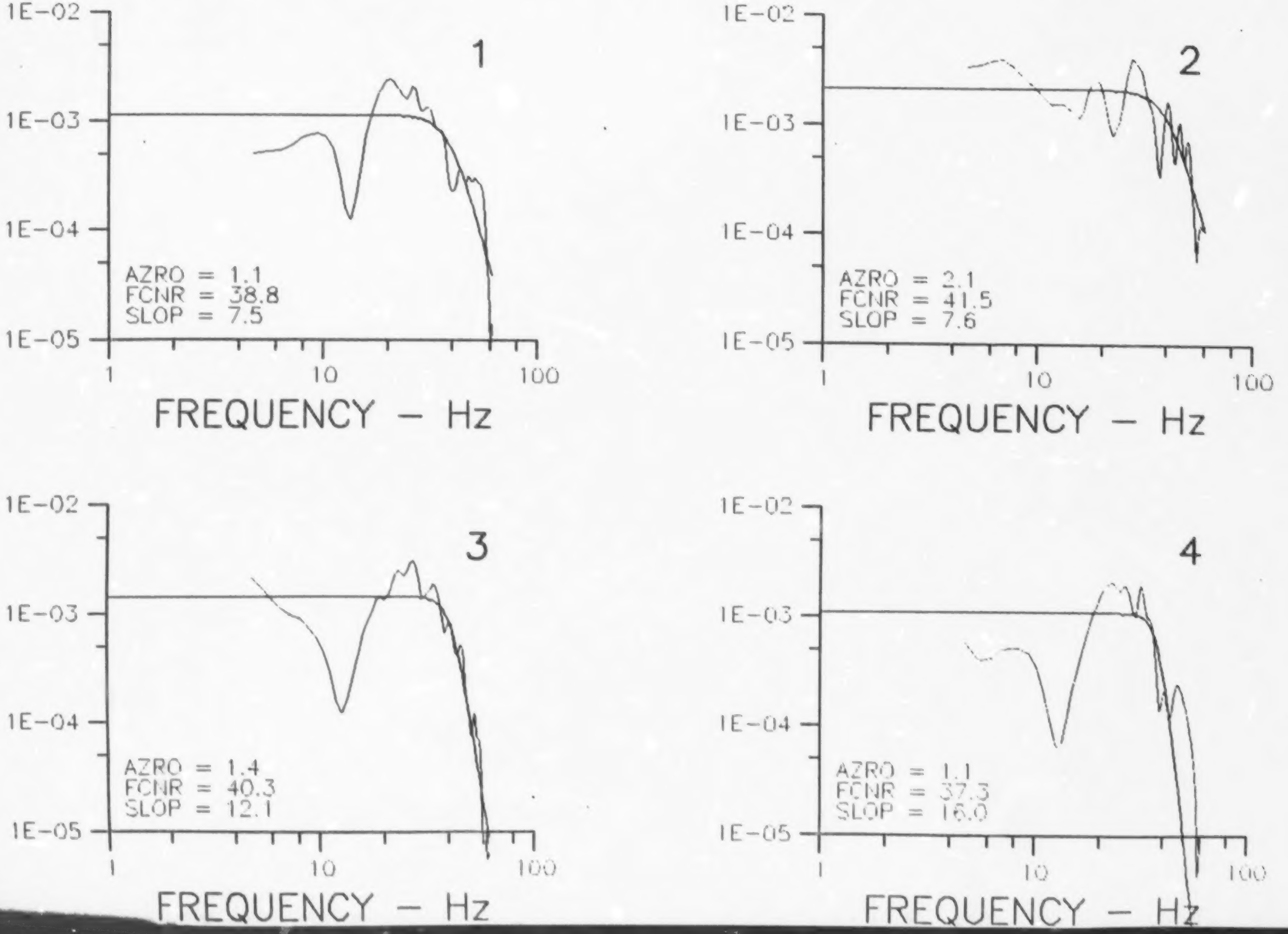

7.1 List of Event Locations

DATE	X-EAST (meters)	Y-NORTH (meters)
1985 OCT. 9	100480.	105150.
	100660.	105250.
	98680.	104355.
	101610.	105920.
	100530.	104525.
	99985.	104205.
	98860.	104420.
1985 OCT. 10	100010.	105025.
	99875.	105510.
	99735.	105130.
	99580.	104755.
	100030.	104415.
	100615.	105580.
	100355.	105035.
	99800.	104200.
	98000.	104205.
	99640.	105145.
	99775.	105075.
	99510.	105555.
	99830.	105275.
	100160.	105285.
	102230.	106060.
	100565.	105640.
	99965.	104205.
	101280.	104205.
	100390.	105820.

*** NO RECORD OCT. 10 16:00 - OCT. 15 14:00 ***

DATE	X-EAST (meters)	Y-NORTH (meters)
1985 OCT. 15	99110.	105380.
	100190.	104205.
1985 OCT. 16	99490.	104835.
	98050.	104205.
	98520.	104620.
	99960.	104335.
	99365.	104655.
	100580.	104205.
	100295.	104205.
	98810.	105375.
	98690.	106100.
1985 OCT. 17	100285.	104930.
	99645.	102855.
	100150.	104955.
	101015.	105410.
	99995.	104205.

	100415.	105045.
	98205.	104755.
	100235.	104850.
	99785.	104205.
	101525.	105085.
	100265.	104795.
	99990.	104935.
	99830.	104080.
	99675.	105200.
1985 OCT. 18	99390.	104500.
	99950.	104940.
	101615.	105200.
	99420.	103765.
	100765.	104830.
	99385.	104065.
	99835.	105400.
	99720.	105100.
1985 OCT. 19	100445.	105070.
	101060.	104205.
	99545.	105275.
	98985.	104305.
	98265.	105375.
	99110.	105380.
	99710.	105175.
1985 OCT. 20	102000.	105400.
	99985.	104440.
	98915.	105315.
	99665.	103090.
	101630.	105130.
	101000.	104855.
	102080.	105140.
	100810.	104850.
1985 OCT. 21	101415.	105710.
	100760.	105085.
	101775.	105295.
	98425.	104205.
	101665.	105200.
	98950.	104205.
	101400.	105170.
	98420.	104320.
	98765.	104415.
	99540.	103655.
	98425.	104335.
	100815.	104990.
	98820.	105030.

*** NO RECORD OCT. 21 23:30 - OCT. 22 15:00 ***

1985 OCT. 22	100885.	105305.
	99415.	103895.

	100515.	104920.
	99640.	104985.
1985 OCT 23	99825.	105955.
	100330.	105935.
	100065.	104835.
	99025.	105085.
	100155.	104535.
	99690.	104180.
	99400.	103800.
	99735.	105185.
	99885.	106040.
	98240.	104205.
	99125.	105790.
	101440.	105295.
	99530.	105625.
	101225.	105280.
	98970.	105485.
1985 OCT. 24	98585.	105340.
	99230.	106490.
	100185.	104915.
	100150.	104810.
	99070.	105420.
	100540.	105955.
	99405.	104050.

*** NO RECORD OCT. 24 18:30 - OCT. 25 15:00 ***

1985 OCT. 25	101115.	104805.
	100160.	104895.
	99125.	104050.
	99300.	104440.
	99410.	104010.
1985 OCT. 26	100230.	105385.
	101665.	105465.
	100070.	104870.
	99895.	104610.
	98960.	105945.
	98950.	104205.
	98750.	104180.
	99235.	106265.
	100310.	104995.
	99765.	104205.
1985 OCT. 27	98885.	103930.
	101485.	105110.
	99415.	103665.
	101525.	105145.
	101265.	104715.
	101690.	105305.
	101860.	104945.
	101370.	105315.

	99245.	104265.
	100440.	104920.
	101055.	105295.
	99625.	104665.
1985 OCT. 28	99895.	104045.
	99200.	106385.
	101790.	105760.
	99800.	105030.
	101285.	104865.
	99440.	104465.
	100475.	103980.
	99910.	105255.
	101690.	104890.
	100460.	104425.
	100850.	106295.
	99645.	102810.
	101330.	104990.
	100505.	105020.
	98800.	104440.

*** NO RECORD OCT. 28 21:00 - OCT. 29 15:00 ***

1985 OCT. 29	99445.	103400.
	100255.	104645.
1985 OCT. 30	100305.	104600.
	99910.	104055.
	99970.	104660.

*** NO RECORD OCT. 29 09:00 - NOV. 13 15:00 ***

1985 NOV. 13	98890.	104545.
	100440.	104560.
	98920.	104500.
	98465.	104550.
1985 NOV. 14	99515.	105450.
	98100.	104610.
	100700.	104870.
	101280.	104820.
	100370.	104995.
	100240.	104825.
1985 NOV. 15	98990.	105525.
	101565.	104590.
	101795.	104670.
	99535.	104610.
	100195.	105005.
	100560.	105210.
	99780.	104705.
	100210.	104820.

1985 NOV. 16	99625.	104825.
	99580.	105050.
	98850.	104525.
	99805.	105170.
	99555.	104460.
	99200.	104100.
	98410.	104965.
	100225.	104975.

*** NO RECORD NOV. 16 16:00 - NOV. 18 15:00 ***

1985 NOV. 18	101155.	103875.
1985 NOV. 19	98790.	104335.
	100805.	105100.
	100590.	105065.
	99525.	104615.
	100185.	105370.
	100250.	105130.
	101135.	105315.
	99670.	104925.
	100525.	105010.
1985 NOV. 20	100710.	104315.
	99370.	105290.
	100095.	104005.
1985 NOV. 21	99370.	105425.
	98635.	105425.
	98635.	104555.
	99115.	105240.
	100540.	104375.
	100390.	104420.
1985 NOV. 22	100825.	105040.
	100010.	103500.
	100620.	104285.
	100195.	104825.
	102070.	105160.
	99570.	104995.
	102225.	105865.
	99015.	105960.
	99215.	104920.
1985 NOV. 23	100745.	104410.
	100520.	104770.
	100140.	105035.
	100595.	104810.
	102005.	105165.
	100005.	103805.
	100360.	103840.
	100185.	104790.
	99900.	103600.
	99370.	104075.

```
                    99365.           104535.
                   101050.           105470.
                    99250.           104170.
                   102060.           106300.
                   101985.           105705.
                    98130.           105215.

1985 NOV. 24       100600.           104700.
                    99145.           106460.
                    99340.           104890.
                   100000.           104200.
                   102340.           106450.
                    98180.           105645.
                    98445.           104275.
                   100525.           104260.
                   100300.           104830.
                   101710.           105640.
                    99260.           104715.
                   100865.           105755.
                    99590.           103780.
                    99640.           103270.
                    98885.           105645.
                    99735.           104510.

  ***   NO RECORD NOV. 25  06:00 - NOV. 26  15:00   ***

1985 NOV. 26       100815.           106520.
                   100470.           104710.

  ***   NO RECORD NOV. 27  01:30 - NOV. 29  15:00   ***

1985 NOV. 29        99820.           105160.
                    99615.           103015.
                    99400.           104970.
                   100500.           104920.
                   100405.           105810.

1985 NOV. 30        99975.           103325.
                    98300.           104190.
                   100670.           105450.
                    99460.           105620.
                   100080.           104985.
                   100175.           104565.
                    98760.           104770.
                   101675.           104865.
                   100855.           104255.
                    99995.           104075.
                    99440.           106525.
                   100140.           103515.
                    99315.           105040.

1985 DEC. 01       100260.           104800.
```

*** NO RECORD DEC. 01 06:00 - DEC. 03 16:00 ***

1985 DEC. 03	100590.	106550.
	100350.	104555.
	99655.	105525.
	99070.	105880.
	101330.	104255.
1985 DEC. 04 ✓	101615.	103425.
	100330.	102960.
	98935.	104730.
	100090.	104595.
	100200.	104830.
	98950.	104520.
	99700.	105275.
	99660.	105315.
	98915.	105280.
	100180.	104805.
	98830.	104590.
	99990.	104815.
	98710.	106230.
	99185.	105055.
	100280.	105670.
	101695.	105530.
	99815.	104890.
1985 DEC. 05	98760.	104200.
	98800.	104200.
	100810.	104240.
	99665.	106550.
	100775.	104240.
	98830.	104620.
	100845.	104255.
	99900.	105250.

Volume

2

McGill University

CONTRACT SERIAL NUMBER 69121-01-SQ
DSS REQUISITION NUMBER 23440-6-9121
CONTRACTOR: POTASH CORP. OF SASKATCHEWAN

A REPORT TO THE DEPARTMENT OF SUPPLY & SERVICES

CONTRACT # 04SQ-23440-6-91210

ON

RESEARCH ON MICROSEISMIC MONITORING

VOLUME II

FEBRUARY 1988

MICROMEDIA

173 pp.

TABLE OF CONTENTS

SECTION 5: COMPUTER PROGRAM FOR AUTOMATION OF ROCK MONITOR UNIT

SECTION 6: ESTIMATION OF GEOSTRESS USING THE KAISER EFFECT OF ACOUSTIC EMISSIONS

SECTION 7: PRELIMINARY STUDY OF THE PETROFABRIC AND STRESS INDUCED MICROFRACTURES IN RELATION TO ACOUSTIC EMISSIONS ON POTASH ROCK SALT

5

Computer Program for
Automation of Rock Monitor Unit

Dr. F.P. Hassani

Mr. Andrew Dasys

McGill University
Department of Mining Engineering

May 6th, 1987

TABLE OF CONTENTS

PROGRAMMING MANUAL

INTRODUCTION 1
DESIGN PHILOSOPHY 2
ADDING A FUNCTION OR MENU TO THE PROGRAM 5
MODIFYING THE ANALOG TO DIGITAL CARD 7

PROGRAM LISTING

type 8
const 9
var 9
procedure DisplayStr 10
procedure TransformFiles 11
procedure InitParam 11
function Keyin 12
function ADConvert 12
procedure Cumulate 12
procedure UnCumulate 13
procedure UpdateDisplay1 13
procedure UpdateDisplay2 14
procedure String_handler 14
procedure Rs232_interupt 16
procedure Rs232_init 17
procedure Initialize 17
procedure Cleanup 17
procedure MenuWindow 18
procedure WindowInit 18
procedure Frame 19
procedure ClearWindow 19
procedure DoFunc 20
procedure ChooseFunc 25
program Main Body 26

PROGRAMMING MANUAL

INTRODUCTION

The following is the programming manual that is included with the RM-6 interface program. It outlines the basic system requirements that are required in order to be able to run the program. Also included in this manual is a list of all of the procedures that are found in the interface program. If modifications are required to the program the method for implementing them is also included. This manual covers Version 1.0 of the program. This is the version of the program that was demonstrated at McGill in April 1987. Version 2.0 is now being tested. The major differences between the two version is:

- Version 2.0 Supports all six channels.
- Version's 1.0 plotting Bugs have been worked out.
- More types of plotting are supported.

The interface program is written in Turbo Pascal, and uses the Turbo Graphics Toolkit to produce the windowing on the screen. Because of this a certain number of files must be included on the disk that contains the interface program. These files are the fonts that are used to print information on the screen. (It should be noted that the Turbo Graphics Toolkit does not use the standard ROM resident IBM text font, and it is for this reason that additional files must be accessed.)

The minimum system that is required in order to run the interface program is an IBM-PC computer (or true compatible) with 2 drives (or a hard disk), a Hercules Graphics Card (or compatible), one RS-232 serial connector (configured as COM1:) and 512K of memory. It is possible to use an IBM CGA card instead of the Hercules Graphics Card, however in this case the interface program will have to be recompiled. The recompilation may also require changing certain parts of the code, since the code was specifically written for the HCG. Finally using the CGA will decrease the resolution of the display, and thus decrease the clarity of the information that is presented on the screen.

DESIGN PHILOSOPHY

Because the system was designed to be user friendly, the user is prompted to use only the function keys to request information or change the program parameters. The function key menu is displayed in the upper left hand side of the screen. The lower half of the screen is used by the program to prompt the user for information (define drive, name files....). This part of the screen is also used to display one of the two possible graphs that can be displayed during the test. (i.e. Event-Count vs. Time and Stress-Factor vs. Time). The second graph is located in the upper right hand side of the screen, and shows the stress-strain curve of the sample under test.

Because the function keys "run" the program, each one of the keys "points to" a given function number. The function number is then used to select an operation inside a case statement. The order of the help menus is implemented in the same manner. This type of multi-branched tree structure allows new functions (or menu levels to easily be added). Adding functions will be outlined in one of the later sections of this manual.

The program interfaces to the outside world by using an Analog to Digital (A/D) card and an RS-232 port. The A/D card is used for the input of the load and displacement readings during testing. The system expects the results of the A/D conversion to be passed as an integer resulting from a function call.

The RS-232 port (configured at 4800 baud) is used to input information from the Rock Monitor. Since the rock monitor sends its information in an ASCII format the program must translate it into numerical values. During the writing of the program it was decided to access the serial port (RS-232) using interrupt driven routines, instead of polling the port. The routines that are used by the program are outlined in this section.

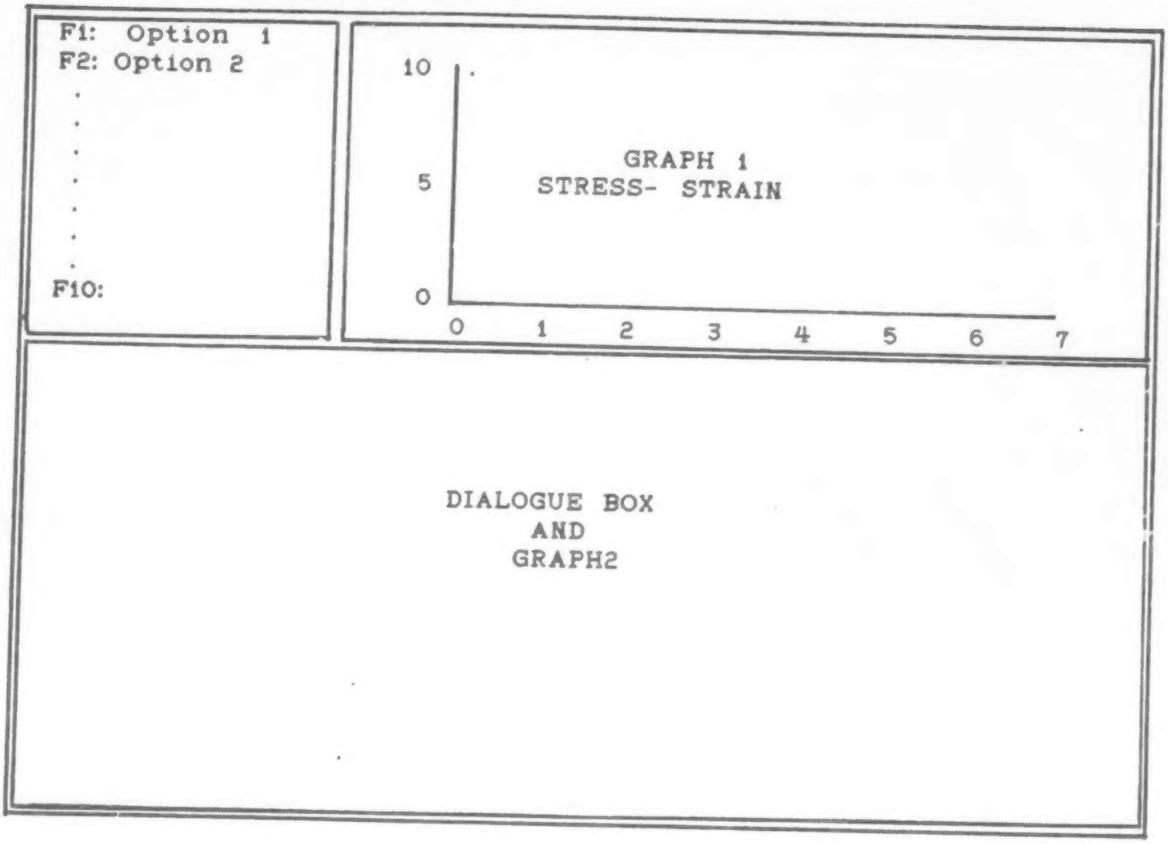
F1: Option 1
F2: Option 2
F10:
10
5
0
GRAPH 1
STRESS- STRAIN
0
1
2
3
4
5
6
7
DIALOGUE BOX
AND
GRAPH2

The above figure gives the general placing of the three windows during the operation of the program. The following section of the manual looks at the programming that is required in order to change the menu options that are located in the upper-left-hand corner of the screen.

ADDING A FUNCTION OR MENU TO THE PROGRAM

Since the program is menu driven it is possible to build new menus for the system. All of the operations are controlled by the function keys. When a key is hit the program jumps out of the main program and goes to the CHOOSEFUNC procedure:

"If Keypressed then ChooseFunc(Keyin) "

KEYIN is a function that returns the scan code for the key that was hit. If keyin corresponds to one of the function keys then DoFunc(function #) is called. "Function #" represents a function number that is associated to the key that was pressed. These function numbers are stored in an array called. f_val[1..10]. Since the array holds integer values the program can have a total of 65,536 different functions.

DOFUNC() is the largest, and most important part of the program. It is within DOFUNC() that all of the other parts of the program are called. DOFUNC() is one large case statement that takes the function number that was passed and executes the appropriate case. Each case contains a set of statements that represent the called function.

As an example function #-999 represents the set of statements that is executed when a function key is hit and there is no associated function. In this case a message is sent to the lower part of the screen informing the user that there has been a mistake and that another key must be hit.

In order to add a function, to the program, the following steps must be taken:

1 - A function number should be added to the list that is located within DOFUNC(). (Make sure the function number does not already exist.)

2 - Write in the statements that are required to execute the new function.

3 - Associate the function number to a function key by placing the function number in the f_val[] array.

4 - Give the function a name that will appear on the screen by placing a word (10 letters maximum) in the array Menu_list[]. The array index should correspond to the function key number that is pressed to access the function. (i.e. same index as that used in the f_val[] array).

5 - Recompile the program.

In order to add a new menu to the program both the f_val[] and the menu_list arrays must be filled in. This is done in function heading number 1 and 11 where the main menu and the graph style menu are created.

The second step in creating a new menu is to link it to a previous menu so that it can be called. In the example of the main menu (function number 1) it is linked in function number 11 under f_val[1] := 1. One of the design standards used was to use function key number 1 to send the user back to the previous menu.

Another standard was to use the function numbers as a path. Thus function number 12 represents the actions that are taken when function key 2 is pressed, in a menu that was called from function key 1.

MODIFYING THE ANALOG TO DIGITAL CARD

The methods that are used to access the A/D cards vary from one producer to the other. Because of this it is unlikely that the A/D card that will be installed has the same protocol as the one that was used to write the software. In order to install a new card follow the manufacturers directions. To interface the card to the program the only function that needs to be modified is the ADConvert FUNCTION.

ADCONVERT expects a channel number which must be integer and returns an integer that is the result of the conversion. Since an integer is 16bytes long, on the IBM PC, a 12bit A/D card can easily be installed in the machine. It may however be advisable to zero the topmost 4 bits in order to make sure that the result of the conversion is in fact 12 bits long. The turbo pascal Port command is used to access the logical address of the card, listed as card_base in the procedure.

PROGRAM LISTING

```
program  ae;
{$I   a:typedef.sys}
{$I   a:graphix.sys}
{$I   a:kernel.sys}
{$I   a:windows.sys}
{$I   a:axis.hgh}
{$I   a:findwrld.hgh}
{$I   a:polygon.hgh}
{$I   a:hatch.hgh}
{$I   a:histogrm.hgh}

type
INS8250  =  record  THR:  integer;
                    RBR:  integer;
                    IER:  integer;
                    LCR:  integer;
                    MCR:  integer;
                    LSR:  integer;
                    MSR:  integer;
               end;

      Registers  =  record
                      AX,  BX,  CX,  DX,BP,  SI,  DI,  DS,ES,Flags:  integer;
                    end;

      Baud       =   (B110,B150,B300,B600,B1200,B2400,B4800,B9600);
      Parity     =  (None,  Odd,  Nevermind,  even);

      data_array  =  array  [1..6]  of  real;

      data_descrip  =  record
                         recnumb  :  integer;
                         stress   :  real;
                         Strain   :  real;
                         Ev       :  Data_array;
                         SF       :  data_array;
                         end;

     long         =   string[200];
     lines        =   string[50];
     words        =   string[10];
```

```
      menu_words  =  array  [1..10]  of  words;

const

   Rs232:array  [1..2]  of  INS8250  =
          ((THR:$3F8;RBR:$3F8;IER:$3F9;
            LCR:$3FB;MCR:$3FC;LSR:$3FD;MSR:$3FE),
           (THR:$2F8;RBR:$2F8;IER:$2F9;
            LCR:$2FB;MCR:$2FC;LSR:$2FD;MSR:$2FE));

     Data_segment:  integer  =  0;
     Card_base               =   632;
     help_win                =   1;
     stress_win              =   2;
     opt_win                 =  3;        { window number definitions}
     gen_win                 =   4;
     tem_win                 =   5;
     max_channel  =  6;

     stress_world  =  1;
     tem_world   =   2;


var
      COM                     :  Byte;
      Rs_error                :  byte;
      Buffer                  :  array  [0..4096]  of  char;
      buf_head, Buf_tail      :  integer;
      Regs                    :  Registers;
      Char_in                 :  integer;
      receipt                 :  boolean;
      lfcount                 :  integer;
      upper, temp,i,ii        :  integer;
      t_sf                    :  array[1..6]  of  real;
      t_ev                    :  array[1..6]  of  real;

      menu_list               :  menu_words;
      f_val                   :  array  [1..10]  of  integer;
                              {  function  number}
      act_window              :  array  [1..15]  of  boolean;
      graph_type,chan_select   :integer;
      text_display,  latch  :boolean;  {  lock  the  second  display  }

      Window_head,  sec_header  :  string[25];
      read_numb                 :  integer;
      running, stop_prog        :  boolean;
      G2_style, channel         :  integer;{  graph2  style  and  channel  }
```

```
{===================}
{=  SAMPLE  DATA   =}
{===================}
      S_height:  real;
      S_diam  :  real;
      S_array :  array  [1..6]  of  lines;

{====================}
{=   FILES   DATA   =}
{====================}
      Files_saved,  Disks_init  :  Boolean;
      data                      :  data_descrip;
     F_data                     :  file  of  data_descrip;
      F_datat,
      F_final                   :  text;
      Fdata_namt  ,
      Fdata_namd  ,
      Ffinal_name               :  string[15];
      f_name                    :  string[8];
      d_name                    :  string[1];

 filvar                         :  text;
 dummy                          :  char;

{================}
{=  AXIS  DATA  ==}
{================}
      Display_1,  display_2  :PlotArray;


procedure   DisplayStr(text_string:lines;  delay:integer);
var  i,  counter:integer;
begin
             SelectWindow(opt_win);
             StoreWindow(opt_Win);
             SetBackground(0);
             DrawBorder;
             DrawText(30,250,2,Text_string);
             for  i:= 1  to  delay  do
               for  counter  :=  1  to  100  do;
             RestoreWindow(opt_win,0,0);
end;   {DisplayString}
```

```
procedure  transformFiles;
{ merge the two files to make a prn file }
var   t:string[100];
begin
  assign(f_final,ffinal_name);
  rewrite(f_final);
  reset(F_datat);
  while  not  eof(F_data)  do
   begin
    read(F_datat,  t);
    writeln(F_final,t);
   end;  {  while  loop}
  close(F_datat);
  reset(filvar);
  while  not  eof(filvar)  do
   begin
    read(Filvar,   t);
    writeln(Filvar,t);
   end;   {   eof}
   close(f_data);
   close(f_final);
end; {transform  files  }



{======================}
{= intialization      = }
{======================}
procedure  InitParam;
begin
   running  :=  false;
   latch    :=  false;
   text_display  :=  false;
   stop_prog  :=  false;
   Read_numb  :=  1;
   Chan_select := 1;          { default to the number 1 transducer }
   G2_style := 1;             { histogram of the event count }
   DisKs_init  :=  false;
   Files_saved  :=  false;
   DefineWindow(tem_win,  XMAxGlb  div  2  -  13  ,  YMaxGlb  div  2  ,
XMaxGlb  -  1,  YMAxGlb  -  1);
   DefineWorld(tem_world,0,100,10,0);

{init  the  value  in  the  array  menu_list}
```

```
           menu_list[1] := 'Initialise';                 f_val[1]   :=   11;
           menu_list[2]  :=  'Start  Test   ';           f_val[2]   :=   2;
           menu_list[3]  :=  'Set  Display  ';           f_val[3]   :=   3;
           menu_list[4] := ' ';                          f_val[4]   :=   -999;
           menu_list[5] := ' ';                          f_val[5]   :=   -999;
           menu_list[6] := ' ';                          f_val[6]   :=   -999;
           menu_list[7] := ' ';                          f_val[7]   :=   -999;
           menu_list[8] := 'Test';                       f_val[8]   :=   -1;
           menu_list[9] := 'Save data';                  f_val[9]   :=    9;
           menu_list[10]:= ' Quit';                      f_val[10]:=   0;

           Window_head := 'Main Menu';
  end;  {  InitPAram  }


  Function  keyin:integer;
  {==================================}
  Var  Key:byte;

  Begin
   Regs.AX:=$0700;
   MsDos(Regs);
   Key:=Lo(Regs.AX);
   if Key = 0 then
     Keyin:=Keyin*256
   else
     Keyin:=Key;
   end;    {Keyin}

 {     ========================================}
    function   ADConvert(channel:integer):integer;
    var  a,b,high,low  :  integer;
     i   :integer;
    begin
      port[card_base] := channel;
      b:= port[card_base + 3  ];
      for i := 1 to 10 do
          a:= port[card_base  +  4];
      for i := 1 to 10 do
          a:= port[card_base  +  5];
       high  :=( port[card_base  +2]  and  15);
       low   :=  port[card_base  +1]  ;
       ADConvert := high * 256 + low;
    end; { of A to D conversion  }
{    ============================================}
{
{       Display management                      }
{                                               }
                                                }
{===============================================}
```

```
procedure  Cumulate(upper:integer;var  display:PlotArray);
var  i:integer;
 begin
  for i:= 1 to upper do
   display[i+1,2]  :=  display[i+1,2]  +  display[i,2];
end;  {cumulate}

procedure  UnCumulate(upper:integer;  var  display:PlotArray);
var i  ,count  :integer;
  begin
   for count:= 1 to upper-1 do
    begin
     i := upper - count +1;
    display[i,2]  :=  display[i,2]  -  display[i-1,2];
    end; {  for  loop  }
  end;  {UnCumulate}



procedure  UpdateDisplay1;
var  tempflip  :real;
begin
          If read_numb <= 3 then
          begin
           SetHeaderToBottom;
            DefineHeader(stress_win,'Stress  Factor');
            SetHeaderOn;
            SelectWorld(stress_world);
            SelectWindow(stress_win);
            SetBackground(0);
            drawBorder;
            DrawAxis(8,8,2,2,2,2,0,0,false);
            for i:= 1 to read_numb do
            DrawPoint(Display_1[i,1],display_1[i,2]);
          end { less than 3 readings}
         else
          begin
           FindWorld(stress_world,Display_1,Read_numb,1,1);
               With  World[stress_world]  do
               begin
                tempflip:=  Y1;
                Y1  :=  Y2;
                y2:=  tempflip;
                y1  :=  0;
           end; { with loop }
        SetHeaderToBottom;
        DefineHeader(stress_win,'Stress  Factor');
        SelectWorld(stress_world);
        SelectWindow(stress_win);
        SetBackground(0);
        DrawBorder;
        DrawAxis(8,8,2,2,2,2,0,0,false);
        DrawHistogram(display_1,read_numb,false,1);
       end;        { if-then-else  }
    end;  {  updatedisplay1}


procedure  UpdateDisplay2(graph_style,  channel:integer);
  var tempflip : real;
  begin

       If read_numb <= 3 then
       begin
         SetHeaderToTop;
         DefineHeader(tem_win,sec_header);
         SetHeaderOn;
         SelectWorld(tem_world);
         SelectWindow(tem_win);
         SetBackground(0);
         drawBorder;
         DrawAxis(8,8,2,2,2,2,0,0,false);
         for i:= 1 to read_numb do
         DrawPoint(Display_2[i,1],display_2[i,2]);
       end { less than 3 readings}
      else
       begin
        FindWorld(tem_world,Display_2,Read_numb,1,1);
           With World[tem_world] do
           begin
            tempflip:=  Y1;
            Y1  :=  Y2;
            y2:=  tempflip;
            y1  :=  0;
           end; { with loop }
         SetHeaderToTop;
         DefineHeader(tem_win,sec_header);
        SelectWorld(tem_world);
        SelectWindow(tem_win);
        SetBackground(0);
        DrawBorder;
        DrawAxis(8,8,2,2,2,2,0,0,false);
        DrawHistogram(display_2,read_numb,false,1);
{       DrawPolygon(Display_2,  1,  read_numb,4,1,0);}
       end;       { if-then-else  }
    end;  {  updateDisplay2}


  {======================}
  {=  RS  232  Parameters  =}
  {======================}


  procedure  string_handler;
     var  i,  ii,  temp  ,  err:integer;
          base   :integer;
          tempflip:   real;
          temp_st:string[9];
          sigma, epsilon:real;            {temp  value  for  the  stress  and  the
 strain}

     begin
      receipt:=false;
      lfcount:=   0;
      base   :=0;
      repeat
        base:=   base+1;
      until  (buffer[base]  =  'E');
      base:=   base+2;

    for  ii:=  0  to  5  do
     begin
       temp_st:='          ' ;
        temp   :=   ii*10+base;
       for  i:=  1  to  9  do
        if  (buffer[temp+i]  <>  ' ')  then
          temp_st[i]:=   buffer[temp+i]
        else
          temp_st[i]:=    '0';
       Val(temp_st,t_ev[ii+1],err);
    {do  the  same  thing  for  the  SF}
    end;
    base:=   80;
    repeat
      base:=   base+1;
    until   (buffer[base]   =   'S');
    base:=   base+2;
    for  ii:=  0  to  5  do
    begin
       temp_st:='          ' ;
         temp   :=   ii*10+base;
       for  i:=1  to  9  do
        if  (buffer[temp+i]  <>  ' ')  then
         temp_st[i]  :=  buffer[temp+i]
```

```
          else
            temp_st[i]  :=  '0';
           Val(temp_st,t_sf[ii+1],err);
       end;
      read_numb := read_numb + 1;

  {send to a test file for analysis}
      write(f_datat,read_numb:5);
       writeln(f_datat,t_ev[1]:8:1,'     ',t_sf[1]:8:1);


  {place the information here for the update of the values}
            Display_1[read_numb,1]  :=read_numb;
              Display_1[read_numb,2]  :=  t_sf[1];
        updateDisplay1;
        { this is temporary }
            Display_2[read_numb,1]  :=  read_numb;
            if G2_style = 1 then
              Display_2[read_numb,2]  :=  t_ev[1]
            else
              Display_2[read_numb,2]  :=  Display_2[read_numb-1,2]  +
 t_ev[1];

      updateDisplay2(g2_style,1);
 { if the latch is set then update second display}
       buf_head:= 0;
       Buf_tail:=0;
 {send the information to the disk file for storage }
 {      with data do
        begin
          recnumb := read_numb;
          for i := 1 to 6 do
            begin
            ev[i]  :=  t_ev[i];
            sf[i]  :=  t_sf[i];
            end;
        end;}
         { with loop }
 end; {  string_handler  }


Procedure  Rs232_interupt;
var  bb:byte;
begin
  inline  ($50/
           $53/
           $51/
           $52/
           $57/
```

```
            $56/
            $06/
            $1E/
            $FB/
            $2E/$a1/Data_segment/
            $8E/$D8);
  Rs_error  :=  port  [rs232[com].lsr];{  and  $1E;}
   bb:=   port[rs232[com].rbr];
   if  bb  =  13  then  lfcount:=lfcount+1;
  Buffer[Buf_tail]:=  char(bb);
  buf_tail:=(buf_tail+1)  mod  4096;
  inline($FA);
  port[$20]:=$20;
  if  (lfcount  >=  2)  then
     string_handler;
  inline  ($1f/
           $07/
           $5E/
           $5f/
           $5A/
           $59/
           $5B/
           $58/
           $8b/$E5/
           $5D/
           $CF);
 end;  {rs232_interupt  }


procedure  rs232_init(speed:baud;  P:parity;  Stop,length:  Byte);
 Begin
  regs.DX::=com-1;
  regs.AX::=ord(speed)*32  +  ord(p)*8  +  (stop-1)*4  +  length  -5;
  intr($14,Regs);
 end;  {rs232_init  }



procedure  initialize;
var  i:integer;
begin
for  i:=  0  to  4096  do
buffer[i]:=char($00);
  Regs.AX:=$250D-com;
  Regs.DS::=cseg;
  Regs.DX::=ofs(Rs232_interupt);
  MsDos(Regs);
```

```
      if com =1 then
       port[$21]:=port[$21]  and  $EF
      else
       port[$21] := port[$21] and $F7;
      port[Rs232[com].LCR]:=port[rs232[com].LCR]  and  $7F;
      port[rs232[com].IER]  :=  1;
      Port[Rs232[COM].MCR]:=$08;
   DisplayStr('in  initialize',100);
    end;

   procedure cleanup;
   var  i:integer;
     begin
      port[$21]:=port[$21]  or  $18;
      port[Rs232[COM].LCR]:=port[Rs232[com].LCR]  and  $7f;
      port[Rs232[COM].IER]:=0;
      Port[Rs232[COM].MCR]:=0;
     end;  {cleanup}


   {****************************************
   {*          WINDOWS & MENUS    ***************************}
   {*******************************************         * }
   {*******************************************************}

  procedure MenuWindow(Menu_list : menu_words);
  var  i  :integer;
      s   :string[2];
  begin
  { Define the help menu window }
    DefineWindow(help_win, 0, 0, XMAxGlb div 2 - 15, YMAxGlb div
  2-10);
    DefineHeader(help_win,Window_Head);
    SetHeaderOn;
    SelectWindow(Help_win);
    SetBackground(0);
    Drawborder;
       for i := 1 to 10 do
       begin
            str(i,s);
            DrawText(10, I*15 + 2, 2, 'F' + s + ' - ' +
 menu_list[i]);
      end; {for loop }
   act_window[Help_win] := true;
 end;  {MenuWindow}

 procedure  WindowInit;
 { set up the screen with three screens}
 { help window, stress window, option window }
 var dum :char;
```

```
begin
      SetWindowModeOn;
        MenuWindow(menu_list);

 {Define the stress_fact window }
     DefineWindow(stress_win, XMAxGlb div 2 - 13 , 0, XMaxGlb - 1,
YMAxGlb div 2 - 2);
     DefineHeader(1,'Stress  Factor');
     SetHeaderOn;
 {set up the axis for stress strain }
      DefineWorld(stress_world,0,100,10,0);
      SelectWorld(stress_world);
      SelectWindow(stress_win);
      DrawBorder;
      DrawAxis(8,8,2,2,2,2,0,0,false);



{Define the options window }
     DefineWindow(opt_win,0, YMaxGlb div 2, XMAxGlb-1, YMAxGlb-1);
     SelectWindow(Opt_win);
     SetBackground(0);
     Drawborder;

end;  {window_init}

procedure  Frame(window,UpperLeftX,  UpperLeftY,  LowerRightX,
LowerRightY:  Integer);

{==================================================================
========}
    { create a text window of the required size }
    var  i  :integer;
   begin  {Frame}
    DefineTextWindow(window,upperleftX,upperleftY,lowerrightx,
lowerRightY,4);
     selectWindow(window);
     SetBackgroundColor(0);
     SetForegroundColor(0);
     SetBackground(0);
     GotoXY(UpperLeftX,  UpperLeftY);
     Write(chr(201));
       for I := (UpperLeftX + 1) to (LowerRightX - 1) do
       begin
         Write(chr(205));
       end;
       Write(chr(187));
       for I := (UpperLeftY + 1) to (LowerRightY - 1) do
       begin
        GotoXY(UpperLeftX  ,  I);  Write(chr(186));
```

```
         GotoXY(LowerRightX,   I);   Write(chr(186));
        end;
         GotoXY(UpperLeftX,  LowerRightY);
         Write(chr(200));
         for I := (UpperLeftX + 1) to (LowerRightX - 1) do
         begin
           Write(chr(205));
         end;
           Write(chr(188));
         end;  {Frame}


 Procedure  ClearWindow(win_numb:integer);
       begin
               SelectWindow(win_numb);
               StoreWindow(Win_numb);
               SetBackground(0);
               DrawBorder;
       end; {  ClearWin  }



{*********************************************************}
{*          FUNCTION CONTROLS                           * }
{*********************************************************}

procedure  DoFunc(choice:integer);
{==============================}
var  sec_choice, i  :  integer;
    dum : char;
  begin
   case  choice  of
     -999  :  begin
              ClearWindow(opt_win);
              DrawText(180,250,2,'THIS FUNCTION IS NOT YET
SUPPORTED');
              DrawText(270,275,2,'Try  again');
              repeat  until  keypressed;
              RestoreWindow(opt_win,0,0);
          end;  {  not  suppoted  }

     -1   :begin
          end;  {  test  function  }

    0 : begin            {  this  is  the  time  to  quit  }
              if  (files_saved)  or  not(running)  then
              begin
                 ClearWindow(opt_win);
```

```
            DrawText(230,240,2,'TO  QUIT  HIT  F10');
            DrawText(230,270,2,'Other  to  Resume');
              if ( Keyin = 17408 ) then
                stop_prog := true
              else
              begin
                SetBackground(0);
               Drawborder;
                RestoreWindow(opt_win,0,0);
              end;  {  else  }
          end
          else
           begin
           ClearWindow(opt_win);
           DrawText(230,240,2,'Files  not  Saved  ');
           DrawText(230,280,2,'Use  Function  9');
           if ( Keyin = 17152 ) then
           Dofunc(9)
           else
           begin
             SetBackground(0);
             Drawborder;
             RestoreWindow(opt_win,0,0);
          end; { if then else Keyin }
         end; { if then else files_saved }
     end;  {  end  Quit}

1      : begin
        menu_list[1] := 'Initialise';              f_val[1]   :=   11;
        menu_list[2]  :=  'Start  Test  ';          f_val[2]   :=   2;
        menu_list[3]  :=  'Set  Display  ';         f_val[3]   :=   3;
        menu_list[4] := ' ';                        f_val[4]   :=   -999;
        menu_list[5] := ' ';                        f_val[5]   :=   -999;
        menu_list[6] := ' ';                        f_val[6]   :=   -999;
        menu_list[7] := ' ';                        f_val[7]   :=   -999;
        menu_list[8] := 'Test ';                    f_val[8]   :=   -1;
        menu_list[9] := 'Save Data';                f_val[9]   :=   9;
        menu_list[10]:= ' Quit';                    f_val[10]:=    0;

        Window_head  :=  'Initialize  Menu';
        MenuWindow(menu_list);
      end;  {  init  second  level  first  choice}

2      :begin       { start the test }
        {init the Rs-232 link }
         running := true;
         com:=1;
         buf_head   :=0;
         Buf_tail   :=0;
         Data_segment   :=Dseg;
```

```
              Rs232_init(b4800, even,1,7);
                 ClearWindow(opt_win);
                 Frame(opt_win,1,14,79,24);
                 gotoxy(29,15);write('GRAPH STYLE INITIALIZATION');
                 gotoxy(10,18);write(' Enter a 1 for events vs.
time');
                 gotoxy(10,19);write(' Enter other for ');
                 gotoxy(10,20);write('                    Cumulative Ev.
Vs. Time');
                 gotoxy(25,22); write(' Choice : ');
                 readln(g2_style);
                 if g2_style = 1 then
                   sec_header := 'Event Count'
                 else
                   sec_header := 'Cumulative Event Count';
                 gotoxy(35,24);write('Hit return');
                 readln(dum);
                 RestoreWindow(opt_win,0,0);
              initialize;
           {once all this is done then set up the bar chart
window}
           {Define the temp window }
    DefineWindow(tem_win, XMAxGlb div 2 - 13 , YMaxGlb div 2 ,
XMaxGlb - 1, YMAxGlb - 1);
{set up the axis for stress strain }
     DefineWorld(tem_world,0,100,10,0);
     SelectWorld(tem_world);
     SelectWindow(tem_win);
     DrawBorder;
     DrawAxis(8,8,2,2,2,2,0,0,false);
          end;       { start test option }

     3    :begin
           menu_list[1] := 'Previous';           f_val[1]  :=  1;
           menu_list[2]  :=  ' Ev.# / time';  f_val[2]  :=  32;
           menu_list[3]  :=  '+Ev.# / time';  f_val[3]  :=  33;
           menu_list[4]  :=  ' ';  f_val[4]  :=  -999;
           menu_list[5]  :=  ' ';  f_val[5]  :=  -999;
           menu_list[6]  :=  ' ';  f_val[6]  :=  -999;
           menu_list[7]  :=  ' ';  f_val[7]  :=  -999;
           menu_list[8]  :=  ' ';  f_val[8]  :=  -999;
           menu_list[9]  :=  '';  f_val[9]  :=  -999;
           menu_list[10]:=  '';  f_val[10]:=  -999;
           Window_head := 'Secondary display';
           MenuWindow(menu_list);
          end;       { set display second window }

     9  :  begin
            if disks_init then
            begin
            files_saved  :=  true;
            close(F_data);
            close(f_datat);
 {
             TransformFiles;}
            displayStr('All  data  files  closed',10);
         end
         else
         DisplayStr('Files  have  not  been  initialized.',200);
         DisplayStr('Use  Function  1  from  main  menu.',200);
        end;       { saving the data files }

   11     :begin
          menu_list[1] := 'Previous';
          menu_list[2] := 'All Data';                       f_val[1]  :=  1;
          menu_list[3] := 'File Data ';                     f_val[2]  :=  12;
          menu_list[4]  :=  'Sample  Data  ';               f_val[3]  :=  13;
          menu_list[5] := ' ';                              f_val[4]  :=  14;
          menu_list[6] := 'Comments ';                      f_val[5]  :=  -999;
          menu_list[7] := ' ';                              f_val[6]  :=  16;
          menu_list[8] := ' ';                              f_val[7]  :=  -999;
          menu_list[9]  :=  'Save  Settings  ';             f_val[8]  :=  -999;
          menu_list[10]:= ' ';                              f_val[9]  :=  19;
                                                      f_val[10]:=   -999;
          Window_head  :=  'Initialize  Menu';
          MenuWindow(menu_list);
          end;  { init  the  parameters  }
  12   :  begin
          DoFunc(13);
          DoFunc(14);
          DoFunc(15);
          DoFunc(16);
          DoFunc(19);
          DoFunc(1);
        end;        { Init all of the data in order }

  13   :  begin
               ClearWindow(opt_win);
               Frame(opt_win,1,14,79,24);
               gotoxy(30  ,  16);write('FILE  INITIALIZATION');
               gotoxy(9,  18);Write('Default  Drive  :  _');
               gotoxy(3,  20);write('Temporary  Disk  File  :
__________');

               gotoxy(3,  22);write('Transfer  Disk  File  :
__________');

               gotoxy(25,  18);  write('->  ');  readln(d_name);
               gotoxy(25,20)  ;  write('->  ');  readln(f_name);
               Fdata_namd  :=  d_name  +  ':'  +  f_name  +  '.dat';
```

```
                Fdata_namt := d_name + ':' + f_name + '.txt';
                gotoxy(25,22);  write('->   ');  readln(f_name);
                Ffinal_name := d_name + ':' + f_name + '.prn';
                gotoxy(35,24);write('Hit   return');
                readln(dum);
                Disks_init := true;
                RestoreWindow(opt_win,0,0);
             end;       { init the files }
   14  :  begin
                ClearWindow(opt_win);
                Frame(opt_win,1,14,79,24);
                gotoxy(29  ,  16);write('SAMPLE  INITIALIZATION');
                gotoxy(3,  18);Write('Sample  Height  (cm)  :
_______');
                gotoxy(3,  20);write('Sample  Diameter  (cm)  :
__________');
                gotoxy(25,18);write('->   ');  readln(S_height);
                gotoxy(25,20);write('->   ');  readln(S_diam);
                gotoxy(35,24);write('Hit   return');
                readln(dum);
                RestoreWindow(opt_win,0,0);
            end;      { init the sample }
   15  :  begin
          end;         { testdata }
   16  :  begin
                ClearWindow(opt_win);
                Frame(opt_win,1,14,79,24);
                gotoxy(29,15);write('COMMENT  INITIALIZATION');
                 for i := 1 to 6 do
                 begin
                 gotoxy(3,16+i);
writeln(i:2,'______________________________________________________________
                end; { for loop }                                            ');
                for i := 1 to 6 do
                begin
                gotoxy(3,16+i);
                write('->');
                readln(S_array[i]);
                end; {for loop}
              gotoxy(35,24);write('Hit   return');
              readln(dum);
              RestoreWindow(opt_win,0,0);
          end;      {comment}
   19 :begin            { save the information to text file }
      If disks_init then
      begin
```

```
              Assign(F_datat,Fdata_namt);
              rewrite(F_datat);
              writeln(F_datat,'"Data                is      stored      in      file
',Ffinal_name,'"'    );
              writeln(F_datat);
              for i:= 1 to 6 do
                writeln(F_datat,'"',S_Array[i],'"');
              writeln(F_datat);
              writeln(F_datat,'"  Diameter   :  "',  S_height:8:2);
              writeln(F_datat,'"  Height   :  "',  S_diam:8:2);
              writeln(F_datat);

              Assign(f_data,Fdata_namd);
              rewrite(F_data);

             end
            else
             Displaystr('Files   have   not   been   initialized,   use
F9',3000);

             end;       { save to text }

     32   :  begin
           { go to the disk file and read in all of the data }
             G2_style  :=  1;
             sec_header  :=  'Event  Count';
             UnCumulate(read_numb,Display_2);
             UpdateDisplay2(G2_style,1);
             DoFunc(1);
            end; {choose  the  first  graph  style}
    33      :  begin
             G2_style   :=2;
             sec_header  :=  'Cumulative  Event  Count';
             Cumulate(read_numb,Display_2);
             UpdateDisplay2(G2_style,1);
             DoFunc(1);
            end; {  choose  the  second  graph  style  }
    39    :begin
           if text_display then
            begin
             text_display  :=  false;
             ClearWindow(opt_win);
            end
           else
            begin
            text_display  :=  true;
            ClearWindow(opt_win);
```

```
              end;

             end;      { setup the window to display the incoming
  data }


      310  :  begin
               if latch then
                  latch := false
               else
                  latch := true;
              end;      { toggle the latch }


    end; {case of choice}
   end; {DoFunc}


 procedure  ChooseFunc(key:integer);
   {======================================}
   begin
     case key of
           15104:DoFunc(f_val[1]);
           15360:DoFunc(f_val[2]);
           15616:DoFunc(f_val[3]);
           15872:DoFunc(f_val[4]);
           16128:DoFunc(f_val[5]);
           16384:DoFunc(f_val[6]);
           16640:DoFunc(f_val[7]);
           16896:DoFunc(f_val[8]);
           17152:DoFunc(f_val[9]);
           17408:DoFunc(f_val[10]);
          {18432:down}
          {20480:up}
           end; {case }
  end; { procedure ChooseFunc }



{Program Main Body }
begin
 {set up the screen}
 initgraphic;
 InitParam;

 clearscreen;
 WindowInit;
```

```
{Main  loop  }
repeat
  if  Keypressed  then  ChooseFunc(Keyin);
until  stop_prog;

cleanup;
LeaveGraphic;
end.
```

Estimation of Geostress Using the Kaiser Effect of Acoustic Emission

This work is part of a study
being conducted for PCS Mining

McGill Microseismic Research Group
Department of Mining and Metallurgical Engineering
McGill University

February / 5 / 1988

Prepared by: Dr. F. P. Hassani
Mr. M. Momayezzadeh

Table of Contents

PAGE

A) INTRODUCTION 1

B) BRIEF LITERATURE SURVEY 4

B.1) UNIAXIAL CYCLIC LOADING 4
B.2) DIRECTIONAL LOADING 5
B.3) CONFINING PRESSURE 6
B.4) RETENTION TIME 7
B.5) PHYSICAL CHANGES 8

C) CASE STUDY 9

C.1) INTRODUCTION 9
C.2) SAMPLE PREPARATION 9
C.3) TESTING EQUIPMENT 10
C.4) TEST RESULTS 11
C.4.1) SAMPLE *5A* 12
C.4.2) SAMPLE *7A* 16
C.4.3) SAMPLE *L13* 20
C.4.4) SAMPLE *L14* 24
C.4.5) SAMPLE *L15* 28
C.4.6) SAMPLE *L16* 32
C.4.7) SAMPLE *U7* 36
C.4.8) SAMPLE *U13* 40
C.5) DISCUSSION 44

D) CONCLUSIONS AND RECOMMENDATIONS 47

REFERENCES 48

A) INTRODUCTION

The evaluation of initial geostress in a mine environment is an important step toward the design of a safe support structure. In practice parameters such as the magnitude of the stress to be carried and the strength of the structure are estimated rather conservatively, to provide an acceptable margin of safety.

More reliable data on the stresses acting on the structure, and more accurate estimates of its capability for carrying more load would result in increased extraction ratios.

Determining the in-situ stress, using conventional methods such as overcoring, hydrofracturing, flat jack, stress-meter, and sound-propagation velocity is often difficult and costly.

A new method would be to determine the in-situ stress by the Kaiser Effect of Acoustic Emission.

ASTM STP-505 defines Kaiser Effect as follows:
"The immediately irreversible characteristic of Acoustic Emission phenomenon, resulting from an applied stress. If the effect is present, there is little or no Acoustic Emission until previously applied stress levels are exceeded."

Dr. Joseph Kaiser of Munich was the first to discover the relationship between the stress and Acoustic Emission rate. He observed that when the stress on a metal under tension is relaxed from a level of historic high, and stressed again, there is little or no AE activity measured before the previous maximum is reached.

Once the level of historic high is exceeded, there is a significant increase in the rate of Acoustic Emission. This phenomenon is generally accepted as Kaiser Effect. Since then, it has been shown that many rock types exhibit Kaiser Effect (Hughson and Crawford, Ref.1).

Many researchers on the other hand have argued that this phenomenon can not be observed in every situation. For instance, Sondergeld and Estey (Ref.2) have reported that the Effect was not observed in tests at high stress levels. Based on their experimental data, these authors seriously question the significance of the Kaiser Effect in uniaxial compression of rocks. Holcomb (Ref.3) also believes that the existence of the Kaiser Effect for uniaxial cycling is unclear as will be further discussed below.

Despite the problems reported by some investigators, there is a lot of information pointing to the contrary. Assuming for now that Kaiser Effect is a reliable method, one can list a number of advantages in using it to estimate paleostress as compared to the more conventional methods.

The most important advantage of estimating previous stress level by measuring Acoustic Emissions is that Kaiser Effect is only dependent on stress; that is, one does not need to measure strain. This fact implies that in-situ measurements of stress using this method does not require a constitutive model of the rock mass under consideration (Holcomb, Ref.3). When employing the conventional methods of stress determination, such a model is usually required and more often than not, the model does not reflect the true characteristics and properties of the entire rock mass.

Other factors in favor of stress estimation via Kaiser Effect, is the fact that tests are reproducible, and it is less expensive and faster to test core samples in the laboratory. Therefore, if Kaiser Effect is proven to be a reliable method of estimating paleostress accurately, it would present an interesting alternative to the traditional methods.

B) BRIEF LITERATURE SURVEY

B.1) UNIAXIAL CYCLIC LOADING

Kaiser Effect studies on uniaxially compressed samples in laboratory have been carried out by a number of researchers. Kanagawa et.al. (Ref.4) may be the first to have made a serious effort to determine previous stress in geological materials using Kaiser Effect. They demonstrated that the Effect exists in tuff samples from boreholes. The cores were cut in various directions and loaded cyclically. The AE output rate versus the stress was plotted and the Kaiser Effect was spotted by the change in the slope of the curve. According to these authors, their values are compatible with those obtained by the overcoring method. Holcomb and Martin (Ref.5) also performed uniaxial tests under strain conditions and observed Kaiser Effect within few MPa of previous stress level.

Sondergeld and Estey (Ref.3) however, have seriously questioned "the significance and existence of the Kaiser Effect in uniaxial stressing of rock". Their results show that during subsequent loading of the Westerly granite sample, an overwhelming number of AE events was detected at stress levels well below the level of historic high. This could be attributed however, to equipment malfunction or the small size of the sample tested (5x1 cm).

Michihiro et.al. (Ref.6) have been successful in estimating Kaiser Effect in cubic (15x15x15 cm) and core (3x6 cm) specimens with 2% accuracy.

Hayashi et.al. (Ref.7) have presented a new method for determining Kaiser Effect with greater accuracy. They propose to plot the sum of AE rate vs stress (S_1) and the sum of AE rate squared vs stress (S_2) on the same graph. The point where the two curves diverge determines the stress at which Kaiser Effect is observed.

All Kaiser Effect studies with the exception of Sondergeld and Estey's (Ref.3) demonstrate that estimating paleostress using Acoustic Emissions is reproducible and in many cases a reliable method.

B.2) DIRECTIONAL LOADING

Directional loading tests are performed on laboratory samples and in-situ conditions by Michihiro et.al. (Ref.6) and Watters and Soltani (Ref.8) respectively. In the first instance, the authors studied the influence of principal stresses in different directions on Kaiser Effect. The three principal stresses which differed in strength, were repeatedly applied to a cubic specimen measuring 15x15x15 cm to obtain a saturated state of strain in the three directions, and a cylindrical specimen (3x6 cm) cored from each of the three principal directions of stress. Their studies show that in general Kaiser Effect in one direction was not affected by the stress from other directions and that the previous stress of a rock specimen in a saturated state of strain can be obtained within an error of ±2% by utilizing the Kaiser Effect method.

The tests carried out by Watters and Soltani (Ref.8) in the field are not as conclusive as the laboratory experiments conducted by Michihiro et.al. (Ref.6). They were successful in obtaining Acoustic Emission response from the rock mass by loading the borehole using a jack. The data showed Mogi and modified Mogi type behavior. In testing a granite boulder of dimensions 1x2x2 m, they observed directional behavior suggesting different AE levels in response to a stress field.

B.3) CONFINING PRESSURE

Holcomb (Ref.3) has conducted a thorough study on the determination of Kaiser Effect under triaxial conditions. He raises the question of non-uniqueness of paleostress estimation, because "the stress state that produces Acoustic Emissions is a strong function of the three principal stresses". He shows that as the confining pressure increases, the load required for the Kaiser Effect to be observed also increases. According to his data, the relationship between confining pressure and the required load is nearly linear for the Westerly granite.

Other researchers such as Tanimoto et.al. (Ref.9) have reported the existence of the Kaiser Effect in triaxially compressed soil samples in laboratory tests. The accuracy of their results are within an acceptable range.

In-situ stress determination tests in a borehole are also carried out by McElroy et.al. (Ref.10). In this case they have measured AE activity in a borehole by loading the side walls, using an Acoustic Emission Jack. They report that in one of the experiments, the previously applied stress could be reliably detected by the Kaiser Effect. The remaining tests (three altogether), revealed no dramatic anomalies in stress vs deformation data. Sudden increases in AE rate was however observed, in narrow stress ranges. These authors attribute this anomalous behavior to some form of in-situ stress.

B.4) RETENTION TIME

The Kaiser Effect retention time is a subject open for debate. For instance Goodman (Ref.11) has reported recovery of Kaiser Effect for two sandstones and quartz diorite within short periods of time. Kurita and Fujii (Ref.12) on the other hand have claimed that they were able to observe Kaiser Effect after a period of one month.

B.5) PHYSICAL CHANGES

Environmental processes may greatly affect the recovery process of Acoustic Emission as well as the stress-strain relation in rock deformation. As demonstrated by Kurita and Fujii (Ref.12) the water content is one of the most important factors in the Kaiser Effect hysteresis. These authors have shown that when a granite core was soaked in a water bath for one day, considerable AE was obtained, in the elastic region, at stresses far below the previous maximum. Therefore, as it is not possible to know the exact physical conditions in the field, comparison between field and laboratory experiments may be difficult. The temperature effect must also be investigated, because it too, plays a major role in Kaiser Effect retention time as shown by Boyce (Ref.13).

C) CASE STUDY

C.1) INTRODUCTION

The purpose of this investigation was to subject potash samples to stress at varying strain rates, to see how changing the strain rate would affect Acoustic Emission activity and the accuracy of stress determination using the Kaiser Effect. A second parameter, the Kaiser Effect retention time was also tested during the course of these experiments. The experiments were carried out using different strain rates on potash samples cut from the same block. Each test consisted of two cycles of uniaxial tests on the same specimen. In each case the first cycle established the reference stress level. The subsequent cycle was performed to search for the first reference stress level.

C.2) SAMPLE PREPARATION

Except for the first two samples presented in this report, all potash samples were cut with a particular angle or direction in mind. This consideration has no bearing on this Kaiser Effect investigation. It is, however, important in microstructural studies such those explained in accompanying report. Care was taken to prepare specimens so that the ends deviated from parallelism by as much as 0.001 centimeters. This produced very little or no corner effects and by the time the second loading cycle started, the ends were perfectly parallel. The samples were kept between one to four days in the laboratory, at room temperature and less than 50% humidity, before they were tested.

C.3) TESTING EQUIPMENT

Acoustic Emission tests were carried out using two different monitoring systems. AET's SAM Phoenix system was used to collect data from the first two samples presented in this report. Physical Acoustic Corporation's LOCAN Jr. was used to test the remaining samples.

The experiments were done on a servo-controlled hydraulic testing machine, capable of providing a maximum load of 2500 kN in compression. As expected, the background noise generated by such a testing equipment was high. No measure was taken to eliminate the noise mechanically, by placing end caps between the specimen and the platens for instance.

The threshold was the only parameter used to control the level of the background noise, and was set at about 0.1 V on the SAM Phoenix system and at 72 dB (out of a possible range of 0 to 88 dB) on the LOCAN Jr. Acoustic Emission activity was monitored over one channel using both systems. The AE equipments were programmed to record signal number, first threshold crossing, rise time, peak amplitude, ring-down count, signal duration, axial strain (as measured by one LVDT transducer) and the load. Of all the Acoustic Emission parameters recorded, the first two (signal number and first threshold crossing time) were of prime concern in this study. The data from some of the remaining parameters are given in the report on microstructural analysis.

One piezoelectric transducer (the same sensor was used on both Acoustic Emission systems) was firmly mounted on the side of each specimen using appropriate acoustic couplant and tape. The transducer had its resonant frequency at about 190 KHz with a bandwidth of approximately 250 KHz.

C.4) TEST RESULTS

The following pages provide a list of relevant information about each sample, stating the different conditions under which they were tested for cycles one and two. Each information sheet is followed by the three representative curves for the second cycle, namely, the event counts vs stress, the AE rate vs stress and the stress-strain curve respectively.

C.4.1) SAMPLE: *5A*

Length:	15 cm
Width:	12.5 cm
Height:	14.5 cm
Strain Rate:	0.42E-3 mm/sec
Delay (between cycle 1 and 2):	same day
Maximum Stress (cycle 1):	2.13 MPa
Maximum Stress (cycle 2):	6.00 MPa
Estimated Stress:	2.06 MPa
Accuracy of Estimated Stress:	96.7%
Threshold Level:	0.1 volt
Equipment Used:	AET's SAM PHOENIX

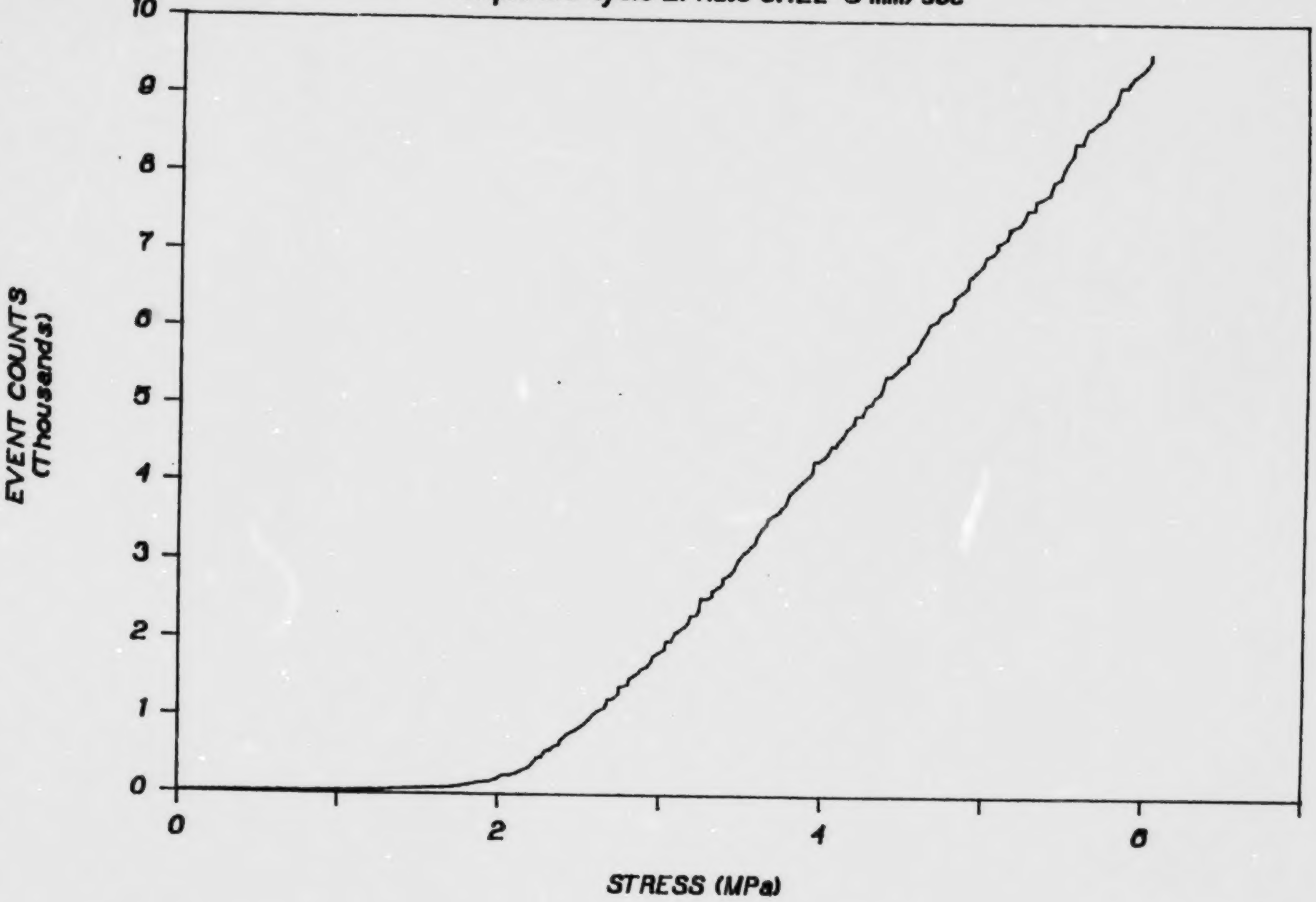

PCS Mining and McGill Project

Sample 5A/Cycle 2/Rate 0.42E-3 mm/sec

PCS Mining and McGill Project

Sample 5A/Cycle 2/Rate 0.42E-3 mm/sec

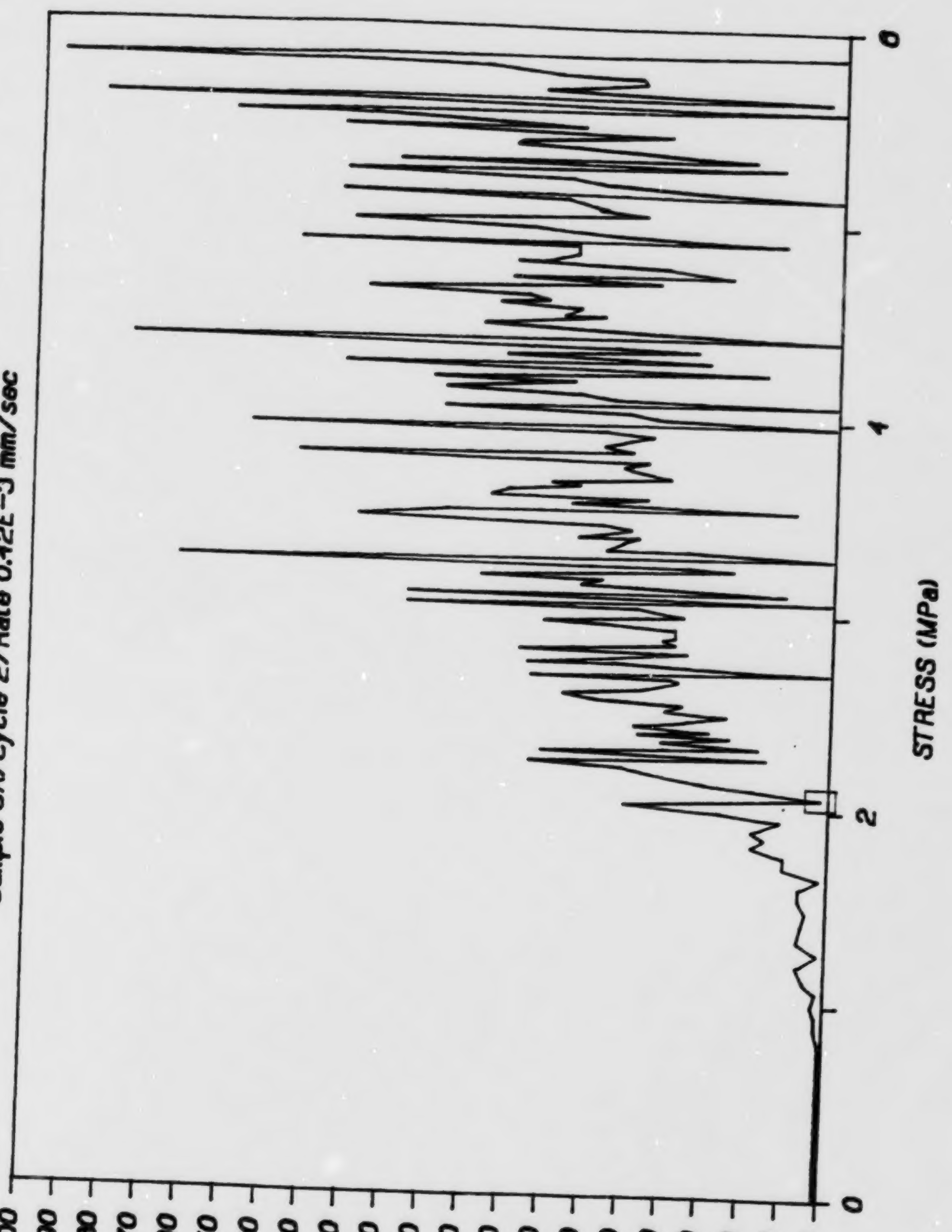

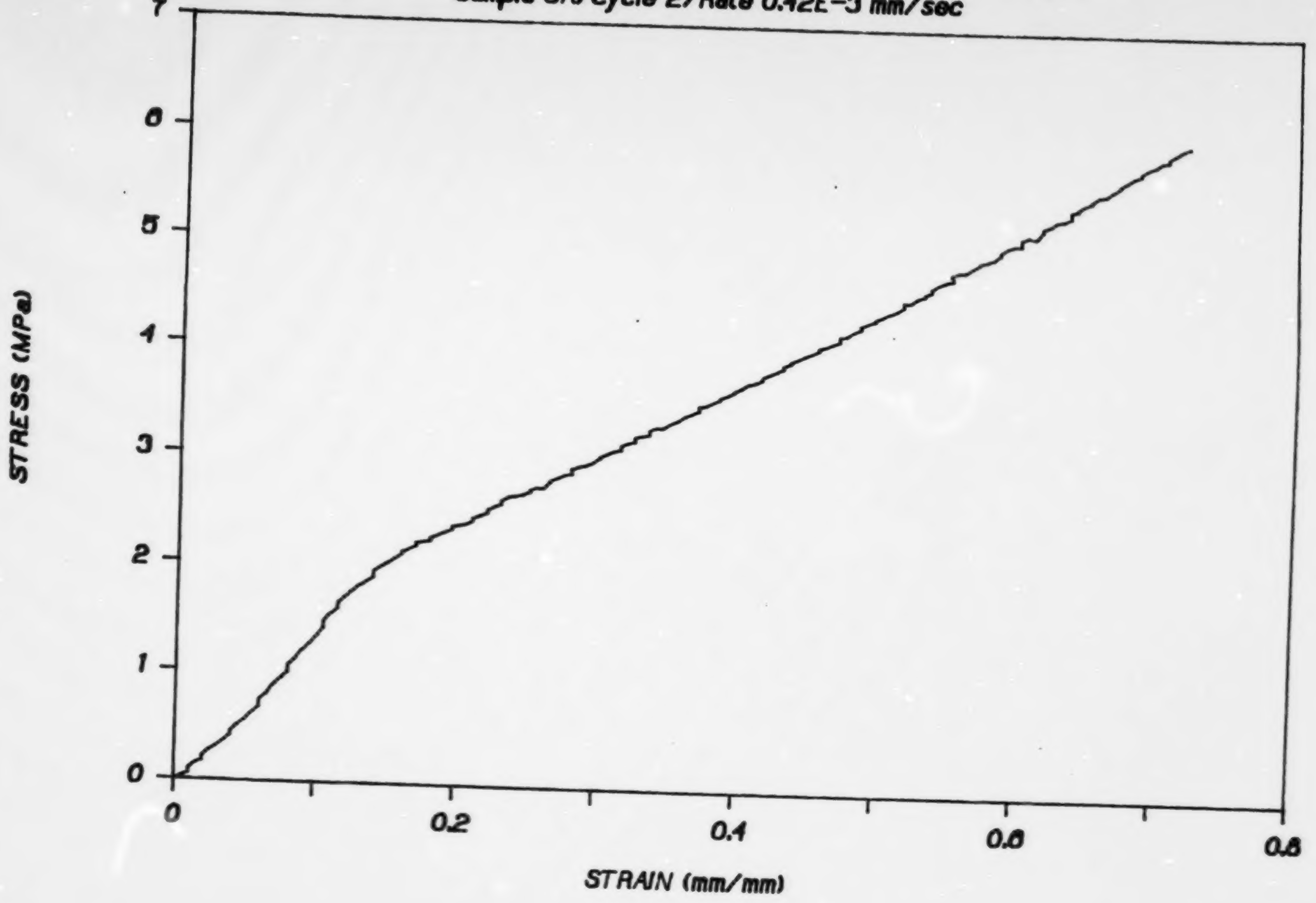

PCS Mining and McGill Project

Sample 5A/Cycle 2/Rate 0.42E−3 mm/sec

C.4.2) SAMPLE: *7A*

Length:	9.5 cm
Width:	8.5 cm
Height:	14.5 cm
Strain Rate:	0.21E-3 mm/sec
Delay (between cycle 1 and 2):	same day
Maximum Stress (cycle 1):	4.92 MPa
Maximum Stress (cycle 2):	9.00 MPa
Estimated Stress:	4.89 MPa
Accuracy of Estimated Stress:	99.6%
Threshold Level:	0.1 volt
Equipment Used:	AET's SAM PHOENIX

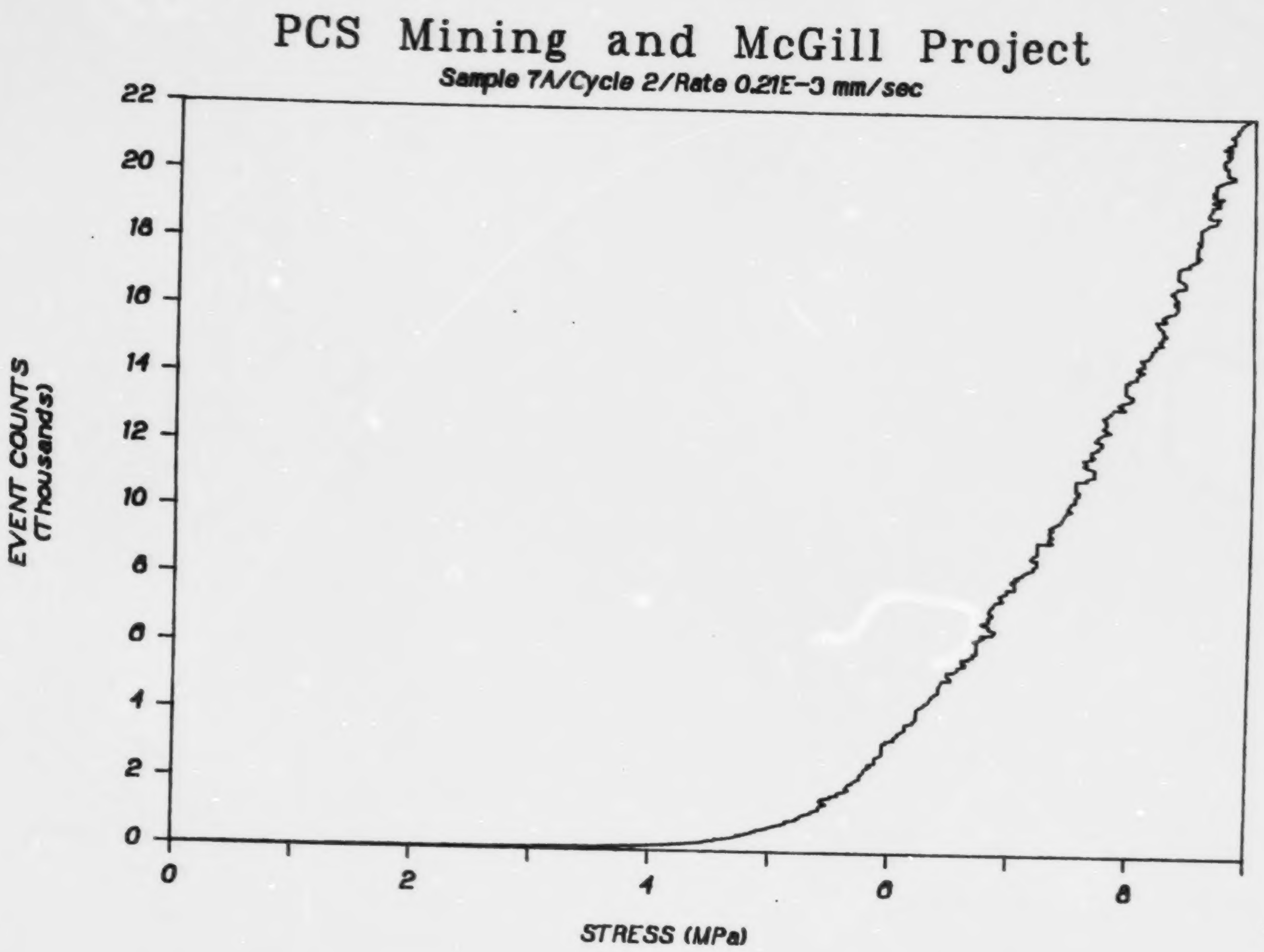
PCS Mining and McGill Project
Sample 7A/Cycle 2/Rate 0.21E-3 mm/sec
EVENT COUNTS
(Thousands)
22
20
18
16
14
12
10
8
6
4
2
0
0
2
4
6
8
STRESS (MPa)

PCS Mining and McGill Project

Sample 7A/Cycle 2/Rate 0.21E−3 mm/sec

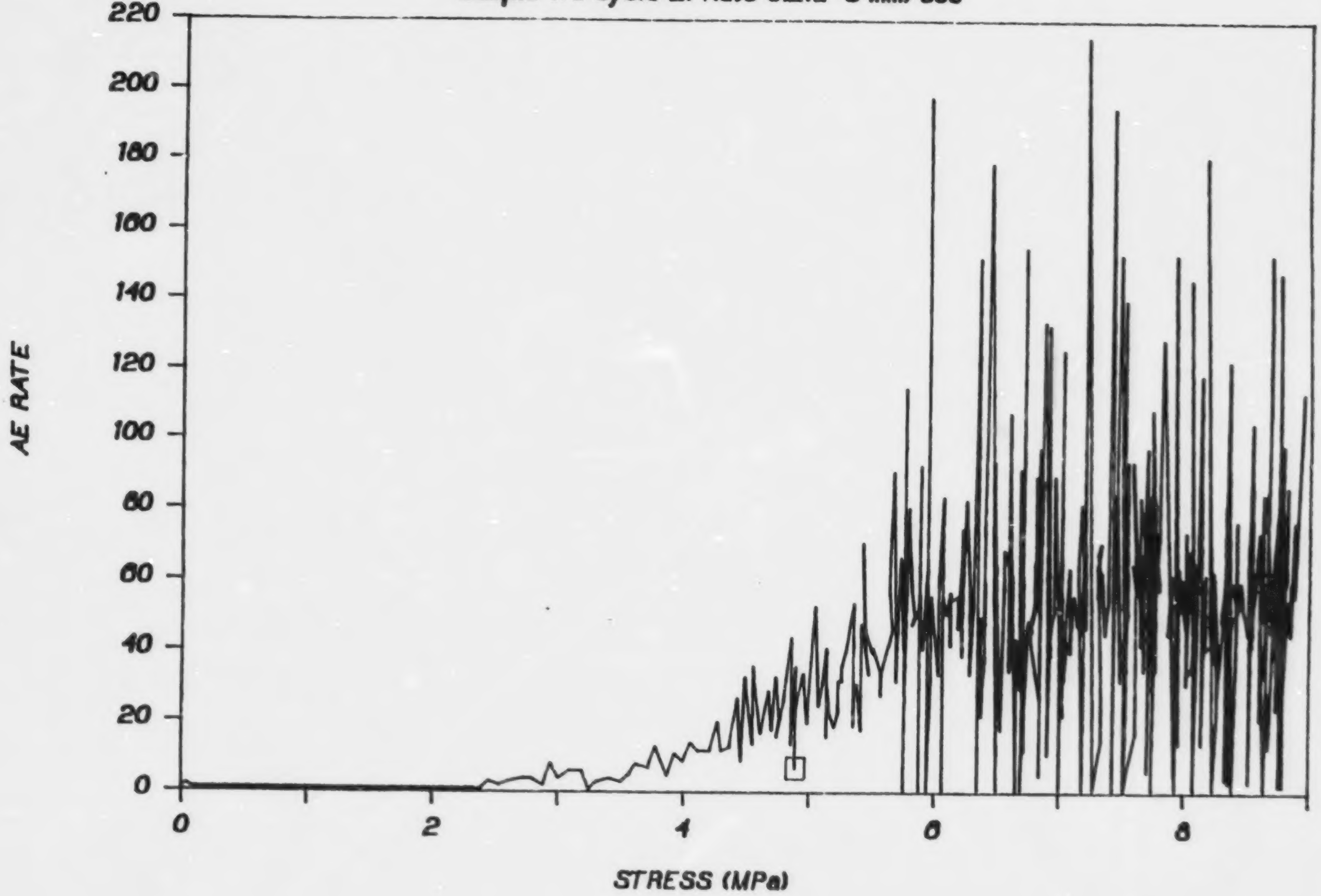

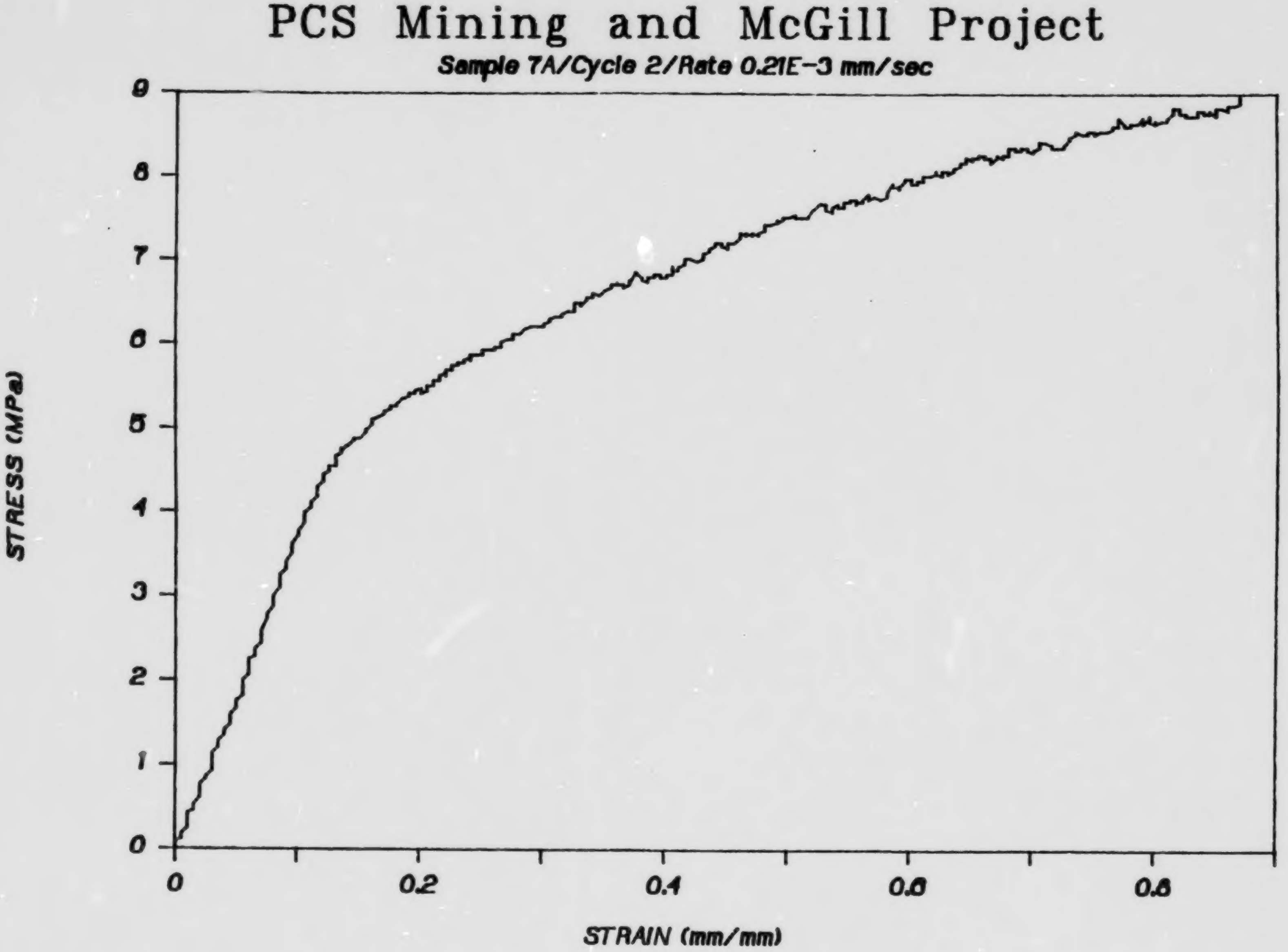
PCS Mining and McGill Project
Sample 7A/Cycle 2/Rate 0.21E-3 mm/sec
STRESS (MPa)
0
1
2
3
4
5
6
7
8
9
STRAIN (mm/mm)
0
0.2
0.4
0.6
0.8

C.4.3) SAMPLE: *L13*

Length:	7.1 cm
Width:	6.6 cm
Height:	10.6 cm
Strain Rate:	0.35E-3 mm/sec
Delay (between cycle 1 and 2):	same day
Maximum Stress (cycle 1):	15.55 MPa
Maximum Stress (cycle 2):	19.80 MPa
Estimated Stress:	15.536 MPa
Accuracy of Estimated Stress:	99.9%
Threshold Level:	72 dB
Equipment Used:	LOCAN Jr.

PCS Mining and McGill Project

Sample L13/Cycle 2/Rate 0.35E-3 mm/sec

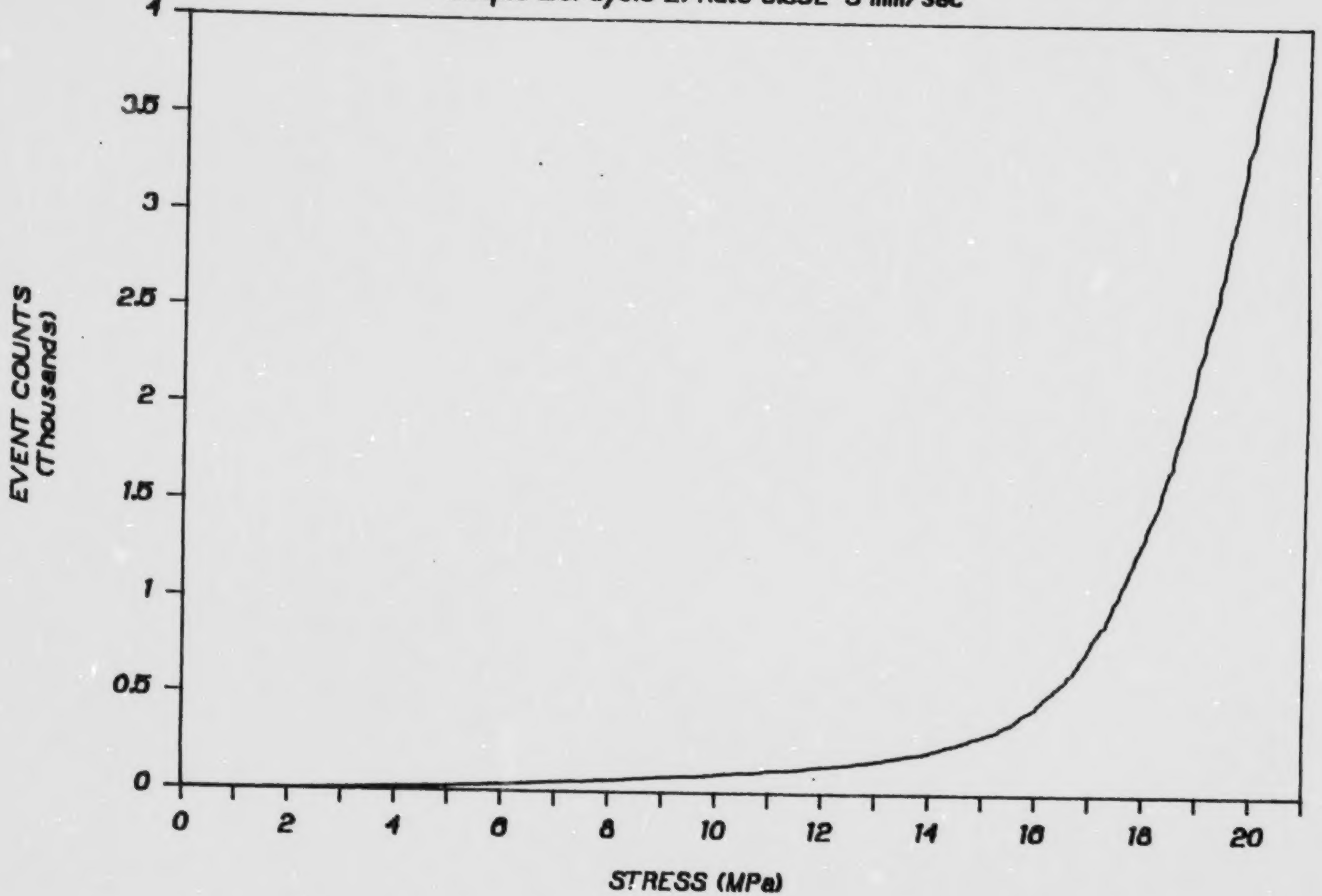

PCS Mining and McGill Project

Sample L13/Cycle 2/Rate 0.35E-3 mm/sec

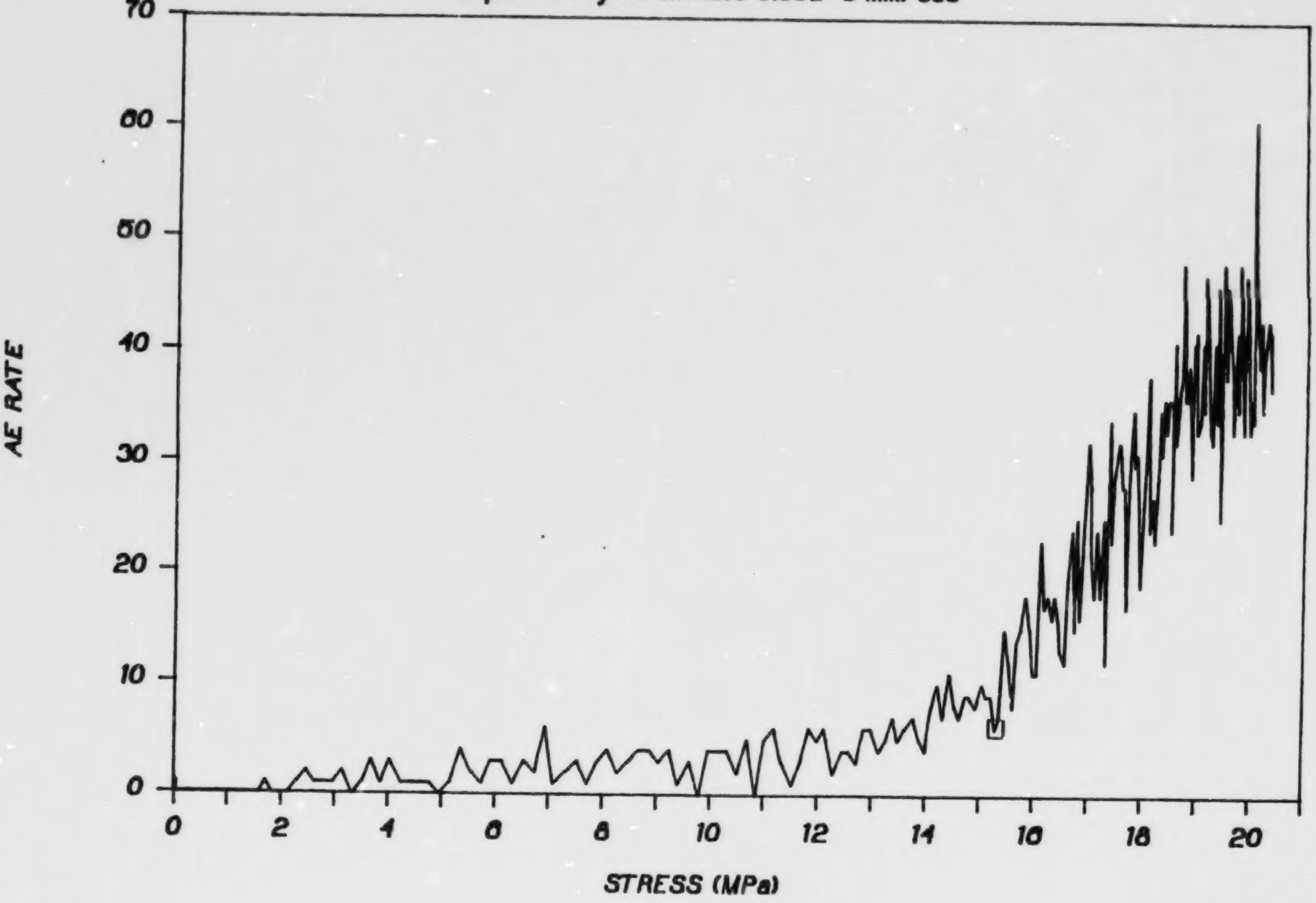

PCS Mining and McGill Project

Sample U3/Cycle 2/Rate 0.35E-3 mm/sec

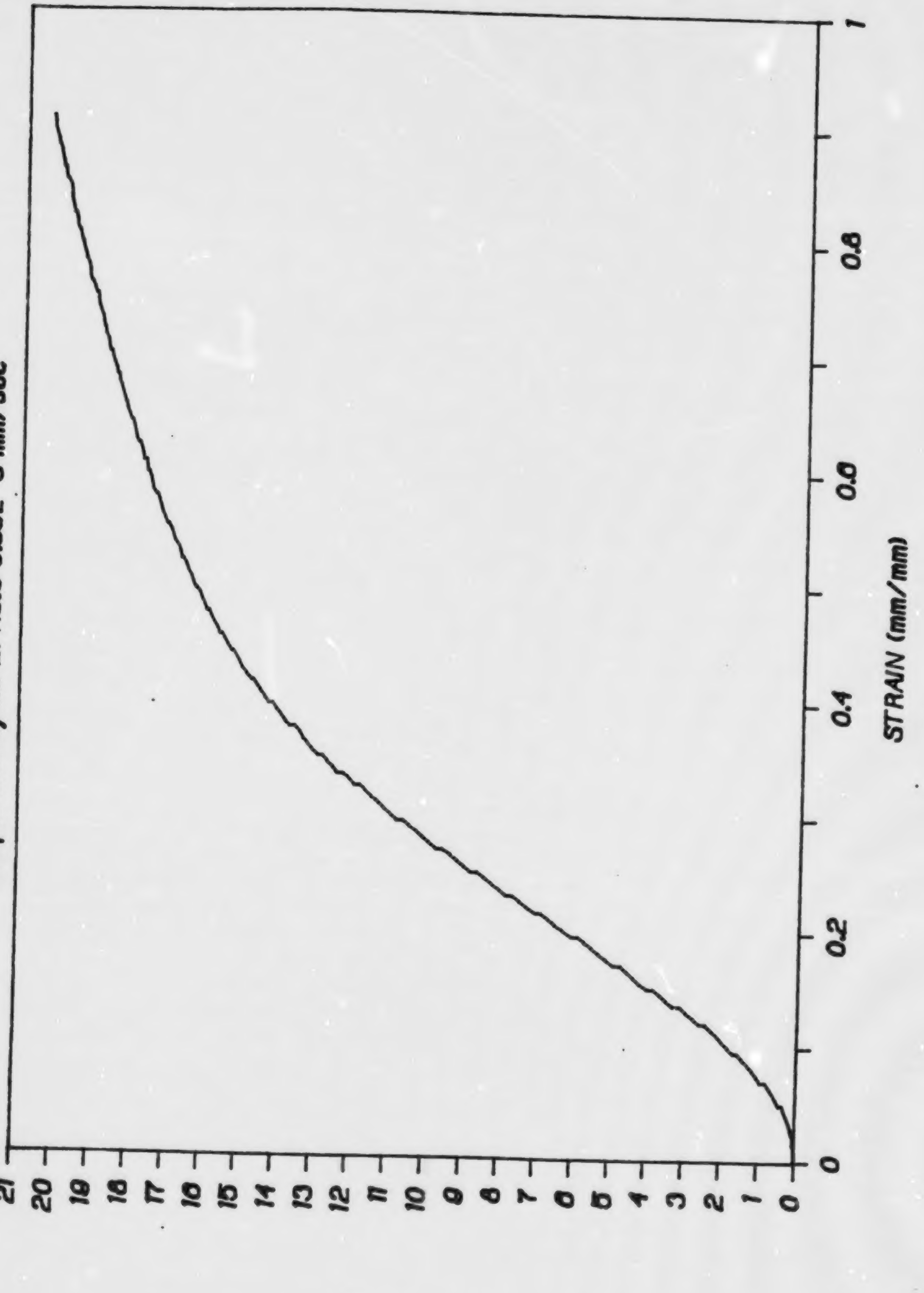

C.4.4) SAMPLE: *L14*

Length:	7.2 cm
Width:	6.7 cm
Height:	10.6 cm
Strain Rate:	0.30E-3 mm/sec
Delay (between cycle 1 and 2):	two days
Maximum Stress (cycle 1):	20.00 MPa
Maximum Stress (cycle 2):	25.85 MPa
Estimated Stress:	19.696 MPa
Accuracy of Estimated Stress:	98.5%
Threshold Level:	72 dB
Equipment Used:	LOCAN Jr.

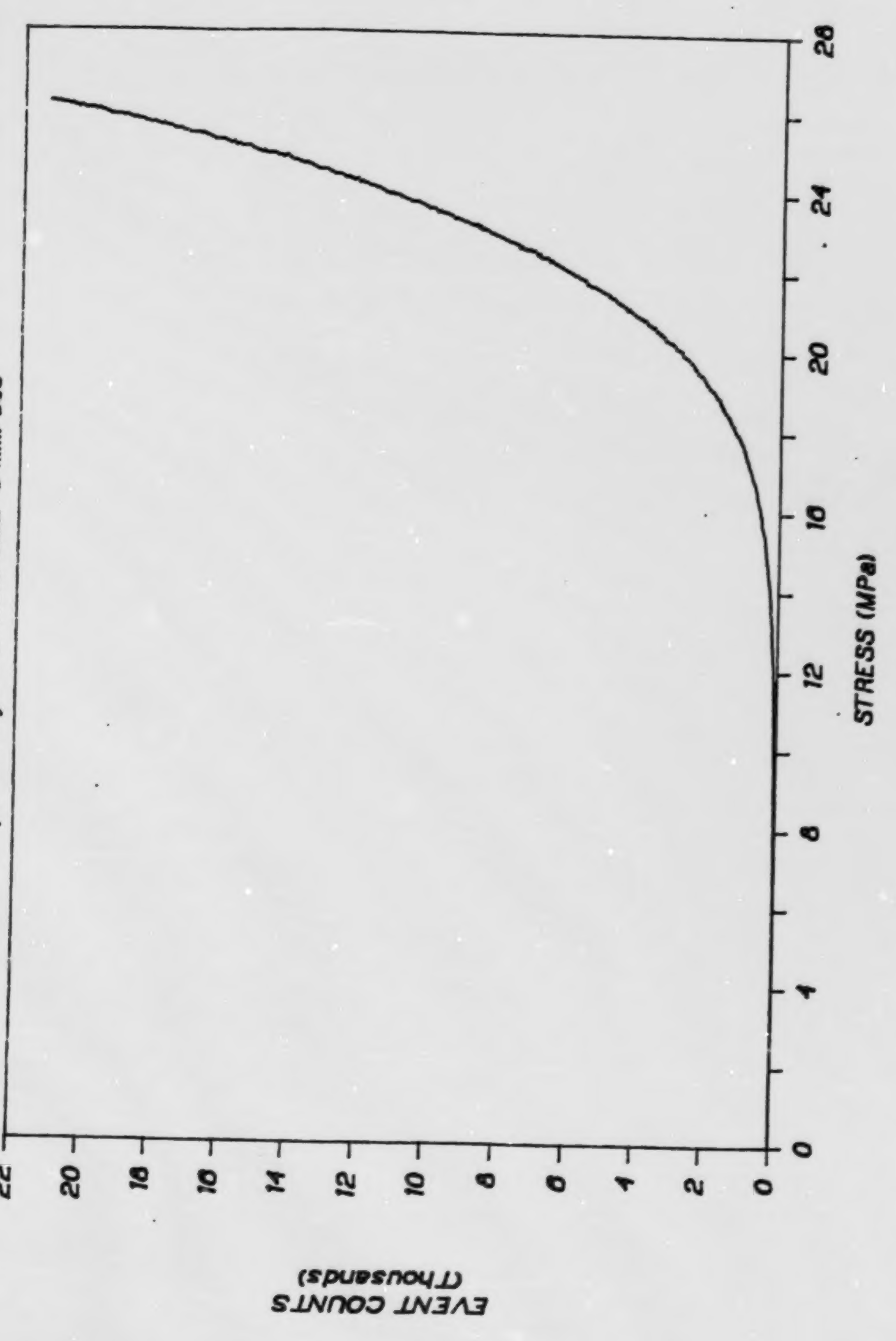

PCS Mining and McGill Project

Sample L14/Cycle 2/Rate 0.3E-3 mm/sec

PCS Mining and McGill Project

Sample L14/Cycle 2/Rate 0.3E-3 mm/sec

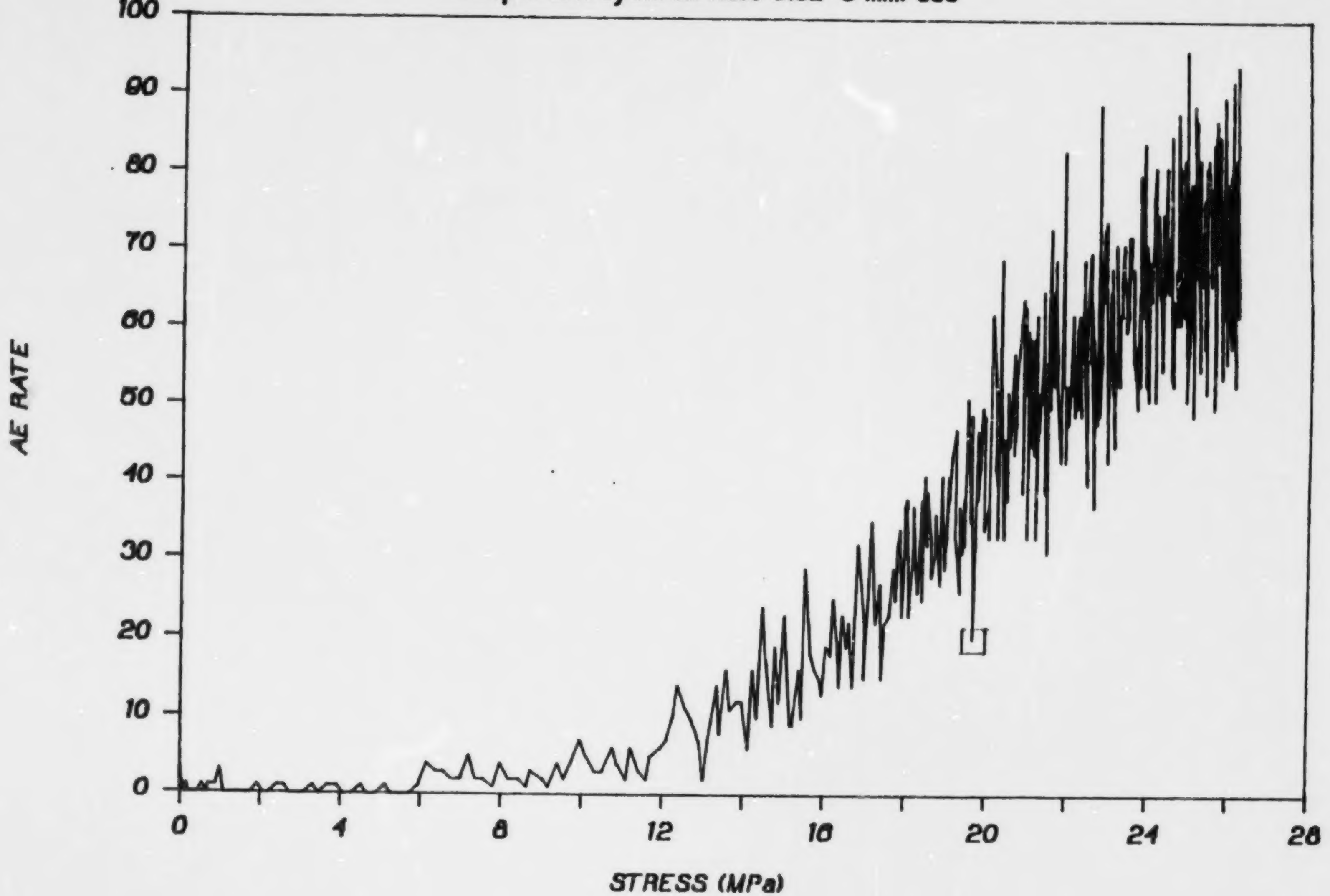

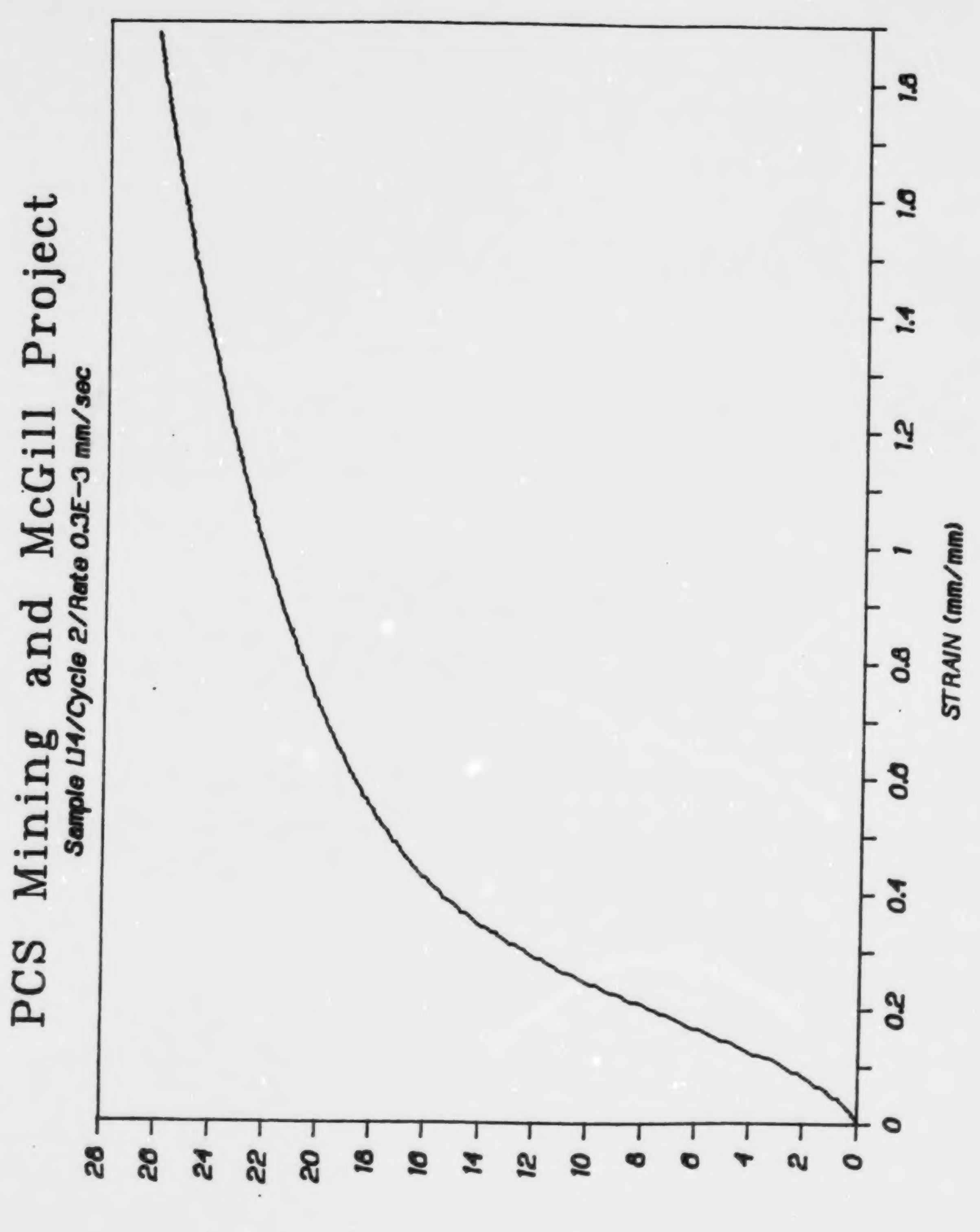
PCS Mining and McGill Project
Sample L14/Cycle 2/Rate 0.3E-3 mm/sec
STRESS (MPa)
0
2
4
6
8
10
12
14
16
18
20
22
24
26
28
STRAIN (mm/mm)
0
0.2
0.4
0.6
0.8
1
1.2
1.4
1.6
1.8

C.4.5) SAMPLE: *L15*

Length: 7.1 cm

Width: 6.8 cm

Height: 12.6 cm

Strain Rate: 0.60E-3 mm/sec

Delay (between cycle 1 and 2): one day

Maximum Stress (cycle 1): 14.00 MPa

Maximum Stress (cycle 2): 18.90 MPa

Estimated Stress: 13.67 MPa

Accuracy of Estimated Stress: 97.6%

Threshold Level: 72 dB

Equipment Used: LOCAN Jr.

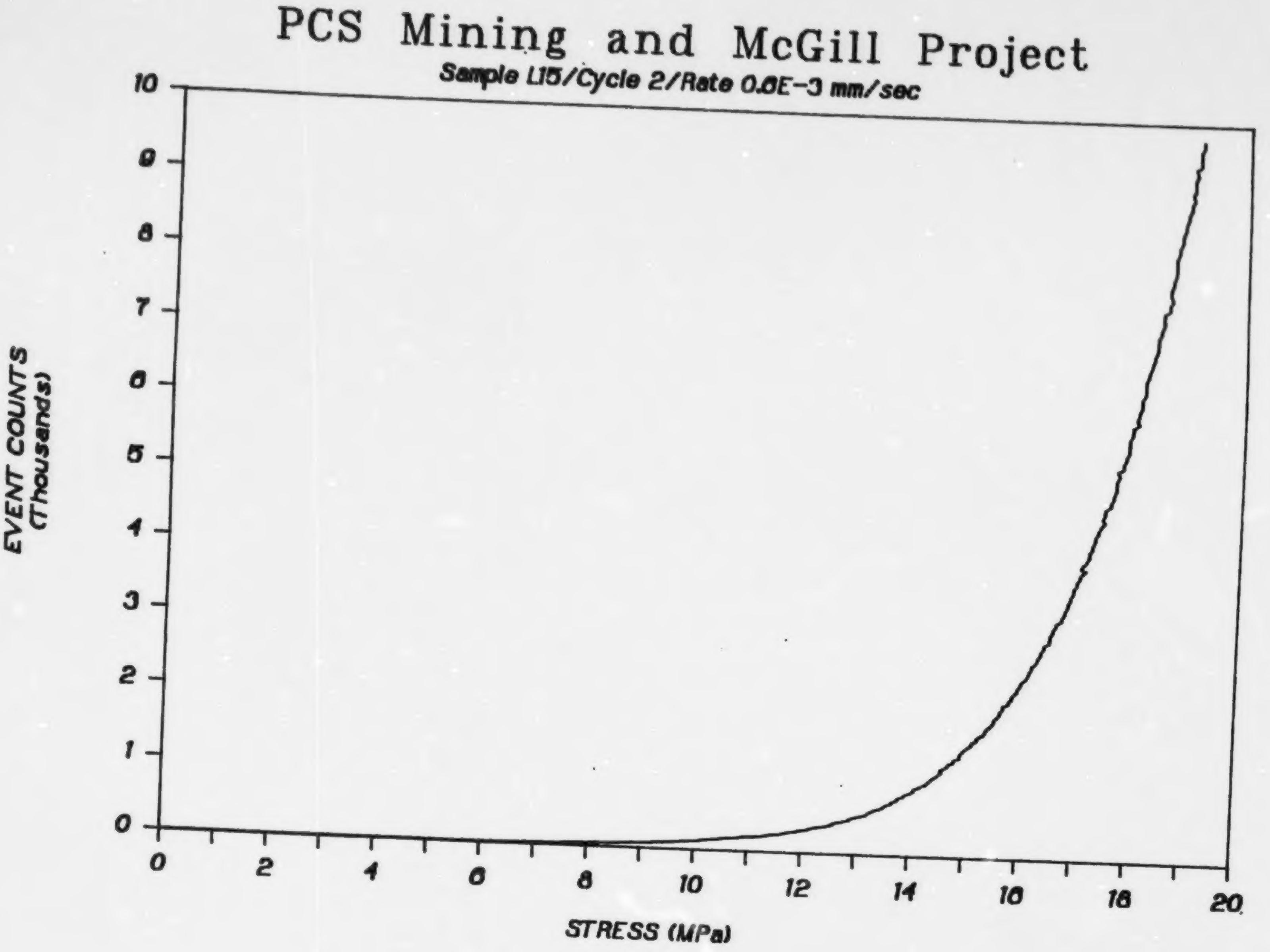
PCS Mining and McGill Project
Sample L15/Cycle 2/Rate 0.6E-3 mm/sec
EVENT COUNTS
(Thousands)
10
9
8
7
6
5
4
3
2
1
0
0
2
4
6
8
10
12
14
16
18
20
STRESS (MPa)

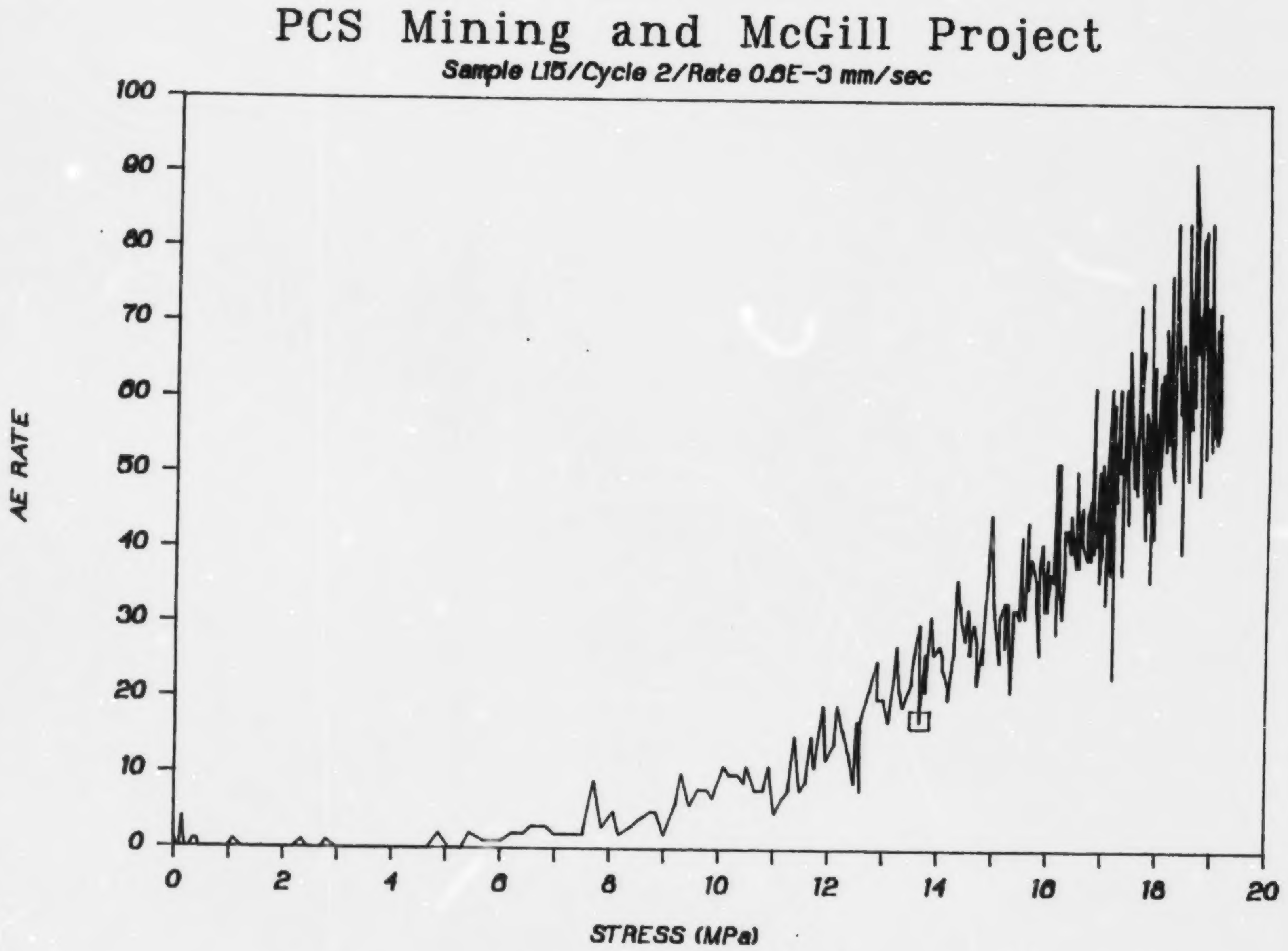

PCS Mining and McGill Project

Sample L15/Cycle 2/Rate 0.6E-3 mm/sec

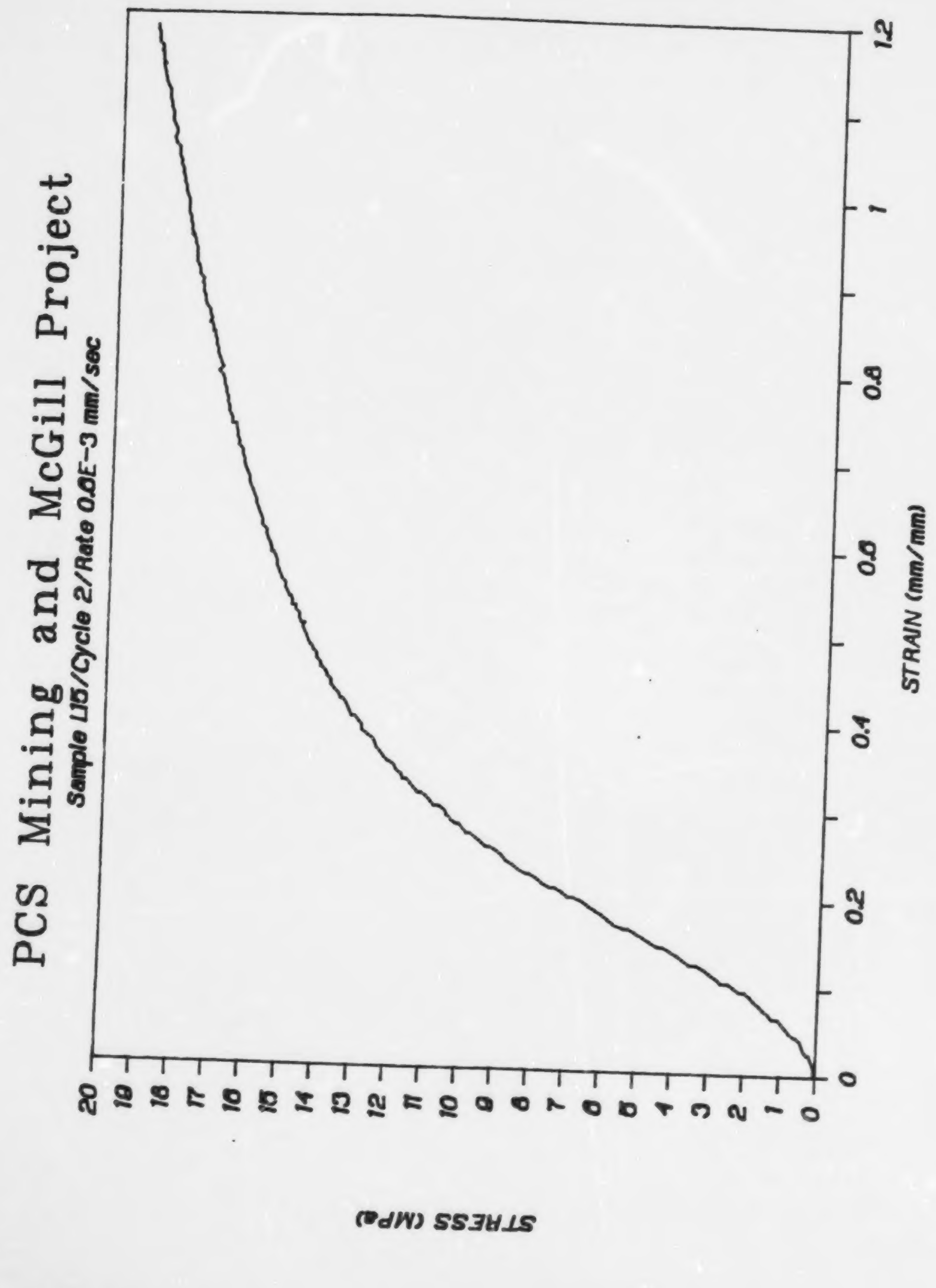
PCS Mining and McGill Project
Sample L15/Cycle 2/Rate 0.0E-3 mm/sec
STRESS (MPa)
0
1
2
3
4
5
6
7
8
9
10
11
12
13
14
15
16
17
18
19
20
STRAIN (mm/mm)
0
0.2
0.4
0.6
0.8
1
1.2

C.4.6) **SAMPLE:** *L16*

Length:	7.0 cm
Width:	6.6 cm
Height:	12.6 cm
Strain Rate:	0.50E-3 mm/sec
Delay (between cycle 1 and 2):	two days
Maximum Stress (cycle 1):	16.00 MPa
Maximum Stress (cycle 2):	21.88 MPa
Estimated Stress:	15.95 MPa
Accuracy of Estimated Stress:	99.7%
Threshold Level:	72 dB
Equipment Used:	LOCAN Jr.

PCS Mining and McGill Project

Sample L16/Cycle 2/Rate 0.5E-3 mm/sec

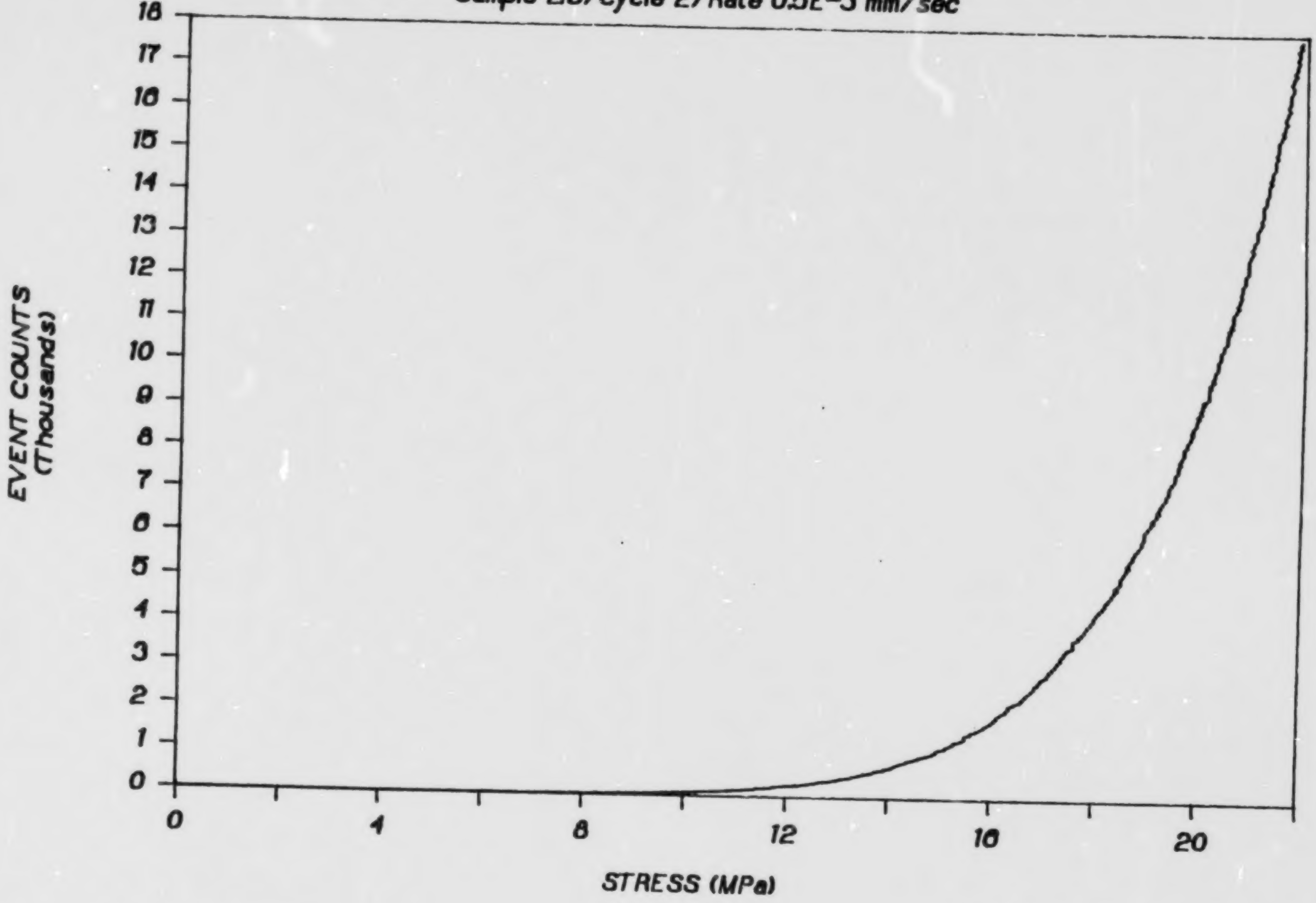

PCS Mining and McGill Project

Sample L16/Cycle 2/Rate 0.5E-3 mm/sec

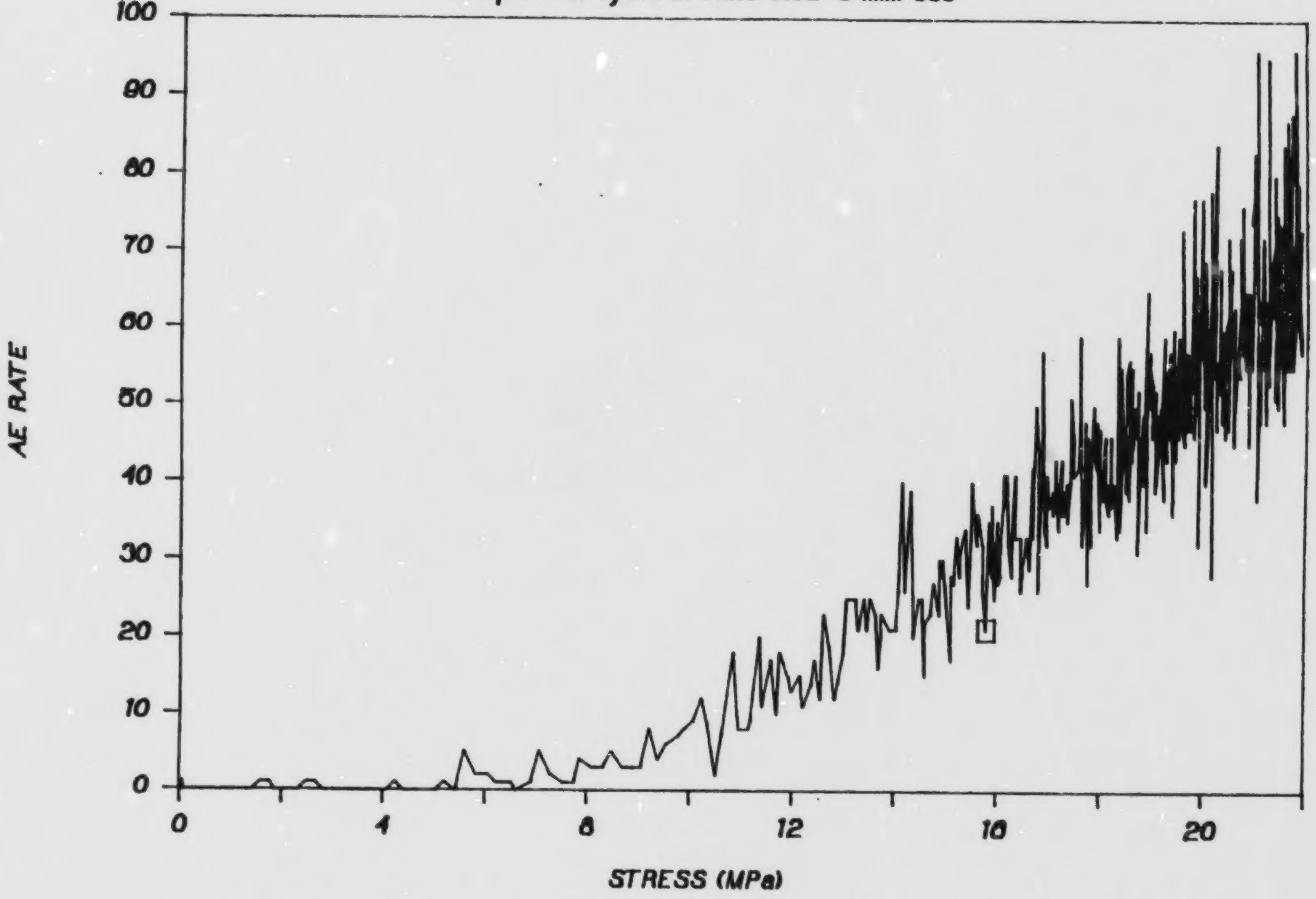

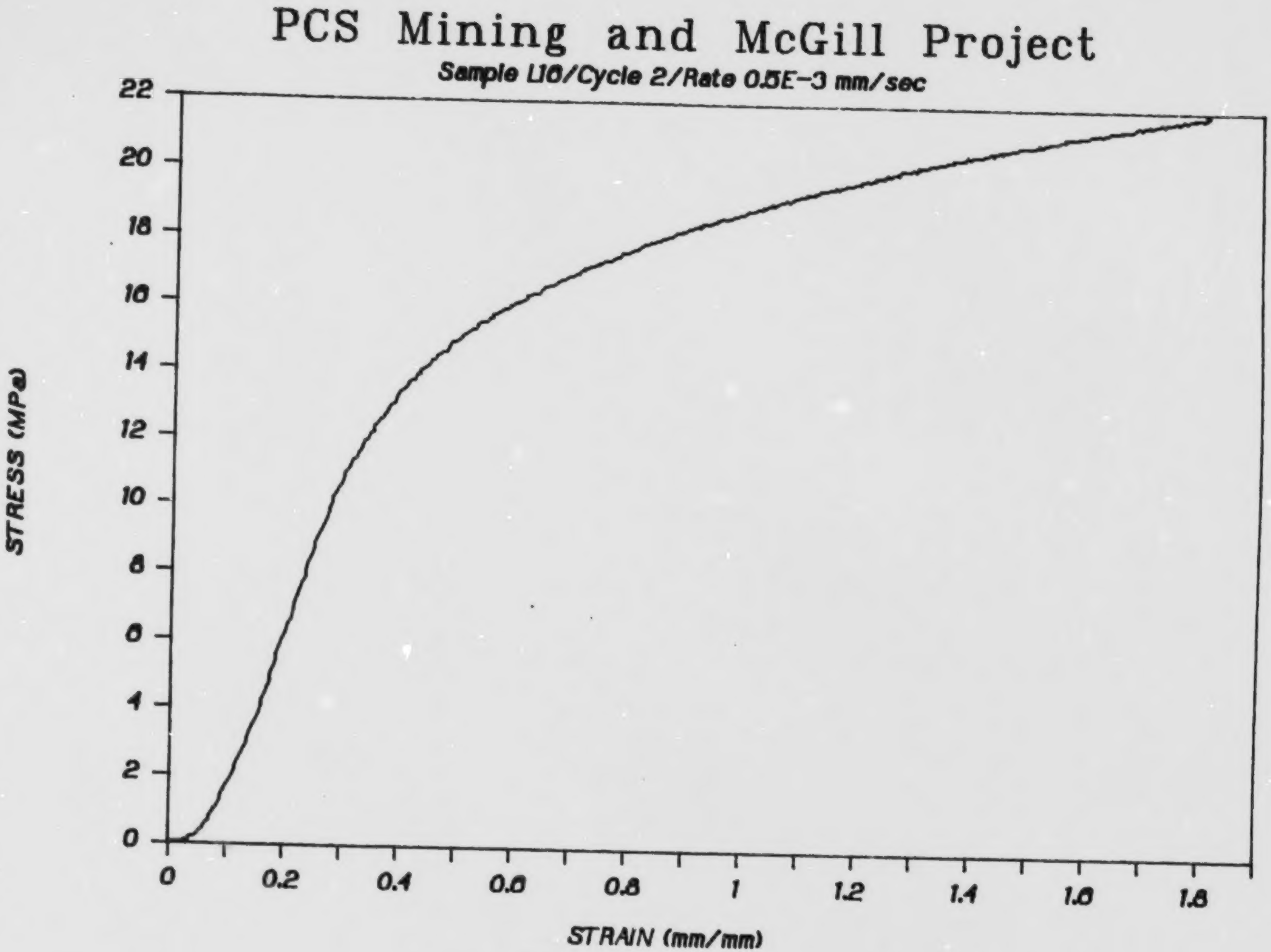
PCS Mining and McGill Project
Sample L16/Cycle 2/Rate 0.5E-3 mm/sec
STRESS (MPa)
22
20
18
16
14
12
10
8
6
4
2
0
STRAIN (mm/mm)
0
0.2
0.4
0.6
0.8
1
1.2
1.4
1.6
1.8

C.4.7) SAMPLE: *U7*

Length:	7.1 cm
Width:	7.0 cm
Height:	9.8 cm
Strain Rate:	0.80E-3 mm/sec
Delay (between cycle 1 and 2):	same day
Maximum Stress (cycle 1):	2.5 MPa
Maximum Stress (cycle 2):	4.9 MPa
Estimated Stress:	2.308 MPa
Accuracy of Estimated Stress:	92.3%
Threshold Level:	72 dB
Equipment Used:	LOCAN Jr.

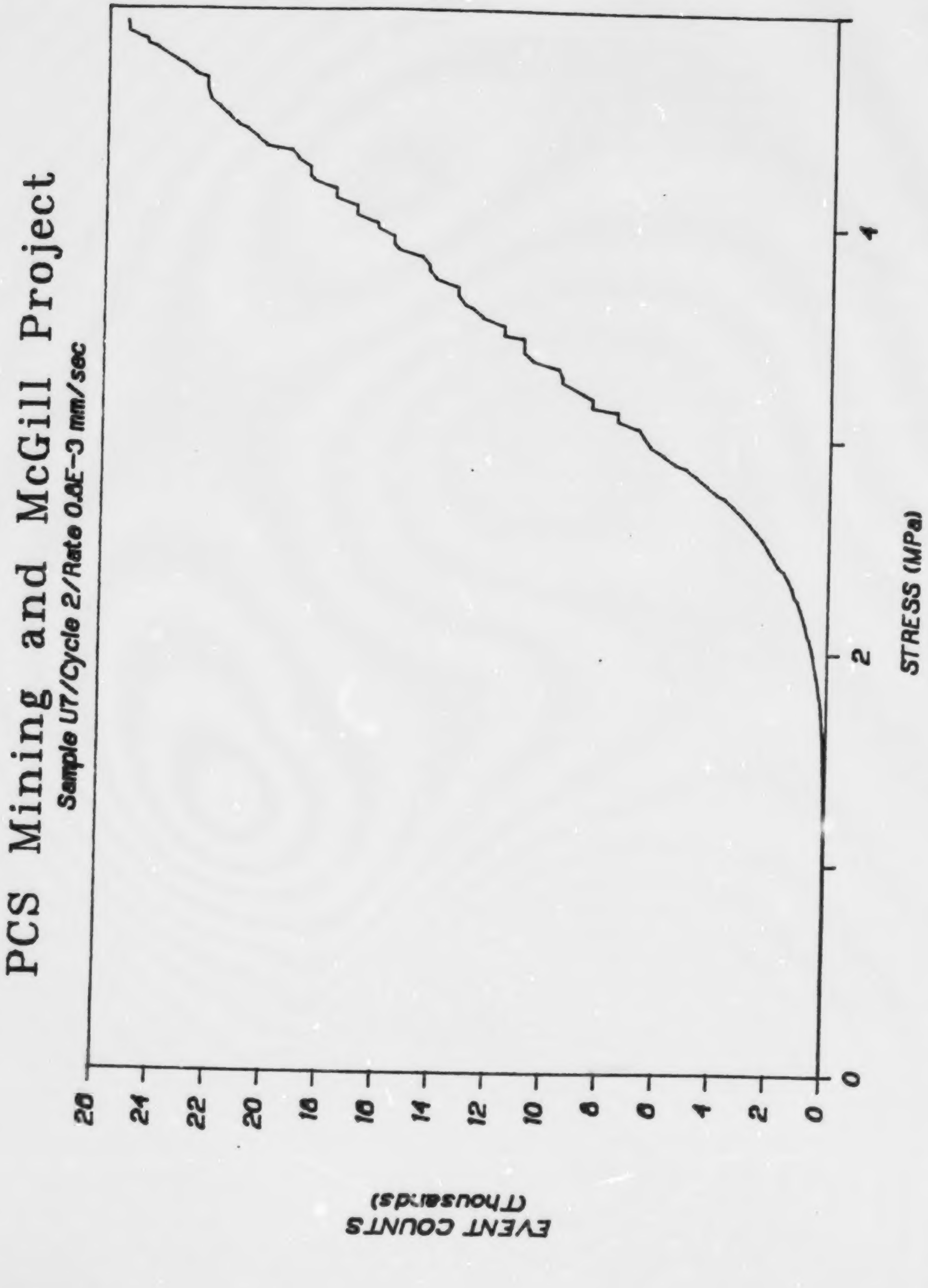

PCS Mining and McGill Project

Sample U7/Cycle 2/Rate 0.8E-3 mm/sec

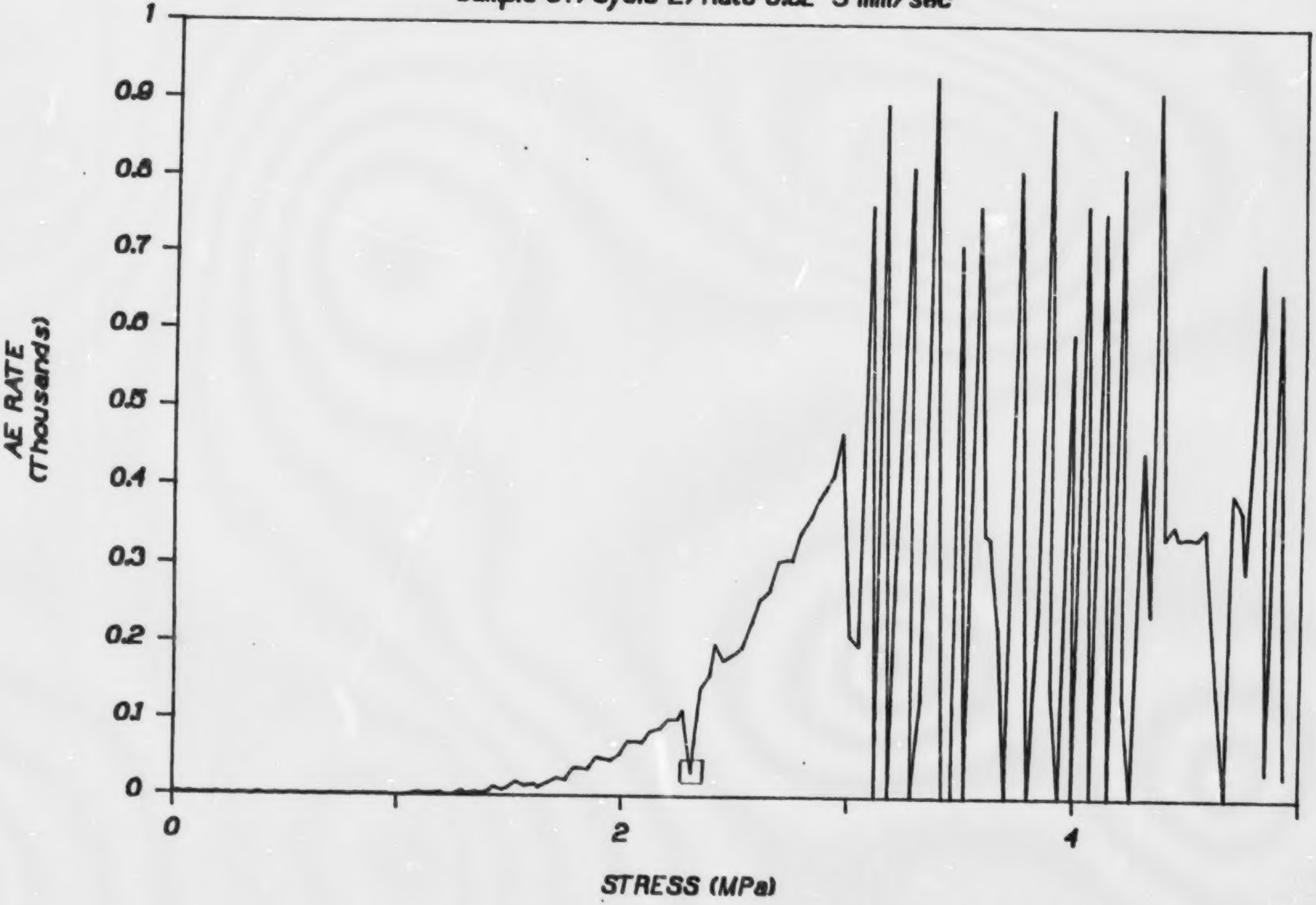

PCS Mining and McGill Project

Sample U7/Cycle 2/Rate 0.8E-3 mm/sec

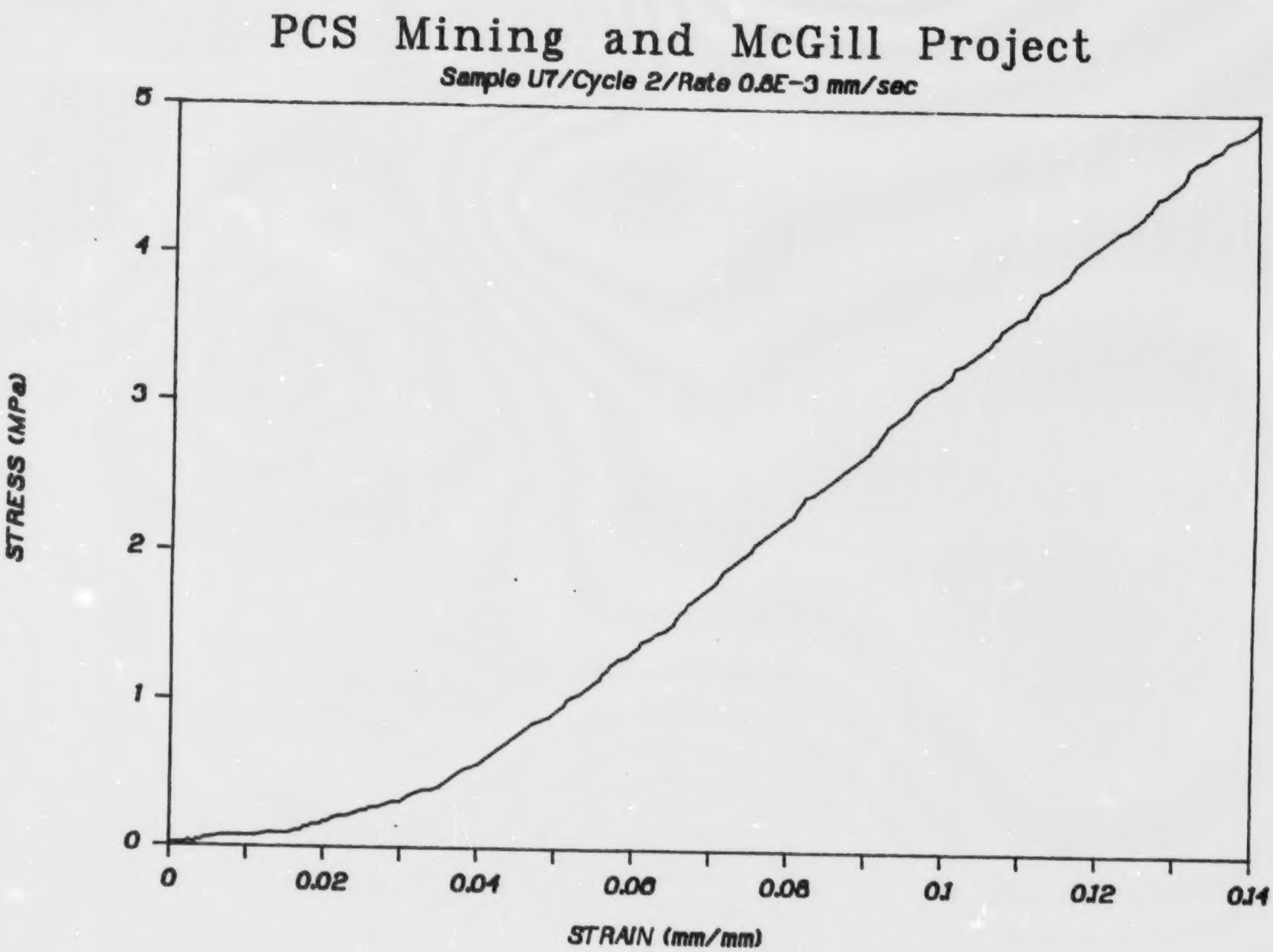
PCS Mining and McGill Project
Sample U7/Cycle 2/Rate 0.8E-3 mm/sec
STRESS (MPa)
5
4
3
2
1
0
0
0.02
0.04
0.06
0.08
0.1
0.12
0.14
STRAIN (mm/mm)

C.4.8) SAMPLE: *U13*

Length:	7.0 cm
Width:	6.5 cm
Height:	10.7 cm
Strain Rate:	1.0E-3 mm/sec
Delay (between cycle 1 and 2):	same day
Maximum Stress (cycle 1):	2.0 MPa
Maximum Stress (cycle 2):	2.60 MPa
Estimated Stress:	1.4-1.6 MPa
Accuracy of Estimated Stress:	70%-80%
Threshold Level:	72 dB
Equipment Used:	LOCAN Jr.

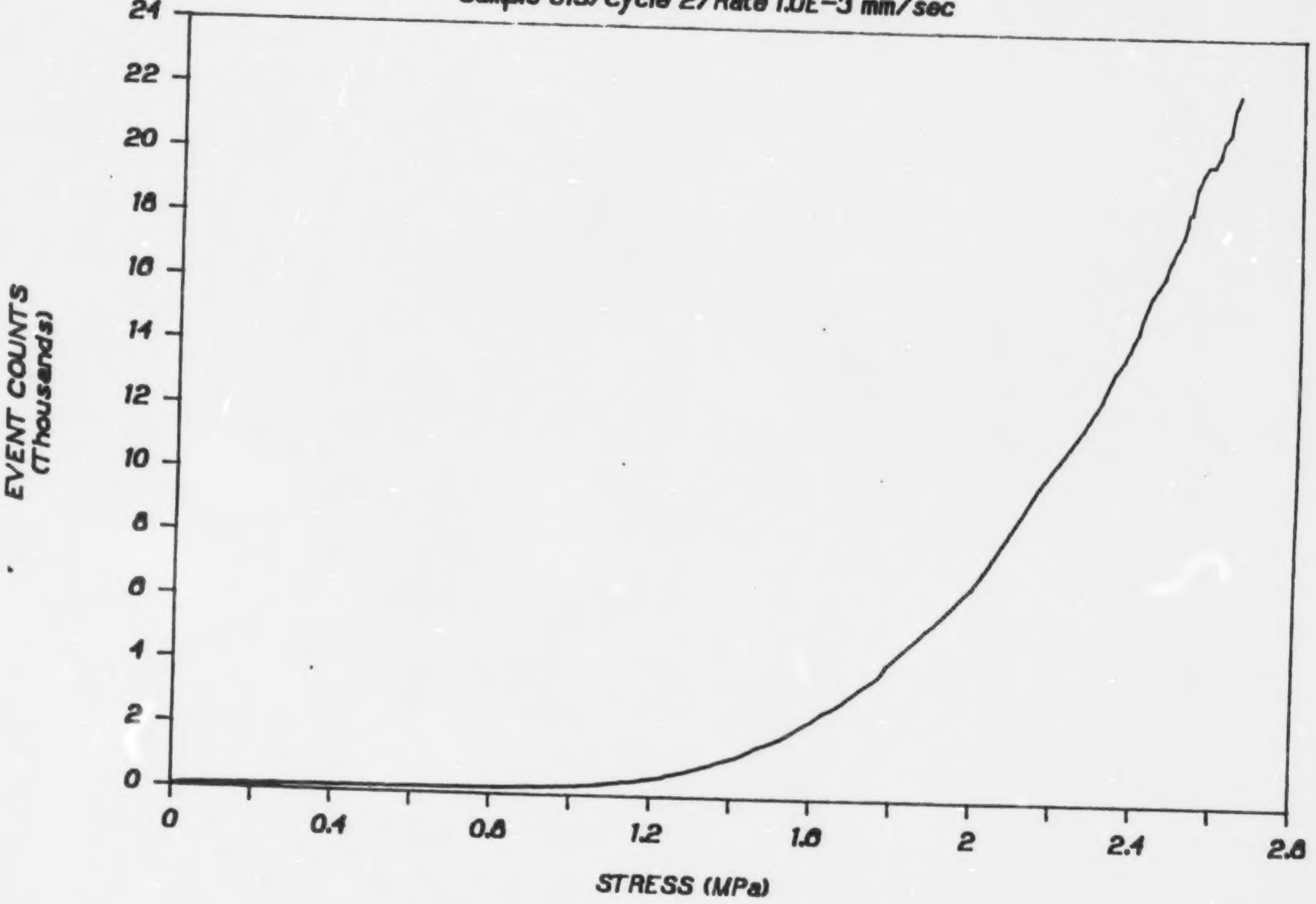

PCS Mining and McGill Project

Sample U13/Cycle 2/Rate 1.0E-3 mm/sec

PCS Mining and McGill Project

Sample U13/Cycle 2/Rate 1.0E-3 mm/sec

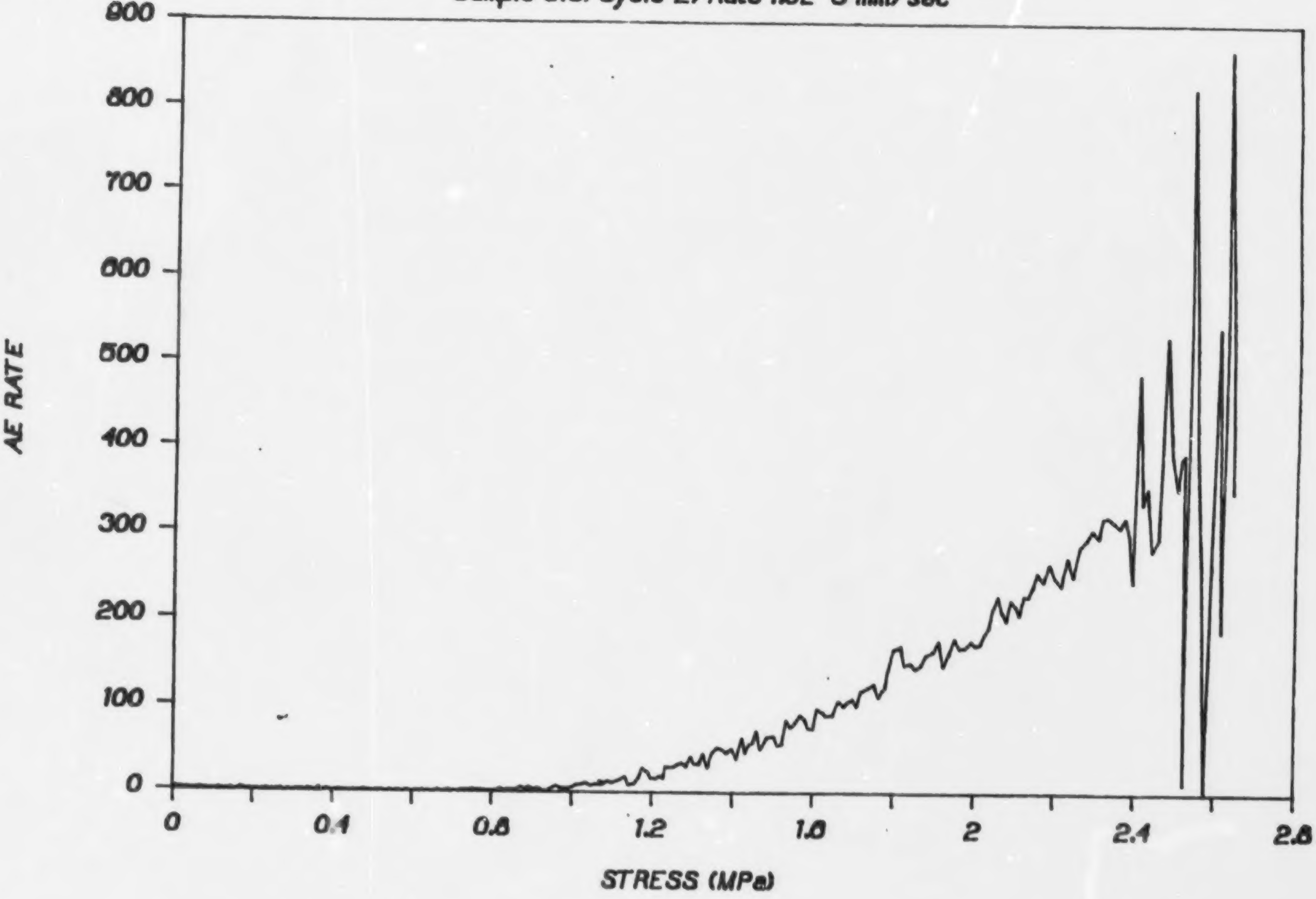

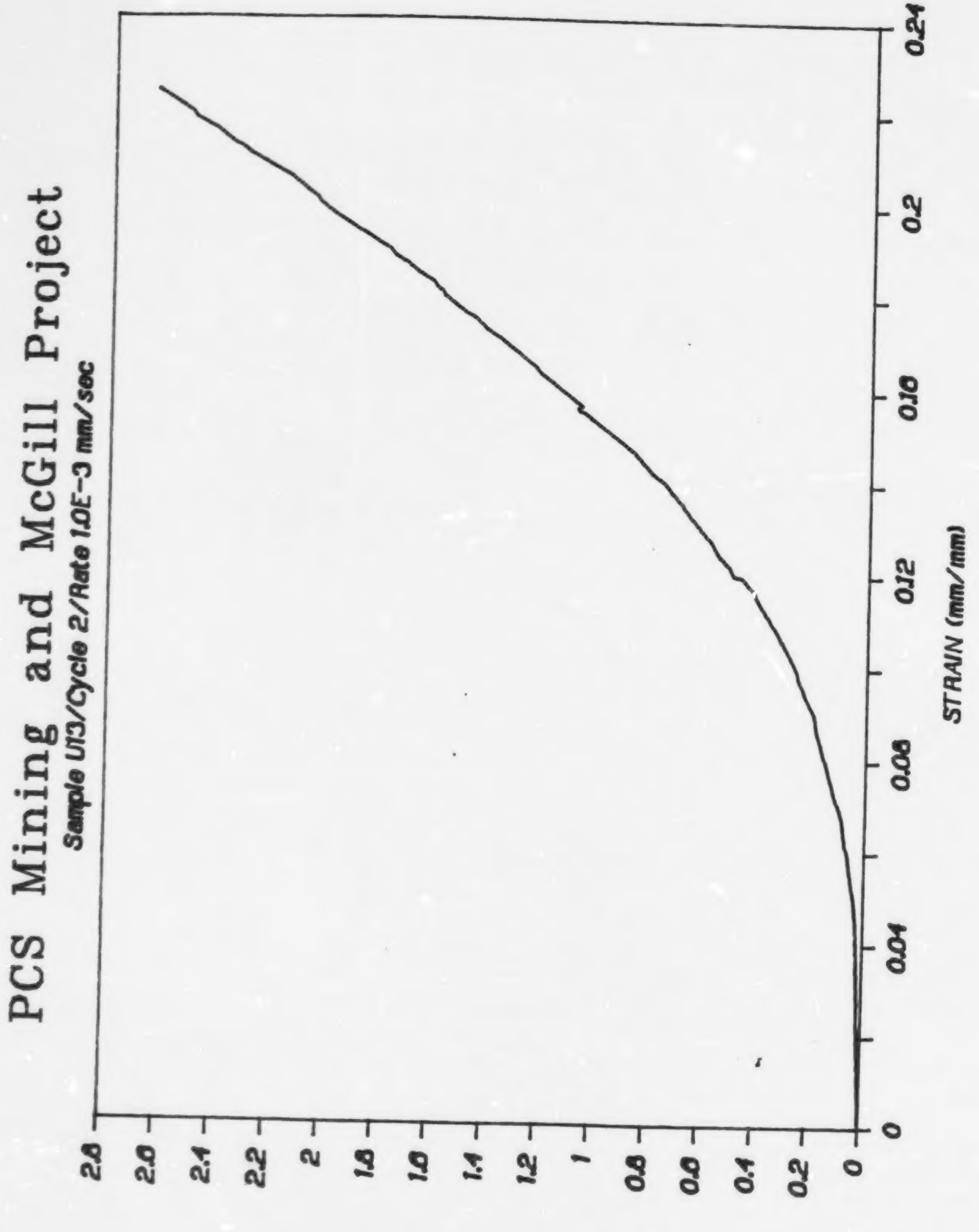
PCS Mining and McGill Project
Sample U13/Cycle 2/Rate 1.0E-3 mm/sec
STRESS (MPa)
2.8
2.6
2.4
2.2
2
1.8
1.6
1.4
1.2
1
0.8
0.6
0.4
0.2
0
STRAIN (mm/mm)
0
0.04
0.08
0.12
0.16
0.2
0.24

C.5) DISCUSSION

All samples were loaded up to a maximum stress level, as mentioned above, and held at that level for three to four minutes. The unloading of the samples took place at twice the loading the rate. After a delay of 5 minutes to two days (see information sheet above for each referenced sample), the second loading cycle was started at the same strain rate as the one used during the first loading. In all cases, the expected Kaiser Effect curves were produced as shown in the event counts vs stress plots. However, not all the Kaiser Effect transition zones are located at the expected position on these curves (see the curves for sample U13 for instance). Therefore, these data must be interpreted carefully, to account for the effect of strain rate, retention time and equipment characteristics.

The method used to locate precisely the previous maximum stress is as follows: the transition zone in the event counts vs stress plots (that portion of the curve where its slope changes rapidly over a small stress interval) tells us where to look for the previous reference level. However, it does not allow one to read off an exact value for the stress. The desired stress estimate can be obtained from the AE rate vs stress plots, at the trough of the curve framed in red.

From these experiments, it is evident that the Kaiser Effect persists in potash samples, after short delays such as one or two days. The test results show that the accuracy of Kaiser Effect stress estimation is better than 96%, except for samples U7 and U13. The lower estimated stresses for these samples can not be due to the amount delay that was allowed between successive loadings, since samples U7 and U13 were reloaded on the same day. In our opinion, short delays should have no effect on the retention time of potash.

A quick survey of strain rate versus the accuracy of stress estimation using the Kaiser Effect method, reveals an interesting point: as strain rate increases, the accuracy decreases. The exception in this trend is sample L16, with an estimated stress that is within 0.3% of the previous maximum for a strain rate of 0.5E-3 mm/sec. The important question is to carry out more experiments to see:

(1) whether these test results can be repeated and,

(2) what happens at both ends of the spectrum, i.e. when very fast or very slow strain rates are used.

One other factor that must be taken into account when interpreting AE data is the design and electrical characteristics of the monitoring equipment. In this case, one particular point that must be mentioned is the value of the threshold set on the LOCAN Jr. For all the runs during the second cycle, this value was set at 72 dB or 3.98 volts. This value is unusually high, considering these tests were carried out in almost identical set of conditions as with the SAM Phoenix system, using the same servo-controlled hydraulic press and the same sensor and preamplifier. This threshold value was programmed in order to eliminate random noise recorded by the LOCAN Jr. system, even when the samples were not loaded.

D) CONCLUSIONS AND RECOMMENDATIONS

The data obtained from this case study suggest that accurate stress estimation is highly dependent on the strain rate used. Short delays (one or two days) introduced between each cyclic loading does not seem to have any effect on the Kaiser Effect hysteresis or its stress determination.

When AE rate vs stress plots are used in conjunction with the event counts vs stress curves, an accurate stress estimate can be obtained for strain rates less than 0.6E-3 mm/sec.

The results presented in this report are very interesting and promising; additional testing programs are required to explore:

(1) the effect of long to very long delay times between each cyclic loading on the retention time of Kaiser Effect.

(2) the effect of very fast or very slow strain rates on accurate stress estimations.

(3) the existence of a strain rate interval that provides the most accurate stress values using this method.

(4) whether this method can unveil more than one historic stress level a given rock specimen has been subjected to in the past.

REFERENCES

1) Hugson, D. R., and Crawford, A. M., 1986,

KAISER EFFECT GAUGING: A NEW METHOD FOR DETERMINING THE PRE-EXISTING IN-SITU STRESS FROM AN EXTRACTED CORE BY ACOUSTIC EMISSIONS

Presented at: International Symposium on Rock Stress and Rock Stress Measurements, Sept. 1-3, Sveden.

2) Sondergeld, C. H., and Estey, L.H., 1981,

ACOUSTIC EMISSION STUDY OF MICROFRACTURING DURING THE CYCLING LOADING OF WESTERLY GRANITE

Journal of Geophysical Research, Vol. 86, No. B4, pp. 2915-2924.

3) Holcomb, D. J., 1983,

USING ACOUSTIC EMISSION TO DETERMINE IN-SITU STRESS: PROBLEMS AND PROMISE

Geomechanics AMD, Vol. 57, pp 11-21.

4) Kanagawa, T., Hayashi, M., and Nakasa, H., 1976,

ESTIMATION OF SPATIAL GEOSTRESS COMPONENTS IN ROCK SAMPLES USING THE KAISER EFFECT OF ACOUSTIC EMISSION

Proceedings of the 3rd Acoustic Emission Symposium, Tokyo, pp. 1-22.

5) Holcomb, D. J., and Martin III, R. J., 1985,

DETERMINING PEAK STRESS HISTORY USING ACOUSTIC EMISSIONS

26th US Symposium on Rock Mechanics/Rapid City, SD/26-28 June

pp. 715-722.

6) Michihiro, K., Fujiwara, T., and Yoshioka H., 1985,

STUDY ON ESTIMATING GEOSTRESS BY THE KAISER EFFECT OF AE

26th US Symposium on Rock Mechanics/Rapid City, SD/26-28 June

pp. 557-564.

7) Hayashi, M., 1979,

ACOUSTIC EMISSION TO DETECT THE GEOSTRESS

Proceedings of the 4th International Congress. Rock Mechanics Symposium in Montreux

pp. 230-231.

8) Watters, R. J., and Soltani, A. M., 1985,

DIRECTIONAL ACOUSTIC EMISSION ACTIVITY IN RESPONSE TO BOREHOLE DEFORMATION IN ROCK MASSES

26th US Symposium on Rock Mechanics/Rapid City, SD/26-28 June

pp. 723-730.

9) Tanimoto, K., Nakamiro, J., and Fudo, R., 1981,

APPLICATION OF ACOUSTIC EMISSION IN IN-SITU TEST

10th ICSMFE, Vol. 2, pp. 573-576, Sveden.

10) McElroy, J. J., Koerner, R. M., and Lord, A.E., 1985,

AN ACOUSTIC EMISSION JACK TO ASSESS IN-SITU ROCK BEHAVIOUR

Int. J. Rock. Mech. Min. Sci. & Geomech. Abstracts, Vol. 22, No. 1, pp. 21-29.

11) Goodman, R. E., 1963,

SUBAUDIBLE NOISE DURING COMPRESSION OF ROCKS

Geol. Soc. Amer. Bull., 74, pp.487-490.

12) Kurita, K., and Fujii, N., 1979,

STRESS MEMORY OF CRYSTALLINE ROCKS IN ACOUSTIC EMISSION

Geophysical Research Letters, Vol. 6, No. 1, pp. 9-12.

13) Boyce, G. M., 1981,

A STUDY OF THE ACOUSTIC EMISSION RESPONSE OF VARIOUS ROCK TYPES

Master of Science Thesis, Drexel University.

PRELIMINARY STUDY OF THE PETROFABRIC, AND STRESS INDUCED MICROFRACTURES IN RELATION WITH ACOUSTIC EMISSIONS ON POTASH ROCK SALT

Dr. F.P. Hassani
Mr. Vincent Mlakar

McGill University
Dept. of Mining Engineering

January 27th, 1988

Table of Contents

Introduction..1

Sample Preparation..2

Defining the Petrofabric in Potash Rocksalt.........................5

1) Quantitative Stereology for Microstructural Analysis..6

  a) Measurement of Average Grain Size..................6

  b) Measurement of Grain Boundary per Unit Volume........7

2) Representation of Crystallographic Orientation by Pole Figure Measurements..........................14

3) Measurement of Compressional Wave Velocity............21

Measuring Techniques...23

Discussion of Results..26

Statistical Analyses of Cracks.....................................52

Variation of Crack Distribution....................................55

Discussion of AE Results...68

a) Constant Strain Rate Experiments...............................68

Conclusion...84

References...87

Introduction

Laboratory testing of Potash RockSalt from PCS Saskatoon is being conducted in order to observe the relationship of AE under various loading conditions. Quantitatively assessed textural parameters and correlation with applied load and AE is under investigation.

Conclusive evidence presented by previous workers has been descriptive and qualitative in trying to relate structure and texture with AE parameters.

This paper characterizes the some of the microstructural and textural properties that characterize the petrofabric of Potash Rocksalt.

Majority of the textural parameters defined in this paper are compatible with existing descriptions of crystalline texture. The purpose of this study is to offer a useful approach in understanding AE output with fracture propagation and fabric 'adjustment' as controlled by the texture of the specimen and applied load conditions.

Sample Preparation

Blocked shaped samples of Potash Rock Salt (approximately 30.00 cm cubed) were obtained from Saskatoon PCS Mines, prepacked in styrofoam and plastic.

The specimen preparation program involved several stages of cutting, grinding, sectioning and polishing. In all cases, the entire block has been manifested to optimize the quality of representatative results. Also, all sectioned and slabbed specimens have been noted for their orientation relative to the original block and inherent bedding, from which it was derived from.

The original block is trimmed down into a well dimensioned block. The trimmed external slabs are retained for later sectioning and analysis. The block is then measured and cut into equally sized rectangular samples (12.75cm. x 7cm. x 7cm.) to be utilized for ultrasonic, compressive load and AE testing. Each test block has been cut so that the vertical axis of the specimen is oriented respectively perpendicular to the inherent bedding. End surfaces of the test samples were sectioned off for texture and petrographic analysis. Finally, each of the block's faces were ground into a smooth, clean surface.

Analyses of slabbed and sectioned specimens involved development of polished thick and thin sections, polished slabs, and composite-epoxied-laminated polished sections. All slabs were photographed prior to being sectioned.

Initial cuts of slabs and test blocks were accomplished by utilizing an automatic continuous rim rock saw. Cutting was also preformed in a dry medium. Finer and more precise cuts were developed by hand held rotating bit outfitted with a miniturized circular cutting blade and low speed precision saw. Such cutting procedures were required for the development of thin and composite polished sections.

Grinding and polishing was accomplished in three stages. Due to the delicate nature of Rocksalt, developing a smooth surface required special care, so as to not introduce artificially generated microstructure. Initial grinding of larger slabs (ie. > 2cm. square) and test sample blocks were produced by utilizing a vertical lap, fitted with dry garnet or Si-Carbide grit paper, ranging in size 100 grit to 240 grit. Polished surfaces were then obtained by polishing with loose Si-Carbide grit set with a mixture of kerosene or commercial varsol paint thinner. Several stages of consecutive grinding is involved, initially starting with a 200 grit and finishing with an 800 grit. Final polishing was accomplished by using various polishing compounds.

Thin sections were developed using standard thin section preparation techniques. Due to the large grain size present in Potash it was necessary to develop a large sample size of thin sections exclusively used to measure cleavage orientation of mineral phases in Potash Rocksalt.

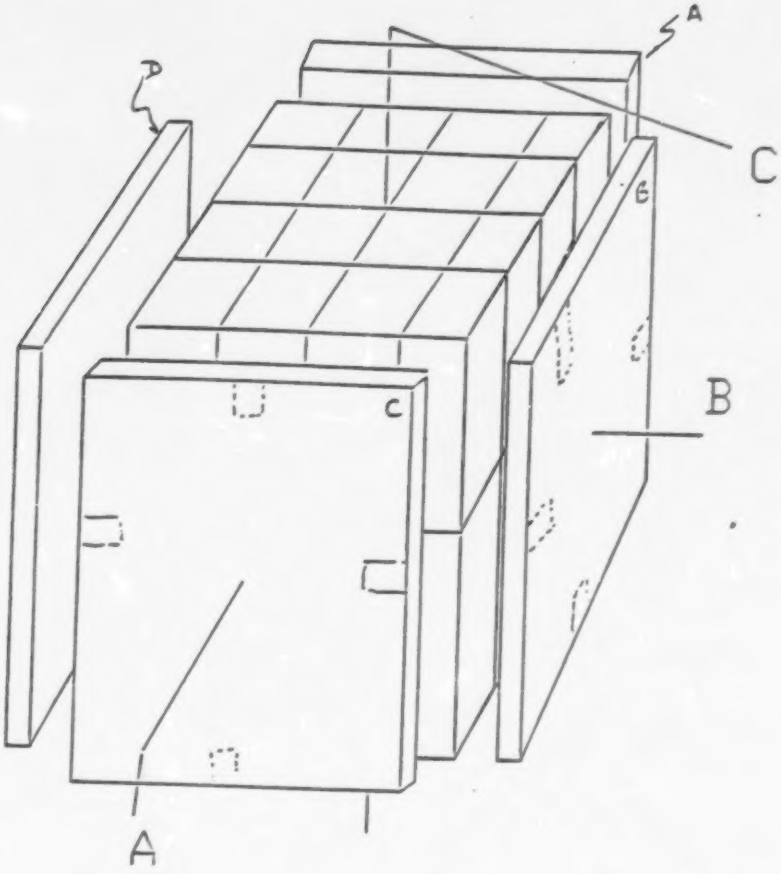

Fig.1. Procedure in which the block was cut, and the designated orientation and direction used in the analyses.

Defining the Petrofabric of Potash Rocksalt

The macroscopic anisotropy of a physical property in a polycrystalline material (such as Potash Rocksalt) may depend on several structural parameters which are summarized into several groups presented in Table A.

The influence of geometrical parameters on macroscopic anisotropies is multivariant. It specifically depends on the details of the structure and the considered property (DeHoff and Rhines, 1968).

The quantification of textural anisotropy of polycrystalline materials can be easily accomplished if the parameters other than grain orientation do not contribute to the influence. The macroscopic properties are then the weighted mean value of the properties of the individual crystal grains, which is also convenient to distinguish orientation and direction dependant properties. In the case of Rocksalt in which there is a strong contribution of parameters other than texture on the macroscopic anisotropy, the quantification correlation between anisotropy, texture and other structural parameters are more complex.

Several measurements must be defined in order to evaluate the textural anisotropy of Potash Rocksalt. Most of the parameters are defined by measuring techniques. These types of sets of values will be observed in order to define the inhomogeneity of the fabric. These include defining parameters derived from Quantitative Microscopy, Xtallographic cleavage orientation of the mineral phases present, and Transmission Ultrasonic Compressional wave velocity measurements.

Quantitative Stereology for Microstructural Analysis

Quantitative Stereology is concerned with the quantitative characterisation of microstructures in terms of their point, lineal and areal elements or constituents. By means of suitable 2-Dimensional measurements on the plane of observation, statistically exact information can be obtained about various microstructural features in 3-Dimensional space occupied by the rock. Elements that can be measured have been broken down into categories.

a) Measurement of Average Grain Size

The average grain size distribution is also under investigation. A slight variation in grain size as evident by inspection of a 1 square foot cut stab of Potash Rocksalt. This variation is gradational and perpendicular to the relict bedding plane.

Grain size has been determined by Heyn's procedure or intercept count method. This method involves a lineal measurement of 'l', from a line projected on the plane of observation. The number of points of intersection between the line and grain boundaries is counted. Then the total length of the line is divided by the number of intersections which results in grain size denoted by 'l'.

Since the grains are nonequiaxed, measurements must be performed in three mutually perpendicular directions. Then, according to the ASTM Designation E 112-60T, the average grain size is calculated from ;

$$N_v = 0.7\sqrt{N_{A(l)}.N_{A(t)}.N_{A(n)}} \qquad (1.1)$$

where N (l), N (t), and N (n) are the numbers of grains/unit of length in directions 'l', 't', 'n'.

b) Measurement of Grain Boundary per Unit Volume, by Lineal Fraction

In order to define some degree of inhomogeneity in fabric, a convenient method to measure percentage of an element occupying a specified volume can be accomplished by means of lineal fraction. Lineal fraction according to DeHoff & Rhines (1968) is defined as a single random traverse is made on a randomly selected plane of polish, then the traverse can be regarded as having been placed at random in the 3-Dimensional structure and the lineal fraction gives a direct estimate of the volume fraction.

This type of measurement will be used particularly for grain boundary lines formed by the intersection of the plane of polish. These structural features (according to DeHoff & Rhines (1968)) can be considered as a 1-Dimensional line in 2-Dimensional surfaces. It is frequently desirable to know this total lenght per unit area.

There are three general equations that relate features of grain boundaries and intersections with an arbitrary test line.

These equations include:

$$L_A = \frac{\pi}{2} N_L \quad \text{mm/mm}^2 \tag{1.2}$$

$$L_V = 2P_A \quad \text{mm/mm}^3 \tag{1.3}$$

$$S_V = 2N_L \quad \text{mm}^2/\text{mm}^3 \tag{1.4}$$

where.... La-length of 'λ' line per unit area

Nl-average number of intersections with 'λ' line, per unit length of test line

Lv-length of 'e' edge per unit volume

Pa-average number of intersections of 'e' lines with test planes per unit area

Sv-interface area per unit volume

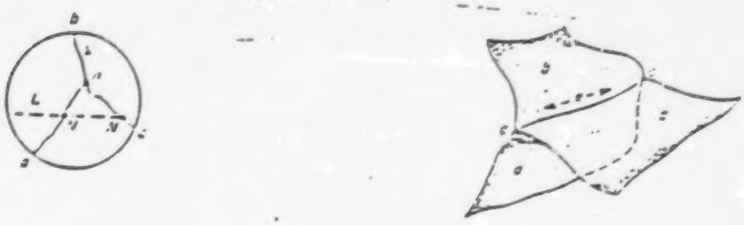

Fig.2. Types of lines & points appearing in three & two dimensions, (after DeHoff & Rhines, 1966).

The technique applied to measure the number of intersectins of grain boundary lines per unit 'l' test line involves constructing random-straight line traverses across the section and counting the number of intersections between the test line and the boundary lines. In order to achieve representative results several lines are required.

It can also be noted that different number of intersections may exist over different positions of the line, but for each microstructure there exists a definite mean value of $\overline{N}_L$, which depends on the total length of grain boundary lines per unit area.

In the case of bedded Rocksalt the methods presented in the previous section can also be modified in order to determine the degree of orientation and ultimately recognize any inhomogeneity in the fabric based on grain shape. The method originally presented by Saltykov, DeHoff & Rhines (1968), and later modified by McCall & Muellen (1973), have shown that one can determine the relative proportions of lineal elements that are randomly directed as homogeneous and those that are not randomly directed as inhomogeneous. Total, partial and no orientation of lines can be distinguished as described by the authors mentioned above.

A numerical expression of degree of orientation has been presented by DeHoff & Rhines (1968). The degree of orientation of a system of lines in a plane may be quantitatively defined as the ratio of the length of oriented portions of the lines to the total length. The oriented portions of the lines are chozen and measured seperately from the isometric portions by measuring N at certain directions relative to the orientation axies. Note, also the fact that, if all the oriented portions of lines in a system are removed, the remaining line elements will be isometric. In such a case, a partially oriented system of lines consists of two superimposed systems. The numerical expression the shape of the grain as an indicator of the shape of the strain ellipse.

Consider a hypothetical situation of a section through an undeformed rock containing initially, uniformlly distributed spheres as shown in figure 3.

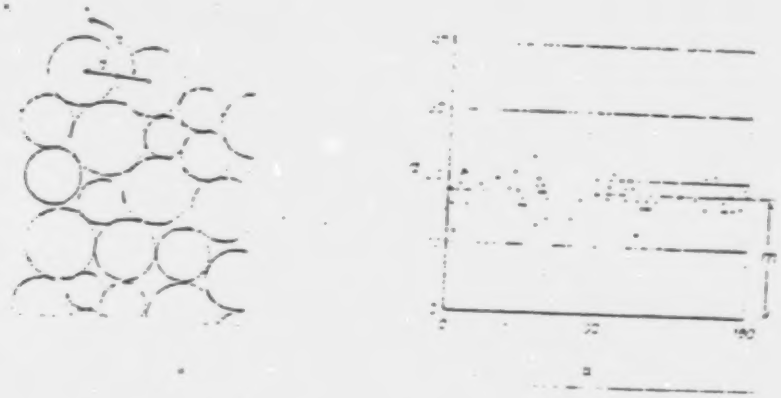

Fig.3. Initial hypothetical case of undeformed particles & their distribution with distance & angle (after Ramsay, 1967).

A line is drawn joining the centres of any two adjacent circular sections and the distance 'd' is measured. This is plotted against the orientation of the line measured from a selected orientation in the section (α). In undeformed material, the plots on the graph would scatter along some mean distance 'm' depending on the frequency distribution of the dimension of the original spheres. As illustrated in Figure 4, if this material is now deformed, the distance between adjacent sphere centres is altered and plots of 'd' vs. 'α' will show a distribution which is proportional to the amount of longitudinal strain in a direction 'd'.

for the degree of orientation 'ω' is determined in terms of fractional percentage by :

$$\omega = \frac{100(L_A)_{or}}{(L_A)_{or} + (L_A)_{is}} = \frac{100[(N_L)_{\perp} - (N_L)_{\parallel}]}{(N_L)_{\perp} + 0.571(N_L)_{\parallel}} \cdot \text{ percent} \qquad (2.5)$$

where La(or) & (La) are oreinted and isometric La's.

The specific application for their relationship can be defined for the system of grain boundary lines that lie in a plane perpendicular and parallel to the so plane, or if there is an external grain shape anisotropy. Therefore, a system for obtaining parallel and perpendicular secants must be established. An accurate method for determining the orientation of these test lines extracted from geometric techniques used in defining the finite strain in rock fabric. The direct method for determining the orientation in naturally deformed Rocksalt requires measuring the shape of the grain and the interparticle distance. Along with the analysis in terms of grain shape, it is imperative that the sample is oriented with respect to a known gross texture or stratigraphic feature, such as bedding, in order to interpret any correlation existing with the external grain morphology and crystallographic orientation.

Ramsey (1967) has presented several useful methods which can be used to evaluate the principal extentions and their axial ratios in the section. His technique is applicable to rocks containing particles which were initially distributed equally throughout the rocks. To determine the the system of oriented test lines and estimate the strain in rocks, one cannot rely on

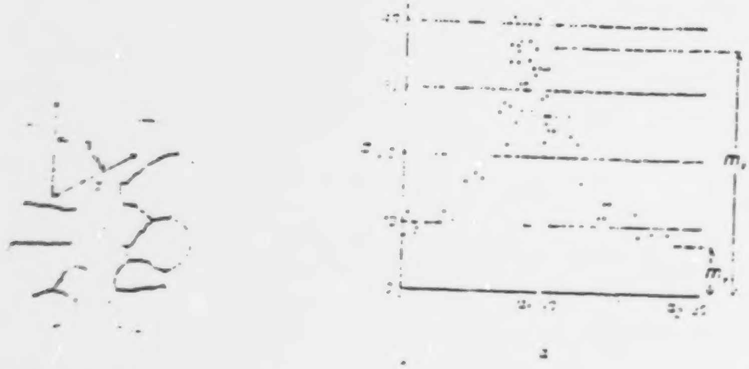

Figure 4. The same material now deformed, and the plot of 'd' vs. '∝', (after Ramsey, 1967).

The direction of maximum and minimum extension ('λ'_{m1}' and 'λ'_{m2}') can be determined from the graph. The principal strain ratios (mX/ mY = X/Y) can also be obtained.

This technique is essential for measuring strain in rock which has suffered pressure solutioning, but is also applicable to any rock containing originally, uniformly distributed particles.

Various strain components of the strain ellipse can be calculated from data obtained by the graphical method (presented above), (Ramsey, 1967). The strain components with reference to two other perpendicular planar sections can be obtained. Assume three sections 'xy', 'yz', and 'zx' with lines intersecting 'x', 'y' and 'z'. Using the ratios of the axes measured from the section, let the ratios be:

$$R_{xy} = \dot{\lambda}_{xy1}\ \dot{\lambda}_{xy2},\ R_{yz} = \dot{\lambda}_{yz1}\ \dot{\lambda}_{yz2},\ \text{and}\ R_{zx} = \dot{\lambda}_{zx1}\ \dot{\lambda}_{zx2}. \qquad (4.1)$$

then the strain components in the 'xy' section can be given by:

$$\begin{aligned} \ddot{\lambda}_{x} &= \ddot{\lambda}_{xy1}(\cos^2\theta_x + R_{xy}\sin^2\theta_x) \\ \ddot{\lambda}_{y} &= \ddot{\lambda}_{xy1}(\sin^2\theta_x + R_{xy}\cos^2\theta_x) \\ \gamma'_{xy} &= \ddot{\lambda}_{xy1}(R_{xy} - 1)\sin\theta_x\cos\theta_x \end{aligned} \qquad (4.2)$$

The strain components in the 'yz' section are given by:

$$
\begin{aligned}
\lambda'_y &= \lambda'_{yz1}(\cos^2\theta_y + R_{yz}\sin^2\theta_y)\\
\lambda'_z &= \lambda'_{yz1}(\sin^2\theta_y + R_{yz}\cos^2\theta_y)\\
\gamma'_{yz} &= \lambda'_{yz1}(R_{yz} - 1)\sin\theta_y\cos\theta_y
\end{aligned}
\qquad (4.3)
$$

Since both eq'n 4.2b and 4.3a give values of 'λ'_x'; 'λ'_{yz} can be calculated in terms of 'λ'_{xy}' ;

$$
\lambda'_{yz1} = \frac{\lambda'_{xy1}(\cos^2\theta_x + R_{xy}\cos^2\theta_x)}{\cos^2\theta_y + R_{yz}\sin^2\theta_y} \qquad (4.4)
$$

Thus, one can express 'λ'_z' and 'λ'_{yz}' in the equivalent form as λ'_x ', 'λ'_y' and 'λ'_{xy}', that is, with the same unknown multiplying factor 'λ'_{xy}' equals to a constant, (Ramsay, 1967). All can be defined in terms of the same unknown multiplying factor.

The parameters 'λ'_{xy}' are the principal reciprical quadratic extensions of the strain ellipse of a sectional plane 'ab'. 'θ_x' is the angle between the major axis of the strain ellipse and the x-axis. ' e ' is defined by;

principle extension: e = (original unit length - change in length)

(change in length)

(1+e)**2 = Sxy (principal stretch parameter)

Reciprical quadratic elongation λ'_{xy} = 1/ Sxy

Representation of Crystallographic Orientation by Pole Figure Measurement

The basic method of representing preferred orientation of structural and crystallographic elements, with a reference specimen plane are discussed in Wenk (1985) and Ramsey (1983). "The crystal direction is first projected onto a sphere of unit radius around the crystal and the point on the sphere is defined by two angles, a pole distance 'α' and an azimuth angle 'β', which is measured from point 'E' counterclockwise (Fig. 5A).

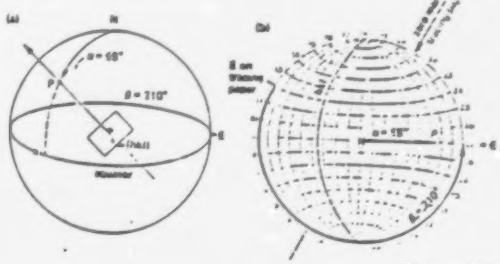

(Fig.5). Spherical coordinates (a) and representation of orientation data in a spherical projection, (after Wenk, 1985.).

This sphere must then be projected onto a plane in order to represent the point on paper.", (Wenk, 1985). Data is conventionally projected onto an equal area stereonet or a Schmidt net. A Wulff net can also be used, but is usually reserved for represenation of planes on a sterecnet. The distribution of points on a stereonet can be interpreted quantitatively. Statistical representation can be developed by replacing point plots by a continuous density distribution. Most techniques involve contouring areas of equal point density.

Various methods for obtaining a contoured pole figure are explained in Wenk (1985), Ramsay (1983) and Priest (1985).

The rocksalt under observation contains large and variable grain size. Sections developed to measure the cleavage orientation have been derived from various different planar locations from the block sample. Thus, polar points from a particular section had to be rotated later into a reference plane, so as to evaluate the distribution. There is a maximum of three measured orientations per grain due to (001) cleavage and a possibility of several (111) dislocation glide planes on a single grain. Both are distinguishable by their intersection.

Grain Orientation analysis by Transmission Optical Microscopy

Pole figure data, and more specifically crystallographic cleavage orientation of individual crystals can be determined by methods in transmission optical microscopy.

The mineral phases in Rocksalt are generally of the cubic system, thus displaying an isotropic optical indicatrix. Such is the case when there is only one velocity and refractive index for light propagating through the medium in any direction. The triaxial ellipsiod, (or the optical indicatrix) which conforms to the crystal symmetry, is represented by a sphere. If the indicatrix is an ellipsiod, light will travel with a different velocity in different directions. Polarized light with two vibration directions attains a path difference ' Δ ', that is longer for thicker crystals and for larger relative difference in refractive indices; which is also referred to as birefringence. Light waves are brought to interference in a polarizing microscope by passing through an analyzer filter, which allow the passage of only those components of the wave that vibrate normal to the originally polarized light and produces an optic image. The optical effects are not useful for cubic minerals since light propagates equally in all directions and every section of the indicatrix. This problem is aleveated by using morphological markers that depend on the crystallographic characteristics of the mineral, such as cleavage; instead of the optic figures.

One of the major factors that control the nature and development of microstructure in Potash Rocksalt is the orientation of mineral grains and more particularily, the orientation of inherent cleavage. Cleavage orientation data of individual crystals can be represented by pole figure plots.

An inexpensive and efficient method used to determine the orientation of crystallographic features in crystals can be established by optical microscopy outfitted with special stage apparatus. Morphological markers (in this case cleavage or alligned fluid inclusions) need to be rotated into a standard setting with respect to the microscope referance coordinate system. This can be accomplished by a Universal Stage mounted on a Petrographic microscope,(see Fig.6). Polished thin sections can be rotated about 3 mutually perpendicular axes in addition, the microscope stage can also be rotated.

Wenk (1985) describes the methodology behind the operation of obtaining measurements of crystallographic features from mineral grains." Observations are possible up to tilt angles of 50 degrees. There is a control axis 'C' perpendicular to the microscope axis 'M' at the normal stage setting in the E-W direction. Usually one tries to align the desired crystal direction, an indicatrix direction (for uniaxial and biaxial mineral phases) or a plane normal (ie. cleavage), parallel to this axis so that it is independent of rotation around 'C'. In this setting the tilt of the specimen about the horizontal axis 'H', which is in the plane of the thin section, provides the pole distance. The rotation around the axis 'N', normal to the thin section, gives the azimuth of the crystal direction in 'C', in standard spherical coordinates."

Glass hemispheres have been introduced to the Universal Stage system, and are mounted at the top and bottom of the thin section to ensure normal incidence at all tilt angles. The section is sandwiched in between the two hemispheres with a thin layer of mineral oil or glycerin between the section and hemispheres. If the refractive induces of the glass hemispheres, glass slide and crystal match, light passes straight through all layers. Deflection occurs in each layer if the refractive induces of the oil and other layers are mismatched. This is important only for the mineral grain which is being measured. The deflection increases with the tilt angle and the difference in refractive index between the various mediums.

Procedures for mounting and aligning the Universal Stage on the microscope and taking measurments are described in Wenk (1985) and Hutchison (1974). In brief, it is common in petrofabric work to plot the normals to all halide cleavages on a sterographic plot. For this the universal stage is used without crossed nicols. Each halide crystal is measured in the section. Thus, the selected grain is transferred into the appropriate field of view. The crystal in turn, is rotated on the innermost 'N' axis until its cleavage is exactly parallel to the E-W crosshair. The crystal is then tilted on the outermost 'H' axis until the image of the cleavage plane becomes as narrow as possible. This makes the cleavage plane exactly vertical and E-W. The pole to the cleavage plane is then recorded and plotted. One then proceeds to the next grain.

The size of the equiaxed Halide crystals ranges from 0.32mm to 2.5cm. thus, composite sections were developed to condense a large area of the crystalline mosaic into an area of a standard thin section. The preferred orientation of 'a' axes can be obtained with the Universal stage measuring cleavage planes. Because of the absence of cleavage traces in some grains, it has been suggested by Wenk (1985) to induce cleavage by quenching the sample in liquid Nitrogen after sectioning.

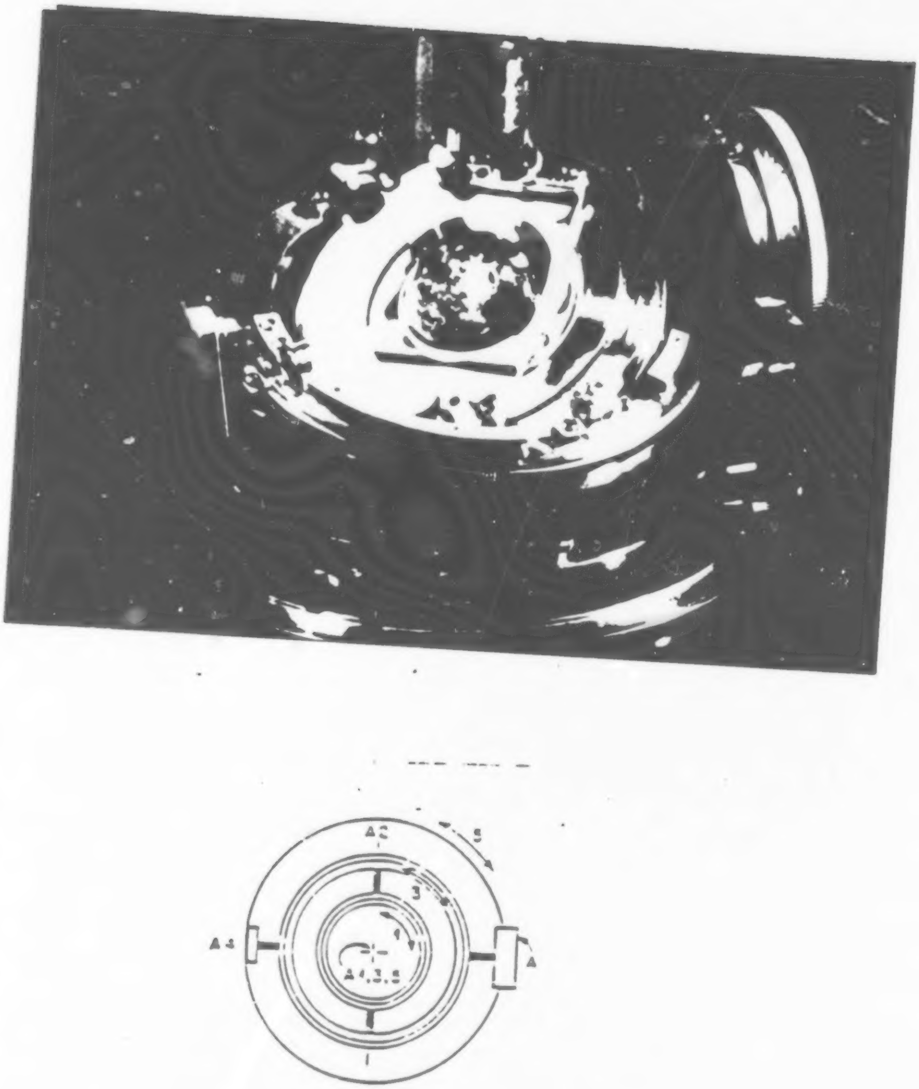
A2
5
3
4
A4
A
A4,3,5
1

Fig. 6. Standard Universal Stage mounted on a Leitz Petrographic Microscope and (bottom) schematic of 4-axes universal stage.

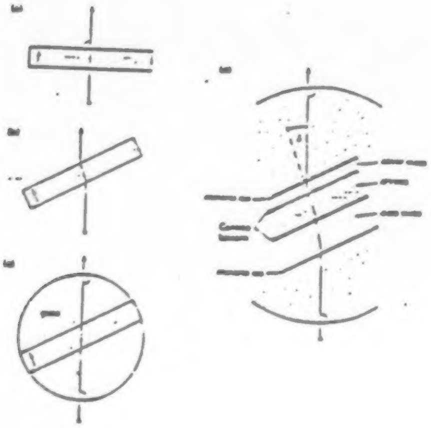

Fig. 7. Principle of Universal stage with glass hemispheres (after Wenk, 1985).

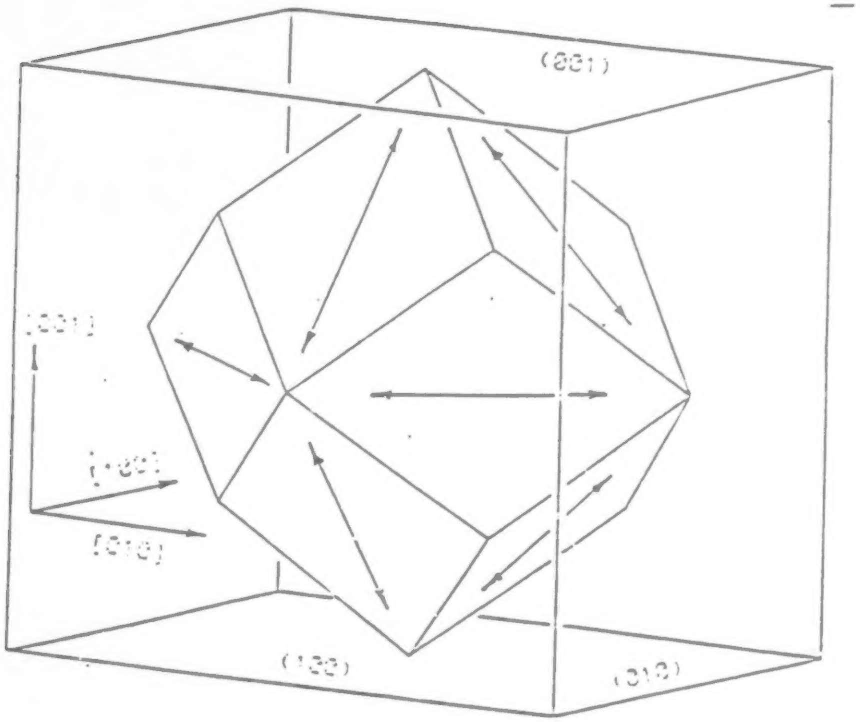
(001)
[001]
[100]
[010]
(100)
(010)

Fig. 8. Crystallographic cleavage & possible glide planes of Halite/ Sylvite.

Measurement of Compressional Wave Velocity

The P-wave velocity was determined by transmission ultrasonic technique, and measured in three orthogonal directions, in order to detect any structural anisotropy in the specimen. Several blocks with dimensions approximetly 12cm. x 6cm. x 6cm. were used to measure the velocities.

The velocity of accustic waves is determined by the elastic tensor, (eg; the Young's Moduli) or the longitudinal waves, (Sharma, 1981). Variations in velocity can occur due to inhomogenieties present in the structure, (Nur & Simmons, 1969). The elastic properties of a rock that initially had a random structure could remain isotropic under a hydrostatic stress field. Anisotropic conditions could result under a non-hydrostatic stress field (Clark & Schwertner, 1965), in terms of development of petrofabric in Potash Rocksalt.

The energy density and intensity is an important factor of any wave, and the energy associated with the motion of the medium as the wave passes through it. The wave velocity is a function of displacement and the kinetic energy contained within each element of volume. (Telford, 1984). The wave also involves potential energy resulting from the elastic strains created during the passage of the wave. The energy density is proportional to the first power of the density of the medium and to the second power of the frequency and amplitude of the wave, (Telford, 1984). A variation in velocity with distance is also detected from graphical results. This would imply a 'λ','I', and "f" variation as a function of distance.

One of the factors controlling crack propagation and orientation is due to the anisotropic behavior of the material, controlled by grain boundary density, grain shape distribution, texture (petrofabric) among other microstructure.

Test results can suggest the possibility that the P-wave velocity mesasurement can be used to quantify gross textural anisotropy by establishing a correlation with various microstructural parameters (Onedara & Kumara, 1980).

Measuring Techniques

Three techniques have been used in order to define the parameters discussed in the previous section.

Parameters associated with quantitative stereology have been obtained by lineal and point count methods preformed on microphotographs and actual slabbed polished samples representing the microstructural planar section in question. Various scales have been implemented, ranging from, macroscopic photographs (without the aid of a microscope), and two microscopic ranges; the former having a magnification stereoscopic range from x4 to x120 and the latter having a magnification range of x40 to x450. All photographs were taken by an accessory camera microscope mount made by NIKON which has a mount universally adaptable for other types and brands of microscopes.

Measurements used to generate pole figure diagrams were obtained by a Lietz 4-circle Universal Stage mounted on a Lietz Petrographic microscope. Grains were large enough and showed enough detail of cleavage at x125 magnification, so that to measure their orientation with respect to the specimen bedding direction. At least two cleavages (intersecting) must be measured per location, in order to ensure (001) cleavage direction. Each location must have three sets of cleavages. The third cleavage plane orientation is determined by planar stereographic projection methods. All points were then plotted on an equal angle stereonet, with respect to their appropriate orientation.

The Compressional Wave measurements were preformed by the use of the PUNDIT Ultrasonic Wave generator and recorder, with two peizoelectric transducers coupled on opposite sides of the sample. The time of the signal transmission was recorded. The velocity was then calculated from the measured dimensions of the block.

TABLE A

SUMMARY OF PARAMETERS

Parameters defined by Quantitative Stereology-

1) Measurement of Lineal Features in Petrofabric
    - a) for random test lines
        - i) total length of grain boundary per unit area
        - ii) degree of orientation
    - b) for oriented test lines
        - i) degree of orientation

2) Measurement of Grain Size
    - a) measurements for inequiaxied grains

3) Measurement of Spatial Distribution of Grains
    - a) Contiguity Ratio
    - b) Inter-particle (grain) distance
        - i) between same mineral phases
        - ii) between different mineral phas

4) Semi-Quantitative Finite Strain Measurements
    - a) approximete calculation of major & minor axes of the Strain Ellip of the structure and its orientation in a 2-Dimensional plane

5) Semi-Quantitative measurement of Crystallographic Grain Orientation
    - a) Pole Figure Diagrams
        - i) Of cleavage orientation of grai

6) Measurement of Compressional Wave Velocity

Discussion of Results

Results have been obtained from the three grouped parameters discussed in the previous section.

The grain size distribution shows a slight variation with respect to the location and orientation of the measurements. The average grain size calculated over the entire range of the bulk block is 1.15cm. This value is representative for the specimen, but local variations exist. These variations are localized within the 'layers' distinguished by either clay rich laminations or percentage of red interstitial Sylvite. The upper and lower bands show on average, smaller grain size than the central portion of the specimen. The central portion being approximetely, 1.68cm and either of the ends having an average grain size of 1.45 cm. (refer to figure 9.).

The degree of orientation, based on grain boundary lengths and orientation of the strain ellipsoid, shows a strong distinction possible between the orthogonal planes. The 'D' plane (which correspond to the 'ac' plane), has been calculated to have a 20% degree of orientation, in relation to relatively low values of 'w' along the other two planes.(see fig. 10).

The strain parameters estimated from inter-particle distance and angular deviation from the horizontal bedding reference frame show a strong grain orientation in the 'ac' plane; a moderate strain ellipsoid in the opposite vertical plane and a circular section of the ellipse in the horizontal dimension. Calculated values are presented:

All interparticle distances and angular deviations from the horizontal are shown in Fig. 11.

Values for Plane 'D' mX=11.45 mm. = 62 degrees

mY=7.63 mm. = 152 degrees

Rac (or Rzx) = 1.5007

S zx = 2.2522

x = 0.6173

z = 0.4930

zx = 0.0922

Values for Plane 'A' mX=10.10 mm. = 57 degrees

mY=8.70 mm. = 127 degrees

Rbc (or Ryz) = 1.1494

S yz = 1.3211

y = 0.8364

z = 0.7905

yz = 0.0565

The average grain boundary length is also reflective of the relative orientation of the strain ellipse. Variations exist along both horizontal and vertical intercepts in both planes, by a factor of as much as a factor of 0.55.

The inter-particle distance between Halite also shows a slight lateral variation. Again, the upper and lower portions of the sample have a lower inter-particle distance, than the central portions of the slab. The upper and lower areas are contain up to

5% of oxide-Sylvite whereas the central portion has less than 1%.

This variation is primarily due to the differential intensity of the strain ellipsiod imposed on the fabric,(see fig.12).

The crystallographic cleavage inherent in both mineral phases present in Rocksalt displays a preferred orientation. Two pole figure diagrams (and one composite diagram) show various point density maxima. If the North direction corresponds to the 'b' direction of the specimen, there is a quazi-axial symmetric distribution of poles. Three sets of pole concentration exist, and trend (in decreasing order of intensity); NW - SE, NE-SW and Horizontal, see figure 14. A total of 97 orientations generating 291 poles have been plotted.

Preliminary measurements of compressional wave velocity display a variation along the different orthogonal axes of the specimen. The average velocities calculated from three sets of 27 measurements indicate that the slowest speed is along the designated 'c' direction and the highest is along the designated 'b' direction. These values have been correlated with the degree of orientation and average grain boundary length along a plane. Results would indicate that the degree of orientation and direction of relict bedding have the most affect on the velocity in a direction of propagation.

The lowest velocity (parallel to the 'c' direction) is perpendicular to the relict bedding. It also corresponds to a homogeneous average grain boundary length along the direction of propagation. The highest average velocity measurement is parallel to the bedding and corresponds to the plane perpendicular to which has the highest degree of orientation., which indicates that the grain boundary lengths are lowest parallel to the direction of maximum grain elongation (ie 62 degrees with respect to thhe horizontal), and high along the minimum grain elongation. The 'ab' plane has a low degree of orientation (< 1.0%). By observation of the strain ellipsoids that intersect the orthogonal surfaces, it can be seen that the grain boundary density is low in the vertical direction and higher in the horizontal direction.

More importantly, is the variation in velocity as a function of distance of propagation. The absorption and/or dispersion, (which has not been experimentally evaluated), can cause the Energy density of the wave to decrease thus increasing the velocity, (as seen in fig. 16.). According to graphical interpretation, the velocity in the 'a' and 'b' direction increases sligthly with increasing distance; whereas, it is constant along the 'c' direction. If the velocity is the same for all the frequencies, the pulse shape will remain the same and the group and the phase velocities will be the same. However, if the velocity varies with frequency, the pulse changes shape as it travles through the medium and the group velocity is different from the phase velocity, which is interpreted as a dispersive medium.

Fig. 9. Grain size distribution based on orthogonal lineal intercepts.

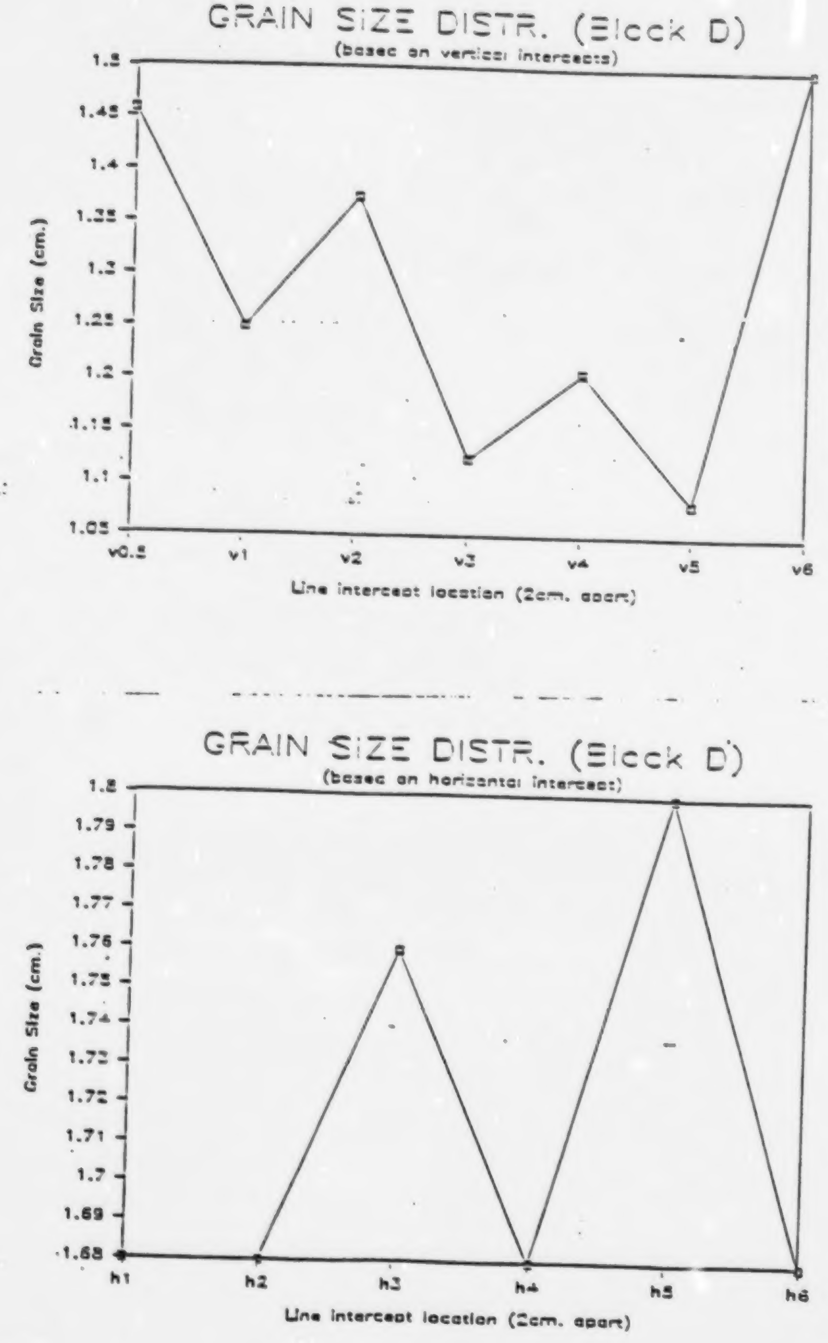

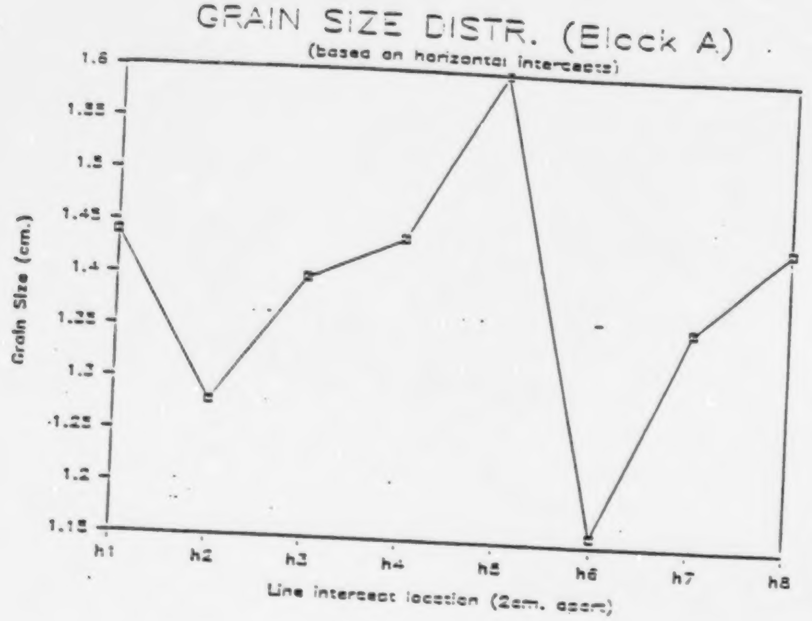
GRAIN SIZE DISTR. (Block A)
(based on horizontal intercepts)
Grain Size (cm.)
1.6
1.55
1.5
1.45
1.4
1.35
1.3
1.25
1.2
1.15
h1
h2
h3
h4
h5
h6
h7
h8
Line intercept location (2cm. apart)

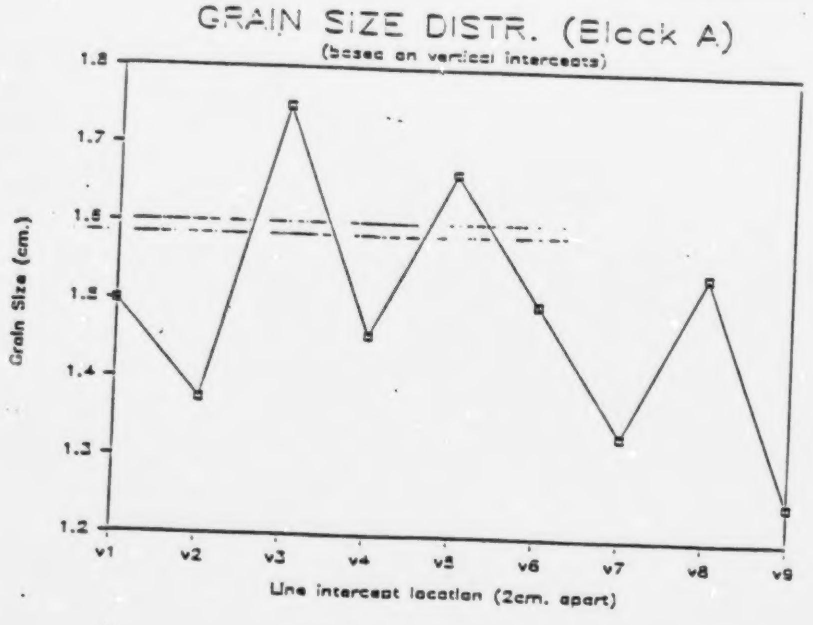
GRAIN SIZE DISTR. (Block A)
(based on vertical intercepts)
Grain Size (cm.)
1.8
1.7
1.6
1.5
1.4
1.3
1.2
v1
v2
v3
v4
v5
v6
v7
v8
v9
Line intercept location (2cm. apart)

Fig. 10. The degree of orientation is based on the grain boundary length per unit area (cm/cm**2). Data presented is the average length along various intercepts for all 4 vertical polished planes.

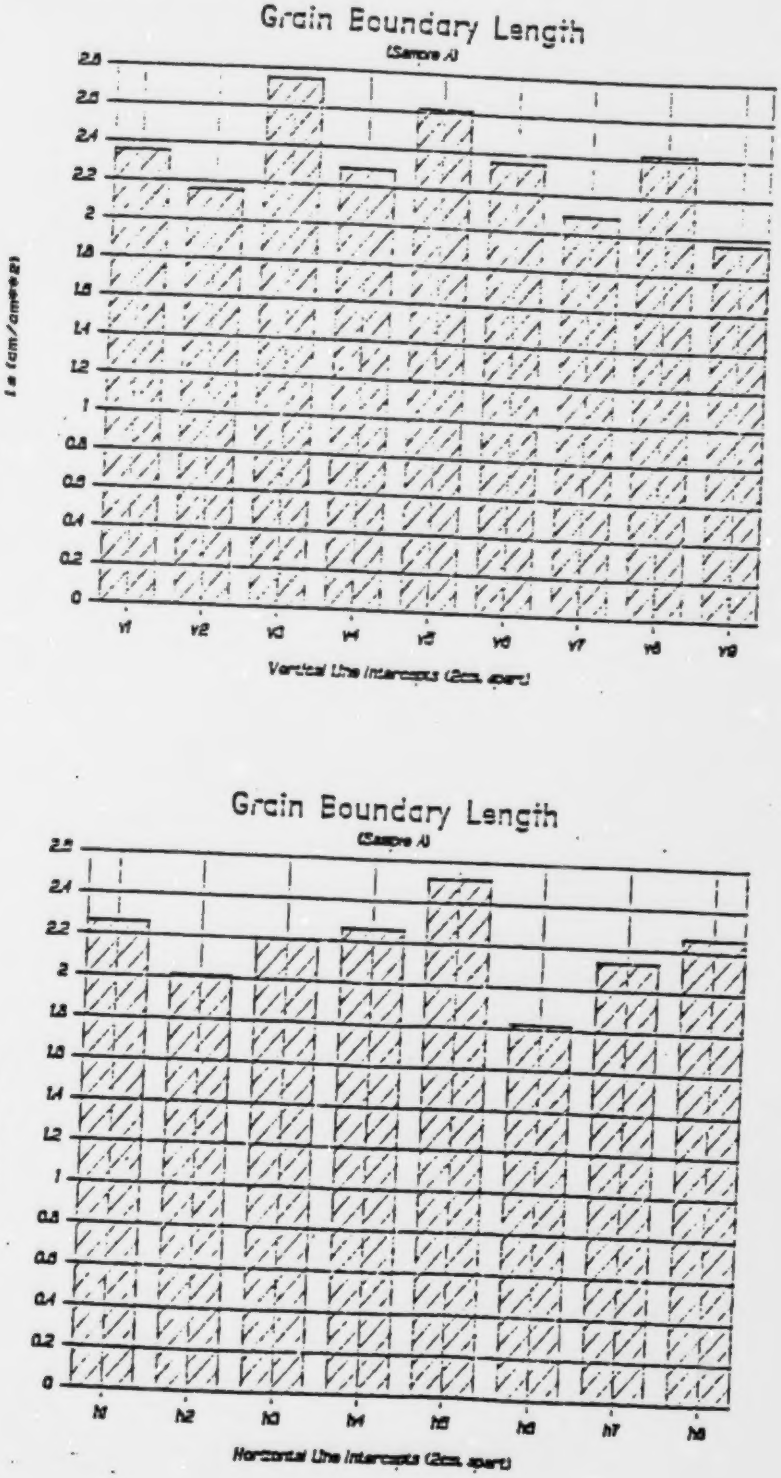

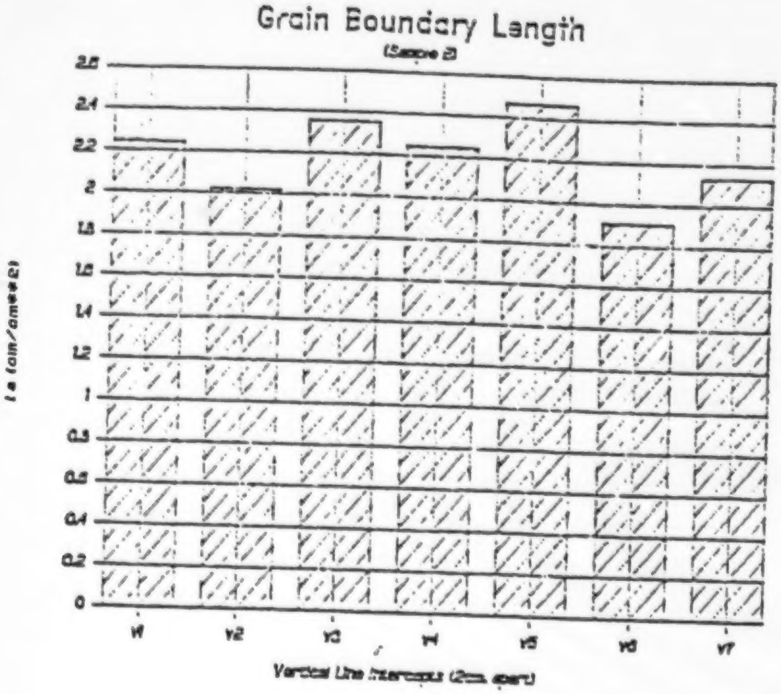
Grain Boundary Length
(Sample 2)
2.6
2.4
2.2
2
1.8
1.6
1.4
1.2
1
0.8
0.6
0.4
0.2
0
l a (cm/cm**2)
v1
v2
v3
v4
v5
v6
v7
Vertical Line Intercepts (2cm. apart)

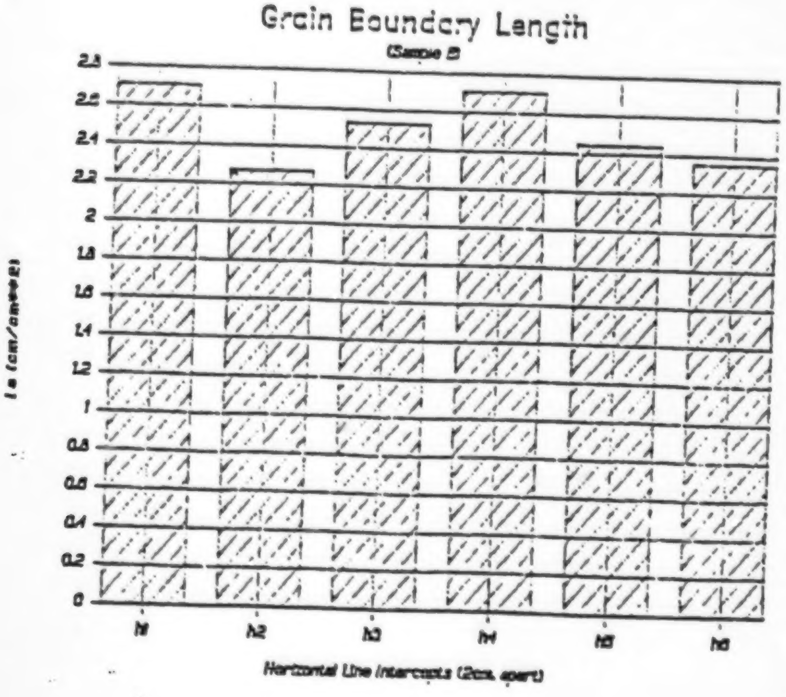
Grain Boundary Length
(Sample 2)
2.8
2.6
2.4
2.2
2
1.8
1.6
1.4
1.2
1
0.8
0.6
0.4
0.2
0
l a (cm/cm**2)
h1
h2
h3
h4
h5
h6
Horizontal Line Intercepts (2cm. apart)

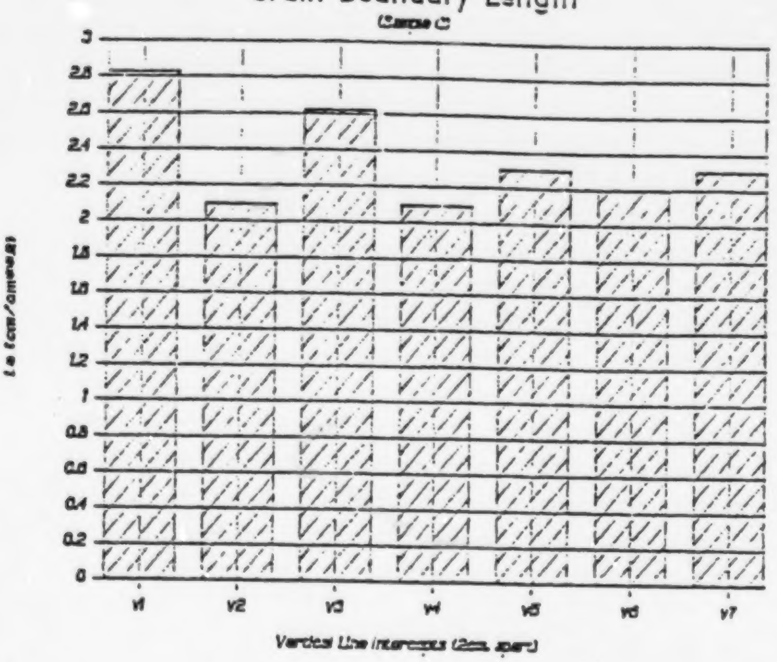
Grain Boundary Length
(Sample C)
3
2.8
2.6
2.4
2.2
2
1.8
1.6
1.4
1.2
1
0.8
0.6
0.4
0.2
0
Le (cm/cm**2)
v1
v2
v3
v4
v5
v6
v7
Vertical Line Intercepts (2cm. apart)

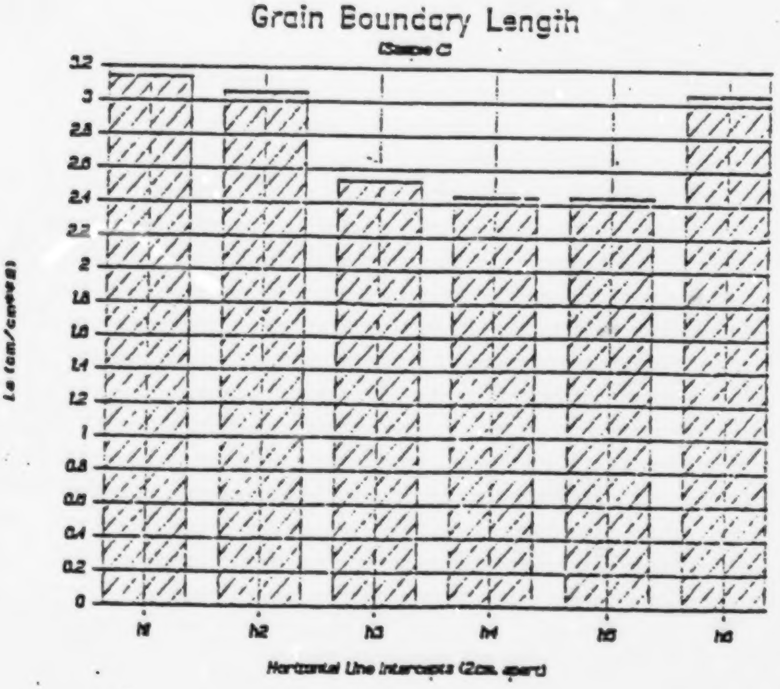
Grain Boundary Length
(Sample C)
3.2
3
2.8
2.6
2.4
2.2
2
1.8
1.6
1.4
1.2
1
0.8
0.6
0.4
0.2
0
Le (cm/cm**2)
h1
h2
h3
h4
h5
h6
Horizontal Line Intercepts (2cm. apart)

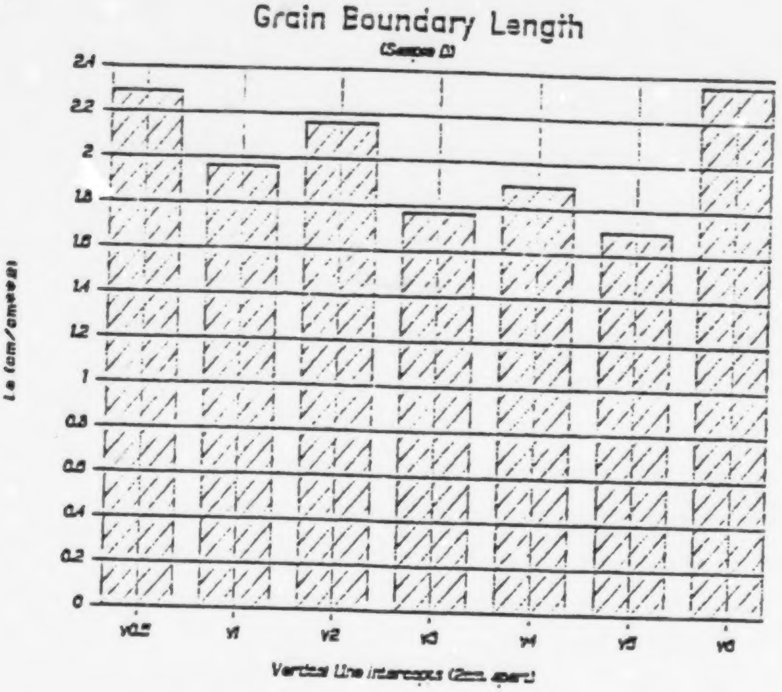
Grain Boundary Length
(Sample D)
Le (cm/cm**2)
2.4
2.2
2
1.8
1.6
1.4
1.2
1
0.8
0.6
0.4
0.2
0
v0.5
v1
v2
v3
v4
v5
v6
Vertical Line Intercepts (2cm. apart)

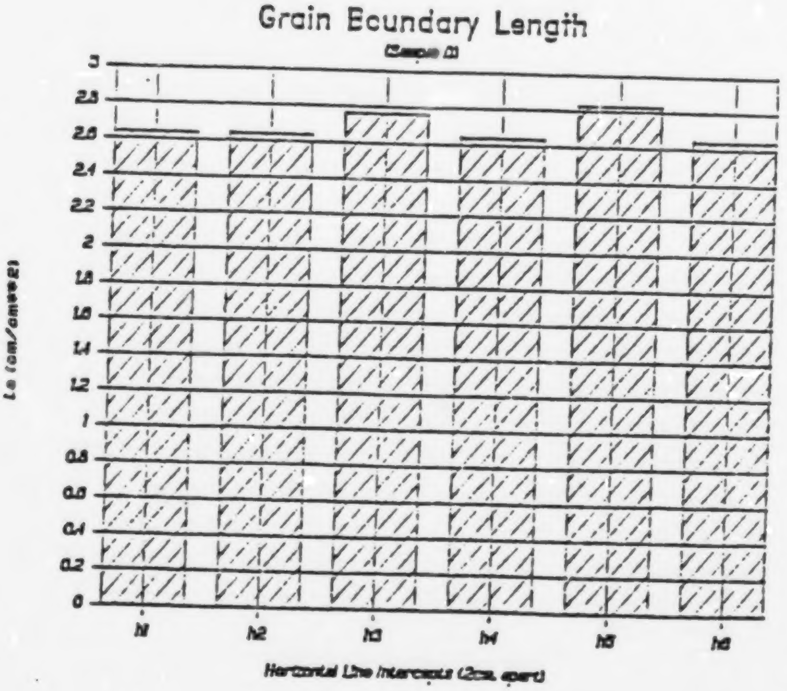
Grain Boundary Length
(Sample D)
Le (cm/cm**2)
3
2.8
2.6
2.4
2.2
2
1.8
1.6
1.4
1.2
1
0.8
0.6
0.4
0.2
0
h1
h2
h3
h4
h5
h6
Horizontal Line Intercepts (2cm. apart)

Fig. 11. Composite plots of 'α' vs. inter-particle distance (based on technique presented by Ragan, 1969).

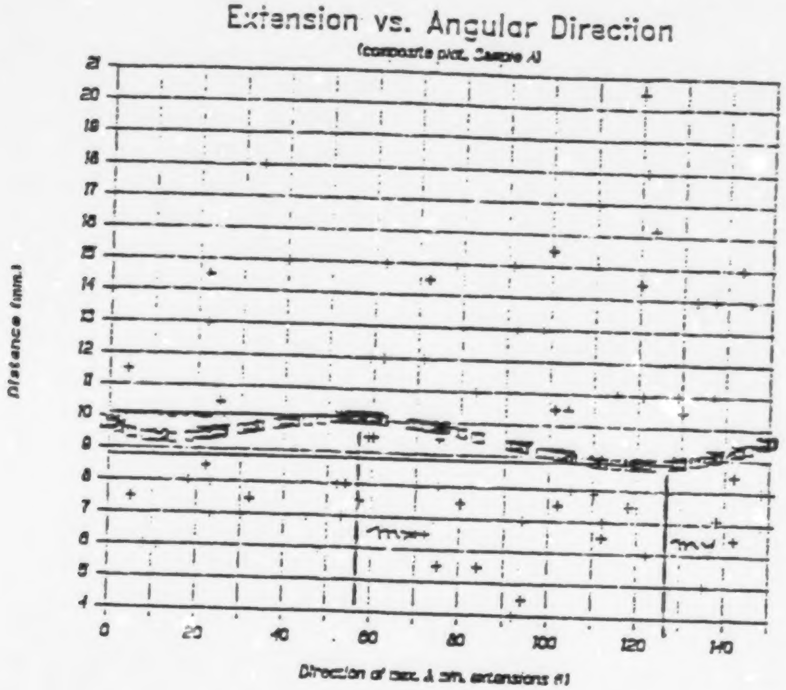

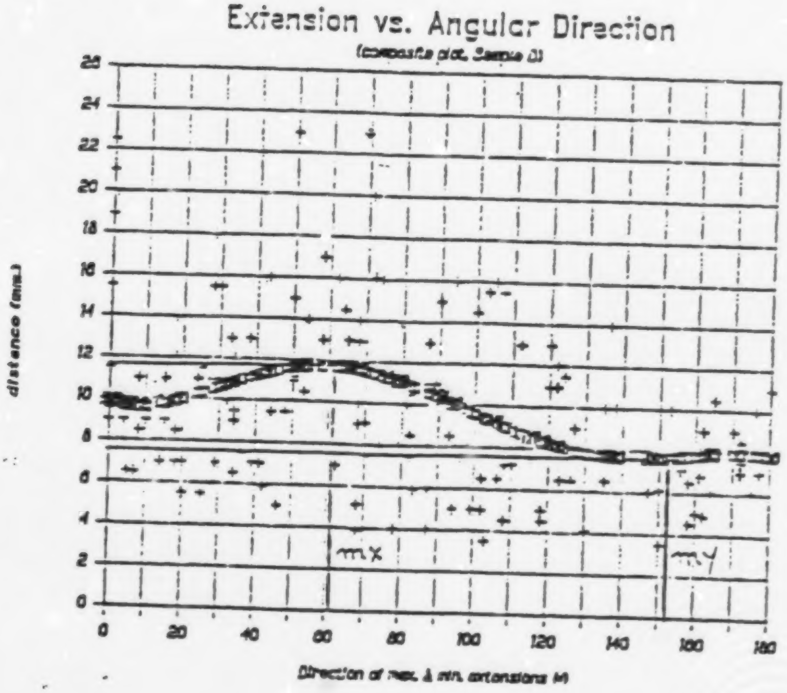

Fig. 12. Frequency distribution for inter-particle distance between adjacent grains for slab 'A' and 'D'.

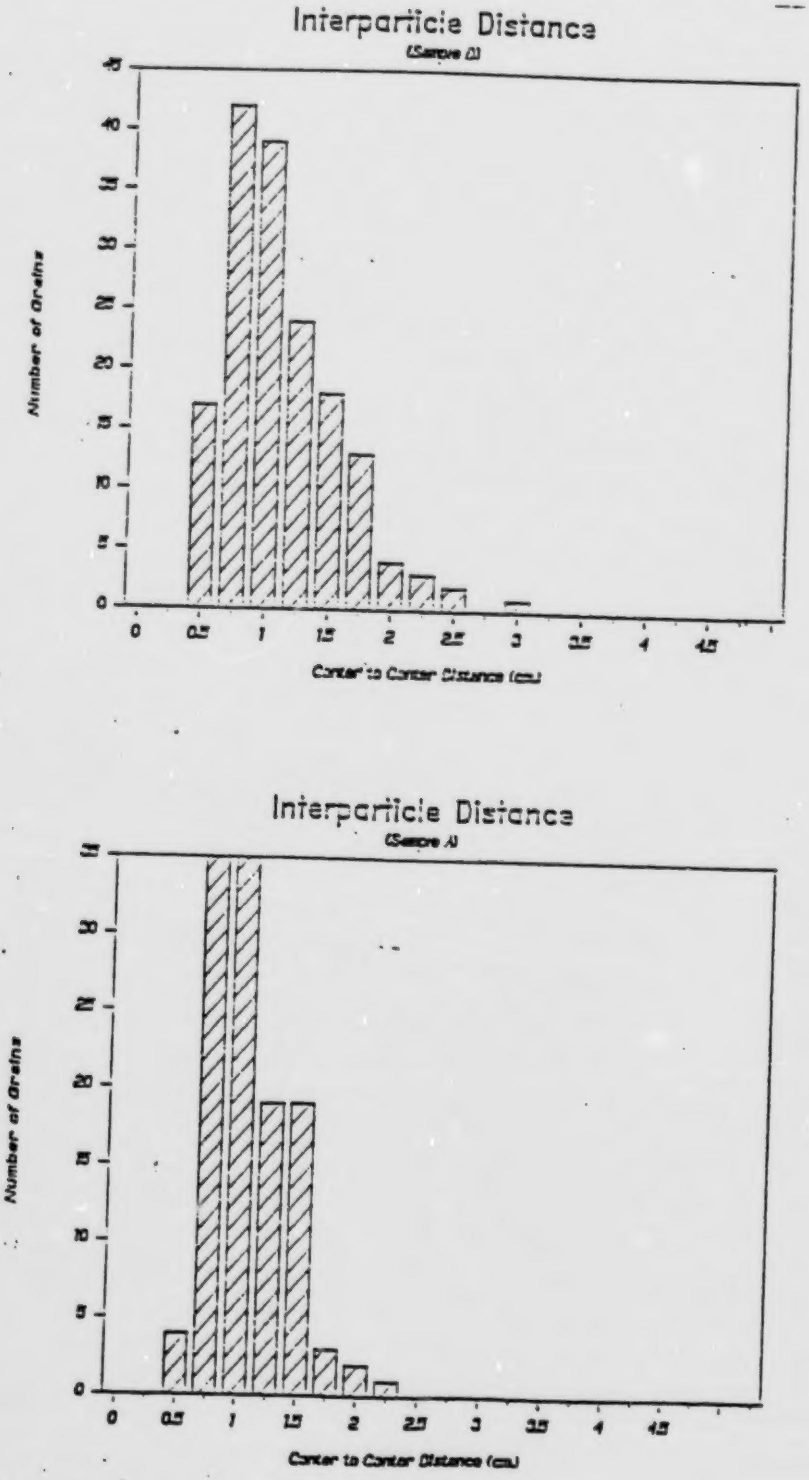

Fig. 13. Grain Boundary length, based on intersections with test lines oriented parallel and normal to the max. and min. extensions.

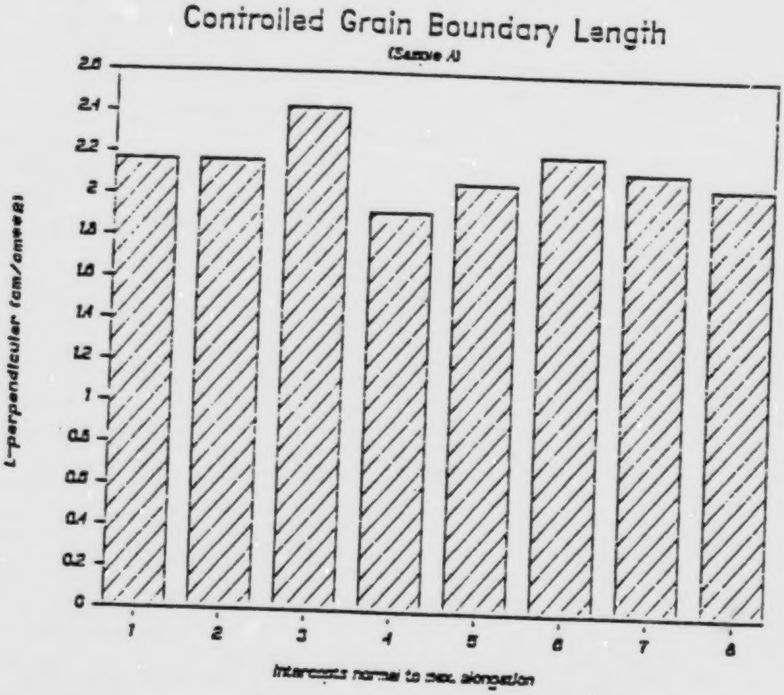
Controlled Grain Boundary Length
(Sample A)

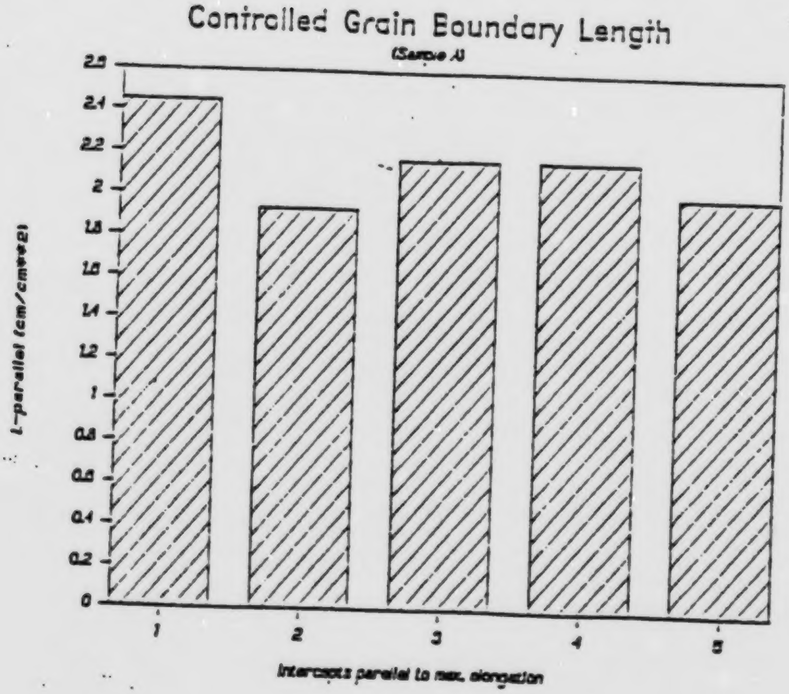
Controlled Grain Boundary Length
(Sample A)

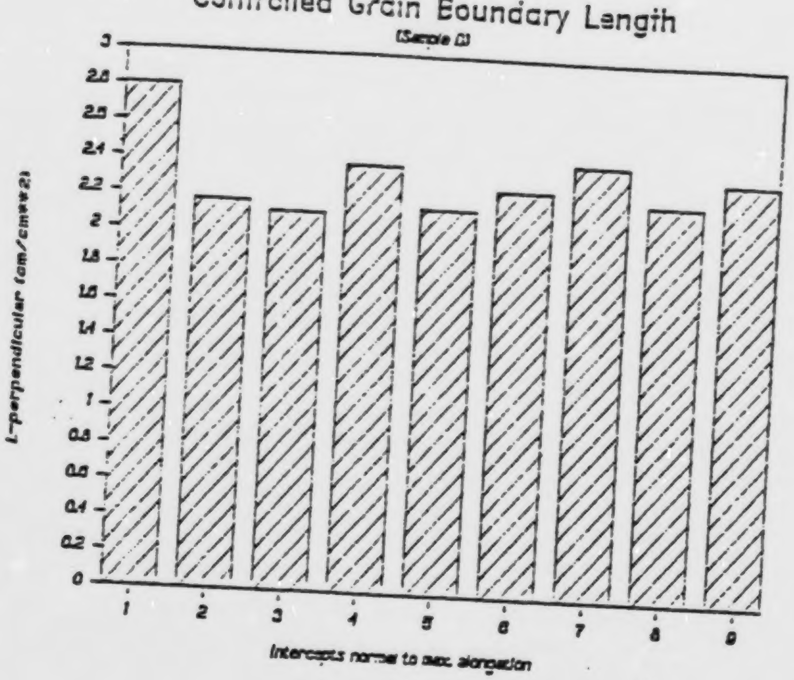
Controlled Grain Boundary Length
(Sample D)
L-perpendicular (cm/cm**2)
3
2.8
2.6
2.4
2.2
2
1.8
1.6
1.4
1.2
1
0.8
0.6
0.4
0.2
0
1
2
3
4
5
6
7
8
9
Intercepts normal to max. elongation

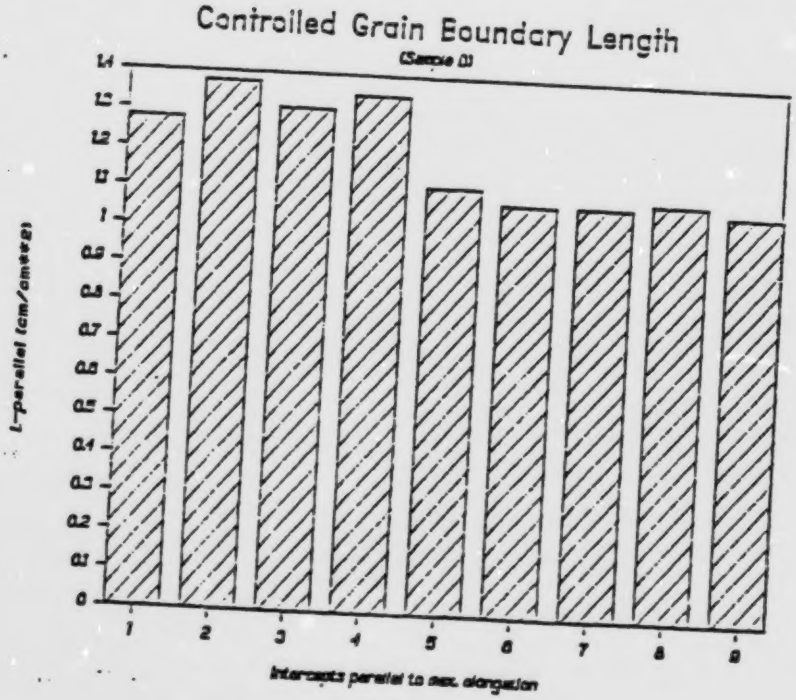
Controlled Grain Boundary Length
(Sample D)
L-parallel (cm/cm**2)
1.4
1.3
1.2
1.1
1
0.9
0.8
0.7
0.6
0.5
0.4
0.3
0.2
0.1
0
1
2
3
4
5
6
7
8
9
Intercepts parallel to max. elongation

Fig. 14.a Contoured pole figure diagram from grain measurements derived from vertically oriented slab. Diagram contains 147 cleavage points for 47 grains.

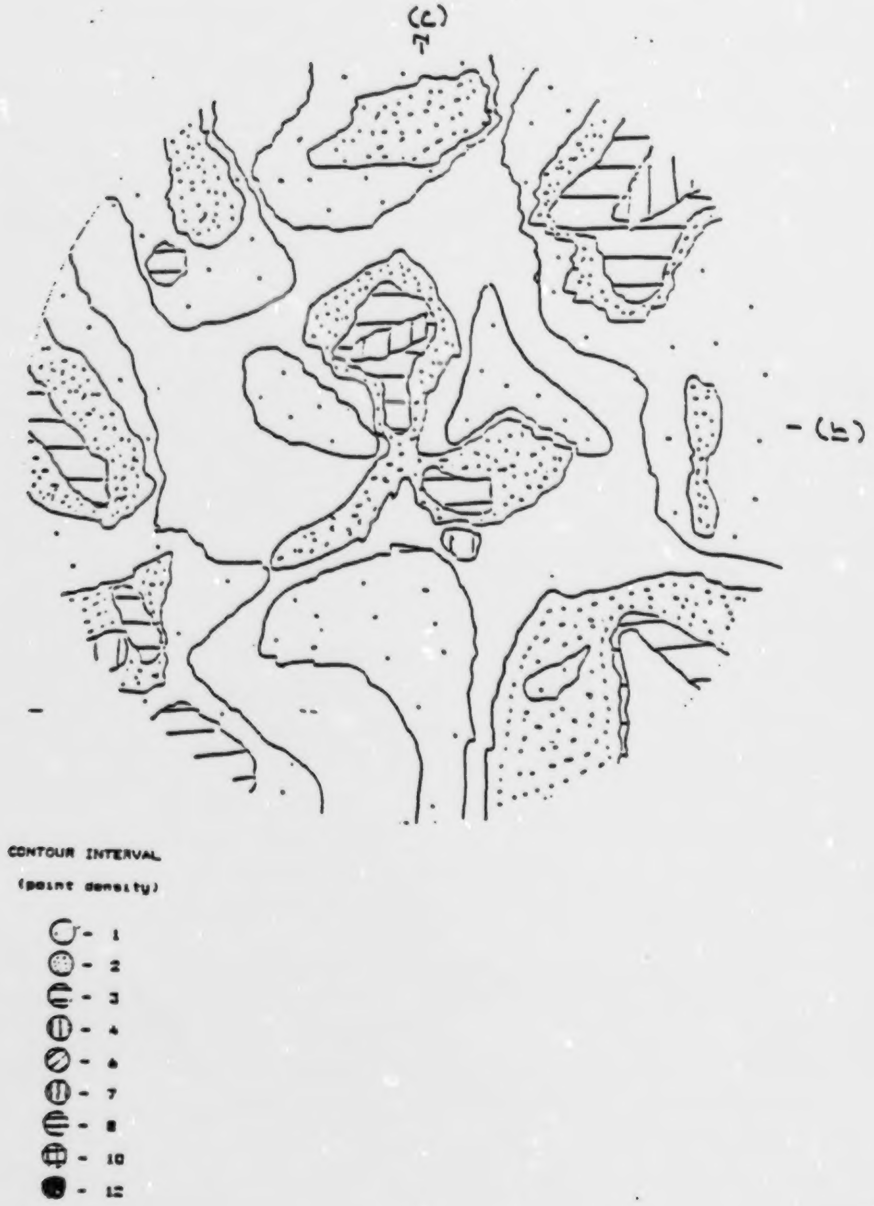

Fig. 14.b Contoured pole figure diagram from grains measured in the horizontal direction. 150 cleavage plots for 50 grains.

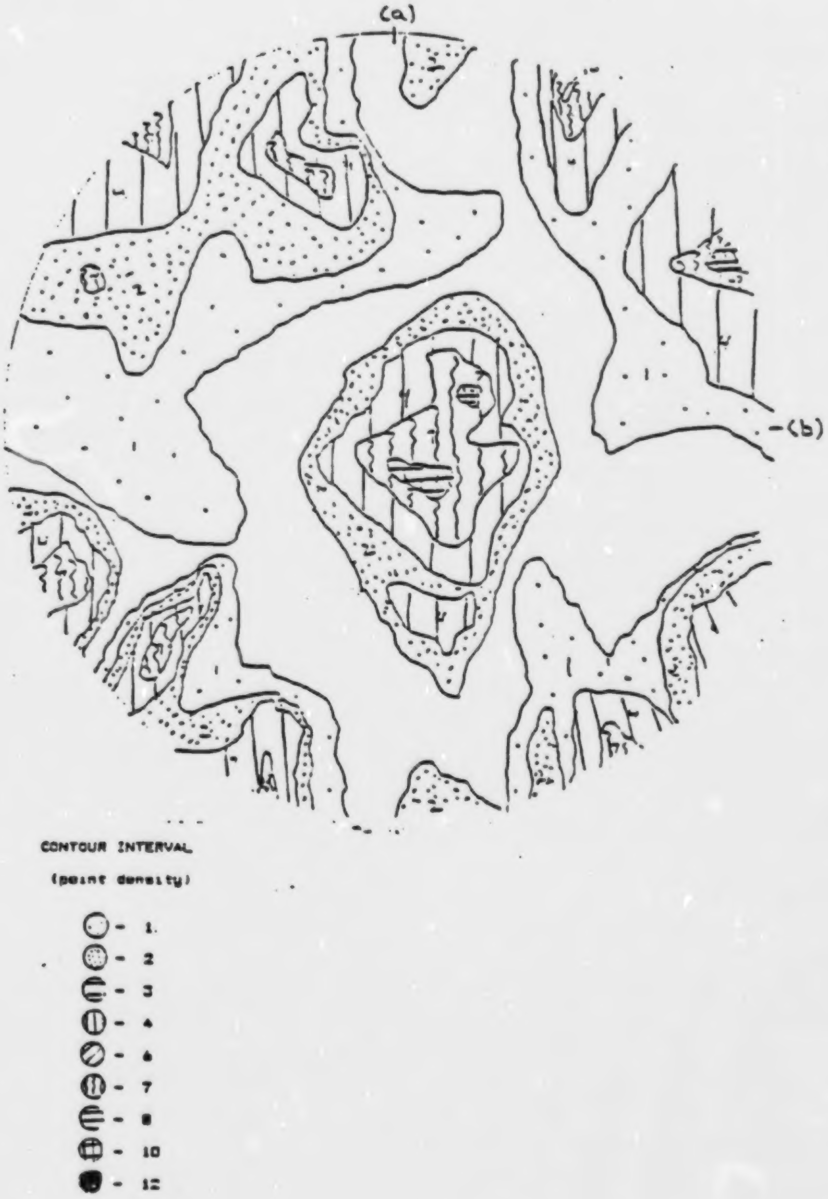

Fig. 14.c Composite pole figure diagram for vertical and horizontal data points.

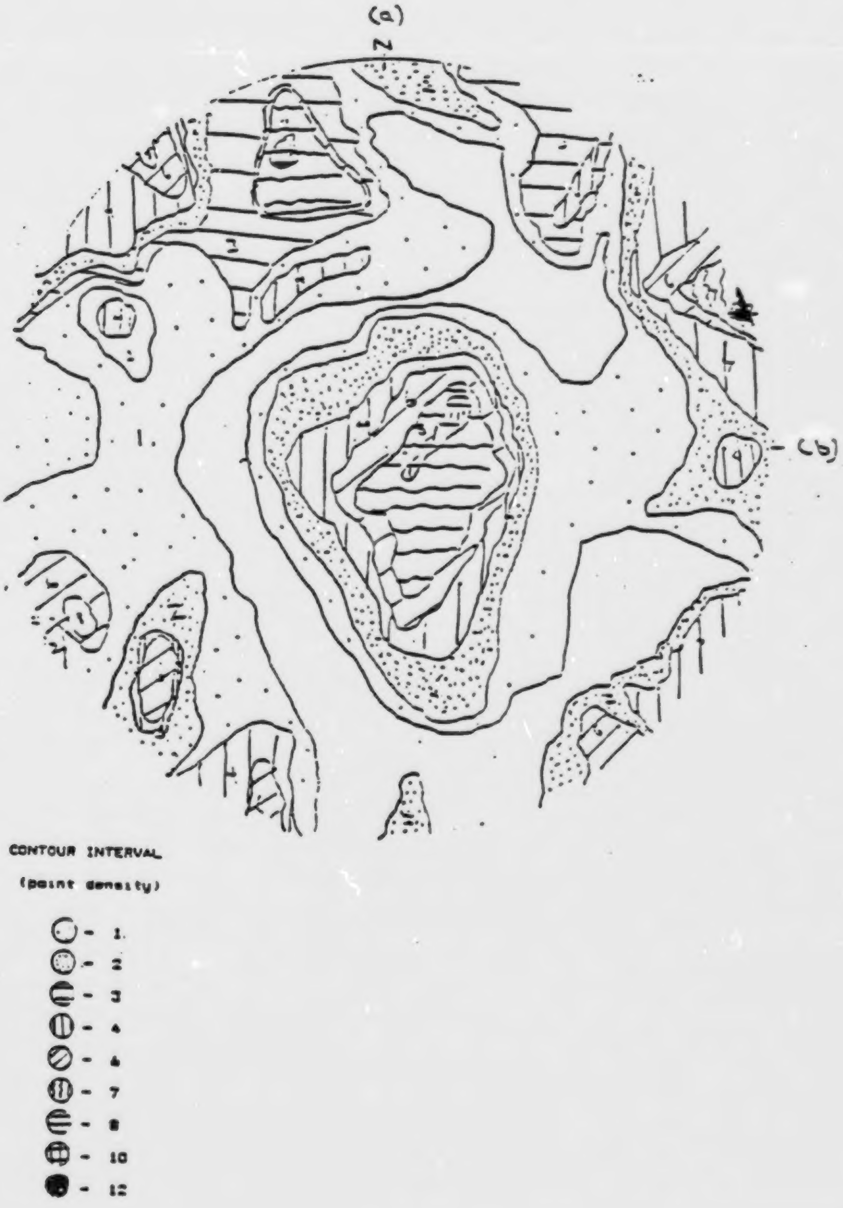

Fig. 15. Compression-wave velocity measurements from the various planes. Different linear relationships exist for each direction, clearly shown in d).

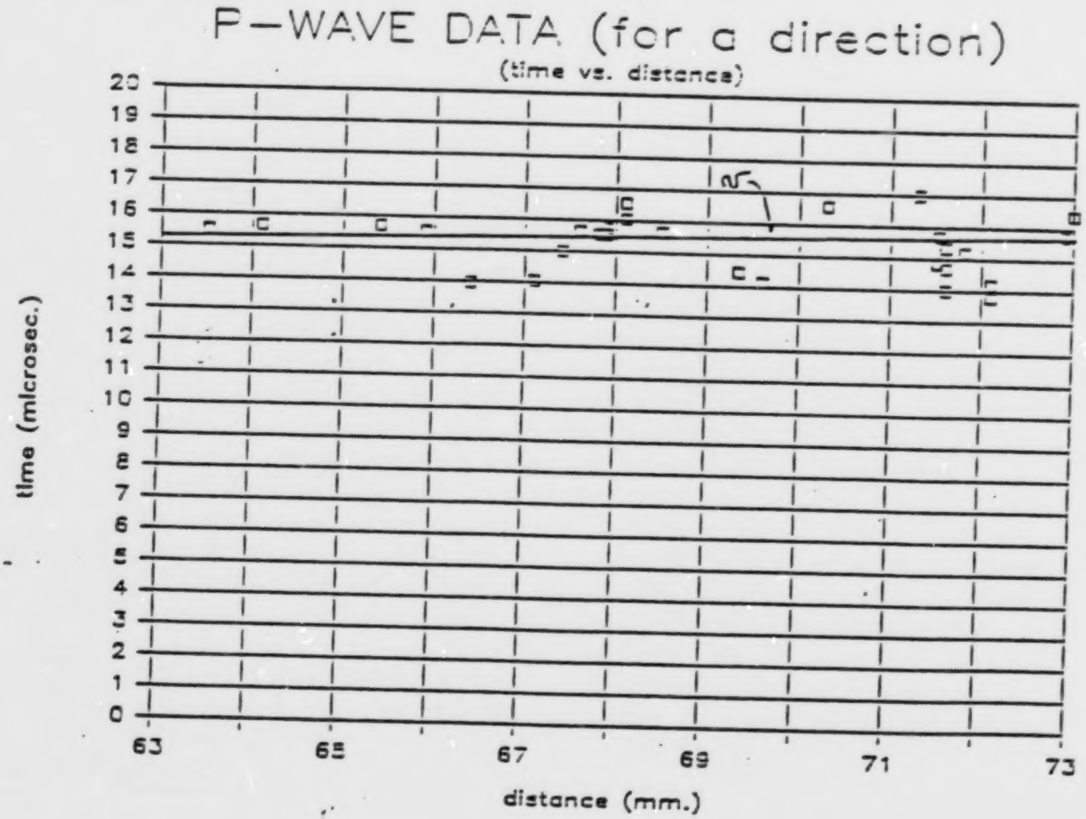

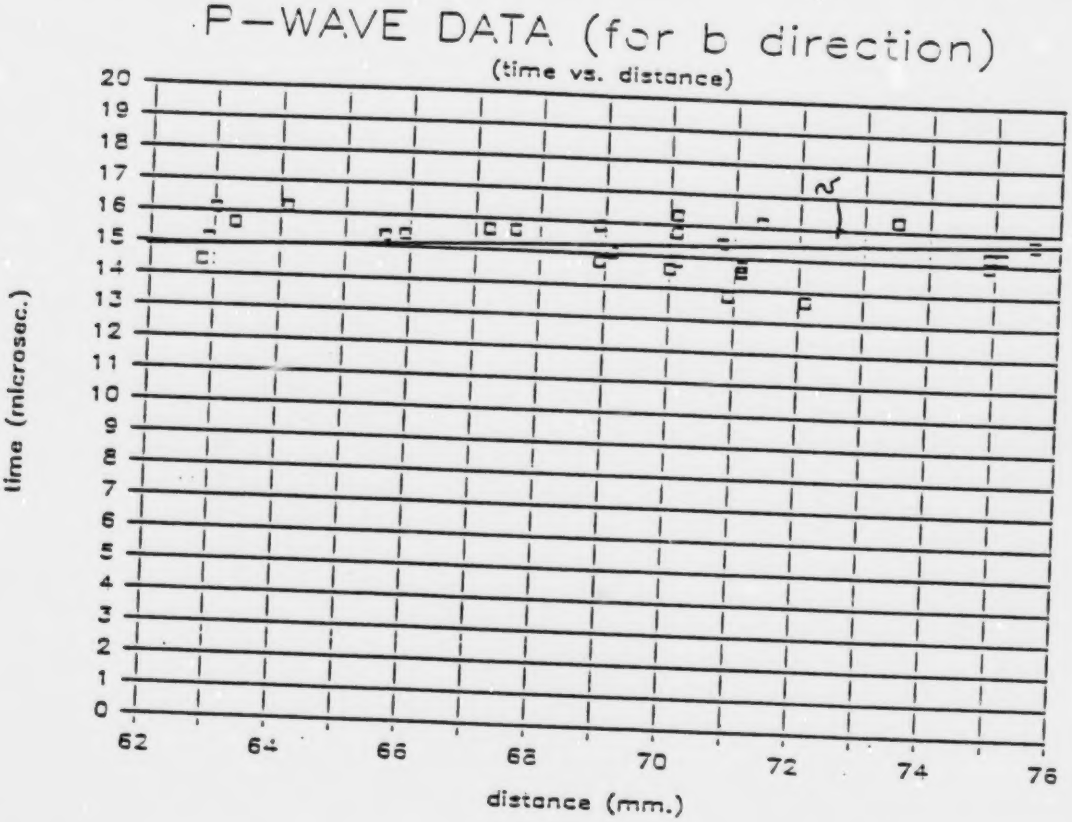
P–WAVE DATA (for b direction)
(time vs. distance)
time (microsec.)
20
19
18
17
16
15
14
13
12
11
10
9
8
7
6
5
4
3
2
1
0
62
64
66
68
70
72
74
76
distance (mm.)

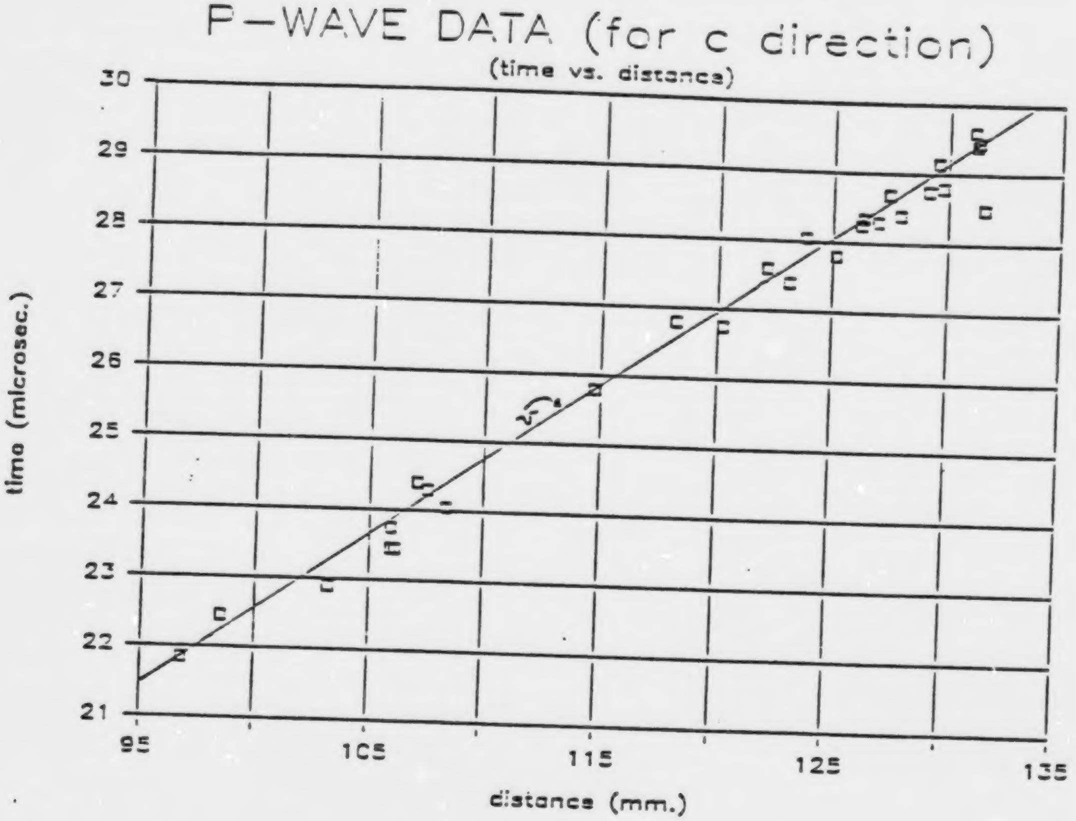
P-WAVE DATA (for c direction)
(time vs. distance)
time (microsec.)
distance (mm.)
30
29
28
27
26
25
24
23
22
21
95
105
115
125
135

Fig. 16. Velocity vs. distance plots indicate a positive correlation. There is an increase in velocity with an increase with distance, with the vertical planes. No variation is observed in direction 'c'.

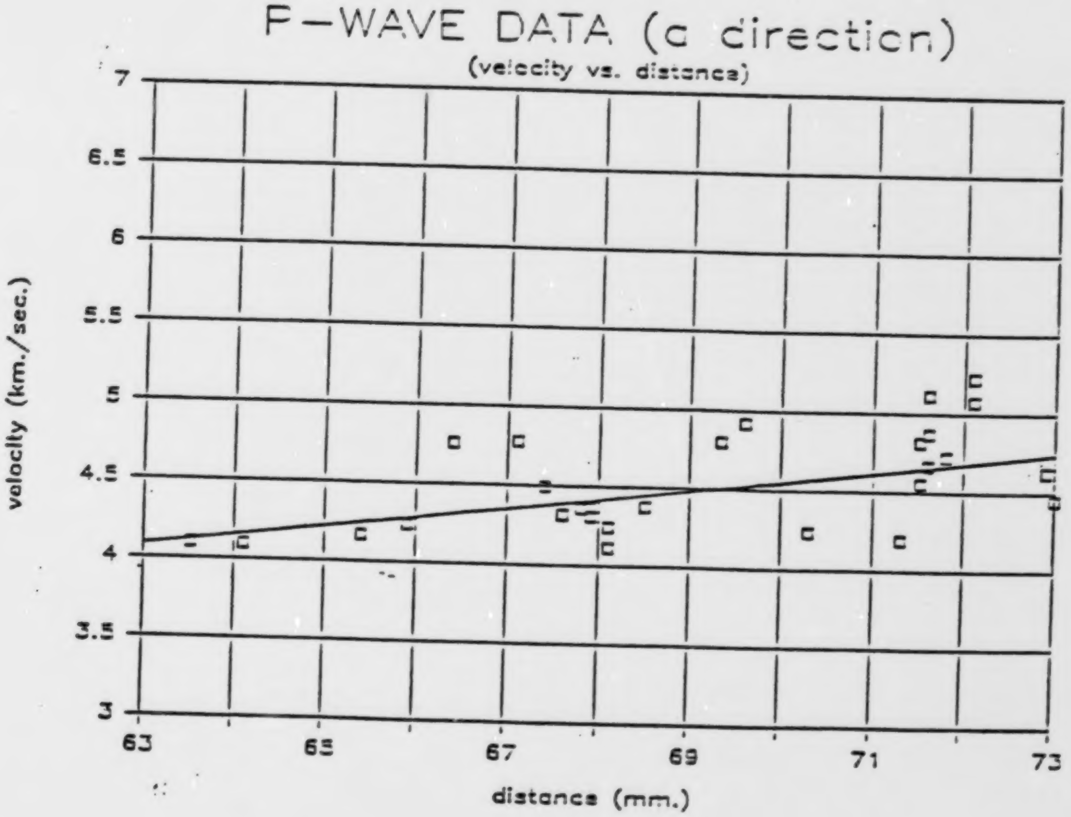

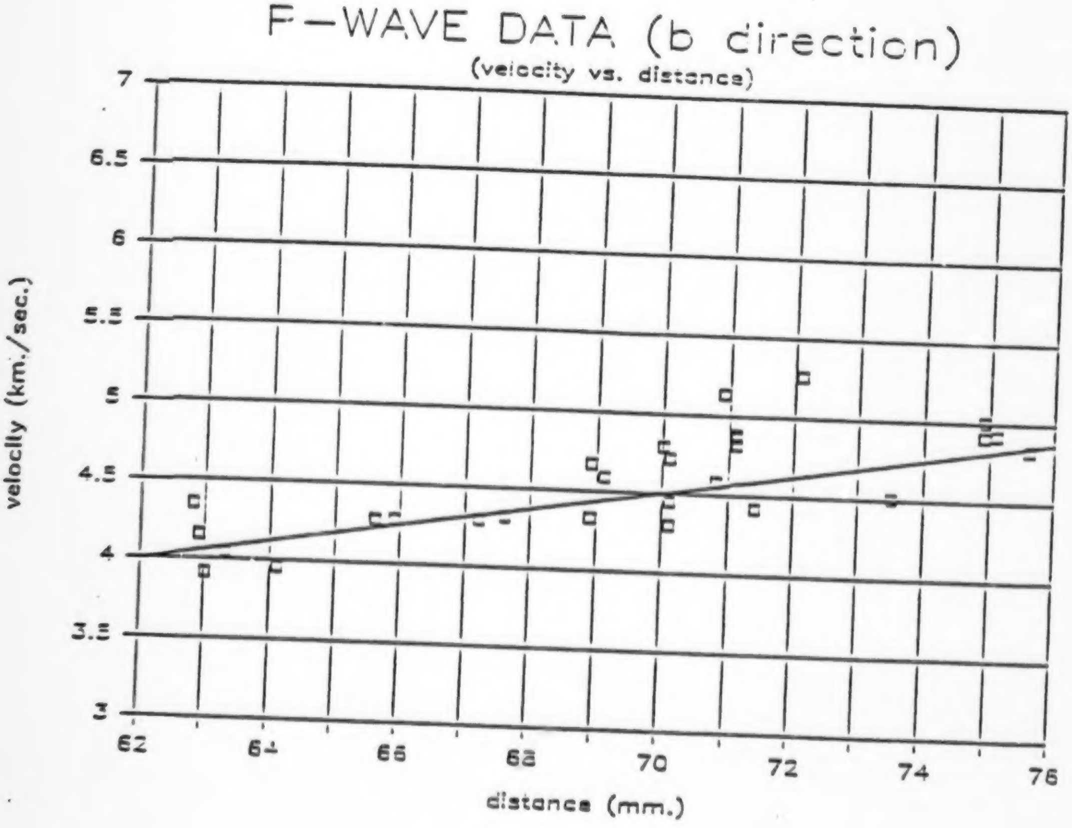
P—WAVE DATA (b direction)
(velocity vs. distance)
velocity (km./sec.)
7
6.5
6
5.5
5
4.5
4
3.5
3
62
64
66
68
70
72
74
76
distance (mm.)

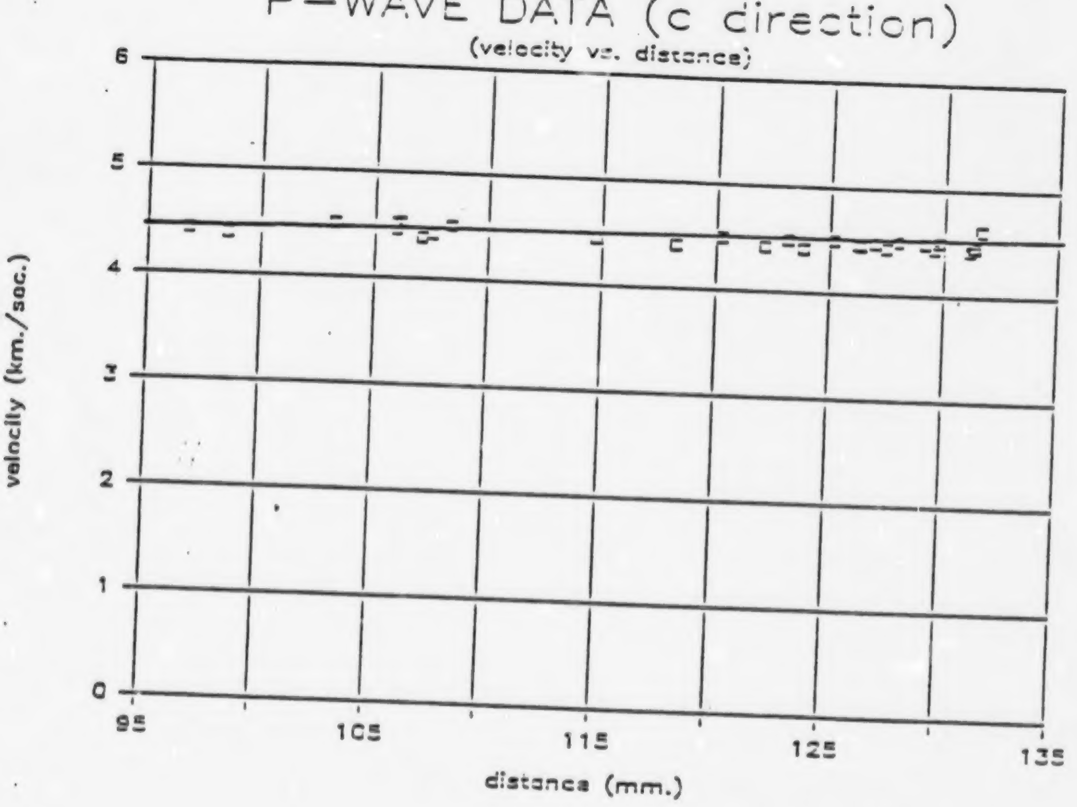
P—WAVE DATA (c direction)
(velocity vs. distance)
velocity (km./sec.)
0
1
2
3
4
5
6
95
105
115
125
135
distance (mm.)

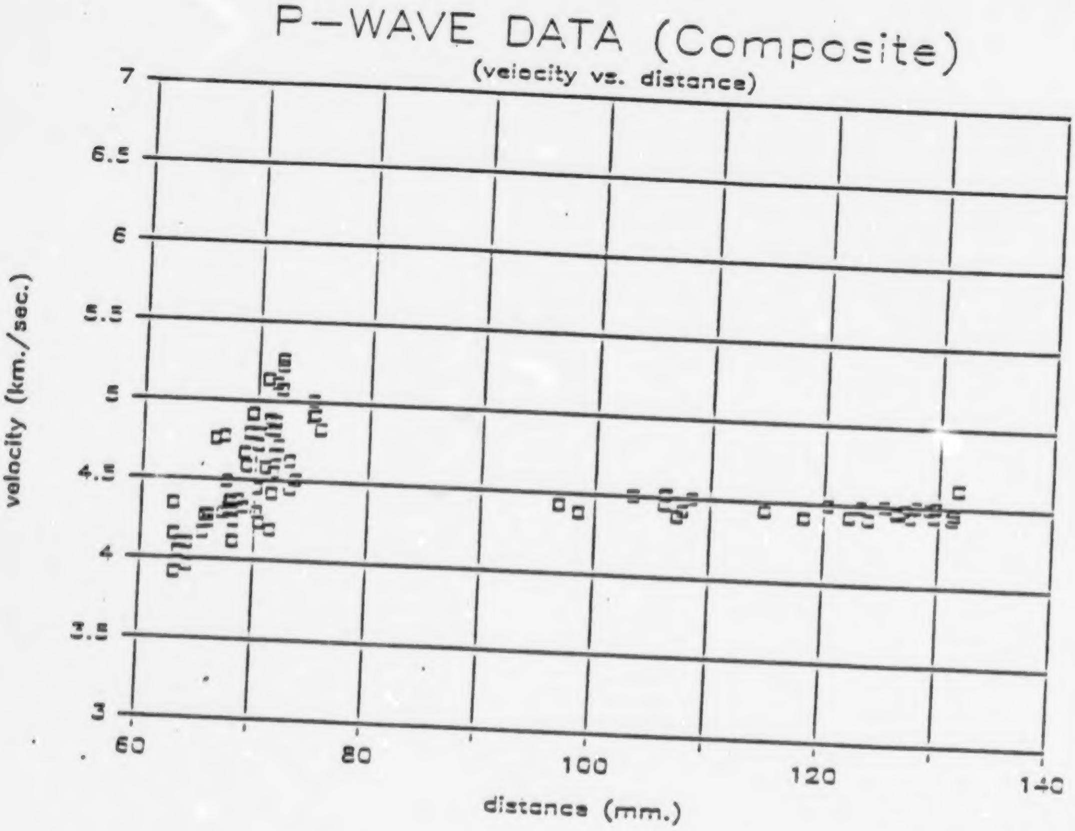
P—WAVE DATA (Composite)
(velocity vs. distance)
velocity (km./sec.)
7
6.5
6
5.5
5
4.5
4
3.5
3
60
80
100
120
140
distance (mm.)

Fig. 17. . Macrophotograph of fabric of specimens. (Upper) Diplays strong grain shape anisotropy, (middle & lower), displays a strong grain shape anisotropy with relict bedding outline. Lower-most photograph displays a fabric with nearly equidimensioned grains. Degree of orientation (from top to bottom) as measured by technique presented by DeHoff & Rhines (1968); ranges from w= 22%, w=10%, w=5 to 2%. (scale x0.5 mag)

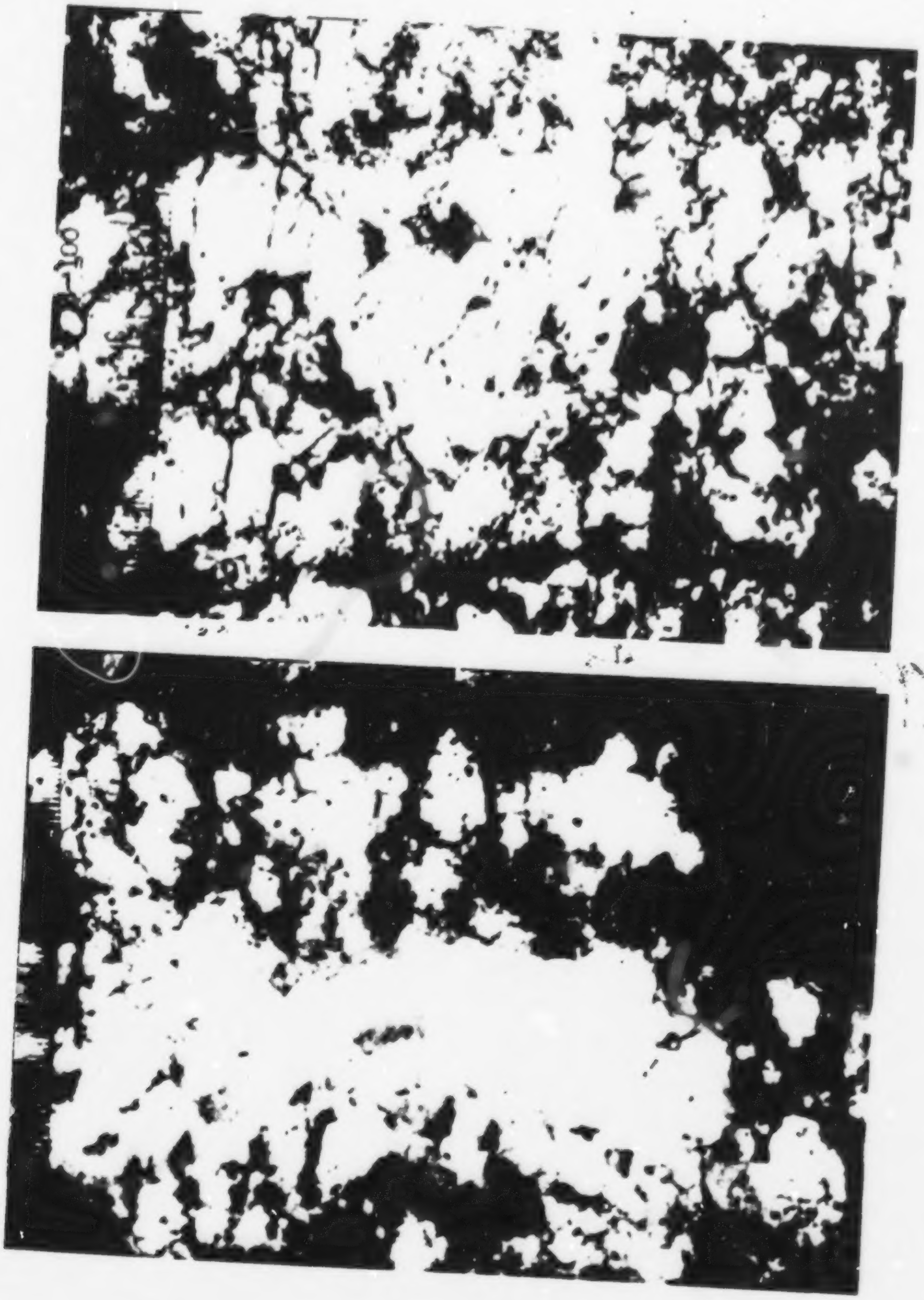

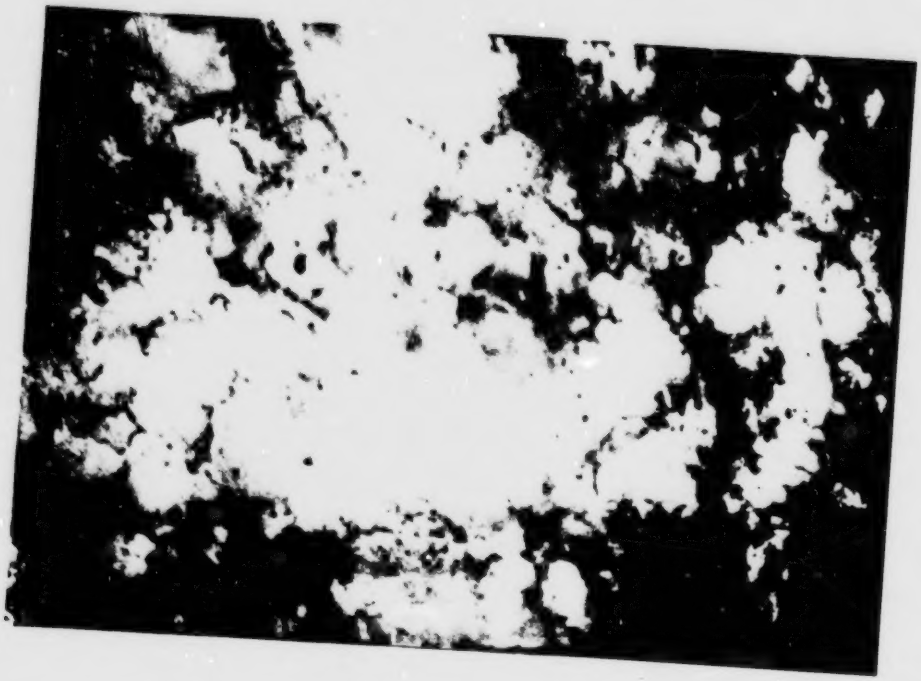

Statistical Analyses of Cracks

All test blocks were examined to confirm cracking patterns. Crack-type features were counted in the same method utilized to count grain boundary density. In a general way, the quantitative stereological data corroborated trends in the AE data.

Attempts to correlate AE results to crack size and distribution from an individual one-to-one basis, can not be directly related to the growth process of individual cracks. At best, a general trend can be observed, between the number of AE Events, Amplitude, Stress Level, Strain and Crack Density.

Three broad catagories of cracks can be observed during a complete loading cycle.

1) Intragranular Cracks.

This variety can be observed at all stages of loading. They can be sub-divided into three catagories, based on size and location and size.

a) Cleavage Microcracks I-

Cleavage microcracks appear in the earle stages of loading, from 0 to 5 MPa. They are characteristically present as small micron-scale slip lines, developing a cross-hatch pattern throughout the entire grain.

b) Cleavage Microcracks II-

A second variety of cleavage microcracks, generated in the 0 to 5 MPa and 5 to 15MPa range, appear as millimeter scale cracks, primarily developed out of the coalescing of type I. They can be either isolated single cracks, or groupped into an en-echelon set.

c) Type III-

The final variety are observed in the late stages of the Regime 2 stage of the loading cycle (approx. 14 to 18MPa), and occur as randomly oriented cracks (ie. not controlled by cleavage), either isolated or formed as a curved tip of a fully developed type II Cleavage crack, thus forming an en-passent type interaction. They are approx. 25 % to 75% of the length of the grain and 0.25 to 1.5 mm. in width.

2) Intergranular Microcracking

Intergranular microcracks can be seen from the last part of the first regime to the final stages of the load cycle. They are characterized as displacements(usually with a shear component), occuring along the grain boundaries. Widths vary from 100 microns to 2 mm. and lengths corresponding to the grain boundary area of the adjacent grains.

3) Transgranular Cracks-

This final group of cracks are observed from the middle to late stages of the loading cycle (ie. 12 to 25 MPa). They are developed by the coalescing of intergranular and intragranular cracks. Lengths can range from just over the length of a grain to through the entire length of the specimen. Their orientation is basically controlled by the anisotropy of the external grain morphology, thus trending parallel to the direction of maximum grain elongation.

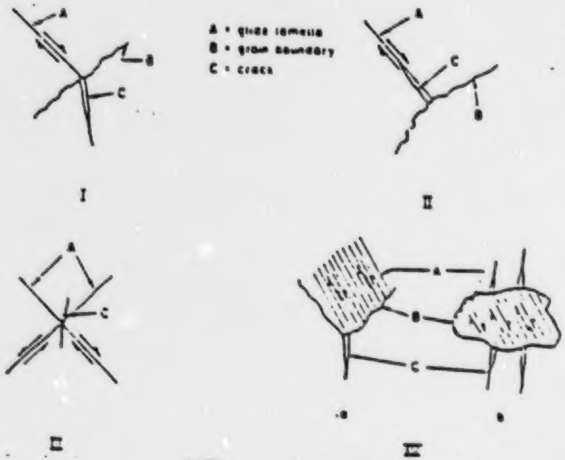

Fig. 18. Four types of microcrack nucleation mechanisms have been observed to operate in the uniaxial compression tests. Types I & II operate at the intersections of cleavage with grain boundaries. The cracks form at high angle to the cleavage in Type I, and parallel to the Cleavage in Type II. The microcracks resulting from type 3 mechanism formed at the intersection of two or more cleavage planes. The Type 4 mechanism is caused by a crack developed by wedging action of a combination of grains oriented in fashion more suceptable to cleavage shear against less suceptable grains.

Variation of Crack Distribution

Variation in both cracck density, distribution and orientation exists in different samples. Results are primarily based on crack intersections with test lines set at equal gridded intervals on each specimen.

Variation in crack orientation is controlled by the external grain shape forming the fabric of the rock. Specimens with strong preferred orientation in the fabric (ie. w => 20%), show a prominent concentration of sub-parallel trending transgranular and intergranular cracks. Based on lateral and vertical intercepts, the area with longer inequidimensioned grains display a higher ratio of intergranular displacement. Eighty (80%) of the observed samples show this pattern, a bulk of which comprize the block samples derived from the lower portion of the original block (designated with subscript 'L').

Crack intercepts show higher density in the central portion of the specimens than on the ends. This corresponds to the area in the fabric with the maximum grain elongation, located in the center of the block samples.

Specimens sustaining loads in the range of 18 to 22MPa show a strong development of transgranular crack. Orientations range from vertical to 70 degrees in the upper and central portions of the samples, and deviate to an alomost subhorizoontal shear displacement in the lower portions. Results are based on lateral intercepts.

The density of intragranular cracks show a dispersed distribution. In general, a crack may form in the grain containing the cleavage, in the adjacent grain, or along the grain boundary, depending on the relationships between the calculated optimal orientation for development of the crack. The intragranular crack distribution irregularity is due to a low concentration of grains with the optimal orientation, required to generate displacements along the cleavage plane. Pole figure data displays low cleavage orientation distribution on an inclined axis. Traverses of variable intercept concentration exist; this situation is due to cracks concentrated in a single grain alone in sub-parallel en-echelon sets.

High counts of intergranular intercepts at low angles have variable interpretable results. Two types of occurences are apparent, where displacement is perpendicular to the observes line of sight, thus measuring an inclined displacement plane in an apparent viewing plane, or a low angle displacement in the specimen plane. The latter is more evident in the lower portions of the samples derived from the bottom section of the original block.

TABLE B. Semi-formal tables of crack density data. 'l' subscript signifies lateral test lines, and 'v' for vertical test lines.

Sample L14
FACE A Transgranular Cracks

Orientation w.r.t. Vertical Axis

Test Line	x90-80	x80-70	x70-60	x60-50	x50-40	x40-30	x30-20	x20-10	x10-0
v1	1	1	1		2				
v2	1	3	1						
v3	3	1	1						
v4		2		2					
v5			1	3					
v6		3	1						
l1		2				1			
l2		4							
l3	1	4							
l4	4	2	1	1					
l5	4		1						
l6		3		2					
l7	1	3							
l8	1	3							

FACE B

Test Line	x90-80	x80-70	x70-60	x60-50
l1	1	1		1
l2	3	2		
l3	2	1		
l4	5			
l5	4			
l6	1			2
l7	1			1
l8	1			4
v2	2			1
v3	2			1
v4	1			
v5	1	3		

FACE B

Intergranular Cracks
FACE A

1

Test Line	x90-80	x80-70	x70-60	x60-50	x50-40	x40-30	x30-20	x20-10	x10-0
v1	1	1	2	1					
v2		2	2				1	4	
v3	7	1	1			1		2	
v4	2	2		1	1			1	1
v5	3	4		1	1				
v6	2	1	2		2				
l1	1	1			4	1			
l2	4	2	2	1					
l3	5	2	1						
l4	9								
l5	3	1		2					
l6	5	1	1		1				
l7	4	4	1						
l8	1	2	1		3				

FACE B

Test Line	x90-80	x80-70	x70-60	x60-50	x50-40	x40-30	x30-20	x20-10	x10-0
v1	1	1	1			3			1
v2	3	2	2						2
v3		2	1			2			2
v4	2	5							1
v5		3	1	1	2				2
l1	1	3	2		3				
l2	5	4				3		1	
l3	2		4	1	1		1		
l4	4	1	1		1	1			
l5	5	1	2						
l6	3	2			1				
l7	4	1	1		1				
l8	1	3		1					

```
                     X90-80   X80-70   X70-60   X60-50   X50-40   X40-30   X30-20   X20-10   X10-0
            V1
            V2                  4                          2
            V3                                    1
            V4                           2                 1        3        1        2
            V5                           4
            V6          2       2        2                 1
            11                  2
            12          1       2                 2                 1
            13          3       2        2        2
            14                           4
            15          1       1        1
            16          6       1                          1
            17                  1        1
PAGE 3      18          1       1
                                2

                     X90-80   X80-70   X70-60   X60-50   X50-40   X40-30   X30-20   X20-10   X10-0
            V1
            V2          1       4        1                          2                          2
            V3          2       6        2
            V4          1       3        3        1
            V5          1       1        2        2
            V6          3       2                 2                 1
            11          1       1        3                          1
            12          1       2
            13                  3        2
            14          3       2        1        2                 2
            15          1       2        1        1
            16          4       4        2                          2
            17
                        2       2        1                          1
```

```
Sample L12

FACE A   Transgranular Cracks

    Test Line
          v1   x90-80  x80-70  x70-60  Orientation w.r.t. Vertical Axis
          v2                2       1  x60-50  x50-40  x40-30  x30-20  x20-10  x10-0
          v3        2       4
          v4        1       2       1
          v5                1       3                               1
          v6        1       4
          11        1       3
          12                3
          13        3       3                                       1
          14        3                               1
          15        2       5
          16        7               1
          17        4       1
          18        2       3
                            4

FACE B

          v1   x90-80  x80-70  x70-60  x60-50  x50-40  x40-30  x30-20  x20-10  x10-0
          v2        1       2       2       2
          v3        1       1
          v4                                1               3
          v5        1       2                                       1
          11        2       1       1
          12
          13        3       1
          14        1               3
          15        4       1                               1
          16        2               1
          17        2       1
          18        3       1                               1
                    2       1                       2       1

Intergranular Cracks
FACE A

          v1   x90-80  x80-70  x70-60  x60-50  x50-40  x40-30  x30-20  x20-10  x10-0
          v2        1       5
          v3        1       6       1               2               1
          v4        2               4       1                               1
          v5        1       2       1               1                       1
          v6        2       3               2
          11        1       1       4                                       1
          12                2                       3
          13                2       1
          14        3       1       1       1
          15        2       3
          16        2       3       1
          17                                                                1
                    1       3       1

FACE B

          v1   x90-80  x80-70  x70-60  x60-50  x50-40  x40-30  x30-20  x20-10  x10-0
          v2        1       4       1
          v3        2       6       2               2               1
          v4        1       3       3       1       1               1       1
          v5        1       1       2       2       1                       1       1
          v6        3       2               2
          11        1       1       3                                       1
          12        1       2                       2                       1
          13                3       2
          14        3       2       1       2
          15        1       2       1       1
          16        4       4       2
          17                                                                1
                    2       2       1

FACE A

          v1   x90-80  x80-70  x70-60  x60-50  x50-40  x40-30  x30-20  x20-10  x10-0
          v2        2       1       3
          v3        3       2       2                       3               1
          v4        2       1                       1       3       1       1
          v5        1       1       1
          v6        3       3                               2
          11        1       1       1               1                       1
          12        3       3       4               1
          13        2       1       2       1
          14        1               1       2
          15        1       1
          16                        2       1               2
          17        1               1               1                       1
                            2                       1
```

Sample L15
Transgranular Cracks
FACE A

Orientation w.r.t. Vertical Axis

	x90-80	x80-70	x70-60	x60-50	x50-40	x40-30	x30-20	x20-10	x10-0
v1	1	3		1	1				
v2									
v3		2					2		
v4					2			2	
v5	1				2				
v6					4				
l1									
l2		1							
l3	1	1							
l4		4							
l5		2	2						
l6	1				2				
l7							3		
l8	1						2		
l9							3		
l10									

FACE B

	x90-80	x80-70	x70-60	x60-50	x50-40	x40-30	x30-20	x20-10	x10-0
v1		2		2					
v2	3			2					
v3	2					1			
v4		2		1				2	
v5		2	1			2			
v6		2							
l1									
l2									
l3	1								
l4	4								
l5	2	2							
l6		1	2						
l7			1						
l8				1					
l9									2
l10									3

Sample U7
Face B
Transgranular Cracks

Orientation w.r.t. Vertical Axis

	x90-80	x80-70	x70-60	x60-50	x50-40	x40-30	x30-20	x20-10	x10-0
l1	3				1				
l2	2								
l3	1				1				
l4									
l5	1	1							
l6	3	2		1					
l7	2		1						
l8	3		1						
v1	1	1					1		
v2	2	2	1						
v3	1						1		
v4	3	1	1				2		
v5	1	1							

FACE A

	x90-80	x80-70	x70-60	x60-50	x50-40	x40-30	x30-20	x20-10	x10-0
l1	2	2							
l2	1	1							
l3	1	2						1	
l4		1							
l5			1					1	
l6	1	1	1	1				1	
l7	2	1						1	
l8	1							1	
v1	2	1						2	
v2	1	2	1	1				1	
v3			2						
v4	2	2	1	2				2	
v5	1	1							

Face 2
Intergranular Cracks

```
     x90-80  x80-70  x70-60  x60-50  x50-40  x40-30  x30-20  x20-10  x10-0
11      3       2       1       1
12      3       1               1
13      4               1               1
14      2                       1
15      1       1               1
16      3
17      2               1
18      3               2
v1      2       1
v2      2       1       1
v3      3
v4      1
v5      2       1       1
```

FACE A

```
     x90-80  x80-70  x70-60  x60-50
11      2       1       1
12      2       1       2
13      3       1       1
14      1               1
15              2
16
17      2
18      2       1
v1      2       2
v2      1       1       1
v3      3
v4      1       2
v5      1       1       1
```

Face 3
Intragranular Cracks

```
     x90-80  x80-70  x70-60  x60-50  x50-40  x40-30  x30-20  x20-10  x10-0
11              2               1       2       1       1
12              2               1       1       1       1               1
13      1       1               1       2               1
14              2                                               1       1
15              1               1               1       2
16                              2                       1       2
17                              2                       2       1
18                              1       3               2
v1                              1       2       1
v2              1                       1       1
v3                              1               1
v4
v5              1                       2
```

FACE A

```
     x90-80  x80-70  x70-60  x60-50  x50-40  x40-30  x30-20  x20-10  x10-0
11              2       1
12      1       1       1                                               1
13      1       2               1
14                              1       1
15                              1       1
16                                      2       1
17                                      1       1
18      1
v1
v2              1       2       1
v3                      1       1
v4
v5              1
```

Fig. 19. Transgranular fracture composed of an intragranular cleavage fracture (type II) (o) and an intergranular fracture (x). (scale x12 mag. red marker = 0.25mm). (At 22MPa)

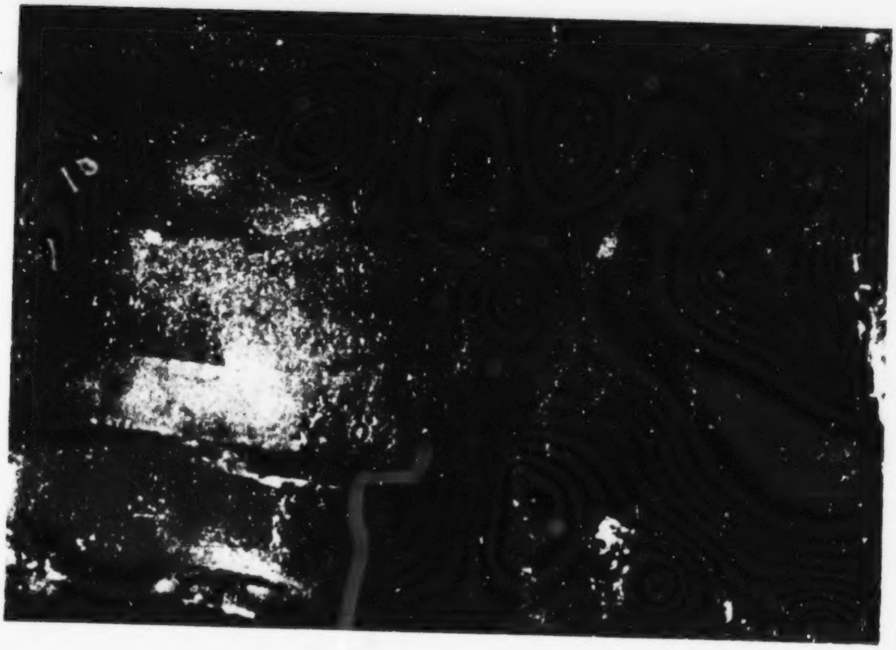

Fig. 20. Small transgranular fracture, composed of en-echelon intragranular cleavage fractures (1) migrating into the adjacent grain (2). (scale x12 mag.) Mode I & II mechanisms control this system. (At 22MPa).

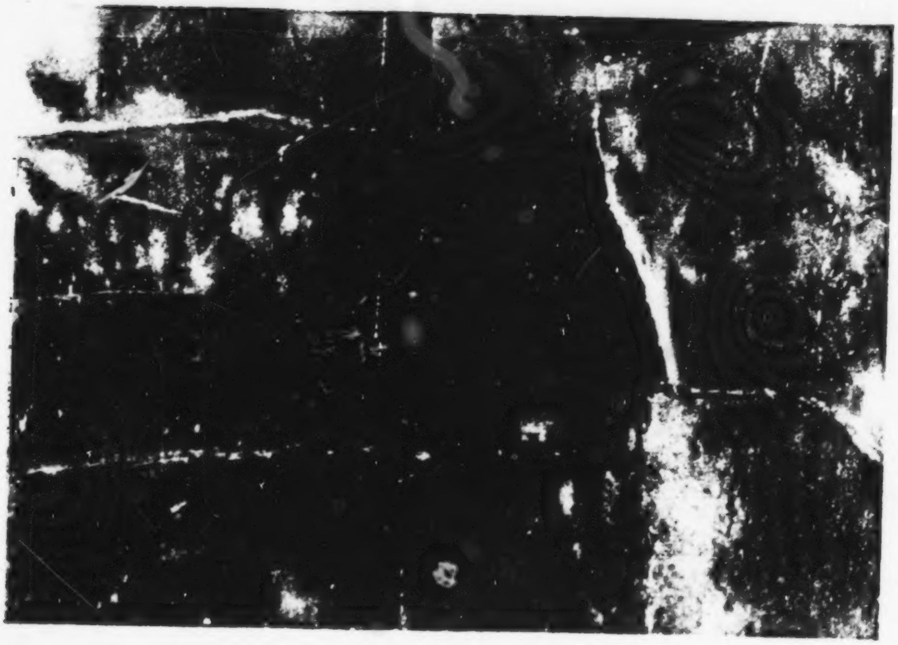

Fig. 21. Intragranular en-echelon cleavage fractures (1) developing into single larger intragranular crack (at 22MPa). (scale x15 mag.).

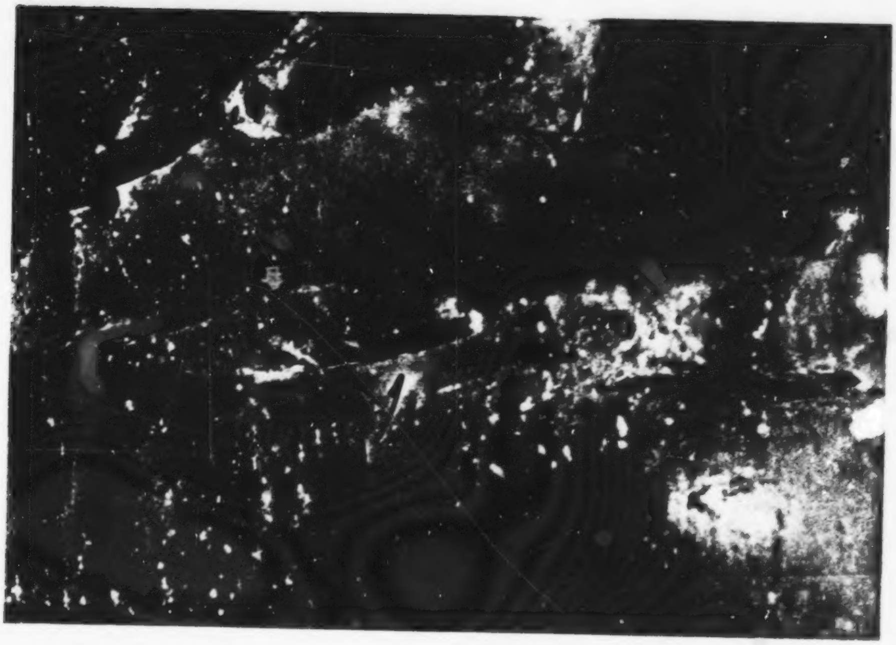

Fig. 22. Intragranular cleavage cracks (type II). (scale x30mag.), sample sustaining load of 25MPa.

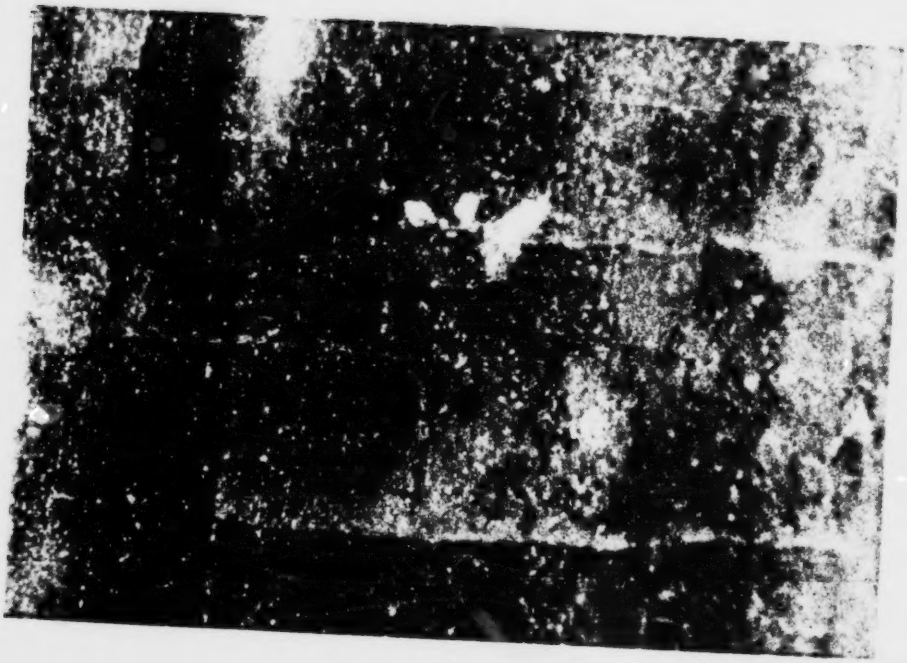

Fig. 23. Advanced intergranular displacement (1) with small cross-hatch cleavage (type I) visible in the darker grain (2). (x43 mag.)

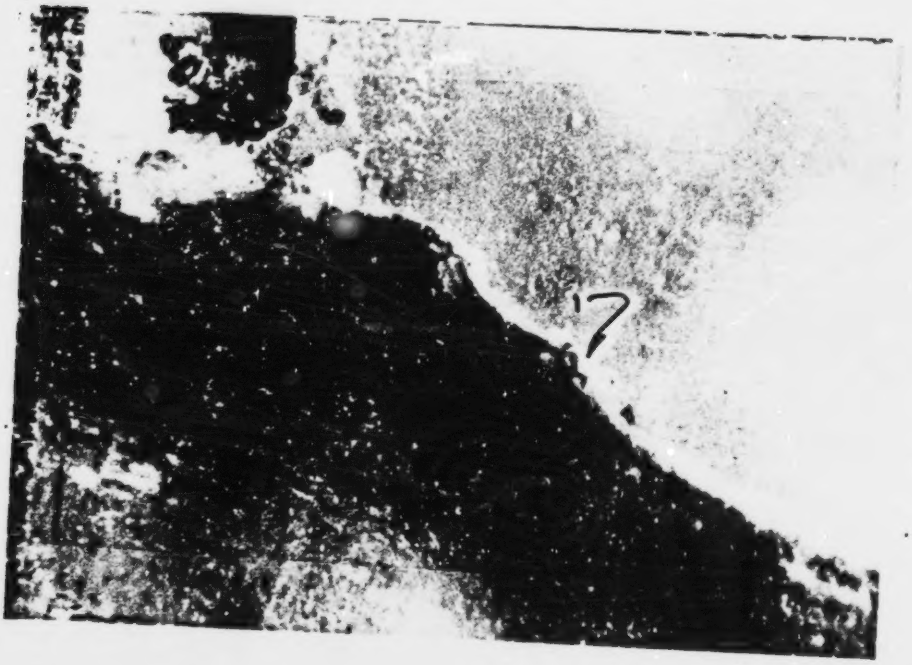

Fig. 24. Intragranular crack (type III) generated from Type I (poorly visible). (x55 mag.).

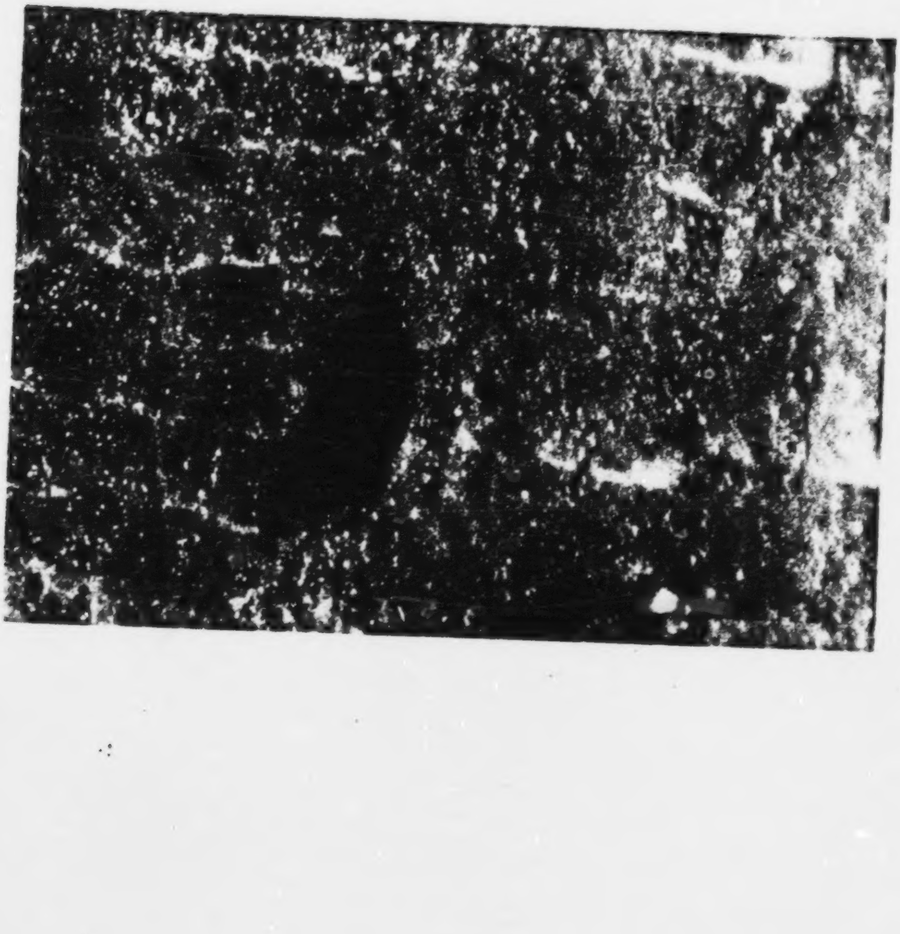

Discussion of AE Results

Acoustic Emission measurements were made during uniaxial compression preformed on Potash Rocksalt specimens. The AE equippment used was made by Dunegan Corp. (Model LOCAN AT, 3000 series). It was used to obtain various AE parameters including; AE amplitude frequency distribution, (amplitude 0 - 100dB, resolution 1dB), ring down counts, energy, duration, rise time and event count. The total capable capable monitoring frequency range was 100 to 300 KHz. The gain has been adjusted to the maximum machine level, with the AE threshold set at 72 dB. The transducers (with a surface area of 1cm x 1cm.), were bonded to the flat specimen surfaces with grease.

Constant Strain Rate Experiments

Load experiments conducted over several load rate ranges, have produced characteristic AE behaviour, which can be sub-divided into three regimes. Such groupings have been observed by earlier authors, including, Fonseka et al., 1985, Brace 1964, Ohnaka & Mogi 1982, among others.

In all of the tests conducted, no decrease in AE rate was observed. This includes the first load cycle of the test, and all of the successive loading tests for the same sample.

Sub-division of the 3 regimes are based on the slope of AE rate vs. stress (see fig. 26) and corresponding observable microfracture characteristics.

The first Regime (from 0 to 5 MPa) is characterized by a steady AE Rate. Corresponding induced microstructure appear mostly as high angle intergranular displacement (w.r.t. the axial load direction), and development of intragranular (type I) cross-hatch cleavage. The interaction between the various elements that display mode I, II and IV type mechanisms, (see fig.18).

The second Regime (5 to 15 MPa) is characterized by an exponetially increasing AE Rate. At this stage, the deformation patterns comprise of more pronounced development of the previous microcracks, into short but extensive transgranular cracks, which extend in length, equivalent of 2 or 3 grain boundary lengths. The intergranular displacements are fully developed, as characterized by dilatent openings, with widths ranging from 0.25 mm. to 1.21 mm. Crack plane orientations are favourably controlled with respect to the external grain shape (ie. fabric). All four modes of mechanical interaction are evident at this stage.

The third Regime (15 to 25 MPa) is characterized by very high AE Rate, culminating towards specimen failure. Most evident feature, is the extensive development of transgranular cracks. From the test line intercept data, transgranular crack intercepts (with the test line) show the highest density, from the previous two regimes. Also, orientation of cracks is similar to the orientation of maximum grain elongation. Towards the end of the test cycle, pieces along the vertical faces of the sample block begin to spaul off (20 to 25 MPa). The pieces are generally single grains, or thin polygranular pieces (approx. 0.5cm to 1.25cm. in width by 2 to 5 cm. in length).

In all of the tests conducted, the bulk of AE events occured at the late stages of the loading cycle, corresponding with in large, with the low frequency AE Amplitudes, (fig. 26). The Amplitude Event Frequency Distribution are reproduceable, and correspond highly to results obtained by Fonseka et al., 1985. The distribution is skewed, with an initial rise, and the fall off at higher amplitudes. Additional cracking observed in the latter two Regimes occur associated with the rapid onset of dilatancy and the rate of low frequency AE events associated with the larger intergranular and transgranular crack volumes.

Fig. 25. Examples of Stress Strain distributions for various specimens tested under uniaxial compression.

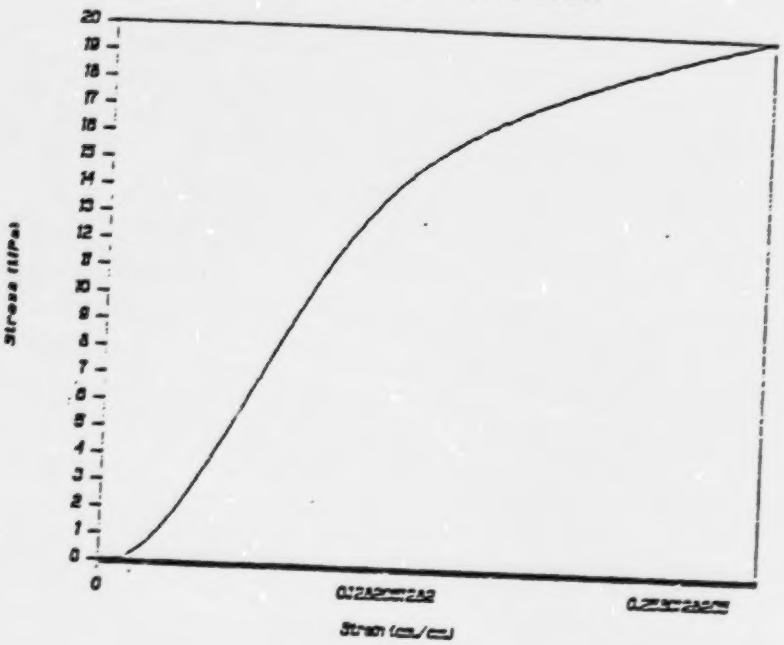

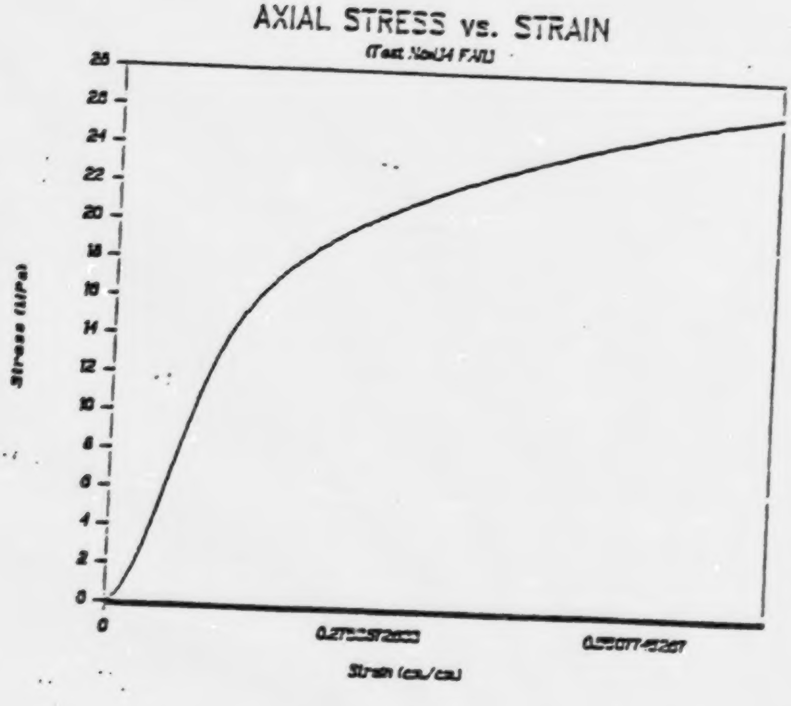

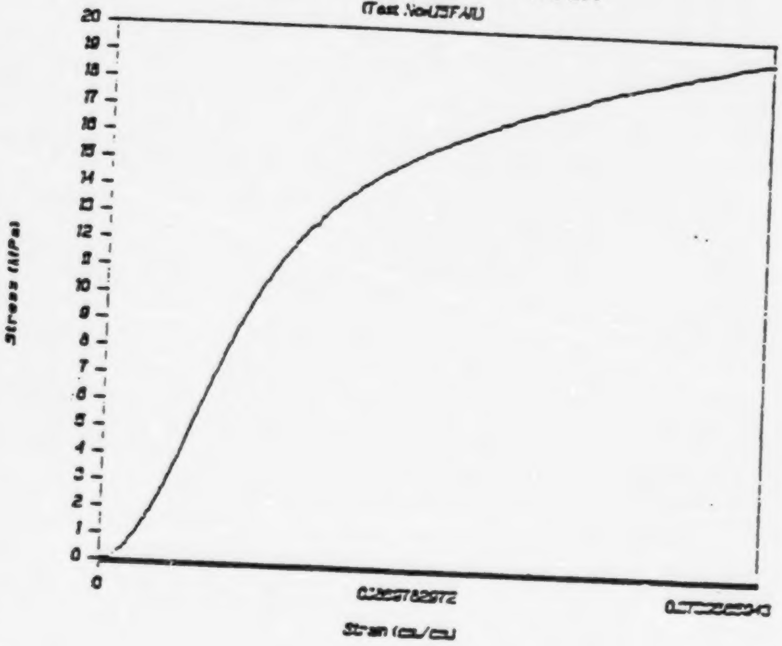
AXIAL STRESS vs. STRAIN
Stress (MPa)
20
19
18
17
16
15
14
13
12
11
10
9
8
7
6
5
4
3
2
1
0
0
Strain (cm/cm)

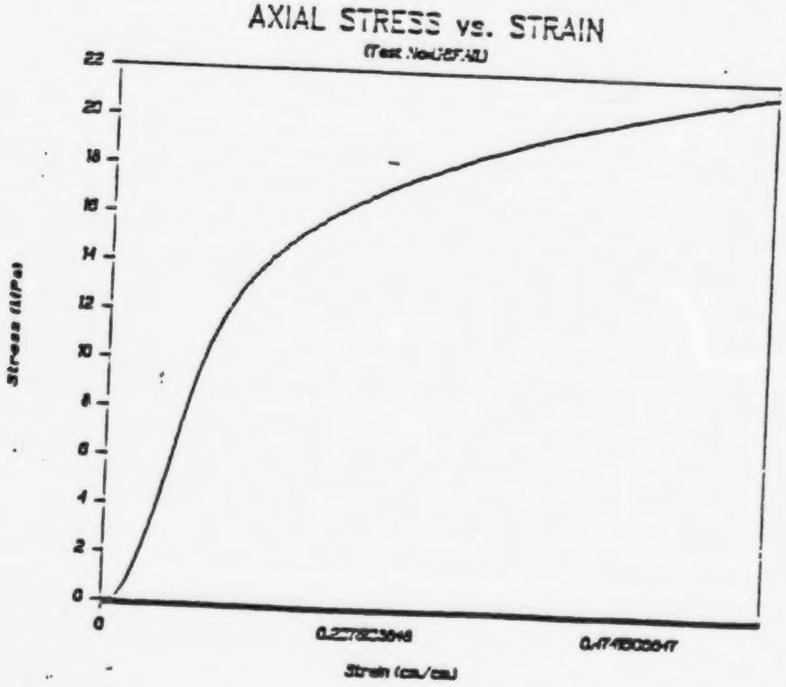
AXIAL STRESS vs. STRAIN
Stress (MPa)
22
20
18
16
14
12
10
8
6
4
2
0
0
Strain (cm/cm)

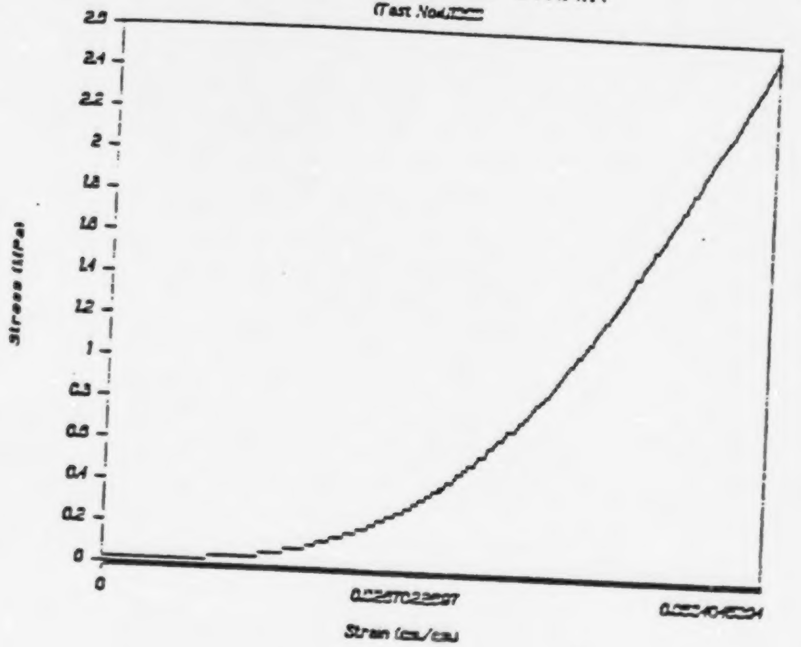
AXIAL STRESS vs. STRAIN
2.6
2.4
2.2
2
1.8
1.6
1.4
1.2
1
0.8
0.6
0.4
0.2
0
Stress (MPa)
0
Strain (cm/cm)

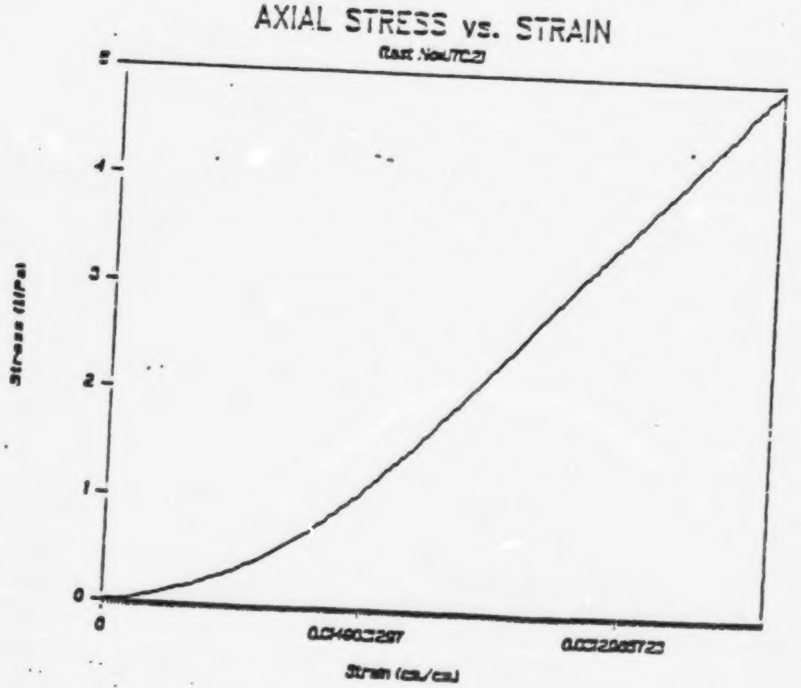
AXIAL STRESS vs. STRAIN
(Test No.UTC2)
5
4
3
2
1
0
Stress (MPa)
0
Strain (cm/cm)

Fig. 26. Examples of various (typical) plots of AE parameters.

a) AE amplitude distribution for various tests. Distribution is for single test cycles.

b) Stress & AE Rate (per 10 seconds) plotted against Strain

c) AE Rate against Stress.

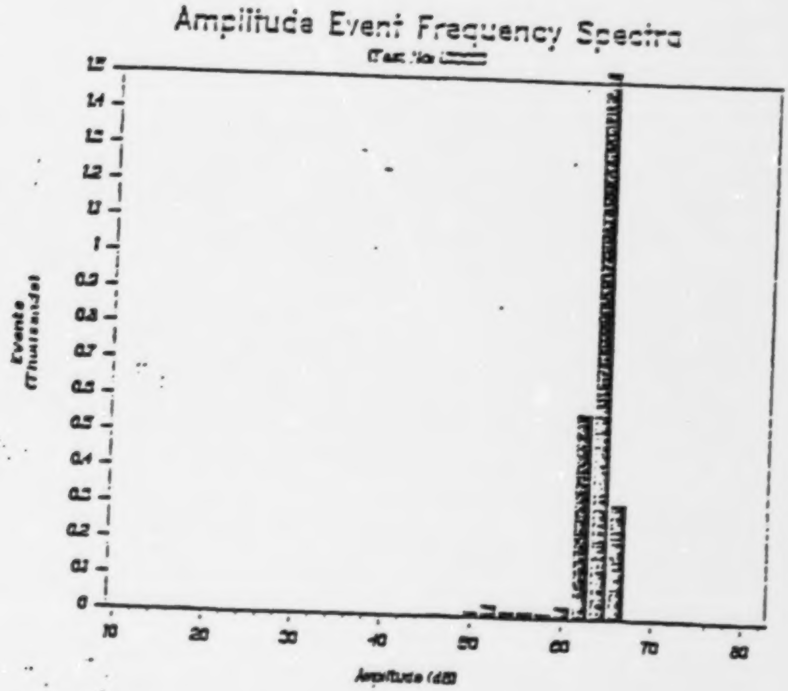

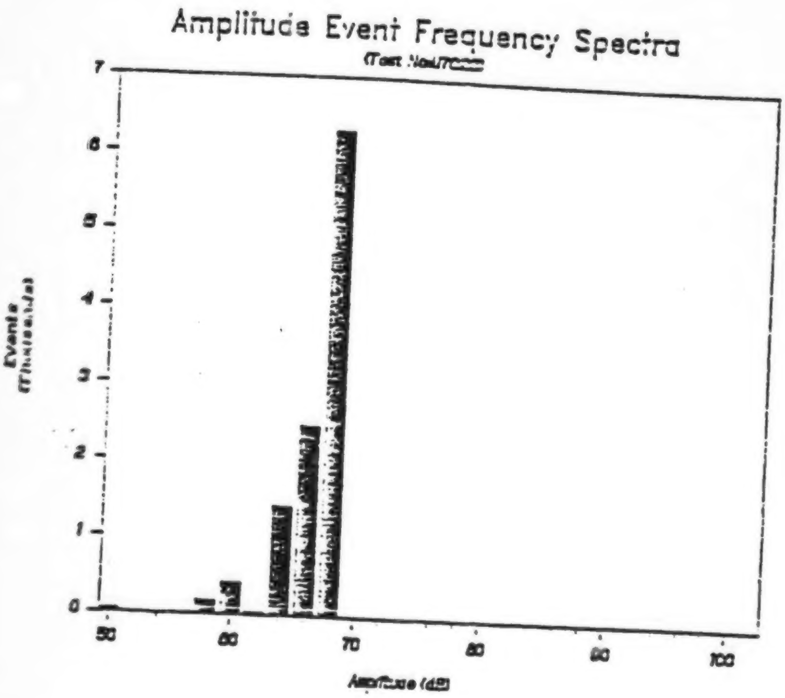
Amplitude Event Frequency Spectra
(Test No.[illegible])
Events (Thousands)
0
1
2
3
4
5
6
7
50
60
70
80
90
100
Amplitude (dB)

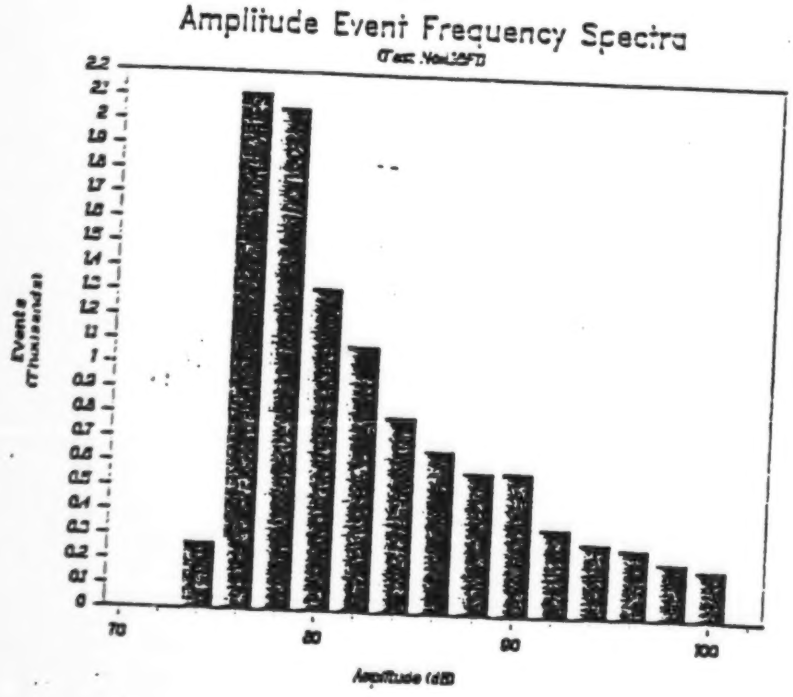
Amplitude Event Frequency Spectra
(Test No.[illegible])
Events (Thousands)
0
0.1
0.2
0.3
0.4
0.5
0.6
0.7
0.8
0.9
1
1.1
1.2
1.3
1.4
1.5
1.6
1.7
1.8
1.9
2
2.1
2.2
70
80
90
100
Amplitude (dB)

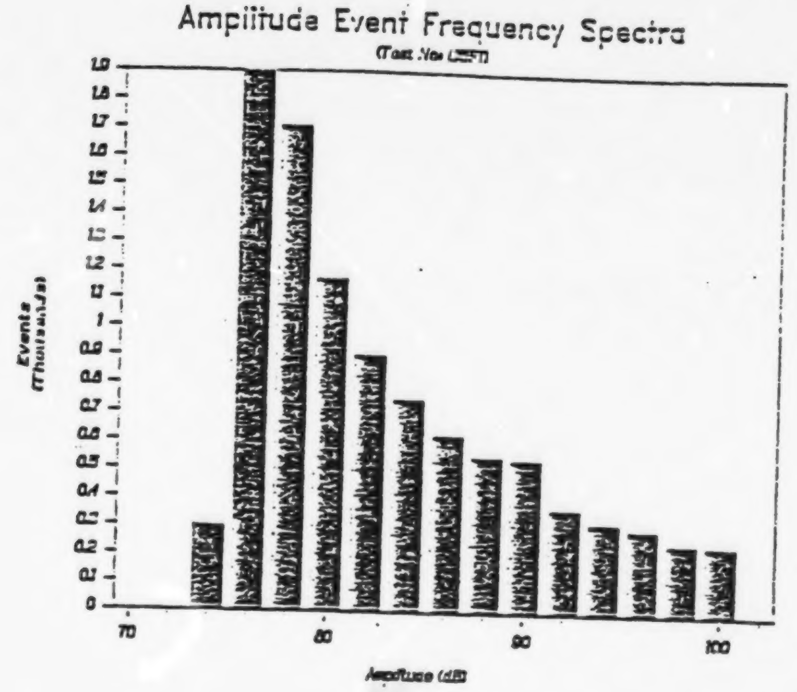
Amplitude Event Frequency Spectra
(Test No. [illegible])
Events (Thousands)
1.9
1.8
1.7
1.6
1.5
1.4
1.3
1.2
1.1
1
0.9
0.8
0.7
0.6
0.5
0.4
0.3
0.2
0.1
0
70
80
90
100
Amplitude (dB)

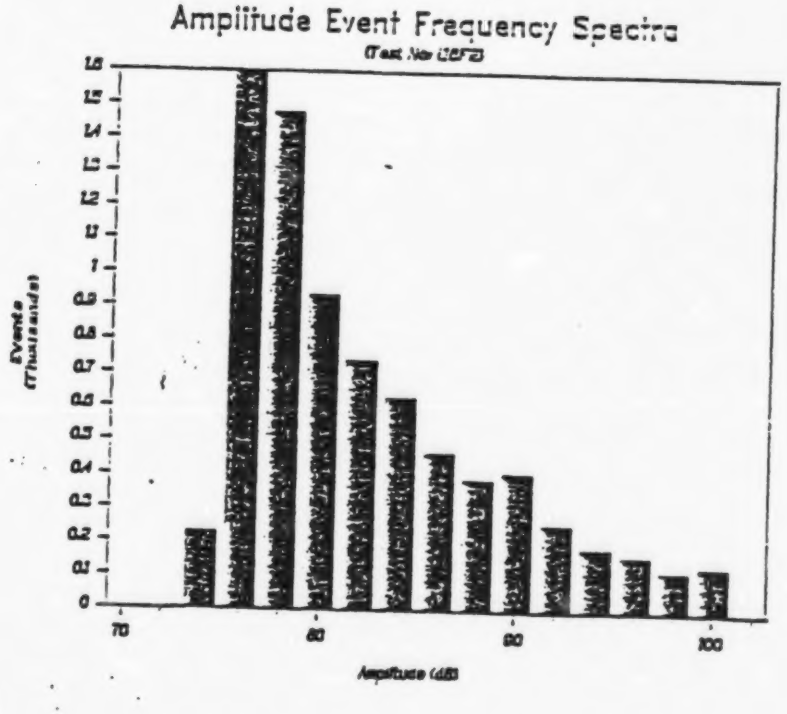
Amplitude Event Frequency Spectra
(Test No. [illegible])
Events (Thousands)
1.6
1.5
1.4
1.3
1.2
1.1
1
0.9
0.8
0.7
0.6
0.5
0.4
0.3
0.2
0.1
0
70
80
90
100
Amplitude (dB)

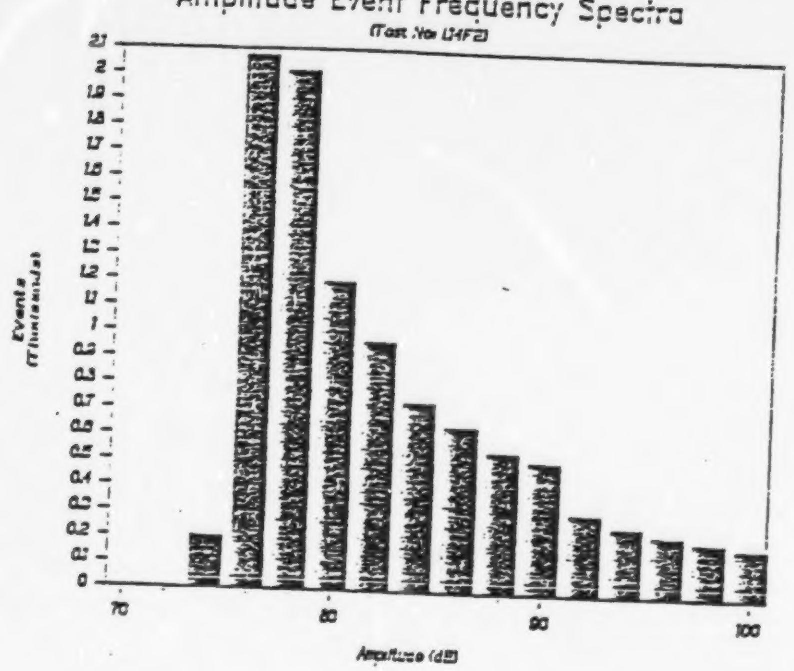
Amplitude Event Frequency Spectra
(Test No: L4F2)
Events
(Thousands)
2.1
2
1.9
1.8
1.7
1.6
1.5
1.4
1.3
1.2
1.1
1
0.9
0.8
0.7
0.6
0.5
0.4
0.3
0.2
0.1
0
70
80
90
100
Amplitude (dB)

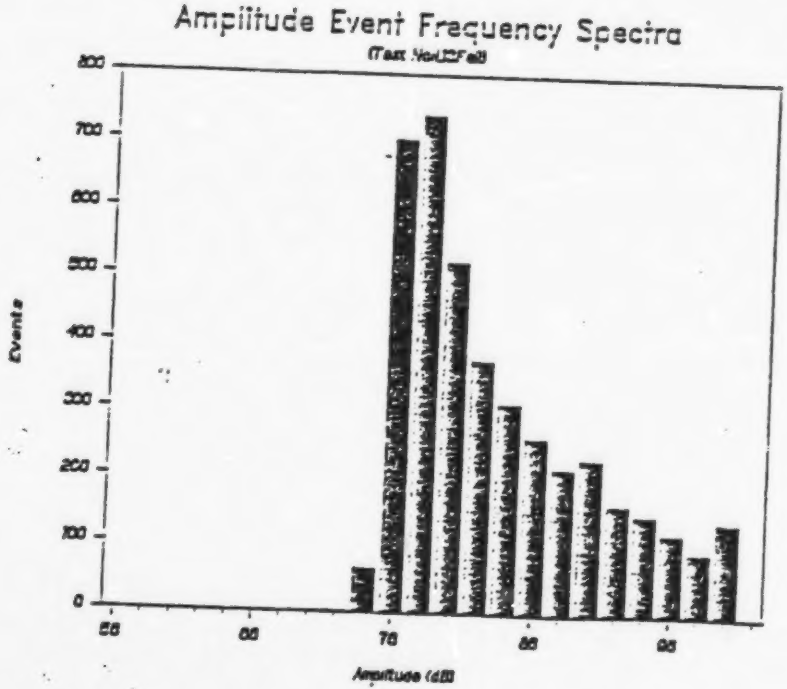
Amplitude Event Frequency Spectra
(Test No: L2Fe8)
Events
800
700
600
500
400
300
200
100
0
50
60
70
80
90
Amplitude (dB)

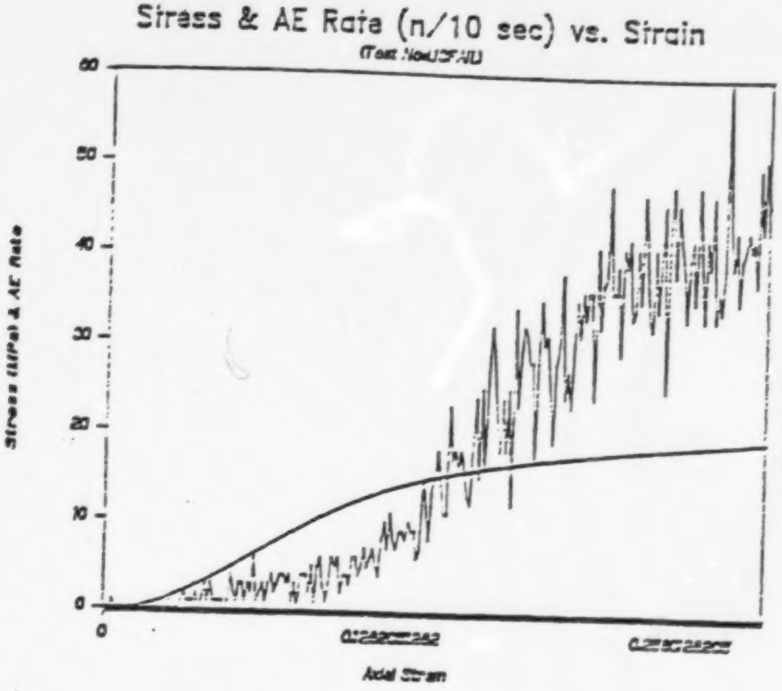
Stress & AE Rate (n/10 sec) vs. Strain
60
50
40
30
20
10
0
Stress (MPa) & AE Rate
0
Axial Strain

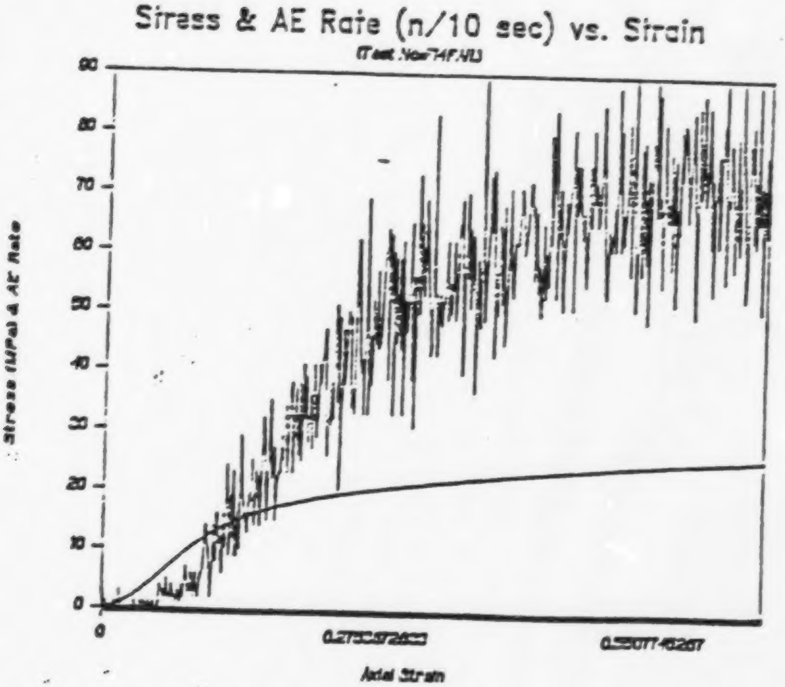
Stress & AE Rate (n/10 sec) vs. Strain
90
80
70
60
50
40
30
20
10
0
Stress (MPa) & AE Rate
0
0.2753872633
0.5507745267
Axial Strain

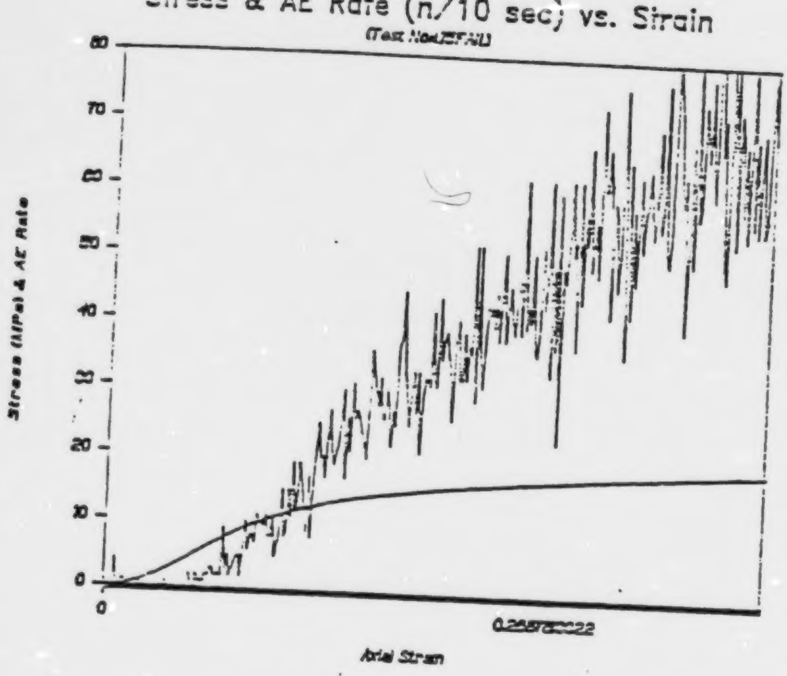
Stress & AE Rate (n/10 sec) vs. Strain
80
70
60
50
40
30
20
10
0
Stress (MPa) & AE Rate
0
Axial Strain

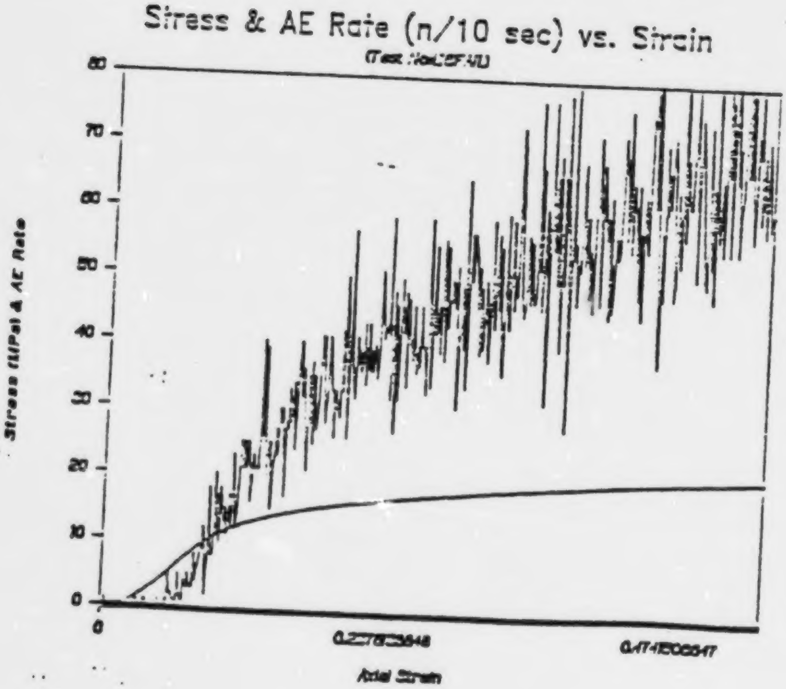
Stress & AE Rate (n/10 sec) vs. Strain
80
70
60
50
40
30
20
10
0
Stress (MPa) & AE Rate
0
Axial Strain

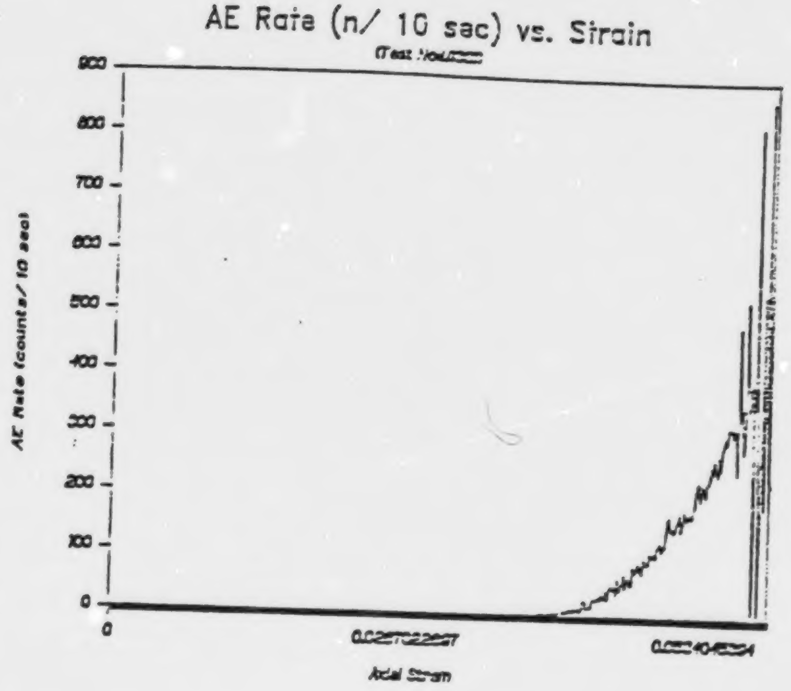

AE Rate (n/ 10 sac) vs. Strain

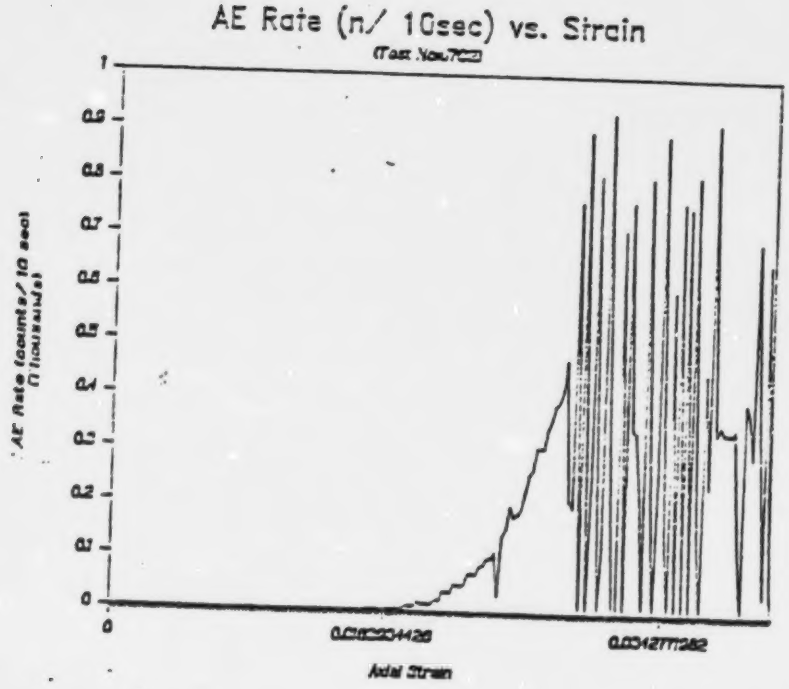

AE Rate (n/ 10sec) vs. Strain

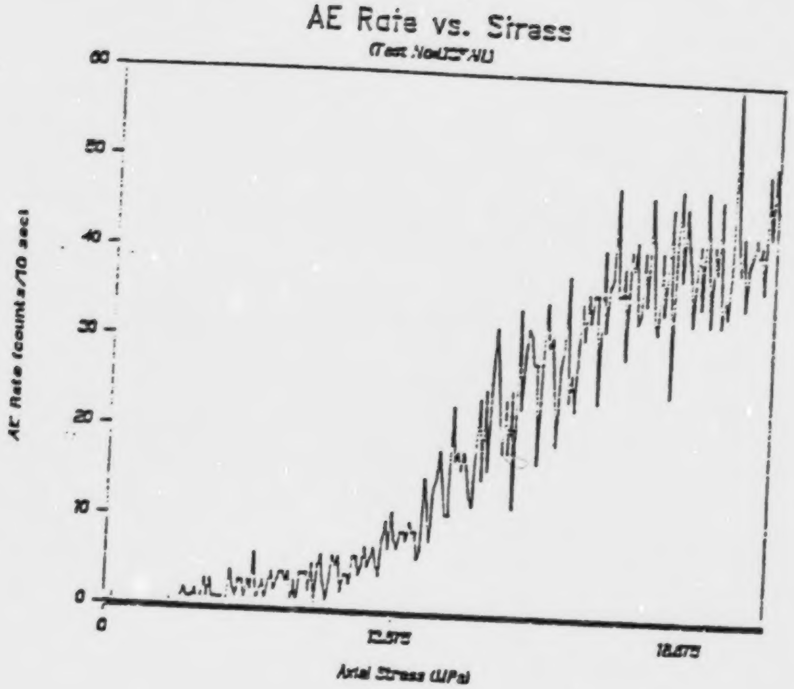
AE Rate vs. Stress
(Test No.[illegible])
AE Rate (counts/10 sec)
0
10
20
30
40
50
60
0
12.375
18.875
Axial Stress (MPa)

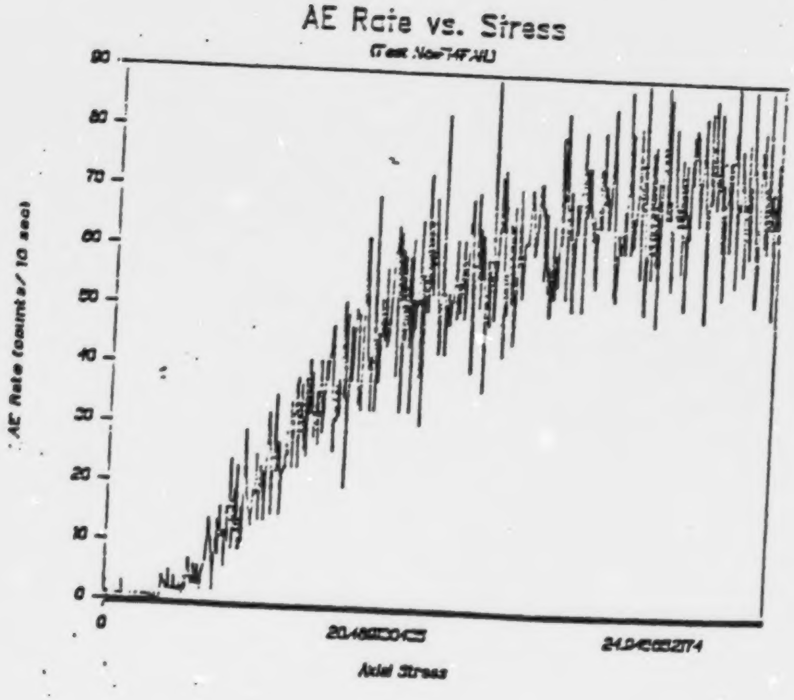
AE Rate vs. Stress
(Test No.[illegible])
AE Rate (counts/ 10 sec)
0
10
20
30
40
50
60
70
80
90
0
20.468300423
24.946052174
Axial Stress

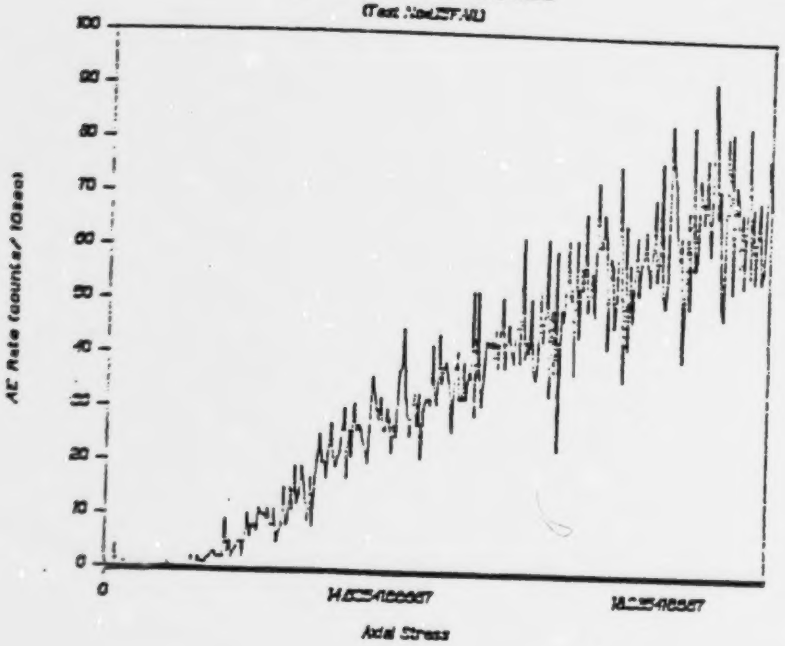

AE Rate vs. Stress

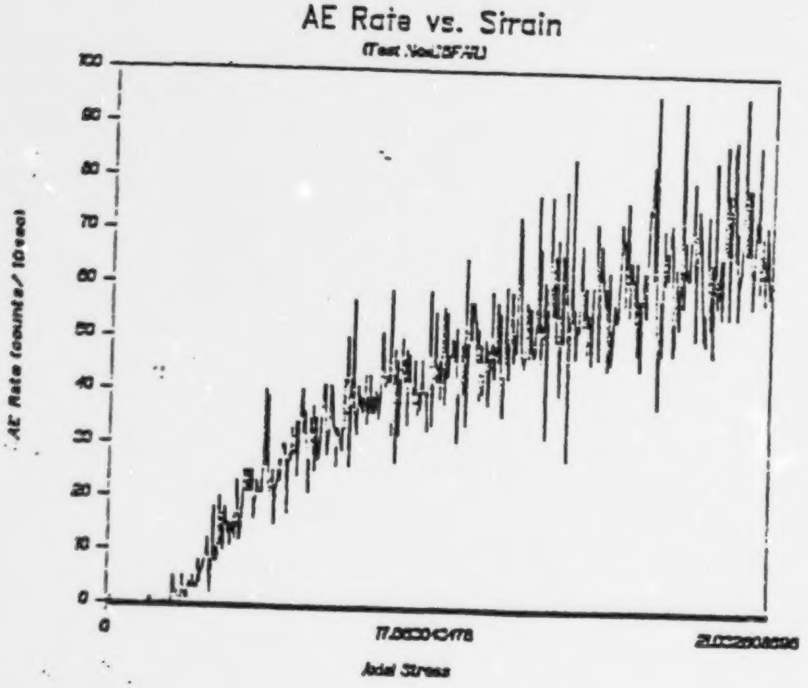

AE Rate vs. Strain

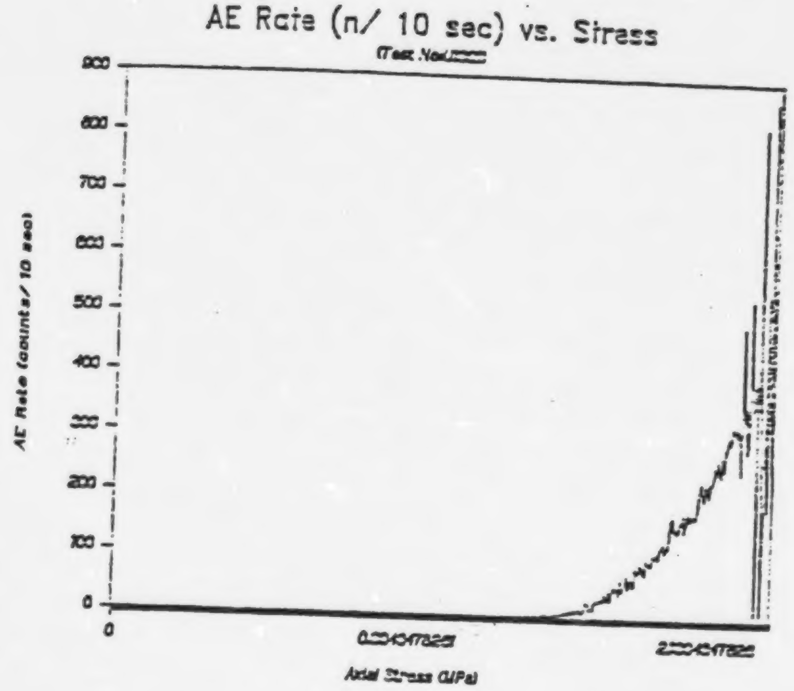

AE Rate (n/ 10 sec) vs. Stress

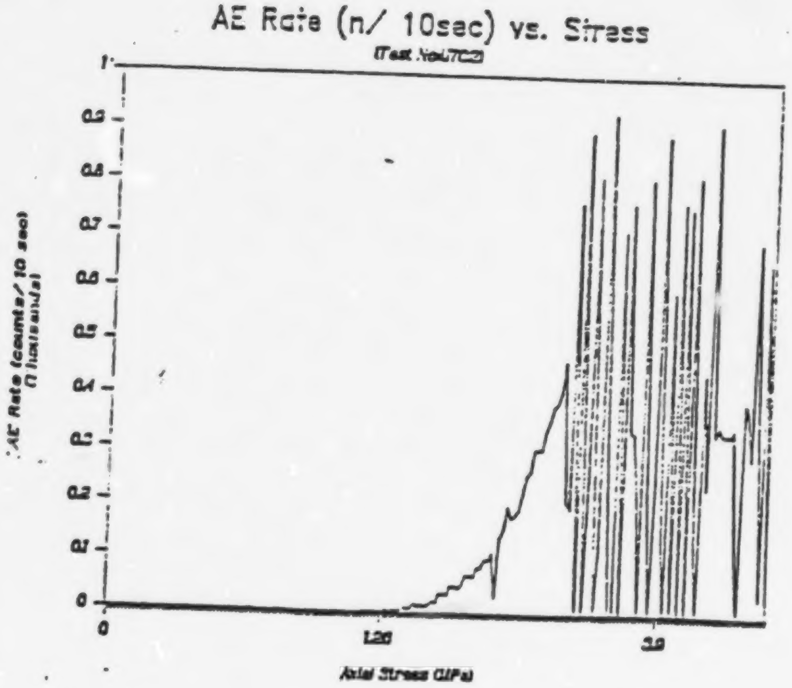

AE Rate (n/ 10sec) vs. Stress

Conclusion

Variations in the petrofabric of Rocksalt are identifiable by the following parameters:

1) The degree of orientation 'w' shows a strong variation along the different vertical planes of Potash Rocksalt. Thus, the measurement of grain boundary lengths per unit area show a variation., in terms of lineal intercepts. Microscopically, these grains characteristically appear elongated.

2) A modified parameter of degree of connectivity of similar phases has shown that a lateral variation exists between inter-particle center to center distances.

3) By utilizing the inter-particle distances and measuring their orientation with respect to a relict horizontal bedding plane marker, one can estimate various finite strain parameters of the sample in study. Results indicate a strong external grain orientation along the 'bc' plane.

4) Preferred orientation is observable in the texture of Rocksalt. This is observed by the pole figure diagram representing the orientation of crystallographic cleavage of the Halide phases making up the Rocksalt.

5) Preliminary ultrasonic P-Wave measurments along various planes of the specimens indicate an average variation of velocity. If velocity is plotted over the corresponding distance of propagation, two out of the three directions show a linear variation of velocity with increasing distance, possibly due to

dispersion. Further measurement of the waveform characteristics are required to fully define this relationship.

The physical parameters of Rocksalt are anisotropic, that is to say, they are dependant on the crystallographic cleavage orientation, distribution of mineral phases, presence of relict bedding, grain shape and grain boundary density. Texture of Potash considers mainly the crystallographic cleavage orientation, the latter contribute to structural parameters in a polycrystalline mosaic, all of which contribute to the anisotropy of the material (Bunge after Wenk, 1985).

Various authors have attempted to derive a correlation function between different microstructural parameters. Of most concern here is one that would define the Cummulative Rate of AE output as a function of microstructural parameters prior to and after successive loading cycles. The corresponding properties measured in a plycrystalline material is then a certain mean value of the properties of the individual crystallites, (Wenk, 1985).

Three different fracture patterns can be identified based on size, location and orientation. Early stages of loading result in the generation of intergranular displacement and type I intragranular cross-hatch cleavage fractures, which in a later stage coalesce into larger intragranular type II fractures. In the later stages of load sustained by the sample, transgranular cracks are generated, which can migrate through the entire length of the sample. Majority of the displacement orientations are controlled by the macroscopic grain shape anisotropy.

Distribution of AE Amplitude Event Counts vs. Stress and Time display reproducable results, and conform to the patterns observed in literature. However, attempts to correlate AE results to crack size and distribution in individual samples is at best qualitative. The number of AE Events, Amplitude Distribution and Stress Level compared to the deformation pattern observed in specimens is consistent, but further research is required to correlate AE with the fracture distribution.

This paper demonstrates the various 'variables' involved in order to define the petrofabric of the rock sample, numerically. In future data analyses, a one-to-one comparison of crack density, texture, and AE parameters will be adopted to develop a correlation function. This can be accomplished by a Discriminant Analysis, which is a multivariant correlation coefficient. This technique can be adopted to discriminate failure modes on the basis of a set of test variables or parameters.

.op

REFERENCES

ASTM Designation : E 494 - 75, Standard Recommended Practice for Measuring Ultrasonic Velocity in Materials. Pp. 466-479.

ASTM Designation : E 500 - 74, Standard Definitions of Terms Relating to Ultrasonic Testing. Pp. 492-495.

CLARK, A.R., and SCHWERDTNER, W.N., 1966, Petrofabric Analysis of Potash Rocks, Esterhazy, Saskatchewan. Third International Symposium on Salt, pp. 103-122.

CLABAUGH, P.S., 1962, Petrographic Study of Deformed Salt : Science. Vol. 136, no. 3514, pp. 389-391.

DEHOFF, R.T., and RHINES, F.N., 1968 Quantitative Microscopy. McGraw-Hill Book Co., New York.

FONSEKA, G.M., and al., 1985, Scanning Electron Microscope Emission Studies of Crack Development in Rocks. Int.J.Rock Mech. Sci. & Geomech., Vol. 17, no 3, pp. 273-299.

HARDY H.G. & LEIGHTON F.W., 1984, AE Microsiesmic Activity in Geologic structures and Materials, Proceedings of the Third Conference, Trans Tech Publ., Penn. State.

HOWARTH, D.F., and ROWLANDS, J.C., 1987, Quantitative Assessment of Rock Texture and Correlation with Drillability and Strength Properties. Rock Mech. and Rock Eng. no. 20, pp. 57-85.

HUTCHISON, C.S., 1974, Laboratory Handbook of Petrographic Techniques. Wiley and Sons Inc., New York.

JOHNSTON, D.H., and TOKSOZ, M.N., 1980, Ultrasonic P and S Wave Attenuation in Dry and Saturated Rocks Under Pressure. J.G.R., Vol. 85, no B2, pp. 925-936.

KEYS, D.A., and WRIGHT, J.Y., 1966, Geology of the I.M.C. Potash Deposit Esterhasy,Saskatchewan. Third International Symposium on Salt, pp. 95-101.

McCall, J.L., and MUELLER, W.M., 1973, Micostructural Analysis Tools and Techniques. Plenum Publishing Co., New York.

NUR, A., and SIMMONDS, G., 1969, Stress-Induced Velocity Anisotropy in Rock : An Experimental Study. J.G.R., Vol. 74, no. 27, pp. 6667-6674.

OLSSON, W.A., 1976, Microcrack Nucleation in Marble. Int. J. Rock Mech. Min. Sci. & Geomech, Vol. 13, pp. 53-59.

ONODERA, T.F., and KUMARA, A., 1980, Relation Between Texture and Mechanical Properties of Crystalline Rocks. Bulletin of the International Association of Engineering Geology, no. 22, pp. 173-177.

PELLISIER, G.E., and PURDY, S.M., 1972, Stereology and Quantitative Metallography. ASTM-504-72, Amer. Soc. for Testing and Mats., Philadelphia.

PHILLIPS, W.R., and GRIFFEN, D.T., 1981, Optical Minerology : The Nonopaque Minerals. W.H. Freeman and Co., San Francisco.

PRIEST, S.D., 1985 Hemischerical Projection Methods in Rock Mechanics. Allen & Unwin Inc., London.

RAGAN, D.M., 1973, Structural Geology. An Intrduction to Geometrical Techniques. Second Edition, New York.

RAMSEY, J.G., 1967, Folding and Fracturing of Rocks. McGraw-Hill Book Co., New York.

SCHOLZ, C.H., 1968, Microfracturing and the Inelastic Deformation of Rock in Compression. J.G.R., Vol. 73, no. 4, pp. 1417-1432.

SCHWERDTNER, W.M., 1966B, Preferred Orientation of Halite in a " Salt Seismogram ". Third International Syposium on Salt, pp. 70-83.

TAPPONNIER, P., and BRACE, W.F., 1976, Development of Stress-Induced Microcracks in Westernly Granite. Int. J. Rock Mech. Min. Sci. & Geomech, Vol. 13, pp. 103-112.

VERHOEVEN, J.D., 1975, Fundamental of Physical Metallurgy. Wiley & Sons Inc., Iowa.

WENK, R.H., 1985, Preferred Orientation in Deformed Metals and Rocks : An Introduction to Modern Texture Analysis. Academic Press Inc., Florida.